WARM COMPACTION OF ALUMINIUM ALLOY ALUMIX 123

By

ĽUBOŠ MELÚCH

A thesis submitted to
The University of Birmingham
for the degree of
DOCTOR OF PHILOSOPHY

UNIVERSITY OF BIRMINGHAM

Department of Metallurgy and Materials
The University of Birmingham
September 2009

ABSTRACT

The aims of this PhD project were to understand and improve the mechanical properties of aluminium Al-Cu-Si-Mg P/M alloy Alumix 123 by application of a warm compaction process. They were achieved by investigating the effect of (a) compaction pressure/temperature, (b) admixed lubricants (e.g. Acrawax C and Kenolube P11) on green/sintered density and mechanical properties of Alumix 123 P/M Al powder.

It was found that compaction at 110ºC led to (1) a reduction in the ejection force up to ~ 40 % and (2) an increase in sintered density up to ~ 98 % of theoretical density. After heat treatment at 200ºC for 5 hours (T6), the tensile strength reached ~ 365 MPa and hardness of ~ 126 HV was achieved. These mechanical properties are comparable to wrought alloy of Al 2014 A (Al-Cu-Si-Mg). Further improvement of mechanical properties of aluminium alloy Alumix 123 can be achieved by reducing the amount of admixed lubricant to 0.5 wt %, and using Acrawax C as the lubricant rather than Kenolube P11. 0.5 wt % of lubricant improved the blending properties of the powder premix thus allowing the most effective filling of the die. Also lower content of lubricant leads to higher amounts of metal-to-metal contacts between powder particles.

Taguchi analysis was used to identify which parameter (compaction pressure, temperature and lubricant content) affected the densities and mechanical properties of Alumix 123 specimens with single lubricants the most. It was observed that the most effective parameter in warm compaction of Alumix 123 specimens with Acrawax C as admixed lubricant was actually the lubricant content. The next parameters are compaction pressure and temperature. A similar effect was noted for Alumix 123 specimens with

admixed Kenolube P11, where the most effective parameter was also lubricant content followed by compaction pressure and temperature.

PREFACE

The work described in this thesis was carried out by the author in the Department of Metallurgy and Materials, The University of Birmingham from February 2006 to September 2009, under the supervision of Dr. I T H Chang.

To the best of my knowledge, the material presented in this thesis is original except where otherwise noted within the text. None of this research has been submitted for any degree at this or any other university.

Part of the present work was published as follows:

L. Meluch, I.T.H. Chang, *Warm compaction of Alumix 123 L,* Powder Metallurgy, In Press;

ACKNOWLEDGEMENTS

This research would not have been possible without the assistance of many people and I would like to gratefully acknowledge everyone who contributed in some way. In particular, I would like to thank:

- Dr. I. T. H. Chang for his support and advice throughout this project. His patience, input and excellent supervision has helped to make this project a very rewarding experience.
- Professor Paul Bowen, Head of the School of Metallurgy and Materials for the provision of laboratory facilities.
- ECKA Granulate GmbH & Co. KG for providing the material support for this project to take place.
- I would like to thank the following technical staff for their invaluable assistance: Mr. Frank Biddlestone; Miss Avril Rogers; Mr. Jaswinder Singh; Mr. John Lane; and Mr. Dave Price. I would also like to acknowledge all the other technical and support staff who have helped make this work possible.
- My group friends, including Dr. P.J. Squire, have ensured a pleasant working environment as well as being the source of many discussions on the practical aspects of Ph.D research.
- Finally, I would like to thank my family for their love, encouragement and support.

TABLE OF CONTENTS

CHAPTER 1 INTRODUCTION **1**

CHAPTER 2 LITERATURE REVIEW **5**

2.1 Powder Production 5

2.1.1. Physical Processing Methods 6

2.1.1.1. Atomization 6

2.1.1.1.1 Gas Atomization 6

2.1.1.1.2 Water Atomization 10

2.1.1.1.3 Centrifugal Atomization 11

2.1.1.1.4 Splat Cooling 13

2.1.1.2. Melt Spinning 14

2.1.1.3 Advantages and Disadvantages of Physical Processing Methods 15

2.1.2 Chemical Processing Methods 17

2.1.2.1 Electrolysis 17

2.1.2.2 Oxide Reduction 19

2.1.2.3 The Pyron Process 20

2.1.2.4 Carbonyl Decomposition 21

2.1.3 Mechanical Processing Method 22

2.1.3.1 Milling 22

2.1.4 Aluminium and Aluminium Alloy Powder Production 23

2.2 Powder Preparation 24
2.2.1 Classification by Particle Size 24
2.2.2 Heating for Purification and Softening 25
2.2.3 Addition of Different Lubricants or Binding Agents to Improve Powder Compaction 26
2.2.3.1 Ferrous Materials 27
2.2.3.2 Nonferrous materials 28
2.2.4 Mixing of Various Particle Fractions or Powder Types 29
2.2.5 Aluminium Powder Characterization 30
2.2.5.1 2xxx Al Alloy 31
2.2.5.2 7xxx Al Alloy 31
2.3 Powder Compaction Methods 32
2.3.1 Cold Compaction 36
2.3.2 Warm Compaction 38
2.3.3 Double Pressing - Double Sintering 41
2.3.4 Isostatic Pressing 43
2.3.4.1 Cold Isostatic Pressing 44
2.3.4.2 Hot Isostatic Pressing 44
2.3.5 Powder Forging / Sinter Forging 45
2.3.6 Hot Pressing 47
2.3.7 Extrusion 48
2.3.7.1 Cold Extrusion 49
2.3.7.2 Hot Extrusion 49

2.4 Sintering 51

2.4.1 Solid State Sintering 53

2.4.2 Liquid Phase Sintering 54

2.4.3 Effect of Sintering Parameters on Material Properties 56

2.4.3.1 Sintering Temperature 56

2.4.3.2 Sintering Time 57

2.4.3.3 Sintering Atmospheres 59

2.4.3.3.1 Endothermic Atmospheres 60

2.4.3.3.2 Exothermic Atmospheres 60

2.4.3.3.3 Dissociated Ammonia 61

2.4.3.3.4 Vacuum 61

2.4.3.3.5 Nitrogen 62

2.4.3.3.6 Hydrogen 63

2.4.3.3.7 Argon 63

2.4.3.4 Heating and Cooling rate 64

2.4.4 Sintering of Aluminium and Aluminium Powder Alloys 66

2.4.4.1. Sintering and Heat Treatment of Aluminium Alloys

2xxx Series 67

2.5 Taguchi Design 71

CHAPTER 3 EXPERIMENTAL TECHNIQUES 76

3.1 Starting Material 76

3.1.1 Powder Premix 76

3.1.2 Lubricants 77

3.2 Mixing Lubricant into Alumix 123 78

3.3 Powder Compaction 79

3.3.1 Cold Compaction Cycle 81

3.3.2 Warm Compaction Cycle 81

3.4 Sintering and Heat Treatment 82

3.5 Material Characterization 83

3.5.1 Thermo Analysis of Used Lubricants 83

3.5.2 Density Measurement 83

3.5.3 Tensile Testing 84

3.5.4 Hardness Testing 85

3.5.5 Microstructure 85

CHAPTER 4 RESULTS 87

4.1 Analysis of Used Materials 87

4.1.1 Particle Size Analysis 87

4.1.2 Thermal Stability of Admixed Lubricants 90

4.2. Effect of Compaction Pressure and Temperature on Ejection Force of Alumix 123 Compacts 95

4.2.1 Acrawax C 95

4.2.2 Kenolube P11 98

4.3. Effect of Compaction Pressure and Temperature on Green Density of Alumix 123 Compacts 101

4.3.1 Acrawax C 101

4.3.2 Kenolube P11 103

4.4 Relationship between Compaction Pressure and Green Density of Alumix 123 Compacts 106
4.4.1 Acrawax C 106
4.4.2 Kenolube P11 109
4.5 Microstructure of Alumix 123 Green Compacts 112
4.5.1 Effect of Lubricant Content on Microstructure of Alumix 123 Green Compacts 114
4.5.2 Distribution of Porosity in Alumix 123 Green Compacts 116
4.6 Effect of Compaction Pressure and Temperature on Sintered/Aged Density of Alumix 123 Compacts 118
4.6.1 Acrawax C 118
4.6.2 Kenolube P11 120
4.7 Mechanical Properties of Sintered/Aged Alumix 123 Compacts 123
4.7.1 Effect of Compaction Pressure and Temperature on Tensile Strength of Sintered/Aged Alumix 123 Compacts 123
4.7.1.1 Acrawax C 123
4.7.1.2 Kenolube P11 126
4.7.2 Effect of Compaction Pressure and Temperature on Hardness of Sintered/Aged Alumix 123 Compacts 130
4.7.2.1 Acrawax C 130
4.7.2.2 Kenolube P11 132
4.7.3 Effect of Compaction Pressure and Temperature on Elongation of Sintered/Aged Alumix 123 Compacts 135
4.7.3.1 Acrawax C 136

4.7.3.2 Kenolube P11 139

4.7.4 Effect of Compaction Pressure and Temperature on Young' Modulus of Sintered/Aged Alumix 123 Compacts 142

4.7.4.1 Acrawax C 142

4.7.4.2 Kenolube P11 144

4.7.5 Correlation between Tensile Strength, Young's Modulus and Porosity 147

4.7.5.1 Correlation between Tensile Strength and Porosity 147

4.7.5.1.1 Acrawax C 149

4.7.5.1.2 Kenolube P11 154

4.7.5.2 Correlation between Young's Modulus and Porosity 154

4.7.5.2.1 Acrawax C 156

4.7.5.2.2 Kenolube P11 158

4.8 Microstructure of Sintered/Aged Alumix 123 Compacts 161

4.9 Fracture Surface of Sintered/Aged Alumix 123 Compacts 164

4.10 Taguchi design 166

CHAPTER 5 DISCUSSIONS

5.1 The Influence of Compaction Pressure, Temperature and Lubricant Content on Ejection Force of Alumix 123 Compacts 172

5.2 The Influence of Compaction Pressure, Temperature and Lubricant Content on Green Density of Alumix 123 Compacts 175

5.3 Heckel Relationships 178

5.4 The Influence of Compaction Pressure, Temperature and Lubricant Content on Sintered/Aged Density of Alumix 123 Compacts 179

5.5 The Influence of Compaction Pressure, Temperature and Lubricant Content on Tensile Strength and Hardness of Sintered/Aged Alumix 123 Compacts 180

5.6 The Influence of Compaction Pressure, Temperature and Lubricant Content on Elongation of Sintered/Aged Alumix 123 Compacts 185

5.7 The Influence of Compaction Pressure, Temperature and Lubricant Content on Young's modulus of Sintered/Aged Alumix 123 Compacts 187

5.8 Correlation between Tensile Strength, Young's Modulus and Porosity 187

5.9 Microstructure of Sintered/Aged Alumix 123 Compacts 190

5.10 Fracture Surface of Sintered/Aged Alumix 123 Compacts 192

5.11 Taguchi analysis 193

CHAPTER 6 CONCLUSIONS AND FUTURE WORK 194

6.1 Conclusions 194

6.2 Suggestions for further work 196

APPENDIX 197

REFERENCES 211

CHAPTER 1

INTRODUCTION

Powder metallurgy (P/M) technology covers a broad subject of powder production, powder consolidation and characterisation of both powder and bulk samples. Consolidation into net-shape forms is achieved by the application of pressure and heat at temperature below the melting point of the major constituent.

Although P/M is just small fraction of the global metal industry, it plays an important role in many sectors because it has many advantages compared to other conventional technologies. They include:

- Fabrication of metals which cannot readily or satisfactorily be produced by alternative processes (porous materials, hardmetals, and composite materials).
- Cost effective production.
- Typically more than 97% of the starting raw material is used in the finished part.
- Elimination or minimisation of machining.
- Long-term performance reliability.
- Good surface finishes.

- Materials with properties that can be improved through secondary processing operations. [1-3]

While P/M materials are dominated by ferrous alloys (which are close to 80 % of global metal powder production) there is a growing interest in Al P/M (8%). Aluminium and aluminium P/M alloys are characterised by a low weight-to-strength ratio, which makes aluminium useful in many applications, e.g. in the automotive sector for production of camshafts, bearing caps, mirror brackets, shock absorber parts and pumps. Aluminium P/M alloys can compete with conventional aluminium casting alloys, as well as with other materials, for cost-effective manufacture of complex or unique shapes impractical with other applications. Also in P/M the microstructure can be more refined and homogenous than in an ingot or a cast. Therefore, the use of aluminium alloys in high-technology applications, such as those in aircraft, aerospace structures and automobile industry is extended. [4]

Other benefits of aluminium P/M parts include:

- Ability to increase strength by alloying and precipitation hardening.
- Good workability.
- Corrosion resistance, (Al in contact with air creates a protective oxide film which reduces corrosion attacks).
- High thermal and electric conductivity. [1-3]

Most of the structural aluminium P/M alloys used today are those based on the 2xxx and 7xxx wrought alloy compositions, being blends of Al-Cu-Mg-Si and Al-Zn-Mg-Cu, respectively. These alloys can achieve similar properties to their wrought equivalents. [5] One of these alloys is commercial blend known as ECKA Alumix 123 from ECKA

Granulate GmbH & Co. KG. During the preparation of compacts from powder blend 1.5 wt % of Microwax C is used as admixed lubricant. Microwax C is a fatty acid amide wax recommended by ECKA Granulate. It is trademark of Hoechst AG Company. Chemical composition and sintered properties of Alumix 123 and wrought Al 2014 A are listed in table 1.1.

Table 1.1: Chemical composition and sintered properties of Alumix 123 and Al 2014 A [6, 7]

Alloy	**Nominal composition**	**Sintered properties**			
		Sintered density [g/cm^3]	**Tensile strength [MPa]**	**Hardness HB**	**Elongation [%]**
Alumix 123	Al-4.5Cu-0.6Si-0.5Mg	2.55 - 2.65*	190 260_{T4} 320_{T6}	64	~5 ~3 ~1
Wrought Al 2014A	Al-4.5Cu-0.8Mn-0.7Si-0.5Mg	2.8	190 430_{T4} 485_{T6}	55 110_{T4} 140_{T6}	20 18_{T4} 12_{T6}

*Sintered density depends on the compaction pressure and heat treatment.

The continued growth of aluminium P/M in automotive applications is dependent on the improvement of dynamic properties through development of higher density. Several approaches have been proposed to increase green density. The warm compaction process is one technique developed for increasing density levels in ferrous alloys by a single compaction process. Typically the powder and tools are heated to 130 and 150°C. In the warm compaction process high temperature polymers are often used as lubricants. The compacts can be sintered in the normal way. This process also provides increased green strength and reduced ejection forces. [8-10]

Taguchi design is used in many industries to optimize the manufacturing process, e.g. to determine the role of process parameters on the final properties at minimal cost. By incorporating orthogonal arrays in Taguchi design of experimental methods it is possible to minimize the number of experiments required to determine the effect of parameters upon performance characteristics. [11]

The main aims of this PhD project were to study the effect of warm compaction conditions on the resultant microstructures and mechanical properties of Alumix 123. This was achieved through the addition of different lubricants in varying amounts, and use of different compaction pressures and temperatures. In addition, Taguchi analysis was applied to the experimental data to study the effect of the warm compaction processing on parameters.

This work is divided into six chapters. In the next chapter (Chapter 2), a literature review of powder production and powder consolidation techniques is presented. Chapter 3 describes the experimental methods applied during this research. This includes preparation of specimens and their characterization. This is achieved by optical microscopy, scanning electron microscopy (SEM), simultaneous thermal analysis (STA), and tensile and hardness testing. In chapter 4 experimental results of this work are presented and in chapter 5 experimental results are discussed. Chapter 6 gives the conclusions of the research and recommendations for future work.

CHAPTER 2

LITERATURE REVIEW

2.1 Powder Production

At present, it is possible to produce powder from more than 50 % of all metals within the Periodic Table. The required physical and chemical characteristics of the powder may be produced by a variety of methods. Generally, these processing methods can be categorized into three main groups; physical, chemical and mechanical. [12]

- Physical: e.g. atomization of a liquid metal by high-pressure air or water jets.
- Chemical: includes electrolysis of solutions or fused salts, thermal decomposition, and chemical displacement.
- Mechanical: machining, crushing, grinding, or milling of metallic stock to powder.

The choice of method depends on many factors including physical-chemical characteristics, reactivity, ductility or brittleness and reducibility of any oxide content and the economic factors. [13-15]

2.1.1. Physical Processing Methods

2.1.1.1 Atomization

Atomization is widely used for production of elemental and alloyed powders. They include powders from: aluminium, iron, copper, tin, cobalt, titanium and nickel systems.

Atomization is commonly used as a powder production method. There are several techniques which fall under the general heading of atomization. However the most common commercial techniques are:

- Gas atomization.
- Water or oil atomization.
- Centrifugal atomization, splat cooling. [12, 16, 17]

The basic principle of atomization involves three steps: (1) melting of initial material to form of a stream of molten metal, (2) disintegration of molten metal into droplets and (3) solidification of droplets to solid particles.

2.1.1.1.1 Gas Atomization

In the gas atomization process, the liquid metal stream is disrupted by a high-velocity gas, up to 4 MPa (Figure 2.1). Gases such as nitrogen, helium or argon, act as a medium for breaking up the molten metal stream. Molten metal of appropriate composition is supplied from a melting furnace held at the required temperature in an atomizing bay. The liquid is drawn from the bay through a liquid delivery tube into the atomizing nozzle. This is achieved

by a suction effect caused at the nozzle end of the delivery tube by the flow of the high-pressure atomizing gas in the nozzle. When the liquid metal meets the high-velocity gas it is broken up into droplets. [19, 20]

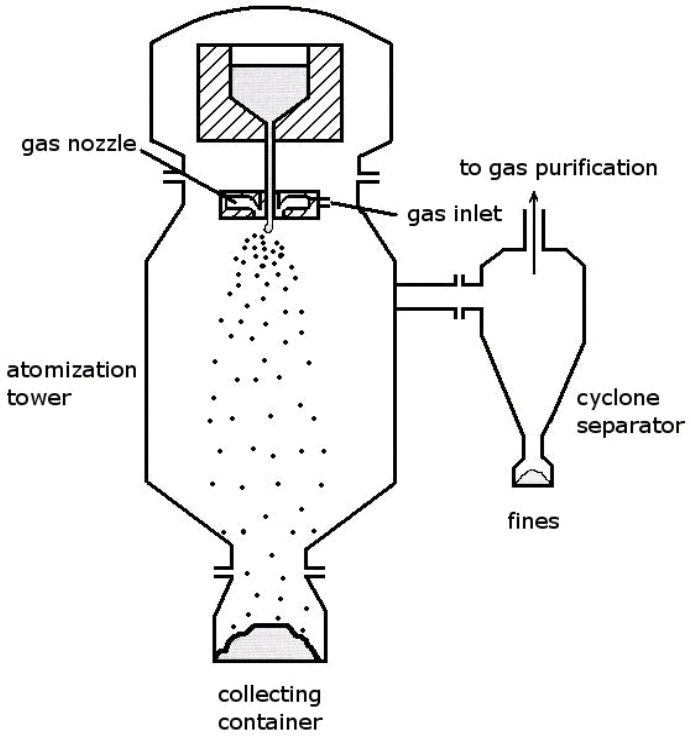

Figure 2.1: Vertical gas atomization. [18]

The creation of droplets can be described in five stages as shown in figure 2.2. In the first stage, waves on the liquid are formed after molten metal is hit by high-pressure gas. This is followed by the transformation into a thin sheet form in second stage. The sheet is unstable because of a high surface area to volume ratio. In the third stage, the liquid continues to respond to the shear and acceleration forces, giving first ligaments and then droplets. The fourth stage is characterized by additional deformation and droplets reduction.

The fifth stage involves collision between particles and creation of agglomerates. Finally droplets solidify into a powder with a wide range of particle sizes. [16]

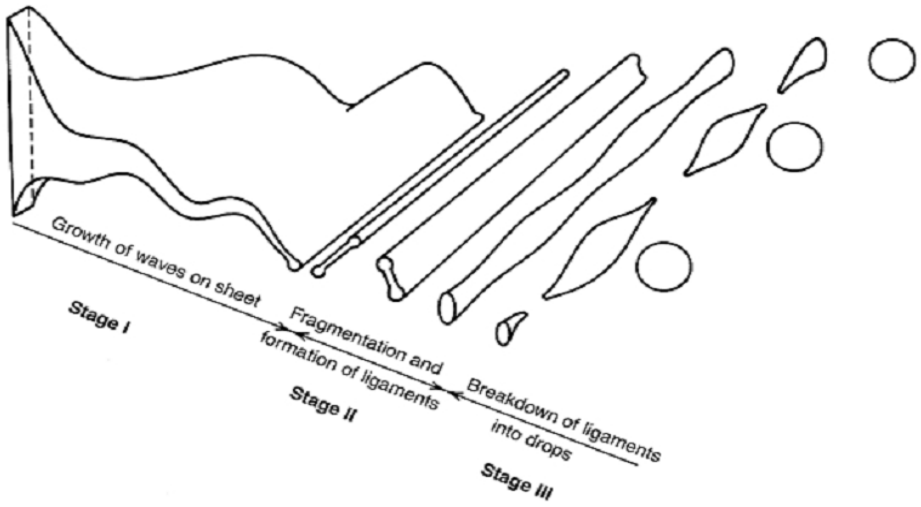

Figure 2.2: Model for the disintegration of a liquid sheet by a high-velocity gas jet. [21]

The median size of droplets produced by gas atomization can be calculated by equation 2.1. This equation has been determined by many experimental observations and is suitable for gas atomization. [16]

$$d_0 = 585\frac{\sqrt{\sigma}}{v.\sqrt{\rho}} + 597\left(\frac{\sqrt{\mu}}{\sqrt{\sigma.\rho}}\right)^{0.45} * \left(1000\frac{Q_t}{Q_v}\right)^{1.5} \quad \text{(eq. 2.1)}$$

where d_0 is the median droplets size [μm], ρ is the specific weight of melting [g/cm^3], σ is the surface tension [dyn/cm], μ is the viscosity coefficient of melting [dyn.s/cm^2], v is the differential speed of gas [m/s], Q_t is the flow velocity of melting, Q_v is the flow velocity of gas.

It is assumed that the size of droplets decreases with decreasing surface tension of molten metal and increasing flow velocity of atomizing medium.

The working pressure for atomizing gases lies between 0.4 and 4 MPa. The gas velocities in the nozzles range from Mach 1 to 3. Typically, mean particle size of gas atomized powder is in the range of 10 to 300 μm with oxygen content of about 100 ppm.

Shorter distances between the gas exit and melt stream lead to better energy transfer, aiding the formation of finer powders. The gas velocity on exit from the atomizer is the dominant factor in determining the resulting particle size. The morphology of gas atomized powders varies from rounded-irregular to spherical (Figure 2.3), with a log normal size distribution. This depends on a range of parameters including base material and atomizing conditions such as atomizing pressure, gas composition and temperature. The temperature at which the molten metal is atomized (i.e. superheat) is generally 75 to 150°C above the melting point of the metal. At superheat temperature, the viscosity of molten metal decreases so smaller particle size can be achieved using a lower pressure of gas. [19, 20, 22]

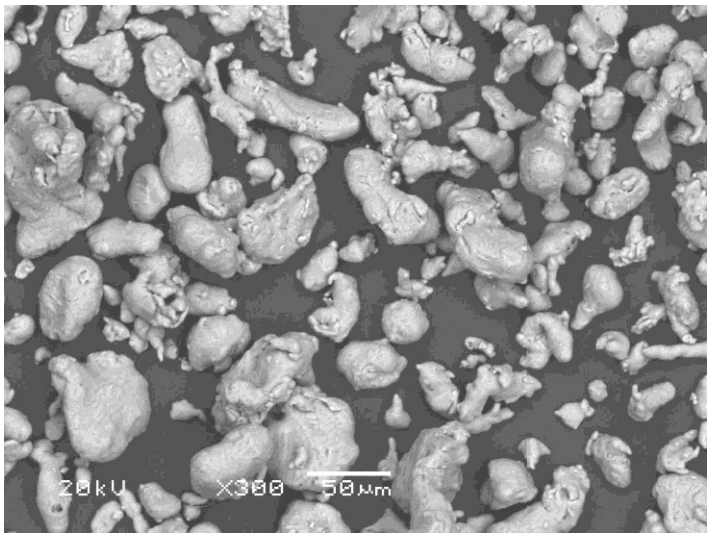

Figure 2.3: Aluminium gas atomized powder.

2.1.1.1.2 Water Atomization

The principle is similar to gas atomization but the molten metal stream is disintegrated by water jets. These two atomization methods have design differences in the shape of the fluid nozzle and the direction of flow as well as in the diameter of the opening for the molten stream. For water atomization a convergent nozzle is used. Figure 2.4 shows an example of the water atomizing process. The water can be delivered in the form of a single jet, multiple jets or an annular ring. The working pressure for commercial water atomizing systems is between 3 to 50 MPa, resulting in mass median particle sizes of 30 to 150 μm. Higher water pressures between 50 to 150 MPa are used to produce finer powders with median particle size of 5 to 20 μm. The cooling rate is higher than in gas atomization due to a better heat transfer coefficient. Water atomized powder has more irregular morphology than gas atomized. Powders produced in this way acquire a film of oxide on the surface of the particles and so in some cases the powder requires a reduction treatment. Therefore, only low oxygen sensitive materials are suitable for water atomization.

The production cost of water atomization is lower than gas atomization; accordingly annual tonnage of water atomized powder is much more than gas atomized powder. [23-25]

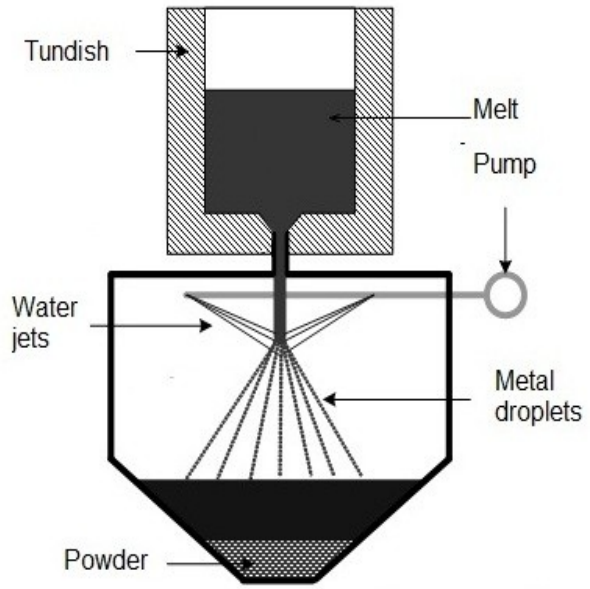

Figure 2.4: Water atomization process. [26]

2.1.1.1.3 Centrifugal Atomization

Centrifugal atomization, also known as the rotating electrode process, is mostly used for reactive metals which are aggressively corrosive in their molten state and attack conventional ceramic crucibles. Primary metals are titanium, zirconium, molybdenum, and vanadium alloys. However it can be used to produce powders of other metals.

Many variations of centrifugal atomization exist. The basic principle is based on the centrifugal force that throws off the molten metal as a fine spray of droplets which solidify into spherical powder particles before hitting the chamber walls. The rotating electrode is schematically shown in figure 2.5. The apparatus (Figure 2.6) consists of a consumable electrode made from the required material. The end of the electrode is commonly melted by an electric arc or plasma generated from a tungsten electrode. The consumable electrode is

the anode and rotates at velocities up to 50,000 revolutions per minute. The cooling rate is higher than 10^5 K/s and average particle size is in the range of 100 to 160 µm.

Centrifugal atomization, like gas atomization, is often performed under an inert gas, or vacuum, to protect the powder from oxidation. The preferred medium is helium, which enhances the heat transfer coefficient and electric arc characteristics. [27-31]

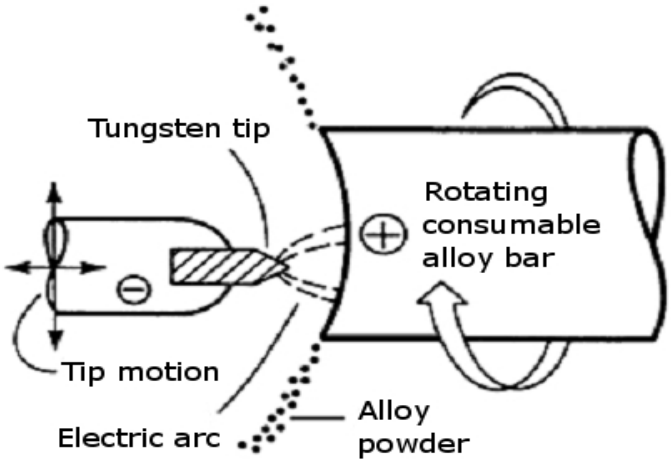

Figure 2.5: Schematic of rotating electrode process. [28]

A median droplet size can be predicted by the equation [29]:

$$d_0 = \frac{3.464}{w}\sqrt{\frac{\gamma}{\rho.D}} \qquad \text{(eq. 2.2)}$$

where d_0 is the median droplet diameter [µm], w is the rotation rate [rpm], γ is the surface tension [dyn/cm], ρ is the density of the alloy being atomized [g/cm^3] and D is the electrode diameter [mm].

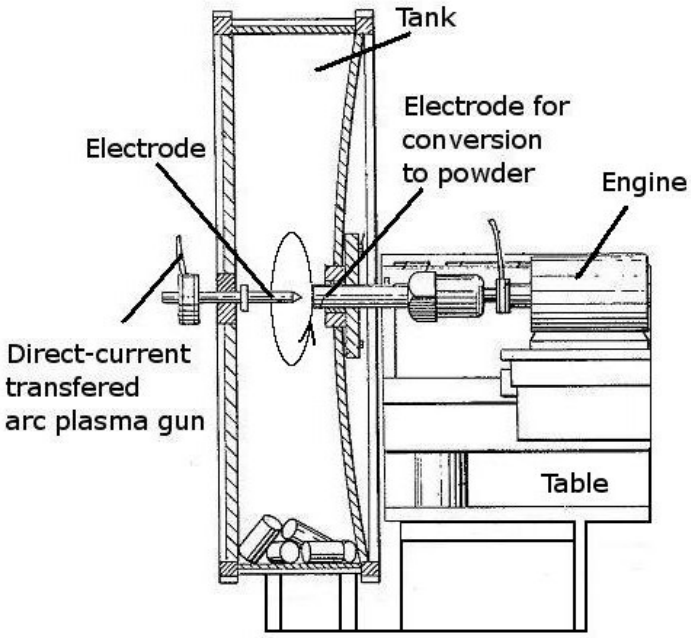

Figure 2.6: Centrifugal atomization by the rotating electrode. [32]

2.1.1.1.4 Splat Cooling

Basically, the metal is melted and liquid droplets are sprayed or dropped against a chilled surface of high thermal conductivity. Figure 2.7 shows a rotating disc from which molten droplets are thrown. They impact against the conical plate where they are deformed to splats and cool extremely fast. As they cool, they shrink from the surface and they are ejected by centrifugal force. The splat cooling process enables cooling rates even higher than those obtained in atomization. Typical cooling rates are 10^5 K/s and particle sizes range from 50 to 100 μm. The speed of the rotating wheel normally ranges from 500 to 4,000 revolutions per minute depending on the required properties of the powder. [33, 34]

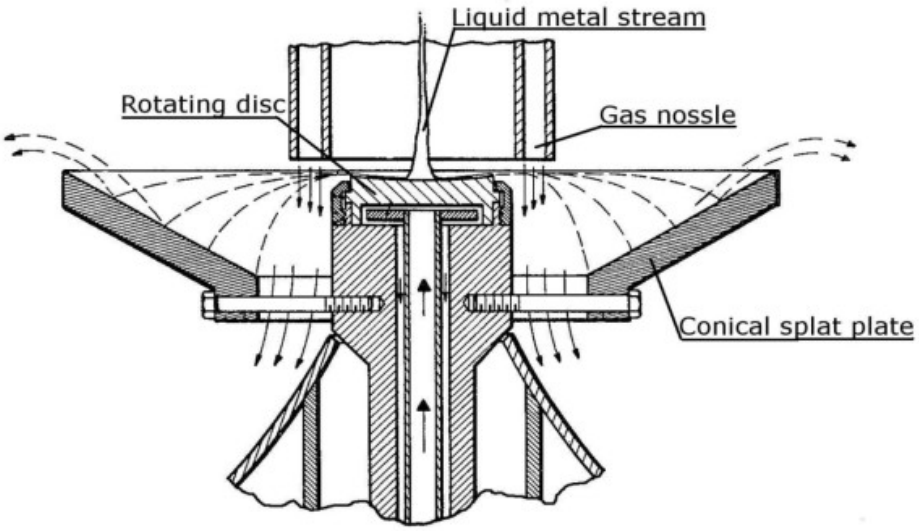

Figure 2.7: The splat cooling process. [34]

2.1.1.2 Melt Spinning

This technique is similar to the splat cooling technique, but the spinning-rotating wheel is in the vertical position (Figure 2.8). Melt spinning is a rapid solidification technique which employs centrifugal force to throw off solidified metal from a rotating chill wheel. Rotation speed can reach up to 25,000 revolutions per minute. This technique is used for production of ribbons or flakes which can be used in secondary processes like milling to get final product. The cooling rate of melt spinning process is between 10^5 to 10^7 K/s and the material thickness is in the range of 10 to 100 μm. The melt spinning process is performed in the vacuum or under protective atmosphere. [35]

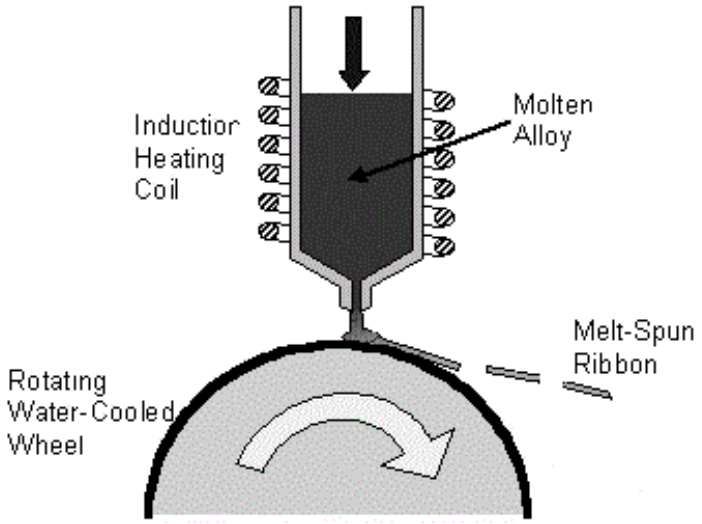

Figure 2.8: Melt spinning process. [36]

2.1.1.3 Advantages and Disadvantages of Physical Processing Methods

Each technique is defined by certain advantages and disadvantages. The most dominant are:

Gas atomization: *Advantages:* - high production rate,

- low pressure requirements,
- low oxide content,
- high range of produced particles.

Disadvantages: - the cost of gases (argon, helium),

- larger-scale facilities,
- lower metal feed rates.

Water atomization:

Advantages: - high production rate,

- low cost of atomizing medium (water),
- low energy use for pressurization.

Disadvantages: - powder impurity,

- irregular shape,
- high oxygen content.

Centrifugal atomization and splat cooling:

Advantages: - powder cleanliness,

- low pressure requirements,
- almost spherical shape,
- minimum level of porosity,
- uniform particle size.

Disadvantages: - low production rate,

- high cost of making a high-quality bar of metal,
- high energy consumption.

Melt spinning*:* *Advantages:* - high ribbon purity,

- production of amorphous structure,

Disadvantages: - cleaning of the nozzle after each run,

- low production rate. [19-35]

2.1.2 Chemical Processing Methods

2.1.2.1 Electrolysis

It is possible to produce powders of about 60 elemental metals and/or alloys by electrolysis. The majority of the metal is obtained from aqueous solutions. Powder production by electrolysis in its simplest form is carried out as follows: two electrodes are connected to direct current, where the anode is made up of the metal whose ions are contained in the electrolyte. As current flows metal dissolves at the anodic electrode and is deposited at the cathodic electrode based on electrochemical reaction e.g. copper sulphate (Figure 2.9):

$$CuSO_4 \Rightarrow Cu^{2+} + SO_4^{2-} \qquad \text{(eq. 2.3)}$$

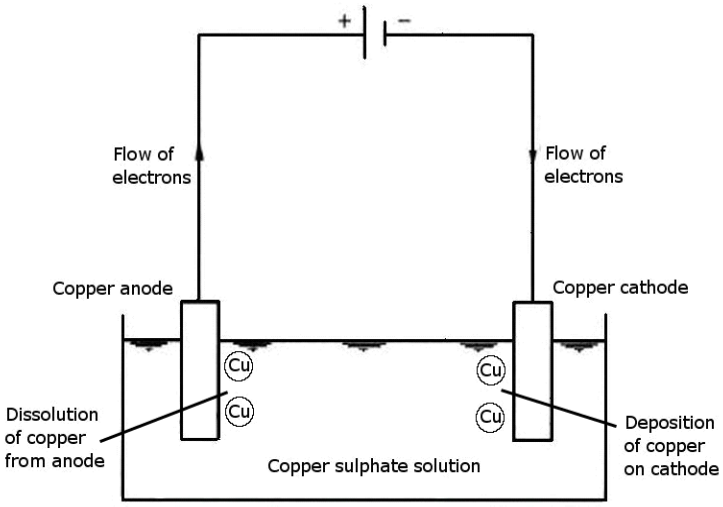

Figure 2.9: Electrolysis of copper sulphate solution. [37]

After deposition, extensive further processing is required. The powder is washed to remove all traces of the electrolyte to prevent the powder from becoming oxidized. The powders are dried, annealed and crushed in high-speed water-cooled hammer mills. They are then classified and blended to the desired particle size distribution.

Metals can be deposited in a spongy or powdery state. Typically the shape of powder particles formed by electrolysis is dendritic, as shown figure 2.10, although considerable control of particle size and shape is possible. The properties of the powder depend on conditions, such as composition and concentration, voltage, type and quantity of the addition agent (e.g. boric acid, glucose, glycerine and glue), temperature of the electrolyte and bath circulation.

The most common metal powder produced by electrolysis is copper. However, iron, chromium, manganese, silver, cadmium and zinc powders can also be produced. Purity of copper powder prepared by electrolysis is more than 99 % copper. [37-40]

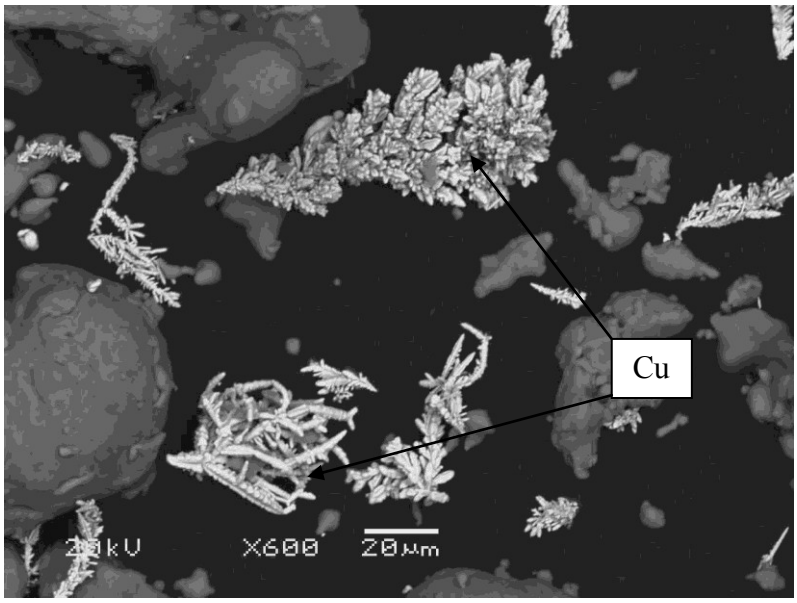

Figure 2.10: Typical dendritic Cu powder.

2.1.2.2 Oxide Reduction

The chemical reduction of metal compounds with solid or gaseous reducing agents plays an important role in powder production. This technique is mostly used for iron, copper, molybdenum and tungsten powders.

The most common process for iron powder production is the Höganäs process. In this process highly pure magnetite ore and pure coke are used as initial compounds. Limestone is also added to reduce the sulphur contained in the coke. The ground mixture of ore and coke-limestone is charged into ceramic tubes and placed into a tunnel kiln, where reduction occurs. The temperature of reduction is 1260ºC and takes approximately 68 hours. The iron is produce by chemical reduction between magnetite and graphite (eq. 2.4):

$$Fe_3O_4 + 2\ C \rightarrow 3\ Fe + 2\ CO_2 \qquad \text{(eq. 2.4)}$$

The resulting iron is known as sponge iron and is then mechanically cleaned and crushed into pieces of 25 mm diameter. This is followed by grinding, magnetic separation and removal of nonmagnetic impurities, to yield powdered iron with particle size about 150 μm. The resultant powder contains approximately 1 wt % of O and 0.3 wt % of C. The powder is consequently annealed in a belt furnace at 870ºC in an atmosphere of dissociated ammonia to reduce the oxide content. Final iron powders contain around 0.3 wt % of O. During annealing, the powder is loosely sintered, but just light grinding and screening is required to yield the final Fe powder. [41-43]

2.1.2.3 The Pyron Process

The alternative process to iron powder production by reduction of oxides is the Pyron process. In this process, mill scale taken from steel mills is used as raw material instead of iron ore.

After cleaning, mill scales are ground to particle size < 150 μm and mixed by layering in a bed. Oxidation at 980ºC converts the mill scale iron oxides FeO and Fe_3O_4, to ferric oxide Fe_2O_3. After oxidation, the reduction of oxides by hydrogen at 980ºC in an electric furnace is performed. The ferric oxide reacts with hydrogen (eq. 2.5) to give iron cake. The cake during reduction is slightly sintered but simple milling operation transforms it to iron powder.

$$Fe_2O_3 + 3H_2 \Rightarrow 2Fe + 3H_2O \qquad \text{(eq. 2.5)}$$

The resulting powder has fine porosity and a sponge microstructure. The pores in the interior structure of Pyron powders are finer than powders produced by Höganäs process because Höganäs is a lengthy reducing treatment at higher temperature that coarsens the pores. Because of the fine pore structure, compacts from Pyron iron powder sinter faster than those from other commercial iron powders. [44, 45]

2.1.2.4 Carbonyl Decomposition

This is a technique for production of very fine powders. Primary iron and nickel powders are produced by decomposition of carbonyl. However, manganese, vanadium, chrome and tungsten can be also produced.

The iron powder is produced by the decomposition of iron pentacarbonyl, $Fe(CO)_5$, (eq. 2.6)

$$Fe + 5\ CO \leftrightarrow Fe\ (CO)_5 \qquad \text{(eq. 2.6)}$$

Firstly, the raw iron pentacarbonyl is formed by passing carbon monoxide over reduced sponge iron at a pressure of 7 to 30 MPa and temperature of 200 to 250ºC. By increasing pressure the gas products become liquids, so iron pentacarbonyl is in a liquid form at room temperature.

Decomposition of iron pentacarbonyl is endothermic. The maximum rates of decomposition are achieved at pressure of 0.13 to 0.18 MPa and temperature of 200 to 250ºC. Released carbon monoxide is reused during production. The final powder has a high purity of up to 99.8 % of Fe (depending on the grade) and spherical shape with particle sizes in the range 2 to 10 μm. [41, 46, 47]

2.1.3 Mechanical Processing Method

2.1.3.1 Milling

In the milling process, the starting material is crushed to finer form via mechanical impaction using hard balls normally either stainless steel or ceramic in a drum. The starting material is usually in the form of turnings, chips, filings, or spongy cakes. Figure 2.11 shows a jar mill in action. As the jar rolls, the balls continuously impact on the material, crushing it to powder.

Milling is widely used for powder production from hard and brittle or some soft and ductile materials (e.g. ferrous alloys, beryllium, chrome and some aluminium alloys). Highly ductile materials are not suitable for the milling process because of their cold welding ability.

There are several types of mills: ball mills; vibratory mills; attrition mills; and hammer and rod mills. Milling can be carried out in dry or wet conditions.

Material with particles up to 6 mm can be milled. The size and density of milling medium is selected based on deformation and fracture resistance of the metals to be milled. Large and dense milling medium is used for grinding of large particles, and smaller sizes are used for fine grinding. The milling speed and time of milling depends on type of mill and required properties of milling material.

Generally, the particle sizes for soft materials are in the range of 5 to 10 μm and for hard material up to 2 μm. [48, 49]

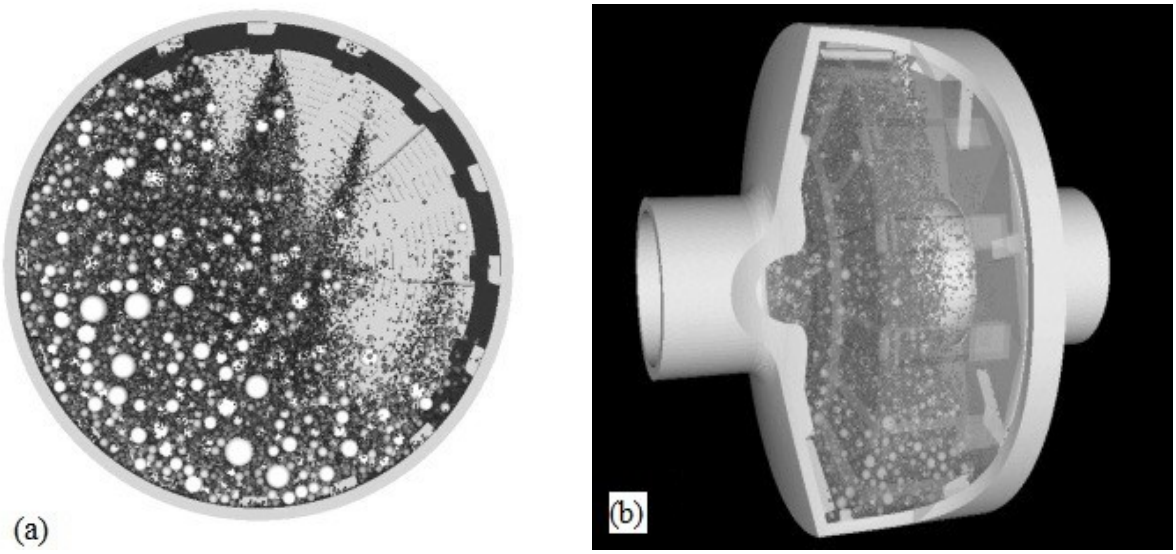

Figure 2.11: A jar mill action movements; (a) the movements of powder and impact balls - front view, (b) the movements of powder and impact balls - side view. [50]

2.1.4 Aluminium and Aluminium Alloy Powder Production

Aluminium and aluminium alloy powders are almost exclusively produced by gas atomization. The atomizing gas can be either compressed air or inert gases (helium, nitrogen, and argon). Air atomized particles are of irregular shape because of the oxygen content in the air, while particles atomized in an inert gas have a spherical shape. Also centrifugal atomization and melt spinning are used for aluminium powder production. In both techniques, molten metal impinges onto rapid rotating wheel where it is rapidly cooled. In a melt spinning process a thin, rapidly solidified ribbon is produced, which is then used as starting material for flake production in rotating mills. [19, 33, 49]

2.2 Powder Preparation

In most cases, before they can be used, powders have to be modified to suit the purpose of their applications. The most fundamental powder preparation operations are:

- Classification by particle size.
- Heating for purification and softening.
- Addition of different lubricants or binding agents to improve powder compaction.
- Mixing of various particle fractions or powder types. [51, 52]

2.2.1 Classification by Particle Size

Powder production methods tend to yield particle sizes with a broad size range. However, a specific range of sizes is needed for powder metallurgy products and so classification of powders has to be defined. [52]

Classification of powders to single narrow size fractions can be done by vibrating sieves. Fine particles (< 45 μm) are classified by sedimentation or by air separation. Gas separation and sedimentation is based on particle size and their speed of falling in gas or liquid environment. Figure 2.12 shows separation of titanium powder. Raw powder is pored to the container. Powders slowly fall to separation chamber through a funnel hole in the bottom of the container. The chamber is divided into sub-chambers by particle size i.e. by weight. As powder falls it is hit by pressurized gas which gives it speed. The trajectory depends on particles volume, shape and weight, and viscosity of environment. The lightest particles have the longest trajectory so the collecting chamber for the finest powders is

located at the end of the separation chamber. Inert gases such as nitrogen and argon are used in the separation and can be recycled. Particles size from 5 to 60 μm can be classified by gas separation. [51-53]

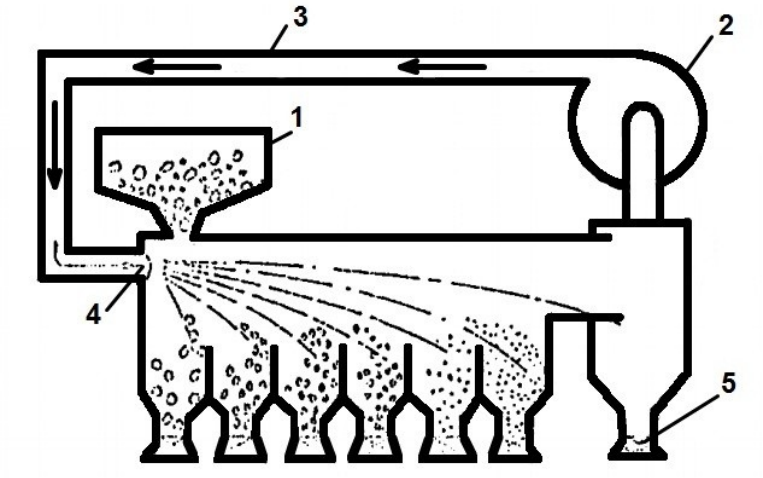

Figure 2.12: Separation of titanium powder. 1 – raw powder, 2 – fan, 3 – argon recirculation, 4 - nozzle, 5 – fine powders. [53]

2.2.2 Heating for Purification and Softening

Powder particles oxidize during long term storage in undesirable environments. Therefore they have to be purified in a heated environment to remove the oxide layer. The heating is performed in conventional furnaces under a reducing atmosphere. Pure hydrogen or cracked ammonia is often used as the reducing agent.

Metal powders with high oxygen affinity like Al, Cr, Mn and Ti are quite difficult to purify in industry. The temperature for purification should be kept as low as possible in order to eliminate a high degree of sintering between the particles. Otherwise the use of greater forces will be required to disintegrate sintered cakes, and there will be a danger of

re-oxidation and cold-working of the powders. Work-hardened powders must be softened by annealing in inert gas atmosphere before pressing. [51, 52]

2.2.3 Addition of Different Lubricants or Binding Agents to Improve Powder Compaction

Lubricants are used to overcome the friction generated between the die wall and the powders and between powders particles. As compaction pressure is increased, the ejection of the powder mass from the die becomes more difficult, so surface quality is detrimentally affected. Therefore, lubricants are used to minimize die wear, ease ejection from the die body and improve the homogeneity of compact. There are two types of lubrications in pressing operations: (1) die wall and (2) powder. [54-55]

Die wall lubricant consist of the solids such as zinc stearate, amide wax and stearic acid, which is mixed with a volatile solvent (methylchloroform or acetone) and is either painted or sprayed on to the tooling. The solvent evaporates and leaves a thin film of dry lubricant on the working surface of the die cavity.

In powder lubrication, the powder is mixed with dry lubricant before it is delivered to the press. The amount of admixed lubricant depends on many factors (e.g. composition of the metal powder, type of tooling, compacted density) and may vary from 0.5 to 1.5 wt %. The choice of lubricant is based on the ability of the lubricant to adhere to the metal particle surfaces. [54-56]

Higher amounts of admixed lubricant reduce the powder flow rate and can lead to difficulties during die filling. Additionally, higher admix lubricant content lowers the green strength of compacts by preventing, or at least reducing, metal-to-metal contacts between particles, thus reducing their cold welding ability. [51]

If powders are not lubricated, fine debris within tool clearances gall the die wall and adjacent punch areas, thereby requiring tool removal and cleaning. The amount of lubricant added to the powder should be proportional to the total surface area of the die assembly that requires lubrication during forming and ejection.

Lubricants have to be removed before the sintering process to allow the growth of particle-to-particle contacts. This happens in a de-waxing chamber in sintering furnaces where the temperature is significantly lower, depending on the type and amount of lubricant, than in the sintering zone. However, residual lubricant left in the compact can contaminate the sintering furnace atmosphere or be deposited on heating elements. In some cases the lubricants, or their residue, may react with the metal during sintering. [54-57]

2.2.3.1 Ferrous Materials

Lubricants play an important role in the powder compaction process. Hoeganaes Corporation has made a study of different lubricants on iron-based premix powder properties. It has been found that large particles of lubricant provide good flow and lower the initial amount of pressure required to eject a green compact from the die. [58]

Powder mixtures used in the P/M industry contain ingredients of different particle sizes and specific gravities that have a strong tendency to segregate during handling. In order to reduce the premix segregation, the powder particles must be bigger than particle size of the lubricants. For example, if iron powder particles are in range of 150 to 200 μm lubricants particles should be in the range of 75 to 100 μm.

The lubricant is removed by heating at 425°C or higher. Moyer showed that no residue was found using commercial waxes (Acrawax and Nopco Wax). However, about 15 % of residue was found using stearates (lithium stearate, zinc stearate) even at temperatures of up to 540°C. [58, 59]

2.2.3.2 Nonferrous Materials

In nonferrous systems (90Cu-10Sn) the zinc stearate, lithium stearate, stearic acid and waxes have been successfully used as lubricants. Often a bi-lubricant system is used (e.g. lithium-zinc stearate).

In bronze, Acrawax alone is used to provide increase of green strength, but it can lower apparent density and retard the flow. [60]

Acrawax was also successfully used for aluminium high-density parts usually with content of 1.5 wt %. The sintered parts achieved high properties, because there was no ash residue after burn-off of waxes that could interfere with particle bonding during sintering. [61]

2.2.4 Mixing of Various Particle Fractions or Powder Types

The problem of homogenising different powder fractions into a uniform powder with a certain particle size distribution is solved by mixing. Mixing can also process different powder constituents into a powder mixture of statistical distribution in terms of size or composition.

For the production of sintered alloys and compound materials, powder constituents of different chemical compositions are used. The mixing process should be realized in the manner that obtains a mixture which is as similar as possible to a random mixture. This is achieved when mixed powders have approximately the same particle size, density and shape. Thus, a mixture reaches the greatest number of point contacts between the components. This results in a uniform fine distribution and satisfactory degree of homogeneity of the components. [62, 63]

The quality of the mix depends not only on the properties of the constituent powders, but also on the method of mixing. The powder can be mixed under dry or wet conditions. Improved homogeneity and decreased agglomeration of the mixture is possible by adding mixing agents such as alcohol, which do not inhibit sintering.

As there are many different types of mixing processes available, it is preferable to classify them according to forces which give rise to particle movements. They include diffusion, convection and shear, as shown in figure 2.13. For diffusion, mixing is performed using a rotating drum and relies on gravity to move the powder. In convection, mixing is provided in screw mixers which include stationary or rotating mixing members and they are capable of higher intensity of mixing. In shear mixing, groups of powder particles are mixed

through formation of slipping planes within the mass of mixture. The movements of powder mass in convection and shear mechanisms are based on the effects of mechanical forces. [62, 63]

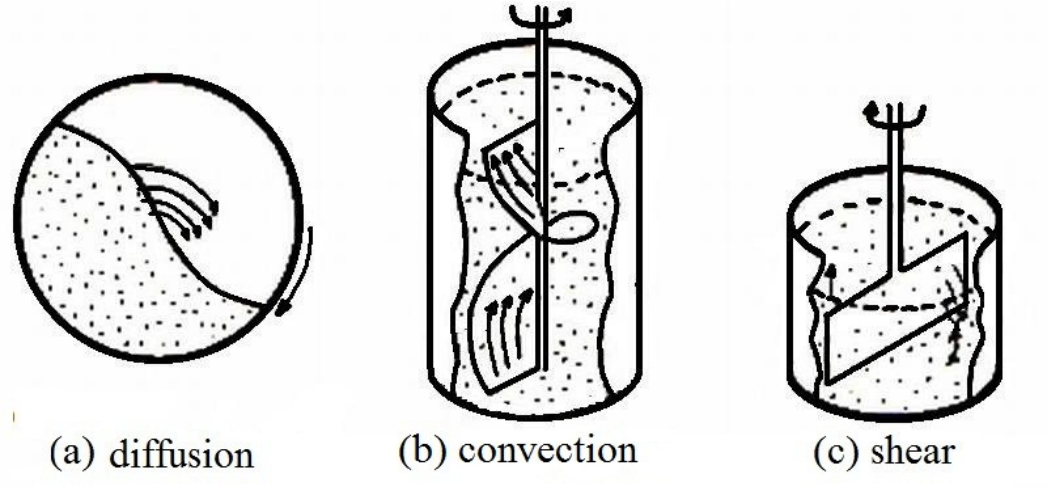

Figure 2.13: Three mechanism of powder mixing; (a) diffusion, (b) convection and (c) shear. [64]

2.2.5 Aluminium Powder Characterization

P/M aluminium alloy powders are commercially available in several grades. They are classified as aluminium powder premixes, prealloyed powders, or aluminium powder composites. Aluminium alloy premixed powders contain elemental Al with alloying additions and Al-based alloy compounds. [65]

As mentioned before, the commercially available aluminium P/M alloys are used in industry for their good mechanical properties and are based on 2xxx and 7xxx series.

2.2.5.1 2xxx Al Alloy

The alloying elements in Al based powders largely determine the mechanical properties of the final component. The principal alloying element in these alloys is copper, with magnesium as a secondary addition, thus allowing material strengthening by precipitation hardening, resulting in very strong alloys. Copper content up to 6 wt % can increase the strength of an alloy through precipitation hardening. Hardening is obtained by precipitation of Al_2Cu intermetallic phases during ageing which leads to high strength. In the presence of Mg and Si, hardening is formed by precipitation of $Al_5Cu_5Mg_8Si_6$. More details of Cu precipitation hardening of 2xxx series is in section 2.4.4.1. Si and Mg content in Al 2xxx alloys is usually in range of 0.5 to 1.0 wt %. 2xxx Al alloys have also good fatigue properties and hardness, with a lower corrosion resistance. [66, 67]

2.2.5.2 7xxx Al Alloy

The major alloying element in 7xxx series alloys is zinc, which can be added in quantities up to 8 wt %, while magnesium up to 3 wt % can be used and only a small percentage of copper (less than ~ 1 wt %). Hardening is obtained by precipitation of $MgZn_2$ with AlZnCuMg components. [66]

This alloy system offers the best combination of strength, fracture toughness and corrosion resistance compared to any other aluminium system. Based on their strength, 7xxx series alloys have been used in aerospace, military, nuclear structures, and also as structural parts in building applications. [67, 68]

2.3 Powder Compaction Methods

One of the most important steps in the P/M process is compaction of the powder. Many compaction methods are known and they cover a large range of applied pressures. Basically the reason for using compaction is to consolidate powders into a useful form. The choice of method depends on many variables e.g. powder composition, powder size and morphology. [69]

Compaction relies on an external pressure source to plastically deforming the metal powders into a high density mass, and to provide the required shape and dimensional control. The main process parameters which determine the resulting densities are the mechanical constrains and the rate of pressurisation.

There are three main zones through powder compaction which relate with compaction pressure (Figure 2.14). In the first zone (A) there is transitional repacking in which the particles rearrange themselves and slide past each other until they can not move further. Rearrangement of the particles is not uniform. Particles situated in ideal locations are rearranged to cavities without restrain. In the second zone (B), rearrangement of the powder particles is maximised, which leads to an increase in pressure but with little increase in density through plastic deformation. The plastic deformation occurring in this stage has just local character. In the third zone (C), the increase of pressure leads to plastic deformation of the particles. Oxide films on particles are broken and particles start to agglomerate by cold welding. Further increase of pressure extends the areas of contacts and increases green strength and density. [69-73]

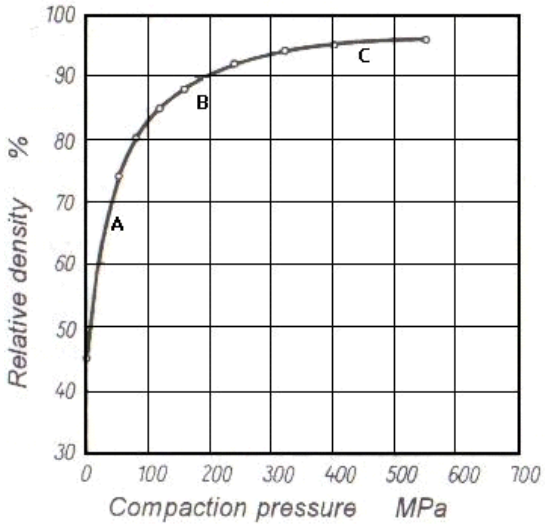

Figure 2.14: Relationship between pressure and relative density of aluminium powder. [73]

In the first and second zone, particle rearrangement is dominant while in the third zone, plastic deformation of particles is dominant. Compaction energy is consumed by friction between particles, friction between particles and die wall and by particle deformation. Deformation of particles is in the direction of the compaction pressure. If the compaction pressure is applied in uniaxial direction from the top by an upper punch, the density of the compact decreases from the top to the bottom as illustrated in figure 2.15 (a). This is caused by increasing length to cross-section ratio, thus it is more difficult to densify the lower end of the compact. Pressure transmission is reduced further from the top punch due to die wall friction. To improve this, compaction should be performed by upper and lower punches simultaneously, where the length to cross-section ratio is effectively decreased, as shown in figure 2.15 (b). [69, 75, 76]

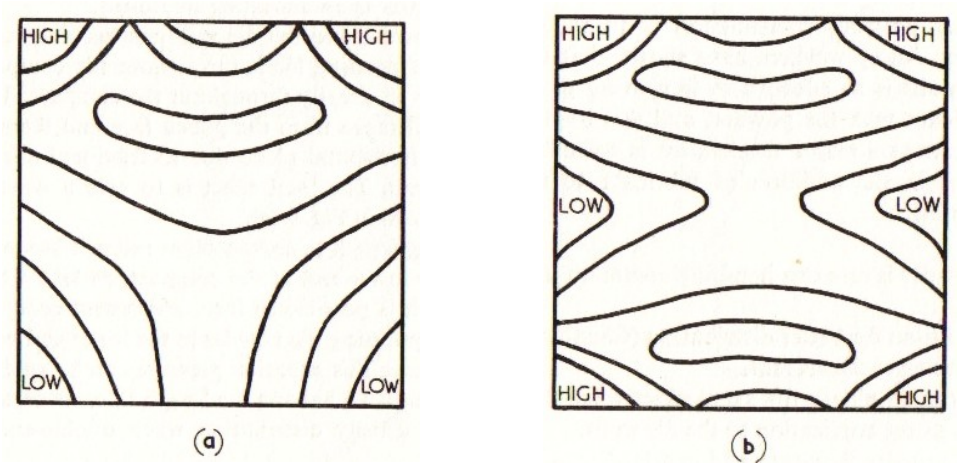

Figure 2.15: Density distribution during die wall compaction (a) single punch pressing (b) double punch pressing. [76]

When the punch load is released the elastic deformation in the compact will try to recover by the radial pressure. During the ejection of a compact from the die it is necessary to overcome the radial pressure and in some cases, if the value of radial pressure is higher than the fracture limit of the compact, then it will cause the compact to fracture. [77]

Also, oxide layers on the particles play an important role during compaction. In some cases, the amount of oxides can be as high as 10 % of whole particle volume. This requires the use of the higher compaction pressures. [69]

The Heckel equation (eq. 2.7) describes the relationship between the relative density and compaction pressure; [67]

$$ln\frac{1}{1-D} = A + k_H P \qquad \text{(eq. 2.7)}$$

where D is the relative density (i.e. $D = \frac{\rho_{measured}}{\rho_{theoretical}}$), P is the applied pressure, A and k_H are constants. A plot of $ln\frac{1}{1-D}$ versus compaction pressure P gives a linear relationship with a slope k_H as shown in figure 2.16. Heckel found that constant k_H is related to the yield stress σ_y of the material by the expression $k_H = 1/3\sigma_y$. So the constant k_H is taken as a material constant which determines the deformation mechanism of materials. [78] Augsburger reported that if the slope is small along the linear portion of Heckel plot then the yield strength of material is high, which suggests that it is more difficult to induce plastic deformation within the powder during compaction. [79]

Generally the Heckel plot (Figure 2.16) has a linear part, with curves at the low and high pressure ends. According to Heckel the linear part of the curve describes the plastic deformation of the material. The non-linear part of the curve at low pressure is associated with particle densification and rearrangement in the absence of interparticle bonding, and that the transition from curved to linear portion corresponds to the minimum pressure necessary to form a compact. The Heckel model is very sensitive to variations in experimental conditions, such as compaction under exceptionally high pressure with high loading, weight of the compact and temperature. [80]

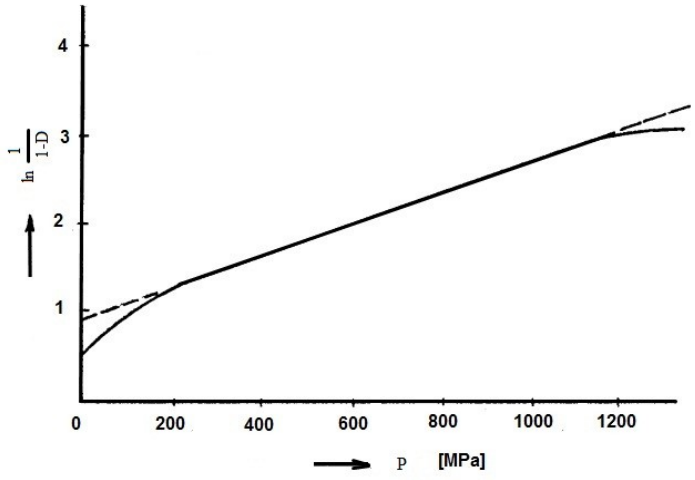

Figure 2.16: A typical Heckel plot of $\ln\frac{1}{1-D}$ *versus P based on theoretical and experimental data. [77]*

Compaction methods can be divided into two main categories: (1) compaction employing pressure and (2) pressureless compaction. These categories include the following processes: (1) with pressure e.g.: cold and warm compaction, double pressing - double sintering, isostatic pressing and powder forging; (2) without pressure e.g.: slip casting or tape casting. [69, 77]

In the following parts of this section, the most common pressure-based powder compaction methods will be introduced and described.

2.3.1 Cold Compaction

Cold compaction is the most common compaction method in the powder pressing. It starts with bulk powders containing small amounts of lubricant to eliminate friction between particles and particles and die wall. The powder is compacted inside a die between upper and

lower punches. Presses for compaction may be either mechanical or hydraulic. Because compaction requires vertical motion, the product size and shape is limited by the constraints of available press capacity. A maximum size of 160 cm^2 for compaction area, part thickness of about 75 mm and a weight of 2.2 kg are normally produced. [69, 75, 77]

The basic tools motions during compaction cycle are illustrated in figure 2.17. During powder filling, the upper punch is retracted to the fill position. The lower punch position during powder entry is termed the fill position. A predetermined amount of powder in an external feed shoe is vibrated into the die. The lower punch position during pressurization differs from the fill position to position which allow pressing in the centre of the die. After filling, the lower punch is dropped to the pressing position and the upper punch is brought into the die. Both punches are loaded to generate stress within the powder mass. At the end of the compaction stoke, the powder experiences the maximum stress. Finally, upper punch is removed and the lower punch is used to eject the compact. Density after compaction is commonly between 70 to 90 %. After compaction the green compacts are sintered, followed by heat treatment if it is needed. Dimensional tolerances of sintered parts depend on the material system, density of compacts and the sintering mechanism. For example, after solid state sintering of Fe based P/M parts, only 0.3 % of size change occurs. However, typically around 1.3 to 2.5 % of dimensional change is found after liquid phase sintering of Al alloys. [69, 70, 72]

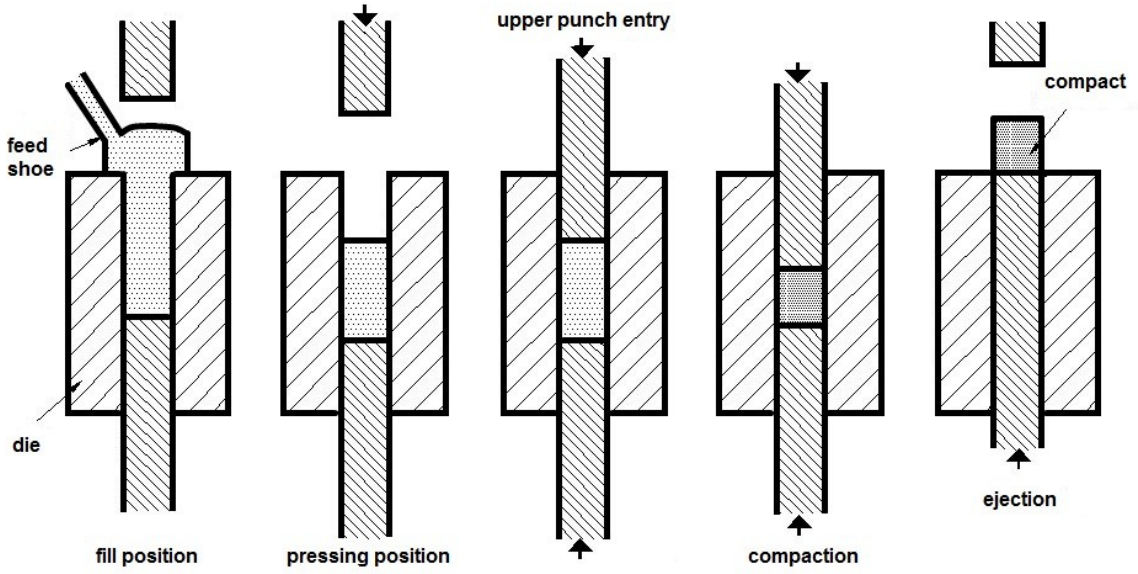

Figure 2.17: Tool motions during a powder compaction process, showing the sequence of powder filling, pressing and ejection. [72]

2.3.2 Warm Compaction

The warm compaction process was practically introduced by Hoeganaes Corporation for use in Fe-based metal powders. Earlier work at MeriSinter pointed at an increase in compressibility of bulk ferrous powder by heating to a temperature around 100°C as compared to the same powders in an unheated condition. Further experimental work at Höganäs AB showed a 30 % reduction in compressive yield strength of iron powder when heated to 150°C. A similar trend has been observed in aluminium alloys as is shown in figure 2.18. It can be seen that a decrease of yield strength with increasing temperature is quite significant. [81, 82]

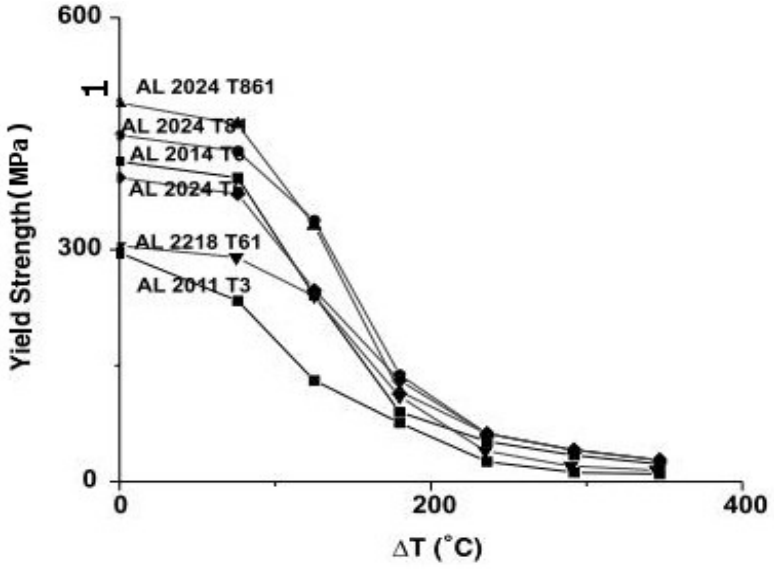

Figure 2.18: Yield strength of aluminium alloys as a function of temperature. [86]

Warm compaction technology provides a means to mass produce high density P/M compacts by a conventional single pressing operation. The tooling design and compaction process for warm compaction is essentially the same as for cold compaction process with just the addition of a heating system which is placed on the die, as is shown in figure 2.19. Temperatures of the powder and die vary from 75 to 250°C depending on the metal powder and type of lubricant. Temperature of the heated powder and tooling system should be controlled in a range ± 2.5°C. [82-85]

As compaction temperature reaches the melting point of a lubricant, it can soften and partially melt the lubricant. This gives better redistribution of the compacted mixture, which increases the green density and reduces the ejection force by 25 to 35 %. However, if the temperature of the powder mixture exceeds the lubricant melting temperature, the lubricant degrades which results in diminished powder flow and causes problems with particle rearrangement. [82-85]

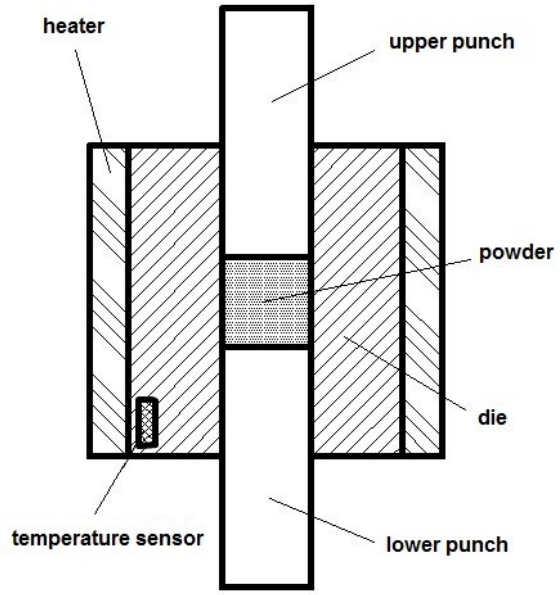

Figure 2.19: Schematic of warm compaction process.

Previous work on Fe-based materials shows that the density of warm compacted and sintered parts increases from 0.1 to 0.25 g/cm^3 over traditional cold pressed and sintered parts. This increase gives attractive improvements in tensile strength. Generally, densities of compacts prepared by warm compaction and sintering are close to those which were produced by double pressing - double sintering (DP/DS) process. However, DP/DS requires additional secondary processing and the referred costs of products increase. Another improvement was observed in the reduction of force necessary to eject the compact from the die, which reduced the risk of crack formation. In addition, the increased green density obtained by warm compaction yields higher green strength and reduces the risk of crack formation at ejection or handling. [87, 88]

In the first decade since the invention of the warm compaction process, the production of Fe-based parts was dominant. However, with increasing demand on aluminium P/M parts, the interest in warm compaction for aluminium alloys has increased.

A similar improvement of green density, ejection force, green strength and subsequent tensile strength in warm compaction of aluminium alloys was noted. Simchi *et al.* [89] and later Eksi *et al.* [90] reported improvement in green density of 7xxx series aluminium alloys up to 7 % of theoretical density, which resulted in improved mechanical properties of sintered parts. Jiang *et al.* [91] found that the green density of Al 2014 with 1.5 wt % of Acrawax increased with increasing compaction temperature up to 200ºC. However, the compaction temperature above 250ºC caused a decrease in green density due to the removal of lubricant during compaction.

2.3.3 Double Pressing - Double Sintering

Double pressing - double sintering is a compaction method where it is possible to get compacts with high density (up to 99 % of theoretical density) and good dimensional tolerance of the final compact. This method is successfully used in Fe-based P/M compaction.

Figure 2.20 shows that two stage pressing with an annealing process between each pressing cycle allows a high density to be achieved using much lower pressure. To reach similar density in single compaction would require a much higher pressure.

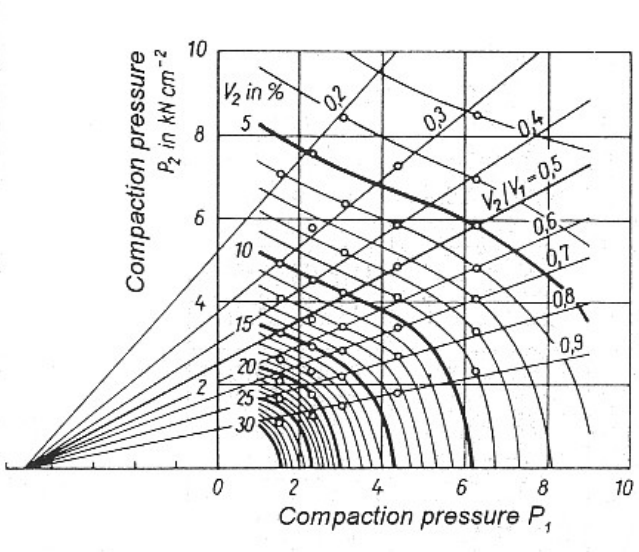

Figure 2.20: Effect of double pressing on porosity of sintered iron: P_1 V_1 - compaction pressure and resultant porosity during first compaction, P_2 V_2 - compaction pressure and resultant porosity during second compaction. [92]

During the first compaction cycle the powder undergoes cold working and the hardness of the particles increases. Annealing of the compact preform at a temperature lower then the sintering temperature can eliminate this strain hardening and leads to softer particles. This means the particles remains deformable in the second compaction stage and continue to provide enhancement in density. By sintering at a higher temperature than the first heat treatment and subsequent sizing in the die, a good dimensional tolerance of the compacted part can be obtained. [92, 93]

2.3.4 Isostatic Pressing

There are two forms of isostatic pressing: cold isostatic pressing (CIP) and hot isostatic pressing (HIP).

In general, compaction of powders is achieved by means of pressurised fluids through a flexible mould (Figure 2.21), which has to have desirable properties. At high pressure the mould has to behave like a liquid to be able to apply pressure on metal powder isostatically. However, at normal pressure the mould behaves like solid material, so after filling with powder it keeps the demanded form of the final product. Powder is filled and sealed outside of the vessel, into which the sample to be pressed is placed. Reaction between mould and metal powder must not occur during the compaction process and also during thermal treatment in HIP process. For CIP the mould is made from rubber, neoprene, urethane or other elastomeric compounds. In HIP the mould is usually made from low carbon sheet steel or stainless sheet steel. The fluids used in pressing are various oils, water and glycerine (CIP) and gasses (HIP).

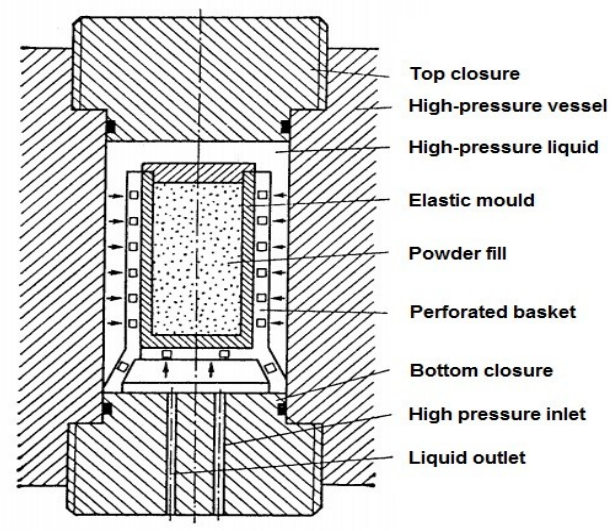

Figure 2.21: Schematic diagram of an isostatic compaction unit. [94]

The green strength of compacts formed by isostatic compaction is generally higher then those by die compaction. The mould moves with the powder as it densifies, therefore friction effects are minimized. Thus applied pressure has an almost unrestricted effect on the compact from all sides. The uniform application of pressure results in the uniform density of compacts and less pressure is required to reach the same compact density as compared to die compaction. In addition, it is possible to compact metals powder which are not possible by die compaction, i.e. mostly very course and very fine powders and also hardmetals. However, dimensional control is not as tight as with die pressing due to flexible tooling. [94-96]

2.3.4.1 Cold Isostatic Pressing

The working pressure for CIP is between 200 and 400 MPa. The dimensions of the vessel are up to 2 m in diameter and 4 m in the height. The compaction pressure needs to be maintained just for a few seconds. However, if compaction of metals with low compressibility is performed, the decompression must be carried out over a period of several minutes to eliminate crack formation caused by elastic springback. [95-97]

2.3.4.2 Hot Isostatic Pressing

Nowadays, HIP is more preferable in the isostatic pressing processes. It can be used as primary or secondary operation process and powder can be compacted up to theoretical density.

HIP process requires high purity powders, which are vibrated in place in a container, sealed and then placed inside a pressure vessel. Finally a heating device is fitted inside the pressure vessel. The dimensions of the vessel are up to 1 m diameter and 2 m length. In the process, pressure is applied by inert gas, such as high purity argon. Working temperature for HIP processes vary between 800 and 1500°C, while the maximum working pressure is usually 200 MPa. The cost of HIP processing is generally high because a long time is required to carry out a full working process, e.g. maximum 2 cycles in 24 hours. [95-98]

2.3.5 Powder Forging / Sinter Forging

The limiting factor in cold powder compaction is powder consolidation. Compaction of powder at elevated temperature allows up to 99.5 % of the theoretical density to be reached, and yields properties similar to wrought alloys produced by ingot metallurgy and hot working processes. Powder forging and sinter forging imply the same process. [101]

A typical process of sinter-forging is illustrated in figure 2.22. A measured quantity of powder is compacted to a preform with a similar shape as the final compact. Density of the preform can be up to 80 % of compacted material. Preforms are heated to the forging temperature in a furnace with controlled atmosphere and subsequently forged to final dimension. Powder forging is normally performed hot at temperatures between 1000 and 2000°C but it can also be executed at warm or cold forging temperatures. Working pressure depends on the material system, for example for steel the pressure can vary from 550 to 950 MPa. High-speed mechanical presses (screw presses) with modifications to allow automated mass production are mainly used for forging. [99-102]

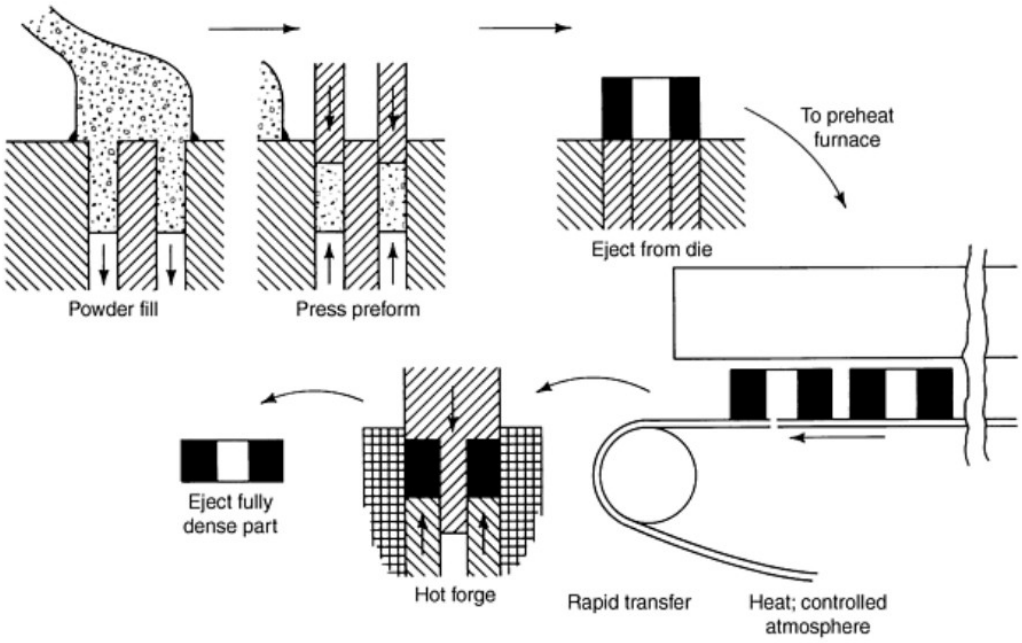

Figure 2.22: Schematic diagram of sinter-forging process. [102]

The modification of this process includes electric induction for heating without protective atmosphere. The main difference is in the method of heating and amount of the heat. The advantages of electric induction are the short heating times required simplicity of the process and high production rates. On the other hand, the difficulties in heating of samples with irregular shape, non-uniform heating in cross-section and possibility of crack formation by high speed of heating, result in the preference of the furnace method. [99-102]

2.3.6 Hot Pressing

The hot pressing process combines compaction and sintering processes in one operation. This process leads to a fully, or near fully dense (less than 1 % of porosity), final compact. Hot pressing is mostly used for materials which at room temperature exhibit low or no plasticity. The commercial application of hot pressing is for the preparation of diamond tools, beryllium components, cemented carbides or tungsten carbides. For example tungsten carbide powders are hot pressed in graphite moulds heated to 1400°C with pressures of up to 17 MPa. Hydraulic and pneumatic presses are used in hot pressing. Because of the high temperature used in hot pressing, die materials have to resist compaction temperatures. They include molybdenum, molybdenum alloy TZM (Mo-0.5Ti-0.1Zr), tungsten, superalloys, and alloy steels that are highly heat resistant. For temperatures higher than 2000ºC, graphite or ceramics are used as die material. In addition, the high temperatures used in pressing increase the ability of the pressed powder to oxidize. Therefore pressing is carried out under argon or vacuum atmosphere. [96, 97]

Heating methods for the hot pressing can be provided directly through induction or electrical resistance heating, or indirectly by heat transfer from the die, which is heated by other means. Indirect heating of the powder through heated die is the most common method for heating. An example of indirect induction heating of the powder is shown in figure 2.23.

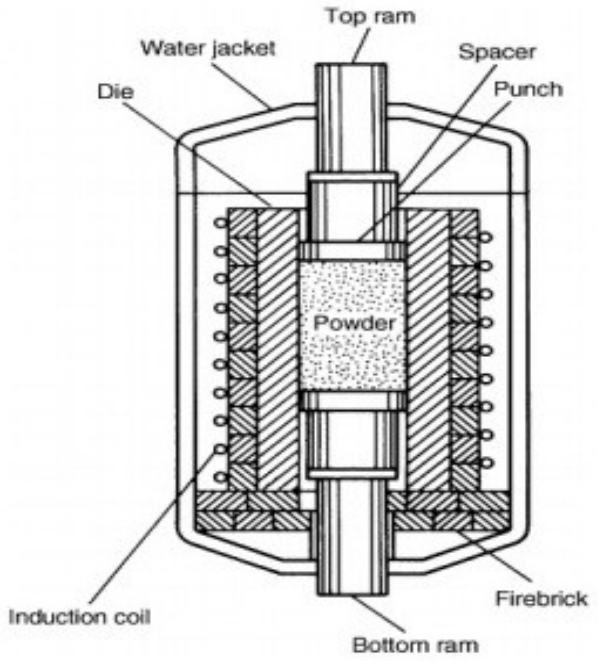

Figure 2.23: Induction-heated graphite die assembly. [102]

The main disadvantage of hot pressing is the need to prevent powder from oxidation, not only during heating and pressing but also during cooling and ejection from the die, which makes the process slow. [102-104]

2.3.7 Extrusion

As well as other compaction processes extrusion can be performed at room temperature as cold extrusion and at high temperature as hot extrusion. This process is mostly used to produce wires, rods and relatively long structure profiles from materials, which are difficult or impossible to prepare by casting or working.

2.3.7.1 Cold Extrusion

In cold extrusion, the powder mixture and lubricant agent are continuously extruded through a die which has a cross-section of the final product. This process is used to prepare P/M parts from lead, tin, aluminium alloys, copper, titanium, molybdenum, vanadium, steel and commercial ceramics. The extruding mixture normally contains 15 to 20 % of lubricating agent. For metal powders, paraffin or waxes are used as lubricants. The production speed of extrusion is quite low, generally about 5 to 10 mm/min. The part then needs to be heat treated in a furnace for de-binding and sintering to full density. [105]

2.3.7.2 Hot Extrusion

Metal powders are predominantly processed by the hot extrusion method. Hot extrusion is performed at a temperature of 50 to 75 % of melting temperature. Depending on the material system pressures vary from 35 to 700 MPa. [107]

Three main approaches to metal extrusion are shown in figure 2.24. In the first, loose material is poured to extrusion container. In this approach relatively coarse powder is used (70 to 450 μm). In the second approach, the material is firstly compacted to a preform followed by heat treatment (if it is required) and consequently extruded through a die. In the third approach, powder is firstly compacted in a can and afterwards is extruded through a die. The can may be evacuated and sealed, e.g. enabling easier handling of toxic materials (beryllium and uranium), or left open for encapsulation of spherical and other difficult-to-compact powders. [105, 108]

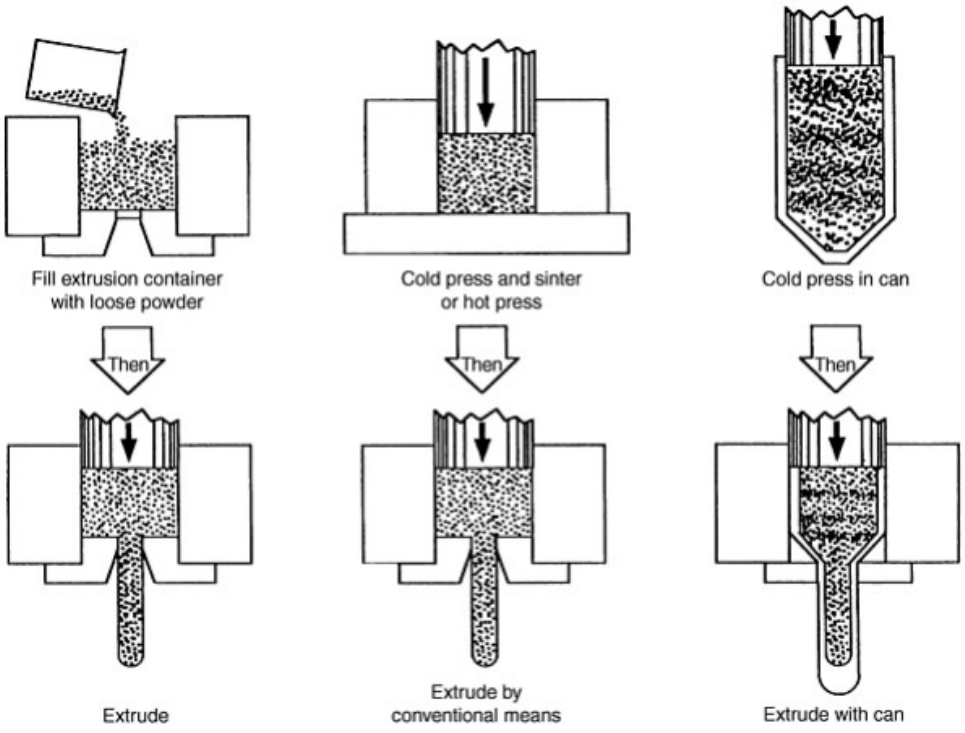

Figure 2.24: Hot extrusion techniques for metal powders. [102]

In hot extrusion, by selection of a suitable die, the powders are well dispersed during extrusion. The high deformation breaks the oxide layers of the particles and allows metallic bonding between them, which leads to a wrought structure of material without the need of additional high temperature thermal treatment. Hot extrusion is applied to materials such as aluminium, titanium and their alloys, high-speed steel, beryllium and uranium. [105, 107]

The limitation of these methods is their slow production cycle which makes them relatively expensive. In addition, high temperature and pressure in hot extrusion adversely affects tool life. Also another limitation is the shape geometry. Only simple shape with uniform cross-section through the length can be extruded. [105]

2.4 Sintering

The sintering process has a huge importance for many technical applications. It is a thermal treatment for the purpose of increasing strength by bonding together of powder particles. Sintering is the process where loose metal powder or powder compact is changed to solid metal in a temperature range of 60 to 90 % of the melting point of the main single element or multi-component system. The driving force for sintering is a reduction in the system's free energy, manifested by decreased surface curvatures and elimination of surface area. The sintering process is accompanied by shrinking.

Sintering can be generally split into four steps (Figure 2.25). The first step is point contact - reorganization of particles. In the compaction process, powder is shaped whereby the starting microstructure is formed and new contacts between particles are created. The second step is the initial-neck creation step. Initial step is characterized by the formation of necks between particles. Oxide is present on the particle surfaces and must be reduced to allow the particle to come in contact. This is achieved by the reaction between the furnace atmosphere and the Oxygen in the oxide layer. The end of this step is when the compact densification increases to about 5 %. The third step is an intermediate step - growth of the neck and grains. The change of contact between particles and the neck growth is a result of enhanced movements of metal atoms. The driving force is the reduction of interfacial energy, including both the surface and grain boundary energy. Pores within the compact have an interconnected structure. The fourth step is the final stage - growth of the grain with pore elimination at grain boundaries. The interconnected pores collapse into isolated spherical

pores which are not effective in slowing grain growth. Spherical pores have lower specific surface and therefore lower free energy. [109]

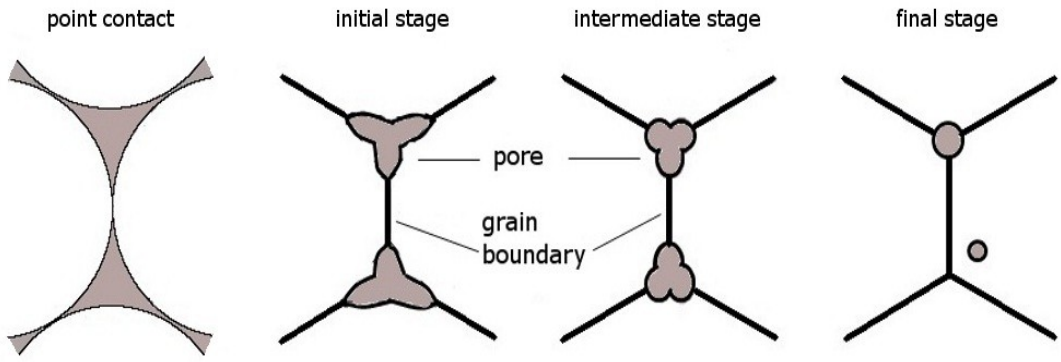

Figure 2.25: Simplify sintering process.

The sintering process can be accelerated by higher sintering temperatures due to increased mobility of atoms.

The most important parameters in the sintering process are temperature, time and protective atmosphere. These variables are specific for each material system and have to be controlled during sintering. Other factors influencing the sintering process are heating and cooling rate.

In multi-component systems the sintering temperature is driven by the component with the highest melting temperature. In some cases this temperature can be higher than the melting temperature of other components (e.g. liquid phase sintering).

There are two broad categories of sintering, namely;

- Solid state sintering.
- Liquid phase sintering.

Figure 2.26 shows these two cases in a schematic binary phase diagram. T_1 is the temperature for solid state sintering in an A-B powder compact with composition X, and T_2 is the temperature for liquid phase sintering in the same powder compact. [109-111]

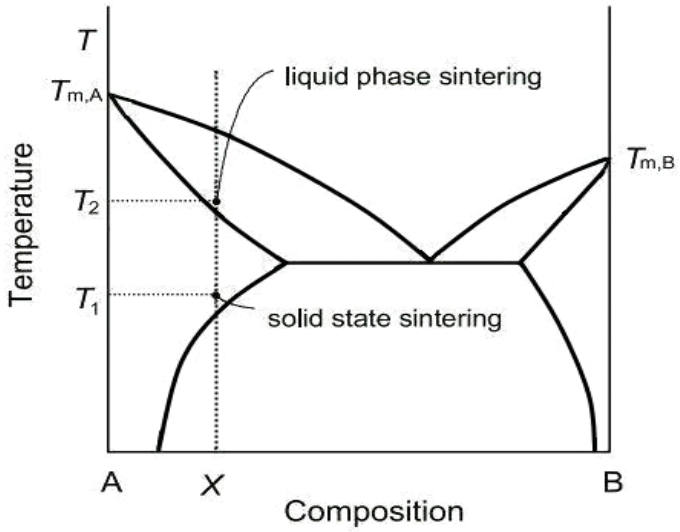

Figure 2.26: Schematic phase diagram with sintering areas. [109]

2.4.1 Solid State Sintering

In solid state sintering all densification is achieved through changes in particle shape, without particle rearrangement or the presence of liquid. The driving force of solid state sintering is the difference in free energy or chemical potential between the free surface of particles and contact points of linked particles.

Mass transfer in solid state sintering can be realized by surface diffusion, viscous flow, lattice or volume diffusion, grain boundary diffusion and evaporation and condensation, as shown figure 2.27. Lattice volume diffusion, viscous flow and grain boundary diffusion are mechanisms which contribute to densification and shrinkage.

Shrinkage occurs because material is removed from the contact area of the particles. On the other hand, in surface diffusion and vapour mechanisms, there is no shrinkage even though the neck growth occurs. These mechanisms lead to coarsening of microstructure, so reducing driving force for densification. [110, 111]

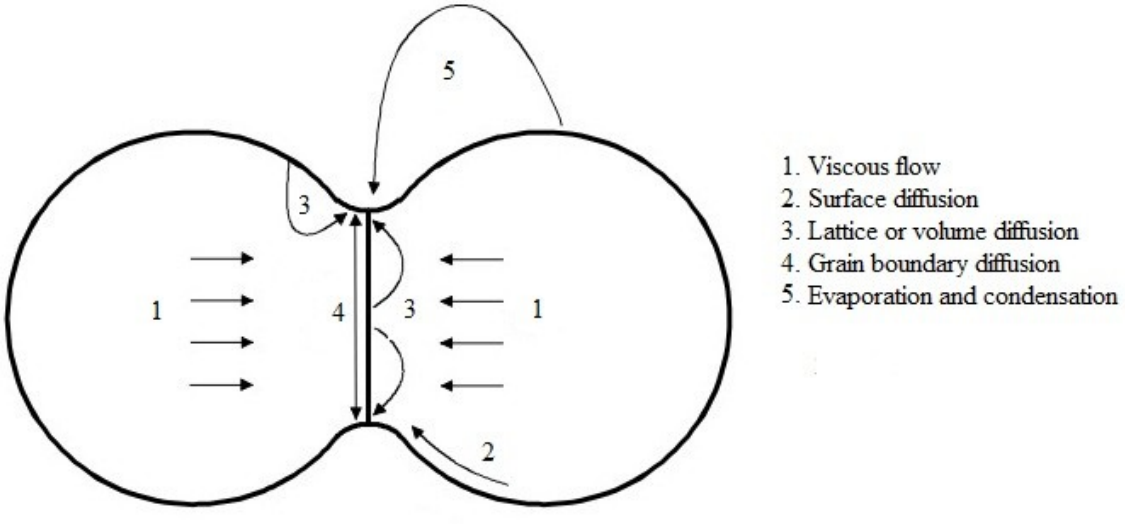

Figure 2.27: Material transport paths during sintering. [110]

2.4.2 Liquid Phase Sintering

Liquid phase sintering describes any sintering technique where a small amount of liquid is used to assist the sintering process. Liquid phase sintering is faster than solid state sintering because of fast material transport through the liquid. This is caused by the fact that surface energy at solid-liquid phase interfaces is lower than the surface energy at solid-vapour interfaces. Therefore, mass transfer is not realized through surface diffusion but through the liquid phase. The formation of a liquid film surrounding the solid phase has the benefit of a surface tension force acting to aid densification and pore elimination. Pore elimination is accompanied by high shrinkage of the compact.

Liquid phase sintering can be divided into three stages:

- Liquid flow.
- Solution–reprecipitation.
- Solid state sintering.

In the first stage, due to capillary forces liquid is responsible for motion of solid particles, and the initial densification of the compact. Capillary forces also exert an attractive bonding force on the particles, resulting in rapid shrinkage. In the second stage, material from the points of solid-solid contact is transferred to the free surfaces of the particles caused by different solubilities of the solid in the liquid. In the final stage, liquid phase sintering ends and permanent solid-solid contacts between particles are formed. [112-115]

Two forms of liquid phase sintering can occur:

1. Persistent liquid phase sintering; where a liquid phase is created by inducing melting in the powder mixture and is persistent during the high-temperature part of sintering process. Persistent liquid phase sintering is widely used in the processing of tool steels, stainless steels, and superalloys.
2. Transient liquid phase sintering; where a liquid phase is temporary and dissolves into a solid or forms a new phase/compound with increasing time. Shrinkage in transient sintering is higher than persistent sintering due to rearrangement of particles. [112, 114]

2.4.3 Effect of Sintering Parameters on Material Properties

The sintering parameters (e.g. temperature, time, protective atmosphere and heating/cooling rate) can influence the properties of the sintered parts.

2.4.3.1 Sintering Temperature

The effect of sintering temperature on mechanical properties of a sintered compact is shown in figure 2.28.

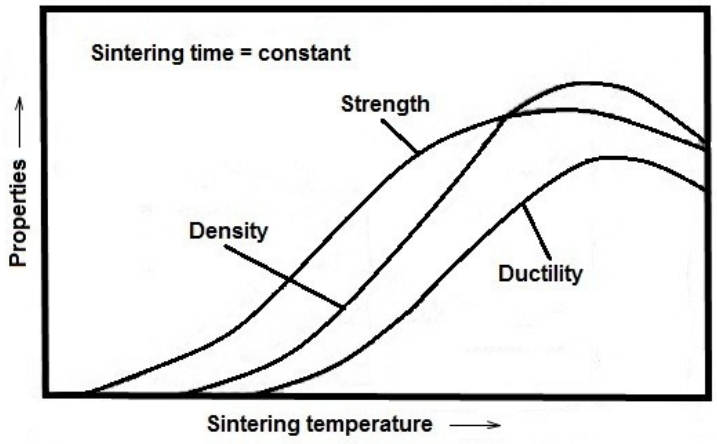

Figure 2.28: The effect of sintering temperature on mechanical properties. [116]

From figure 2.28 it can be seen that properties of the compact increase with increasing sintering temperature. However, sintering in the highest temperature levels can cause a drop in the properties because of excessive grain growth. [116]

An example of effect of sintering temperature on microstructure and subsequently on transverse rupture strength of Fe-1.25C test bars is shown in figure 2.29. In figure 2.29 (a)

sintering temperature was 1010ºC and rupture strength was measured to be 138 MPa. At a sintering temperature of 1175ºC (Figure 2.29 (b)) the rupture strength increased to 655 MPa. Strengthening at higher temperatures is caused by increased sintering, as evidenced by the elimination of grain boundaries and spheroidization of pores. [117]

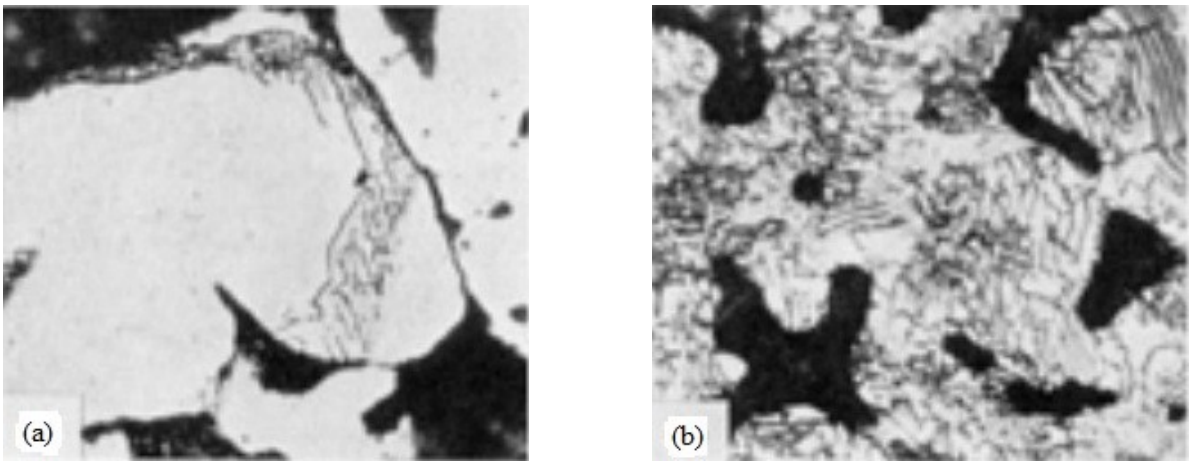

Figure 2.29: Effect of sintering temperature on microstructure of Fe-1.25C. Magnification of the figures is 800 X. [117]

In general, the sintering temperature of single component system should be about 80 % of melting temperature of the component. In multi-component systems, if liquid phase sintering is involved, the sintering temperature depends on the melting temperature and composition of the liquid phase. [116, 118]

2.4.3.2 Sintering Time

At the start of sintering process, if the temperature is constant, physical and mechanical properties increase rapidly. This rate of change of properties with time decreases and reaches a maximum value as illustrated in figure 2.30.

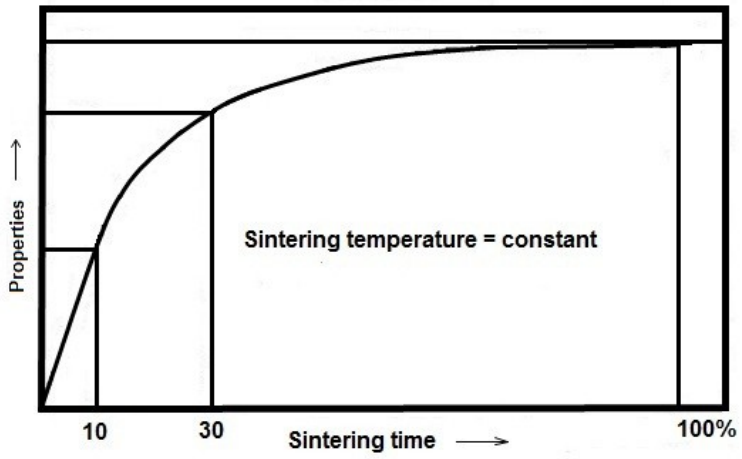

Figure 2.30: The effect of sintering time on mechanical properties. [116]

Sintering time depends on particle size and shape of powdered compact. Fine powders sinter more quickly but if the sintering time is too short, creation of contacts between particles is not sufficient, leading to an open porous structure with sharp-edges. However, if sintering time is too long, the fine powders become coarse-grained with reduced mechanical properties. This happens mainly in liquid phase sintering process. [116]

The effect of the sintering time on the microstructure of Fe-1.25 C is shown in figure 2.31. The sintering temperature of prepared specimens was 1120ºC. A sintering time of 5 minutes is represented in figure 2.31 (a) where numerous grain boundaries are visible, and the porosity is quite angular. The strength of the specimens is ~ 421 MPa. Figure 2.31 (b) shows the microstructure of a specimen sintered for 30 minutes, with some disappearance of grain boundaries and slight spheroidization of pores. The strength of specimen sintered for 30 minute was ~ 552 MPa. [117]

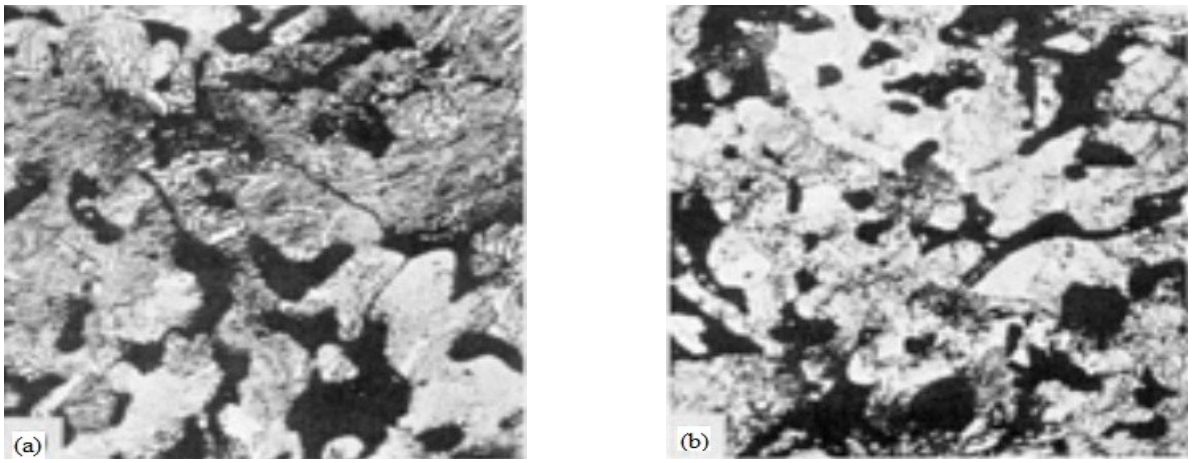

Figure 2.31: Effect of sintering time on microstructure of Fe-1.25C. Magnification of the figures is 800 X. [117]

2.4.3.3 Sintering Atmospheres

Sintering atmospheres are essential for almost all sintering processes. This is due to the fact that a majority of metals react with air and subsequently oxide layers are created on the surface. A suitable atmosphere is required to protect powder compacts against oxidation. In addition, sintering atmospheres have been used to prevent or to control chemical reactions and to remove lubricant from the sintering zone. It also protects the surface of sintered parts and furnaces from degradation. [118]

The protective atmospheres commonly used in sintering of metal powders are endothermic and exothermic atmospheres, nitrogen, dissociated ammonia, hydrogen, argon, and vacuum. [119]

A protective atmosphere must have a low dew point in order to eliminate the reaction of compacted material with water moisture contained in sintering atmosphere. A dew point is the temperature at which condensation of water vapour occurs at a given pressure. Water

vapours at this temperature condense in the form as dew, cloud droplets, ice crystals, mist or fog. In general, dew points of protective atmospheres for sintering are in the range of – 50 to 20ºC. Typically, for sintering of aluminium alloys protective atmospheres with dew point of – 50 to – 40ºC are used. [120]

2.4.3.3.1 Endothermic Atmospheres

Endothermic atmospheres are produced by catalytic combustion of air and hydrocarbon gas. The nickel catalyst chamber is heated externally to produce the carbon and nitrogen rich gas.

Endothermic atmosphere typically contains 40 % nitrogen, 40 % hydrogen, and 20 % carbon monoxide, carbon dioxide, or methane with small amounts of water. Usually 60 % of the gaseous constituents are combustibles, which are oxide reducing agents. Carbon monoxide and methane are carburizing agents, while carbon dioxide and water decarburizing agents, which also act as oxidizers, and de-lubricants.

The mechanical system used to produce an endothermic atmosphere is significantly more expensive than the exothermic design and the nitrogen atmosphere. [121, 122]

2.4.3.3.2 Exothermic Atmospheres

Exothermic atmospheres are produced by the partial combustion of natural gas or propane to produce heat and an atmosphere rich in nitrogen, carbon monoxide, carbon

dioxide, and hydrogen. They typically contain 67 to 87 % of nitrogen. Oxide reduction of the exothermic atmospheres is significantly lower than in endothermic atmospheres or nitrogen based atmospheres. Exothermic atmospheres are used for decarburizing of steel at temperature above 700°C. Also because of water and carbon dioxide content, an exothermic atmosphere is an effective de-lubricating agent.

Exothermic atmospheres are normally used for sintering of bronze and some other copper base parts. [119, 121]

2.4.3.3.3 Dissociated Ammonia

Dissociated ammonia is obtained by catalytic reaction of gaseous NH_3. It is used in the sintering of brass, bronze, and ferrous alloys, as well for aluminium alloys.

Dissociated ammonia contains high concentrations of flammable hydrogen of 75 vol. % and 25 vol. % of nitrogen. So care must be taken in handling.

Dissociated ammonia is commonly used as the sintering atmosphere for reason of low cost, high purity, consistency and dryness. Because of its dryness, it does not provide optimum burning off of the lubricant during de-waxing. [119, 123]

2.4.3.3.4 Vacuum

Vacuum is the principal alternative to dissociated ammonia or nitrogen atmosphere. Because of its low oxidation potential, vacuum is used for sintering of stainless steels,

carbides, magnetic alloys and metals such as titanium, zirconium, uranium, tantalum, and other refractory metals and compounds that react with hydrogen, nitrogen, and carbon-monoxide atmospheres.

Most P/M green compacts contain a lubricant or binder, must be removed before sintering in vacuum, in order to keep the vacuum pump free from contamination. Burn-off of lubricant is mostly occurs in the controlled atmosphere.

Conventional vacuum sintering offers low operating costs. Vacuum sintering is mostly performed in batch type furnaces. [124, 125]

2.4.3.3.5 Nitrogen

Nitrogen is produced from air by cryogenic and non-cryogenic methods. In cryogenic methods, air is rapidly depressurized to an ultra-cold liquid and distilled to separate out the high-purity molecular nitrogen. In non-cryogenic production, a stream of compressed air is passed through an absorbent, where water vapour, oxygen and carbon dioxide are preferentially retained.

Nitrogen is widely used as an atmosphere for its availability, moderate cost, high purity and ease of handling. [119, 123]

2.4.3.3.6 Hydrogen

Hydrogen is produced by extraction from natural gases or hydrocarbon fossil fuels via a chemical path. Hydrogen is widely used for its high reducing ability. However, dry hydrogen is highly explosive and is a relatively expensive gas, so care must be taken during handling. Minimum ignition temperature is 574ºC. Commercial hydrogen has a purity of 99.995 %. Because of its low dew point (- 40ºC) hydrogen is non-decarburizing and also is not effective as de-lubricating agent.

Hydrogen atmosphere is used for sintering of stainless steels and magnetic alloys. [118, 127]

2.4.3.3.7 Argon

Argon is produced as by-product of oxygen and nitrogen production. Atmospheric air is compressed and cooled. Initially, the liquid nitrogen is separated by distillation of the cooled air. The residual liquid, containing approximately 10 % of argon, is subsequently refined in a separate distillation column to produce argon with 98 % purity. [126]

An argon atmosphere is used for sintering of aluminium, steel, titanium and their alloys. However, production of argon is quite expensive so it is mostly used for heat treatment rather than sintering atmosphere. [119]

2.4.3.4 Heating and Cooling Rate

Particle size, purity of the powder, and compact size, shape and density all play a role in the choice of heating rate.

Fine powders (< 45 μm) have higher specific surface area and higher volume of impurities (e.g. oxides). The oxygen content of fine powders atomized in air can approach 1 % wt. To eliminate these impurities, the heating rate for fine powders and compacts with high green density (95 % of theoretical density) have to be slow (< 15ºC/min).

Depending on the material system, high heating rates during sintering of large compacts (> 305 mm diameter) can cause crack formation due to thermal shock. [128, 129]

A controlled cooling rate is important for materials that contain carbon, such as ferrous alloys, where an increase in mechanical properties is required. The cooling rate affects the phase transformation in Fe-based alloys, so changes the mechanical properties, predominantly hardness and strength. Table 2.1 show three cooling rates and their effect on the mechanical properties of Fe-1.25C. The specimens were sintered at 1120 ºC for 30 minutes. The higher the cooling rate the finer pearlite spacing was observed (Table 2.1). [128, 130]

Table: 2.1 Effect of cooling rate on Fe-1.25C alloy [117]

Sample No.	Cooling rate [ºC/min]	Transverse rupture strength [MPa]	Hardness [HRB]	Pearlite spacing
1	1.9	462	37	Very coarse
2	64	565	50	Medium
3	125	600	57	Very fine

An example of the effect of cooling rate on the microstructure and mechanical properties of Ancorsteel 4300, Cr-Si-Ni-Mo P/M steel with 0.6 wt % C is shown in figure 2.32. Ancorsteel 4300 was sintered at temperature 1120ºC and then cooled at the rates of 0.7ºC/s (Figure 2.32 (a)) and 2.2ºC/s (Figure 2.32 (b)), respectively. At a cooling rate of 0.7ºC/s the tensile strength was measured to be 1062 MPa and hardness 66 HRA. At a higher cooling rate of 2.2ºC/s, the tensile strength increased to 1241 MPa and hardness to 71 HRA. With a higher cooling rate the microstructure of Ancorsteel 4300 is almost entirely martensitic. [131]

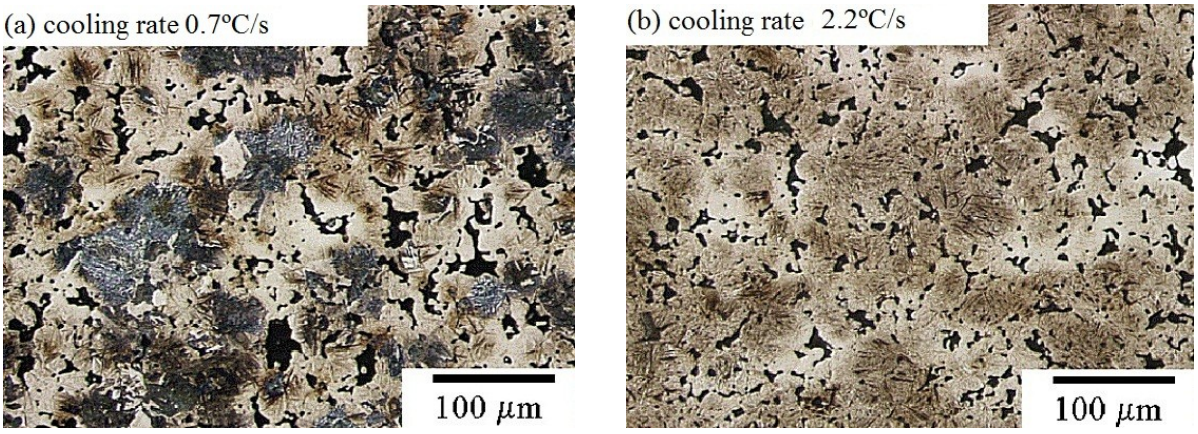

Figure 2.32: Effect of the cooling rate on the microstructure of Ancorsteel 4300-0.6 wt % C; (a) cooling rate of 0.7 ºC/s and (b) cooling rate of 2.2ºC/s. [131]

2.4.4 Sintering of Aluminium and Aluminium Powder Alloys

Choice of sintering temperature and sintering time is based on composition of the alloy and its sintering mechanism. Sintering time depends on part section thickness. The recommended minimum time for parts 6.4 mm thick is between 10 to 15 minutes, whereas parts of 20 to 50 mm thick require 30 to 40 minutes. Liquid phase sintering is mostly used for sintering of aluminium alloys. During sintering, alloying elements form a liquid phase which helps rupture the oxide layers and allows bonding between aluminium particles. Generally, sintering temperatures are in the range 595 to 625°C and sintering time varies from 10 to 30 minutes. [132, 133]

Sintering of aluminium P/M parts can be carried out in a controlled inert atmosphere or in vacuum. The most common inert atmospheres for sintering of aluminium alloys are nitrogen or dissociated ammonia. Nitrogen is the preferred atmosphere because its use results in high mechanical properties and it is also more economical than other atmospheres. The recommended dew point for a nitrogen atmosphere is - 40°C or lower. [132, 133]

The types of sintering furnaces used for manufacture of P/M aluminium parts include: batch, continuous or vacuum furnaces. Sintering requires these furnaces to maintain the temperature to within ± 2.8°C. [132] Heating cycles for batch, continuous and vacuum furnaces are shown in a figure 2.33.

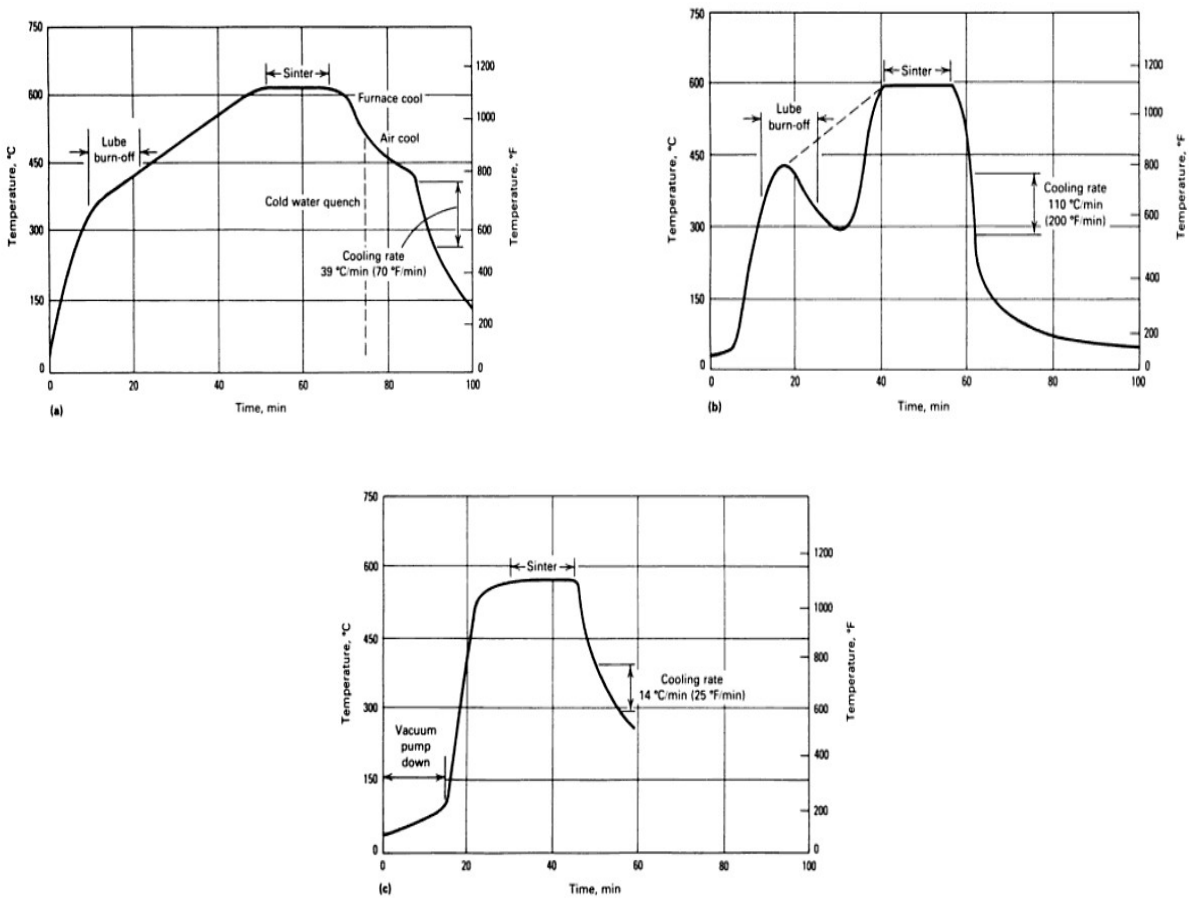

Figure 2.33: Typical heating cycles for aluminium P/M parts sintered in: (a) a batch furnace (b) a continuous furnace (c) a vacuum furnace. [132]

2.4.4.1. Sintering and Heat Treatment of Aluminium Alloys 2xxx Series

Early work by Martín *et al.* [134] and later work by Min *et al.* [135] showed that the best density and hardness of 2xxx series alloy are given by liquid phase sintering in a temperature range of 590 to 620ºC in nitrogen atmosphere during 30 minutes. Sintering at temperature below 590ºC results in a decrease of density (~ 90 % of theoretical density) as produced by swelling of the specimens. Sintering at temperature above 620°C increased the density (~ 97 % of theoretical density) since a larger amount of liquid was produced,

however this also led to larger amounts of shrinkage by typical liquid phase sintering mechanisms.

The main alloying element in aluminium alloys 2xxx series is copper. It is added to these alloys principally to improve the wetting behaviour of the liquid phase of aluminium and also because it contributes to precipitation hardening.

Figure 2.34 illustrates solution treatment and quenching of an aluminium alloy containg 4 % Cu. Point 2 in figure 2.34 represent temperature when Cu goes into solid solution in the alumium matrix. Fast quenching, cooling to point 1, is necessary to freeze into supersaturated Cu-rich solid solution.

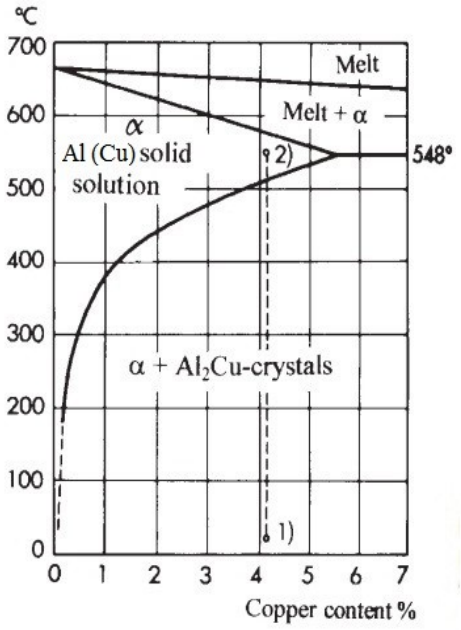

Figure 2.34: Solution treatment and quenching before aging of an aluminium alloy containing 4 % Cu. [136]

By quenching and then reheating to the aging temperature in an Al-4Cu alloy, a fine dispersion of Al_2Cu precipitates forms within the α grain. These precipitates are effective in hindering dislocation motion and, consequently, increasing alloy hardness and strength. The main precipitation sequence for 2xxx alloys is: [66]

$$SSSS\alpha \rightarrow \text{GP zone} \rightarrow \theta'' \rightarrow \theta' \rightarrow \theta\ (Al_2Cu) \qquad \text{(eq.2. 8)}$$

where *SSSSα* is the supersaturated α solid solution, *GP* zone (Guinier-Preston zone) is the mono atomic layers of Cu on $(001)_{Al}$, *θ''* is the coherent precipitate phase, *θ'* is the semi-coherent precipitate phase and *θ* is the equilibrium phase within the α matrix.

GP zones are formed at low temperature around 130ºC. θ'' coherent phase is created at temperature around 130ºC over a long time, or at temperature below 180ºC for a shorter time. The equilibrium phase θ is formed at temperature above 190ºC. The presence of single phases depends on aging temperature and time as can be seen in figure 2.35. Figure 2.35 shows the relationship of hardness versus aging time for various Al-Cu alloys. It can be seen, that alloys with higher content of Cu reached highest hardness. This is caused by creation of higher amount of precipitates.

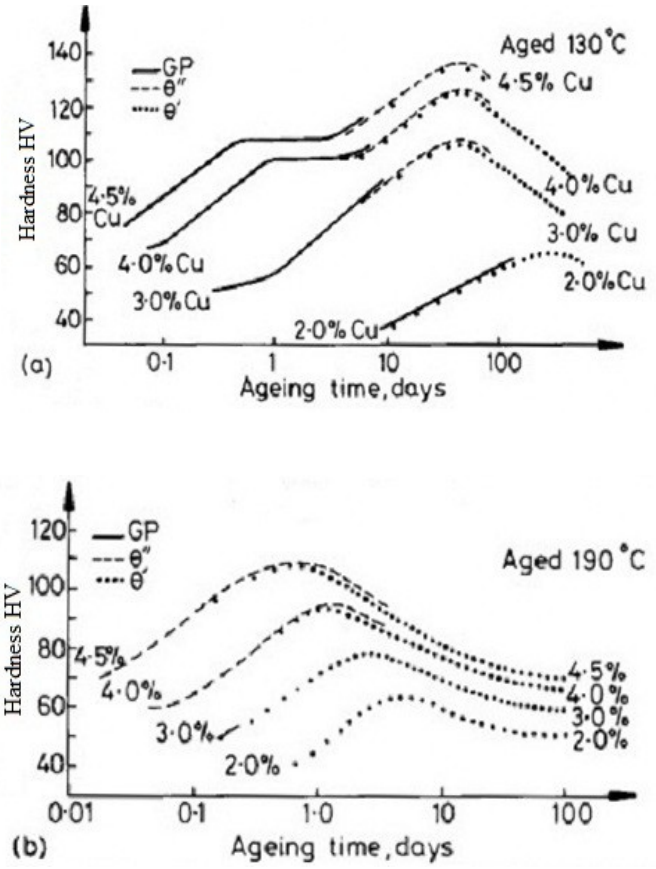

Figure 2.35: Hardness versus aging time for various Al-Cu alloys; (a) aging temperature 130ºC, (b) aging temperature 190ºC. [137]

Raviprasad *et al.* [138] and Song *et al.* [139] suggested a temperature of 200ºC as the best aging temperature for Al 2xxx series. At this temperature, the peak hardness and abrasive resistance was found within the microstructure of rod-shaped GP zones along $<100>_{\alpha}$ together with X' ($CuMgAl_2$) and Ω (orthorhombic Al_2Cu phase) precipitation. Both X' and Ω are plates on the {111}α planes. In recent work, Falticeanu [140] found that aging at 200ºC for 5 hours gives the best mechanical properties for aluminium alloy Al-4.4Cu-0.8Si-0.5Mg. In addition, longer aging times led to a decrease in mechanical properties due to a coarsening of the Al_2Cu precipitates.

2.5 Taguchi Design

Taguchi design - also known as the Taguchi method was developed by Japanese engineer Dr. Genichi Taguchi. It is a statistical method based on products or processes and it is used to improve industrial productivity by reducing the variation in a process through robust design of experiments. The main aim of the design is to find factor settings that minimize response variation. Design with fewer variables is more robust. Taguchi design is based on testing pairs of combinations of parameters rather than testing all possible combinations. This gives the necessary data to define which factor most affects product quality with minimum experimentation. To organize the parameters affecting the process and the levels at which they should be varied an orthogonal array is used. Use of an orthogonal array allows the analysis of many factors with least number of runs. [141-144]

For example if we have 3 parameters and each of them has 2 levels, an L4 (2^3) array is the proper array to use. The model for an orthogonal array is L_{Runs} ($Levels^{Factors}$). A sample of an L4 orthogonal array is shown in table 2.2. L4 means the array requires four experimental runs. It is the number of rows in the array and describes the number of test cases that will be generated. The values inside the array (1, 2, 3 and 4) represent levels and should be replaced with the actual level values to be varied, and P1, P2 and P3 should be replaced with the actual parameters. [141-144]

Table 2.2: L4 orthogonal array [142]

Experiment	**P1**	**P2**	**P3**
1	1	1	1
2	1	2	2
3	2	1	2
4	2	2	1

When the experiments include numerous runs, and results are measured in quantitative terms, Taguchi recommends signal-to-noise ratio analysis. The signal-to-noise ratio is a log function of desired output characteristics. Signal is the change in the quality characteristic of the product in response to the factor introduced in experimental design. Signal factors can be controlled and their level can be fixed. The external factors are called noise factors and they are difficult or very expensive to control. [145]

Taguchi effectively applied this concept to establish optimum conditions for experiments and also to identify which parameter has the most effect on the experiments. [136]

Depending on the quality characteristic, parameter design can be classified and evaluated into three types:

1. Smaller is better, when the aim is to minimize the response.

$$S/N = -10\,log\left[\frac{1}{n}\sum_{i=1}^{n} y_i^2\right] \quad \text{(eq. 2.9)}$$

2. Larger is better, when the aim is to maximize the response.

$$S/N = -10\,log\left[\frac{1}{n}\sum_{i=1}^{n}\frac{1}{y_i^2}\right] \quad \text{(eq. 2.10)}$$

3. Nominal is better, when the aim is to target the response and it is required to base the S/N ratio on standard deviations only. [147]

$$S/N = 10\,log\frac{\bar{y}_i^2}{s_i^2} \quad \text{(eq. 2.11)}$$

where *S/N* is the signal-to-noise ratio; y_i is the mean value and s_i is the variance, $\bar{y}_i$ is the value of the performance characteristic for a given experiment.

$$\bar{y}_i = \frac{1}{n}\sum_{i=1}^{n} y_i \quad \text{(eq. 2.12)}$$

$$s_i^2 = \frac{1}{n-1}\sum_{i=1}^{n}(\bar{y}_i - y_i) \quad \text{(eq. 2.13)}$$

where i is the experiment number, u is the trial number, n is the number of trials for the experiment. [141]

Even if each type is determined by a different formula to calculate the appropriate S/N ratio, the interpretation of the results is always the same, the higher the S/N ratio, the better. [148]

An advantage of the Taguchi method for experimental design is that it is straightforward and easy to apply to many engineering situations, and can be used to identify problems in a manufacturing process from data already in existence. Also the Taguchi method allows testing of numerous different parameters at once.

The limitation of Taguchi method is that it is offline, and therefore inappropriate for a dynamically changing process. It also requires specialized statistics knowledge to understand the results. Another disadvantage of the Taguchi method is that by using orthogonal arrays, it assumes the noise factors are independent, which may be helpful in setting up the experiment, but is not necessarily a good assumption. In addition, Taguchi ignores the interactions between controllable and noise variables. [141-150]

Taguchi design is mostly used in the industrial environment, but it can also be used for scientific research. Taguchi design has been successfully applied to P/M. For example, Hong *et al.*[151] used the Taguchi method to determined the effect of processing parameters, i.e. vacuum hot pressing temperature, pressure, extrusion temperature, pressure and extrusion ratio on mechanical properties of $SiC/_w$ 2124Al. It was found that the vacuum hot pressing parameter is the most sensitive parameter to the tensile strength.

Selcuk *et al.* [152] applied the Taguchi method to optimize the conventional sintering process of porous tungsten. The study showed that tungsten can be reactively sintered at temperatures (< 1200ºC) which are much lower than those (> 2000°C) employed in conventional sintering.

Another successful application of Taguchi method was for the injection molding process. Jamaludin *et al.* [153] used it to optimize the sintering process of specimens made

from water atomized 316L stainless steel powder by injection molding, for its best sintered density. They found, that all sintering process parameters (e.g. temperature, time, heating/cooling rate) influence significantly the sintered density. The optimal sintering condition was found to be: sintering temperature of 1360°C, heating rate of 6°C/min, sintering time of 240 min and cooling rate of 8 °C/min, with possibility to achieve a sintered density of 98.52 % of theoretical density.

CHAPTER 3

EXPERIMENTAL METHODS

3.1 Starting Material

3.1.1 Powder Premix

The material used in this project was the Al commercial premix alloy ECKA Alumix 123 (without lubricant). Lubricant was introduced subsequently during powder blending. The composition of this alloy is comparable with the wrought aluminium alloy Al 2014A. The starting premix used for the manufacture of green/sintered aluminium parts in this study was supplied by ECKA Granulate Metal Powders Ltd. The premix was analyzed at ECKA Granulate Velden GmbH Quality Control laboratory with the following size analysis data:

Table 3.1: Analysis of ECKA Alumix 123

Screen analysis ISO 4497 residue		wt %
> 200 Micrometer	1.3	%
> 160 Micrometer	4.8	%
> 100 Micrometer	29.1	%
> 63 Micrometer	36.0	%
> 45 Micrometer	13.9	%
< 45 Micrometer	14.9	%
Apparent density ISO 3923/1	1.04	g/cm^3
Chemical analysis:		wt %
Copper (Cu)	4.5	%
Magnesium (Mg)	0.5	%
Silicon (Si)	0.6	%

3.1.2 Lubricants

The role of lubricants was to improve compaction and mechanical properties of green specimens. In this study, two types of conventional synthetic amide powdered waxes were used. They were Acrawax C supplied by Lonza Inc. and Kenolube P11 supplied by Hoganas GB. Tables 3.2, 3.3 and 3.4 list the physical properties and composition of these two waxes.

Table 3.2: Characteristic of lubricants [154, 155]

Lubricant type	**Density [g/cm³]**	**Melting point [°C]**	**Boiling point [°C]**
Acrawax C	0.97	140 to 145	285
Kenolube P11	1.006	~100 to 145	250 to 450

Table 3.3: Composition of added lubricant Acrawax C [154]

Acrawax C		
Substance	Ethylenebisstearamide	Stearic acid
wt % content	98	2
CAS Number	110-30-5	57-11-4

Table 3.4: Composition of added lubricant Kenolube P11 [155]

Kenolube P11		
Substance	Ethylenebisstearamide	Zn-Stearate
wt % content	75	25
CAS Number	110-30-5	557-05-01

3.2 Mixing Lubricant into Alumix 123

Blending of lubricants with powder premix was performed inside a blending container using a Turbula T2F Shaker Mixer (Figure 3.1) operated at a speed of 45 rpm for 20 minutes. Lubricant in the amounts of 0.5, 1.0 and 1.5 wt % was added into the powder premix. The blending container during the blending operation was filled to between 45 to 50 % to ensure homogeneity of final blend.

Figure 3.1: Turbula T2F shaker mixer.

3.3 Power Compaction

Cold and warm compaction of powder blends were performed in this study. Cold compaction was performed at room temperature (RT) while warm compaction was performed at 60, 80 and 110°C.

In both types of compaction, the mixed powder with a given amount of lubricant was pressed using a standardized die set to produce a standard tensile test specimen shape (MPIF Standard No. 10) [156], as shown in figure 3.2. All compactions were carried out using a Denison uniaxial hydraulic operated press. Arrangement of the die set is displayed at figure 3.3. The die was supported by two rectangular blocks of soft foam to allow movement of the die during compaction, and also to make die behave as a floating die as this provides pressing in both directions. [141] The cleaned surfaces of die wall and tools (upper and lower

punch) were sprayed with a lubricant-saturated solution of Acrawax C in acetone (10 g of Acrawax C and 100 ml of acetone), prior to each compaction event.

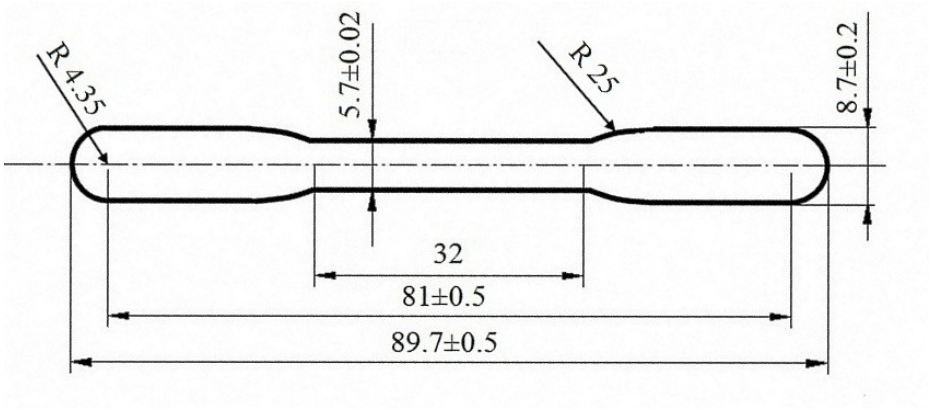

Figure 3.2: Standard tensile specimen. [157]

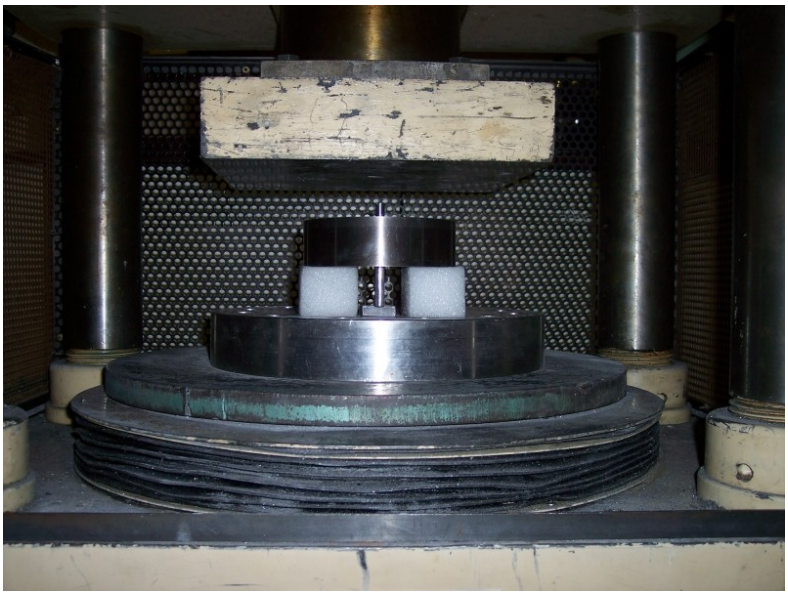

Figure 3.3: Arrangement of die set for cold compaction.

3.3.1 Cold Compaction Cycle

8 g of premixed powder with lubricant was weighed on a digital scale. The die wall and tools were lubricated, followed by filling of the powder into the cavity. Once the punches were placed into the powder filled die, the press was switched on and the punches were forced into the die to compress the powder. Compaction pressure varied between 200 to 400 MPa, at 50 MPa intervals and typically held for a period 30 seconds. After releasing the compaction pressure, compacts were ejected from the die. Prior to the ejection process, the die was turned over and a rectangular steel stands replaced the foam supports, so as to force the compact from the die when the press was switched on.

3.3.2 Warm Compaction Cycle

Warm compaction of the specimens was performed under the same conditions as cold compaction with modification of die equipment to accommodate pressing at elevated temperature, as illustrated in figure 2.19 (Section 2.3.2). Because of the heat during compaction the foam blocks were replaced by support made of steel springs. The correct mass of powder was filled into the heated die and held to pressing position for 2 minutes to ensure the powder had reached the required temperature. Throughout the process, heating was monitored and controlled via a feedback loop from a thermocouple situated on the die.

3.4 Sintering and Heat Treatment

Sintering of both cold and warm compacted specimens was carried out in a Thermal Elite^{TM} tube furnace model TSH12/38/500.

Sintering at 600°C for a time of 30 minutes was followed by solution treatment at 550°C for 120 minutes and subsequently quenched to room temperature in a solution of water and ethanol. The quenched specimens were stored in freezer prior to aging. Ageing of quenched specimens was performed in a Thermal Elite^{TM} box air furnace, followed by air cooling to room temperature. Aging was carried out at 200ºC for a period of 5 hours. Sintering temperature, solution treatment temperature and aging temperature were selected based on previous reports (Section 2.4.4.1).

The heating rate of the sintering cycle was set to 10°C/min. Oxygen-free nitrogen with a dew point of - 45°C, was used as a protective atmosphere during sintering and solution treatment. The furnace was flushed before the sintering cycle with a flow of 5 l/min of nitrogen gas for 10 minutes to eliminate all influences of surrounding air. The flow of nitrogen gas was adjusted to a value of 2 l/min for the duration of complete sintering. The sintering and the ageing cycle is shown in figure 3.4.

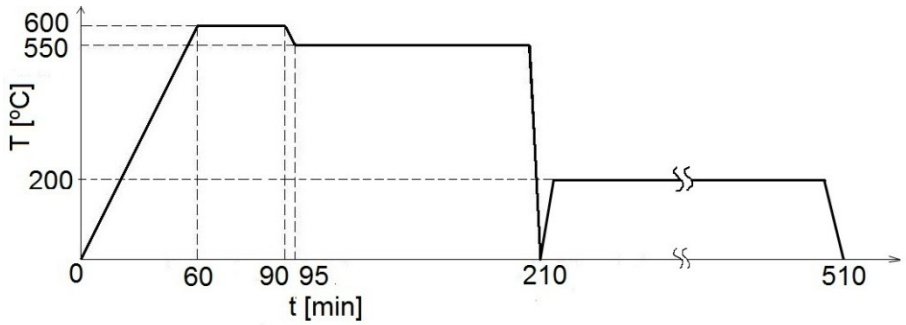

Figure 3.4: The sintering and the ageing cycle.

3.5 Material Characterization

3.5.1 Thermo Analysis of Used Lubricants

A NETZSCH STA 449 C Jupiter^{TM} (simultaneous thermal analyzer STA), was used to determine the melting/boiling points of waxes and to study the de-binding behaviour. STA was performed under nitrogen atmosphere with a heating/cooling rate of 10ºC/min.

3.5.2 Density Measurement

The densities of green/sintered compacts were measured by an immersion technique based on Archimedes principle, i.e. by weighing the specimen in air and subsequently in liquid with a known density. This method is standardized as per Metal Powder Industries Standard No. 42, "Determination of Sintered Density of Compacted or Sintered Metal Powder Products". [156] Ethanol with density of 0.789 g/cm^3 was used as a liquid rather than distillate water which is used in Standard No.42 (to minimize reaction of water with Al and Al-50Mg powders). The mass was measured using a scale with an accuracy of 0.001 g. This method can be applied for parts of any geometry. The density of specimen is calculated from a following equation:

$$\rho = \frac{m}{V} = \frac{m_a}{m_a - m_l} \times \rho_l \qquad \text{(eq. 3.1)}$$

where m is the mass, V is the volume of the dry specimen in air, ρ_l is the density of the known liquid at its measuring temperature, and m_a and m_l are the masses weighed in air and liquid, respectively.

3.5.3 Tensile Testing

A computer controlled Zwick Roell universal tensile test machine was used to measure the maximum breaking force and extension of tensile test specimens. The preparation of test sample was described in "Powder Compaction" (Section 3.3). The extension of tensile specimens was monitored through an extensometer with 20 mm gauge length. The cross head speed of the tensile machine screw was set to a value of 0.6 mm/min.

The ultimate tensile strength was calculated by:

$$\sigma = \frac{F}{S_0} \qquad \text{(eq. 3.2)}$$

where F is the maximum breaking force and S_0 is the original cross-sectional area through which the force is applied.

The elongation is defined as:

$$e = \frac{\Delta l}{l_0} \times 100 \qquad \text{(eq. 3.3)}$$

where Δl is the amount by which the length of the object changes, and l_0 is the original length.

Young's modulus is given by the following equation:

$$E = \frac{tensile\ \ stress}{tensile\ \ strain} = \frac{\sigma}{\varepsilon} = \frac{F_e/S_0}{\Delta l_e/l_0} = \frac{Fl_0}{S_0 \Delta l_e} \qquad \text{(eq. 3.4)}$$

where F_e is the elastic force applied to the object, S_0 is the original cross-sectional area through which the force is applied, Δl_e is the amount by which the length of the object changes under the application of elastic force, and l_0 is the original length of the object.

3.5.4 Hardness Testing

A Vickers micro hardness machine was used to determine the HV values. An Indentec hardness machine of model type 5030SKV was used with a load of 10 kg and time period of 10 seconds. The surfaces of the specimens were finished by grinding and polishing to remove all errors. An average of 5 hardness measurements was recorded for each specimen.

3.5.5 Microstructure

The microstructures of as-supplied powder, green/sintered specimens were examined by scanning electron microscopy, using either a Joel 6060 or Philips XL30 operated at 20 kV. A combination of secondary electron imaging (SEI) and backscattered electron imaging (BSI) was used to examine loose powder morphology and the resultant microstructures. The chemical composition of the starting material and the studied specimens was evaluated by energy dispersive microanalysis (EDX).

The samples for powder morphology study were prepared by spreading the powder onto a conductive adhesive carbon disc stuck on top of an aluminium stub. The microstructure of specimens was interpreted by mounting the samples in the conductive bakelite. This was followed by mechanical grinding and final polishing on a semi-automatic polishing system, using abrasive grinding paper up to 1200 μm and diamond paste up to 1μm. In addition, compacted specimens were etched in HNO_3 + H_2O solution to reveal the grain structure of the green compact.

CHAPTER 4

RESULTS

This chapter presents results on the study of thermal stability of various admixed lubricants and effect of processing conditions (e.g. compaction temperature, compaction pressure, admixed amount of lubricant and lubricant type) on the microstructure, density, mechanical properties of specimens before and after sintering at optimum conditions, as specified in the sections 3.3, 3.4 and 3.5.

4.1 Analysis of Used Materials

4.1.1 Particle Size Analysis

A Joel 6060 SEM and INCA software were used to characterise the particle size of the starting material (Alumix 123) and lubricants (Acrawax C and Kenolube P11). From figure 4.1 and screen analysis of Alumix 123 (Section 3.1), it can be seen that aluminium powder size varied within the range from 200 μm to 45 μm. In table 4.1, the average particle sizes of powders in the Alumix 123 mixture are presented.

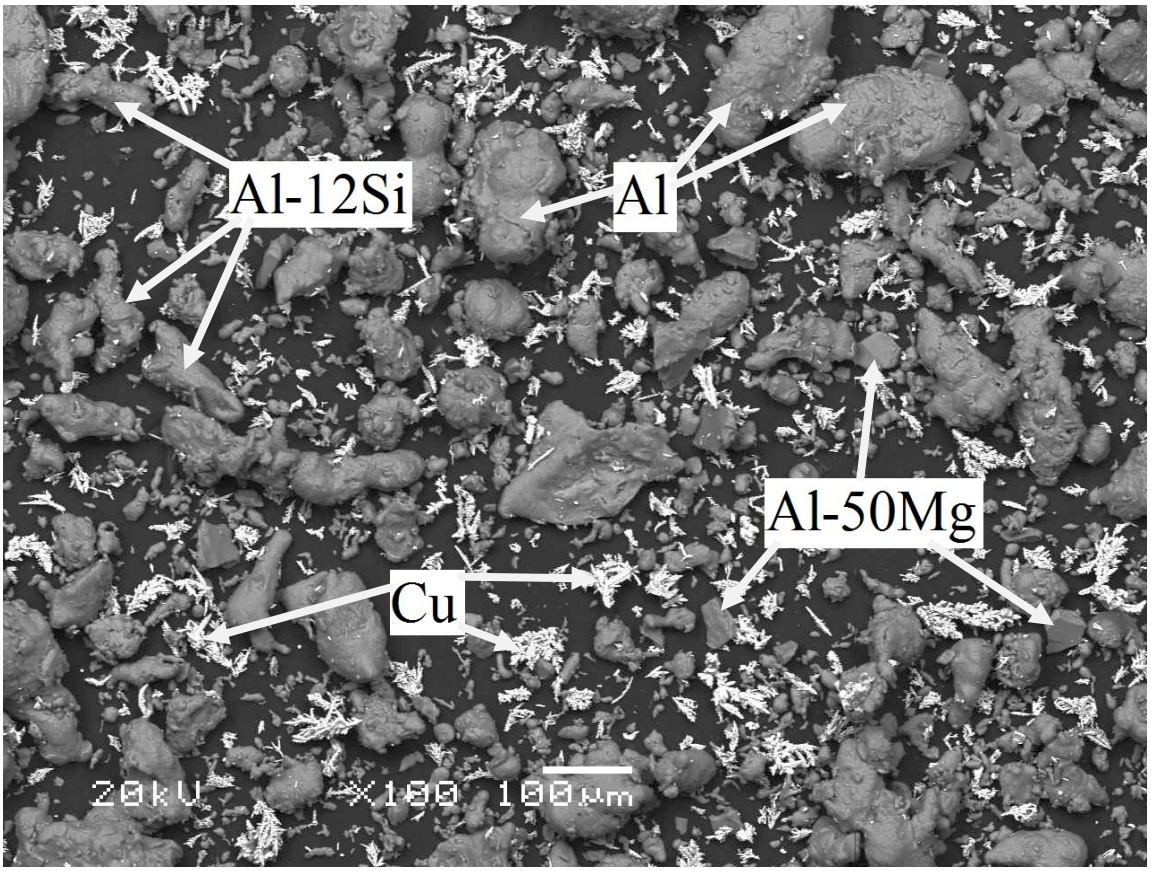

Figure 4.1: SEM micrograph of Alumix 123 without lubricant

Table 4.1: The average particle size of aluminium, copper, and prealloyed powder

Powder	**Average particle size [µm]**
Aluminium	from 200 to 45
Copper	< 75
Al-12Si	< 110
Al-50Mg	< 75

Figure 4.2 shows X-ray maps of the starting material Alumix 123 using Al, Mg, Si and. It can be seen that the Al powder represents major part of the mixture followed by Cu powder and prealloyed powders Al-12Si and Al-50Mg.

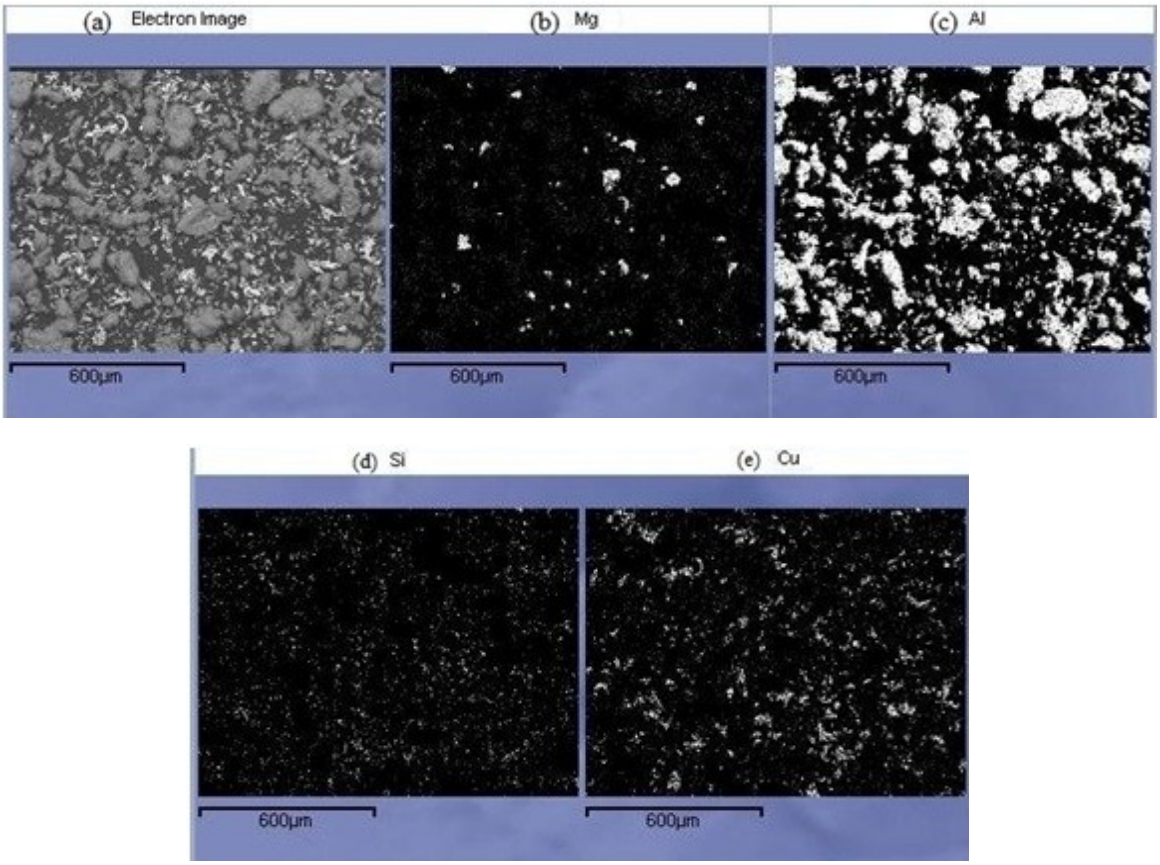

Figure 4.2: X-ray of Alumix 123 (a) BSI (b) Mg, (c) Al, (d) Si and (e) Cu.

The particle size of the lubricant varied in the range 25 to 100 µm. Figure 4.3 shows the average particle size of lubricants (a) Acrawax C and (b) Kenolube P11. It was noted that particles of Acrawax C are approximately twice as large as Kenolube P11 particles.

Table 4.2: The average particle size of used lubricants

Lubricant	**Average particle size [µm]**
Acrawax C	~ 75
Kenolube P11	~ 35

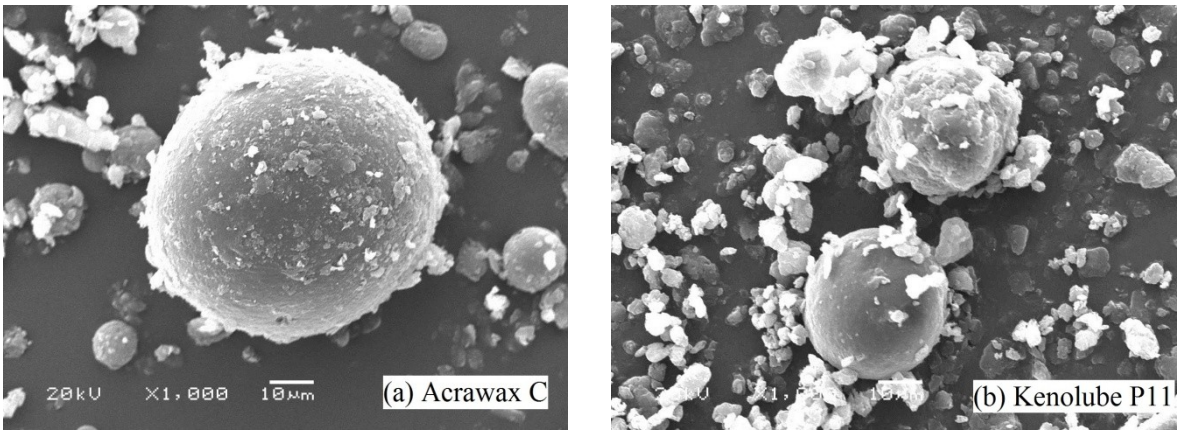

Figure 4.3: SEM micrograph of used lubricants; (a) Acrawax C and (b) Kenolube P11.

4.1.2 Thermal Stability of Admixed Lubricants

Simultaneous thermal analysis of the admixed lubricants was carried out in order to understand the thermal stability of lubricants with increasing temperature, in terms of heat flow as for DSC and mass change as for TGA. Figure 4.4 shows heat flow versus temperature spectra for Acrawax C and Kenolube P11 admixed lubricants. They consist of multiple endothermic peaks occurring at two temperature regions. The low temperature region was found to be between 80 to 160ºC while the high temperature region was found to be in excess of 200ºC. The low temperature region corresponds to the melting of the waxes while the high temperature region corresponds to the evaporation of the waxes. The melting behaviour of Acrawax C is represented by two endothermic peaks, suggesting two melting events. The perturbation in the trace just below 100ºC represents softening of Acrawax C. Acrawax C remains in a powdered form up to 142ºC. The second endothermic peak of Acrawax C starts at 142ºC and finishes at 153ºC. The melting behaviour of Kenolube P11 is represented by three endothermic peaks suggesting three melting events. At a temperature around 80ºC Kenolube P11 is softened. The second peak occurs at 100ºC. This peak finishes

at 120ºC where the wax is mainly in powdered form. The third endothermic peak starts at 120ºC and finishes at 145ºC where the Kenolube P11 is fully molten. The difference in melting behaviour of lubricants may be due to the presence of various additives in the waxes (Tables 3.3 and 3.4).

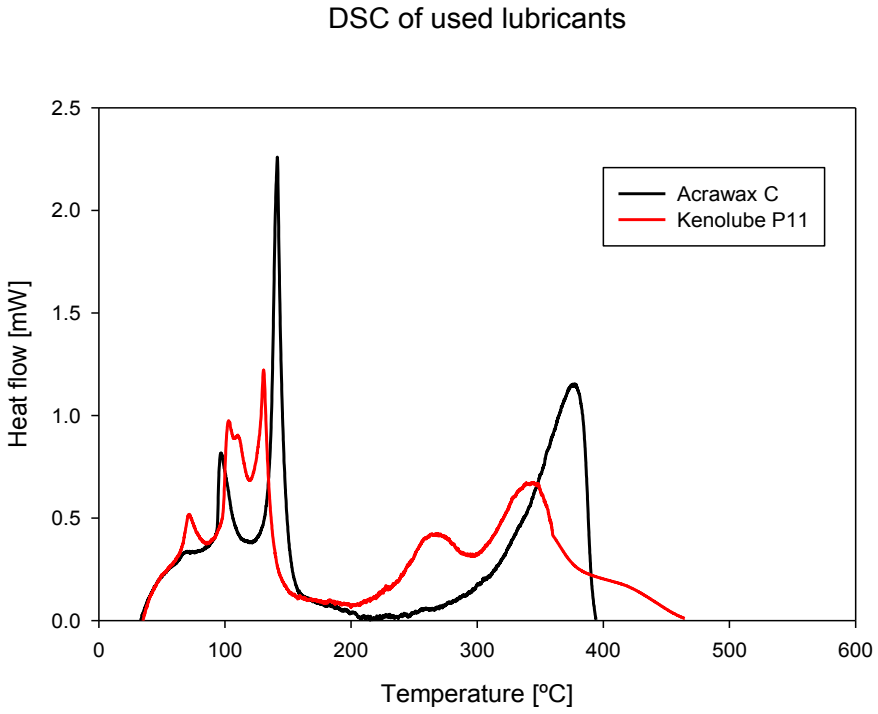

Figure 4.4: DSC of used lubricants: Acrawax C and Kenolube P11.

As previously mentioned, the high temperature region in figure 4.4 corresponds to the evaporation of lubricants. This is clearly shown in figure 4.5, where the mass change versus temperature for lubricants is illustrated. The evaporation behaviour of Kenolube P11 occurs in three stages as in melting. The first stage of Kenolube P11 mass change is close to 200ºC but this change is quite small. With increasing temperature this change grows and at 250ºC Kenolube P11 starts to evaporate, complete burn-off of Kenolube P11 is at 452ºC. It can be seen that the range of evaporation for Kenolube P11 occurs much wider compared to

Acrawax C. The evaporation of Acrawax C is a simple de-binding process. Little mass change occurs at temperature below 260ºC. The evaporation process of Acrawax C starts around 260ºC. The whole process of evaporation is complete at 395ºC.

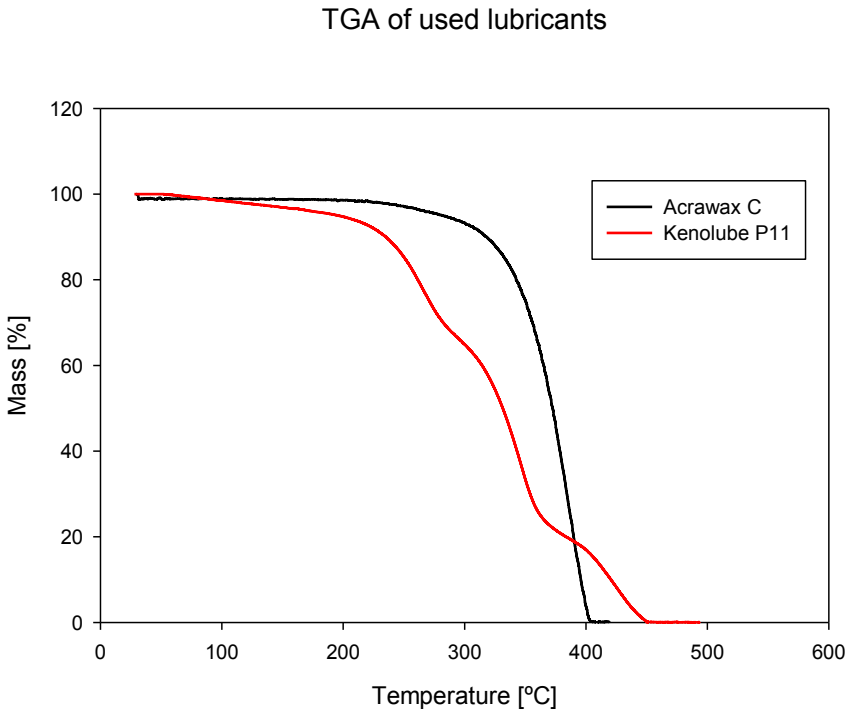

Figure 4.5: TGA of used lubricants: Acrawax C and Kenolube P11.

In addition, figure 4.5 shows that both lubricants burn-off completely leaving behind no residues. As mentioned in section 2.2.3.1 zinc stearate in pure form leaves about 15 % residue which can reduce the sintered part by hindering more complete and uniform sintering of the powder particle and also may result in less favourable pore structure. [158] However, Kenolube P11 contain just 25 wt % of zinc stearate so no residues was found.

Figure 4.6 shows the optical observation of melting behaviour of Kenolube P11. This refers to the low temperature region in figure 4.4. Kenolube P11 was heated up at three

different temperatures. The powders remain solid at temperatures up to 80ºC, as shown in figure 4.6 (a). At temperatures around 80ºC the fine particles of Kenolube P11 are partly molten and they begin to agglomerate (Figure 4.6 (b)). As the temperature is increased to 100ºC, some of the powdered lubricant is changed to the liquid form (Figure 4.6 (c)). At 145ºC the lubricant is completely molten (Figure 4.6 (d)).

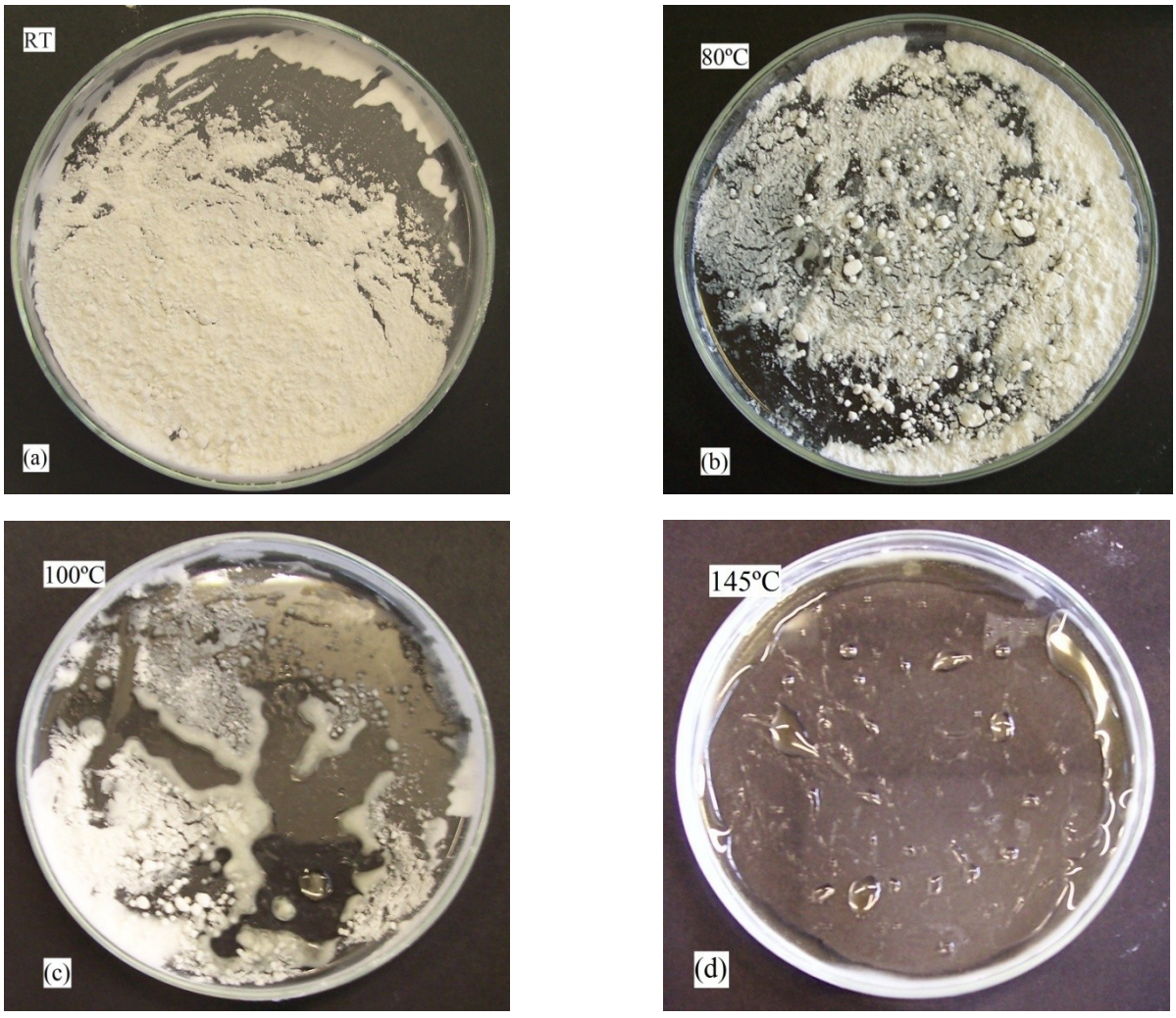

Figure 4.6: Temperature dependence of Kenolube P11; (a) RT, (b) 80ºC, (c) 100ºC and (d) 145ºC.

A similar observation of melting behaviour for Acrawax C compared with Kenolube P11 has occurred, and is shown in figure 4.7. As mentioned above, the melting behaviour of Acrawax C has two endothermic peaks. Acrawax C powders remain solid at temperatures up to 100ºC (Figure 4.7 (a)). At temperatures above 100ºC Acrawax C is partly molten, while some lubricant particles are agglomerated and some small particles are transformed to liquid (Figure 4.7 (b)). As the temperature increases more Acrawax C is transformed to liquid and at 153ºC Acrawax C is completely molten (Figure 4.7 (c)).

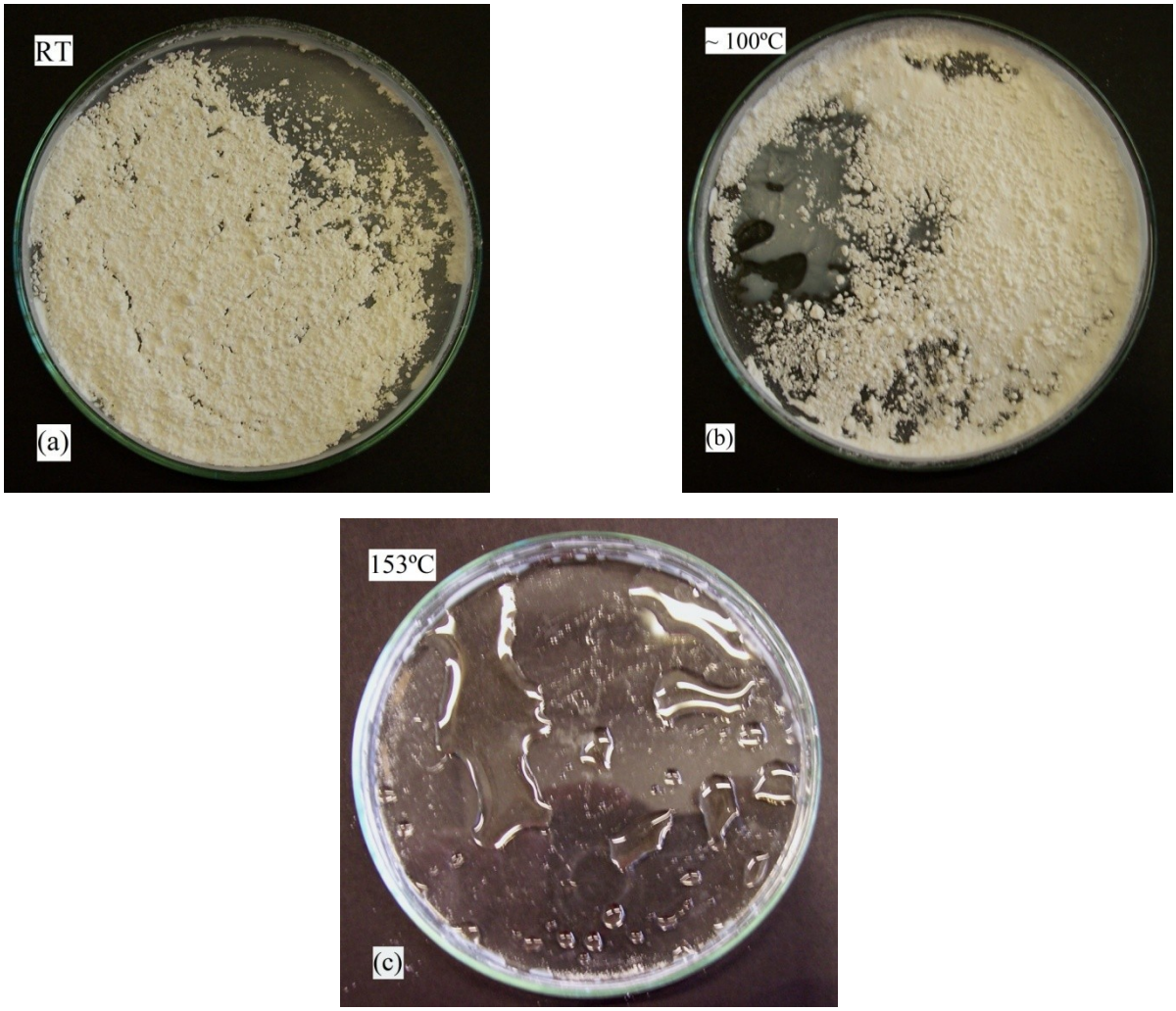

Figure 4.7: Temperature dependence of Acrawax C; (a) RT, (b) ~ 100ºC, (c) 153ºC.

4.2. Effect of Compaction Pressure and Temperature and Lubricant Content on Ejection Force of Alumix 123 Compact

Compacts of Al powder Alumix 123 with lubricant amount of 0.5, 1.0 and 1.5 wt % were pressed using an uniaxial hydraulic press to standard tensile specimen shape as described in "Experimental Methods" chapter. The force required for ejection of compacts was measured. An average of highest ejection forces needed to initiate movement of the specimen from the die was calculated using 4 specimens.

4.2.1 Acrawax C

Figure 4.8 shows plots of the ejection force versus various compaction pressures, temperatures and Acrawax C contents of 0.5, 1.0 and 1.5 wt %. The ejection force was found to increase with increasing compaction pressure at RT.

For compacts ejected from the die at RT the maximum value of the ejection force was measured to be 12.97, 7.2 and 10.1 kN for specimens prepared using 0.5, 1.0 and 1.5 wt % of Acrawax C, respectively.

For Acrawax C content of 0.5 wt % the decrease of the ejection force between compaction temperatures of RT and 110ºC (Figure 4.8 (a)) was found to be 33.3, 41.6, 46, 46.4 and 47.6 % for compaction pressures of 200, 250, 300, 350 and 400 MPa, respectively.

For 1.0 wt % of Acrawax C (Figure 4.8 (b)) the decrease of the ejection force between compaction temperatures of RT and 110ºC was found to be 50.7, 56.4, 68.6, 60.9 and 68.7 % for compaction pressures of 200, 250, 300, 350 and 400 MPa, respectively.

For Acrawax C content of 1.5 wt % (Figure 4.8 (c)) the decrease of the ejection force between compaction temperatures of RT and 110ºC was found to be 40.6, 31.6, 32, 27.6 and 40.1 % for compaction pressures 200, 250, 300, 350 and 400 MPa, respectively.

A list of measured values of the ejection force for specimens compacted at various pressures, temperatures and Acrawax C contents are illustrated in table A1 in the appendix.

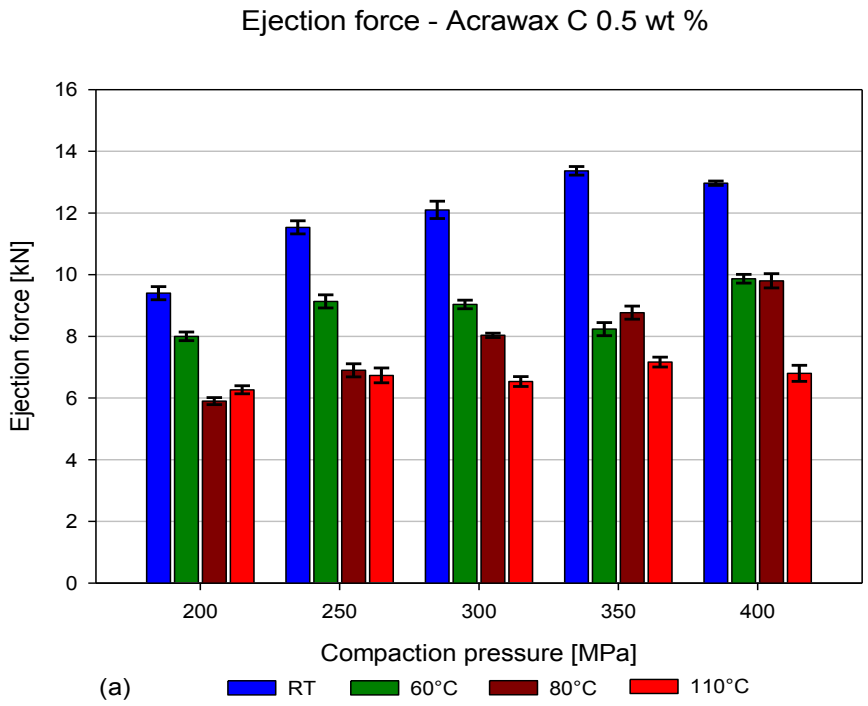

Figure 4.8 (a): Ejection force of specimens with Acrawax C with contents of 0.5 wt %.

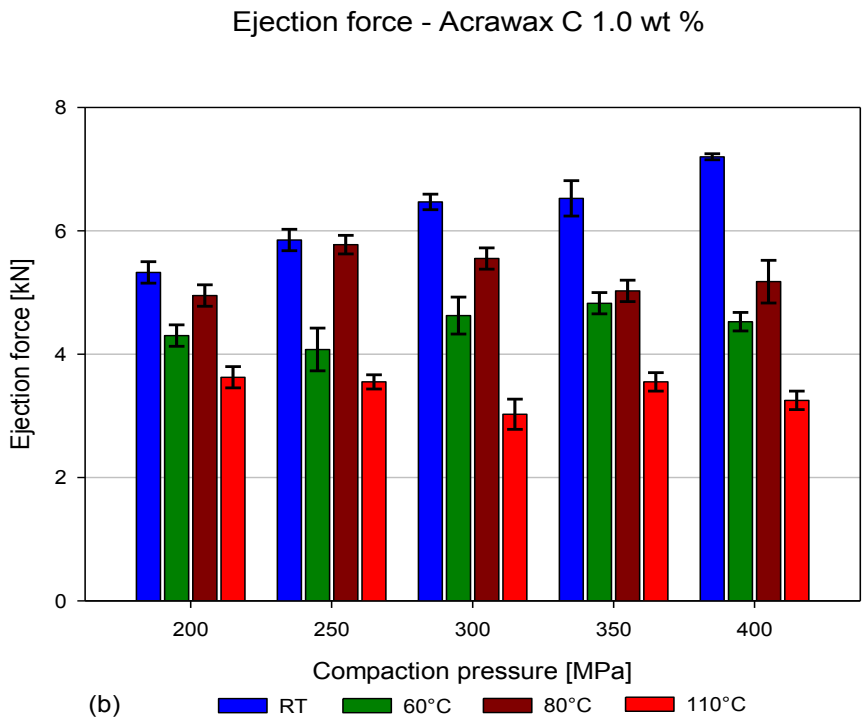

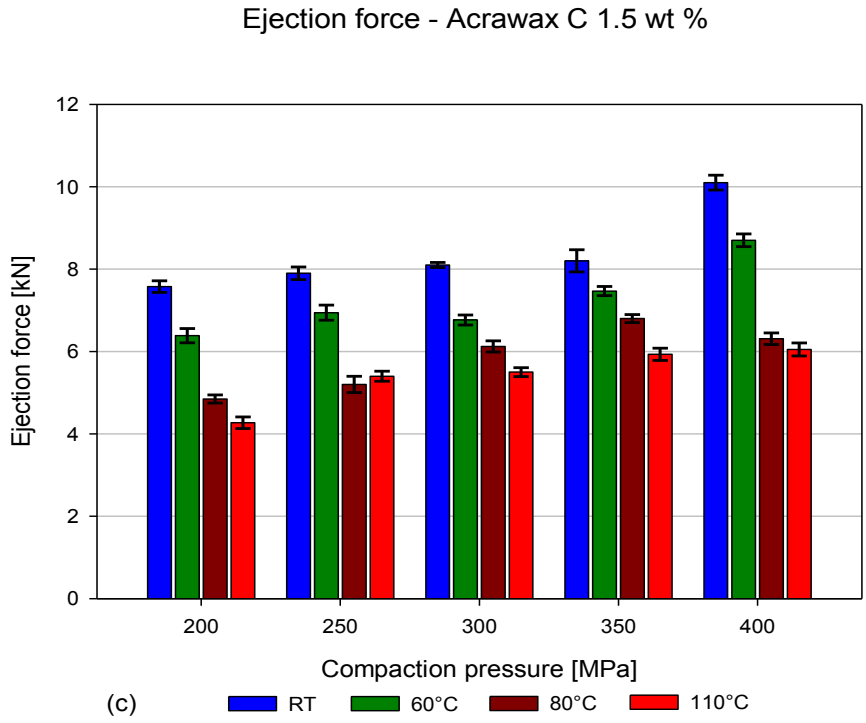

Figure 4.8(b-c): Ejection force of specimens with Acrawax C with contents of (b) 1.0 wt % and (c) 1.5 wt %.

4.2.2 Kenolube P11

Figure 4.9 shows plots of ejection force versus various compaction pressures, temperatures and Kenolube P11 contents of 0.5, 1.0 and 1.5 wt %. A similar trend of the increase in ejection force with increasing compaction pressure at RT compared with Acrawax C occurs.

For compacts ejected from the die at RT the maximum value of the ejection force was measured to be 10.58, 10.75 and 10.13 kN for specimens prepared using 0.5, 1.0 and 1.5 wt % of Kenolube P11, respectively.

For Kenolube P11 content of 0.5 wt % the decrease of the ejection force between compaction temperatures of RT and 110ºC (Figure 4.9 (a)) was found to be 35.7, 42.3, 45.8, 42.8 and 28.4 % for compaction pressures of 200, 250, 300, 350 and 400 MPa, respectively.

For Kenolube P11 content of 1.0 wt % (Figure 4.9 (b)) the decrease of the ejection force between compaction temperatures of RT and 110ºC was found to be 48.8, 50.5, 40.7, 53.1 and 51.8 % for compaction pressures of 200, 250, 300, 350 and 400 MPa, respectively.

For Kenolube P11 content of 1.5 wt % (Figure 4.9 (c)) the decrease of the ejection force between compaction temperatures of RT and 110ºC was found to be 29.5, 34, 36.8, 35.2 and 50.1 % for compaction pressures 200, 250, 300, 350 and 400 MPa, respectively.

A list of measured values of the ejection force for different compaction pressures, temperatures and Kenolube P11 contents is displayed in table A2 in the appendix.

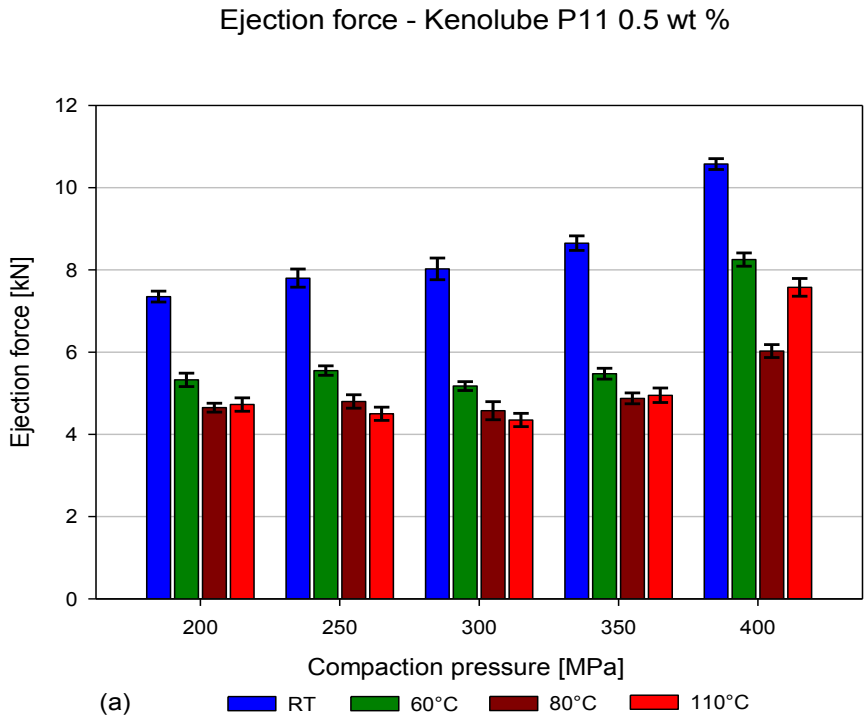

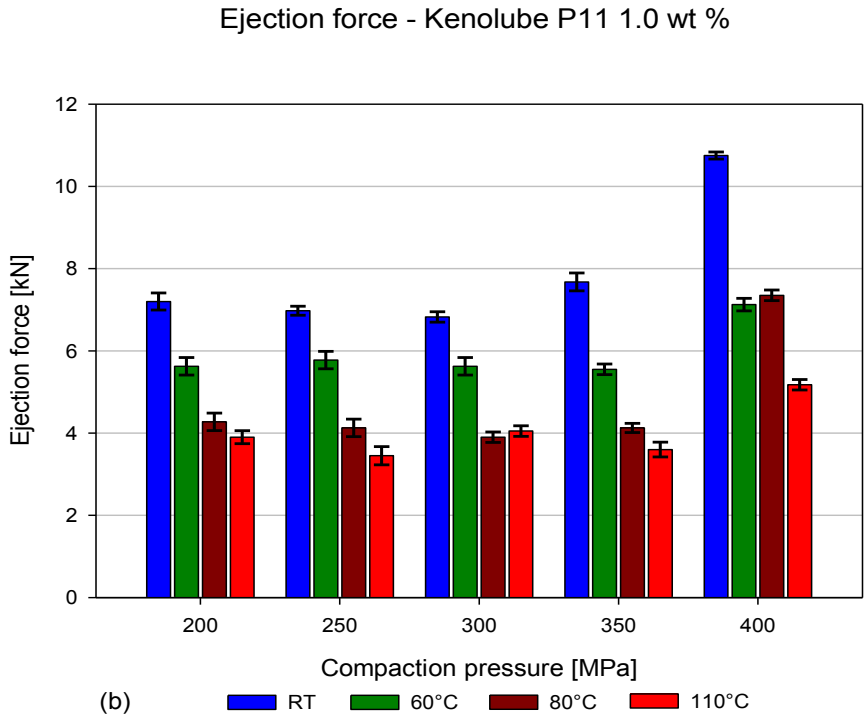

Figure 4.9 (a-b): Ejection force of specimens with Kenolube P11 with contents of (a) 0.5 wt % and (b) 1.0 wt %.

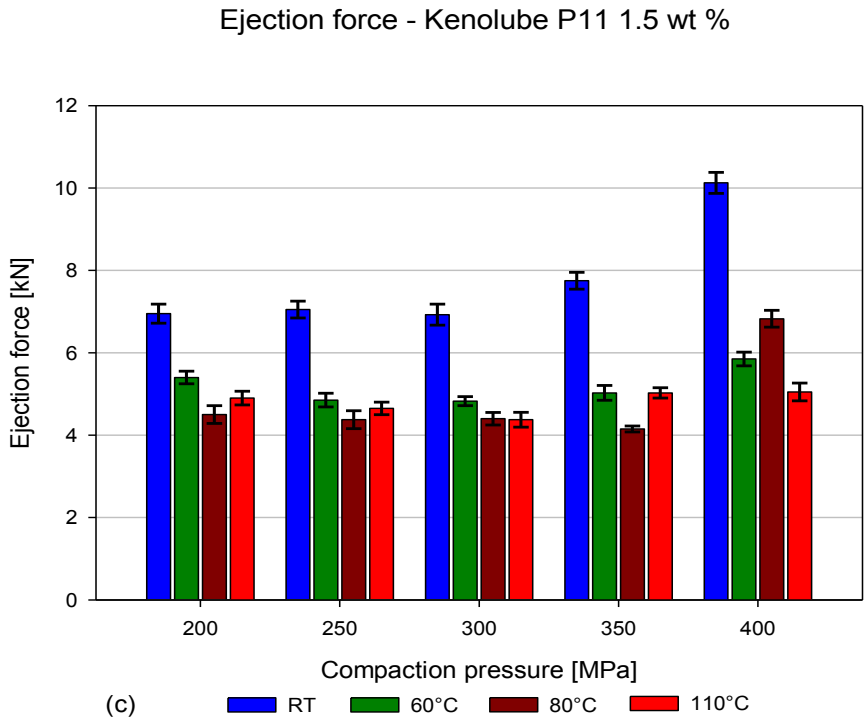

Figure 4.9 (c): Ejection force of specimens with Kenolube P11 with contents of 1.5 wt %.

In general, the ejection force was found to decrease with higher compaction temperature. Ejection force was reduced when the compaction temperature increased from RT to 110°C. It should be noted, that the amount of decrease in ejection force was over 40 %. This is because a larger number of fine particles of lubricant on the die wall are softened and pushed to the boundary between the green compact and the internal die wall surface, leading to a reduction in die wall friction, as the compaction temperature is increased.

Use of Acrawax C and Kenolube P11 resulted in similar development of the ejection force. This could be caused by the use of compaction temperatures below the melting point of both lubricants.

4.3. Effect of Compaction Pressure and Temperature on Green Density of Alumix 123 Compacts

4.3.1 Acrawax C

Figure 4.10 shows the green density of compacts (a-c) and relative green density (d-f) versus different compaction pressures, temperatures and various Acrawax C contents. The relative densities were determined by equation (eq. 4.1):

$$D_{Rel} = \frac{\rho_{measured}}{\rho_{theoretical}} \times 100 \qquad \text{(eq. 4.1)}$$

where D_{Rel} is the relative density, $\rho_{measured}$ is the measured compact density and $\rho_{theoretical}$ is the theoretical density of alloy.

As theoretical density of Alumix 123 alloy the density of 2.8 g/cm^3 was used.

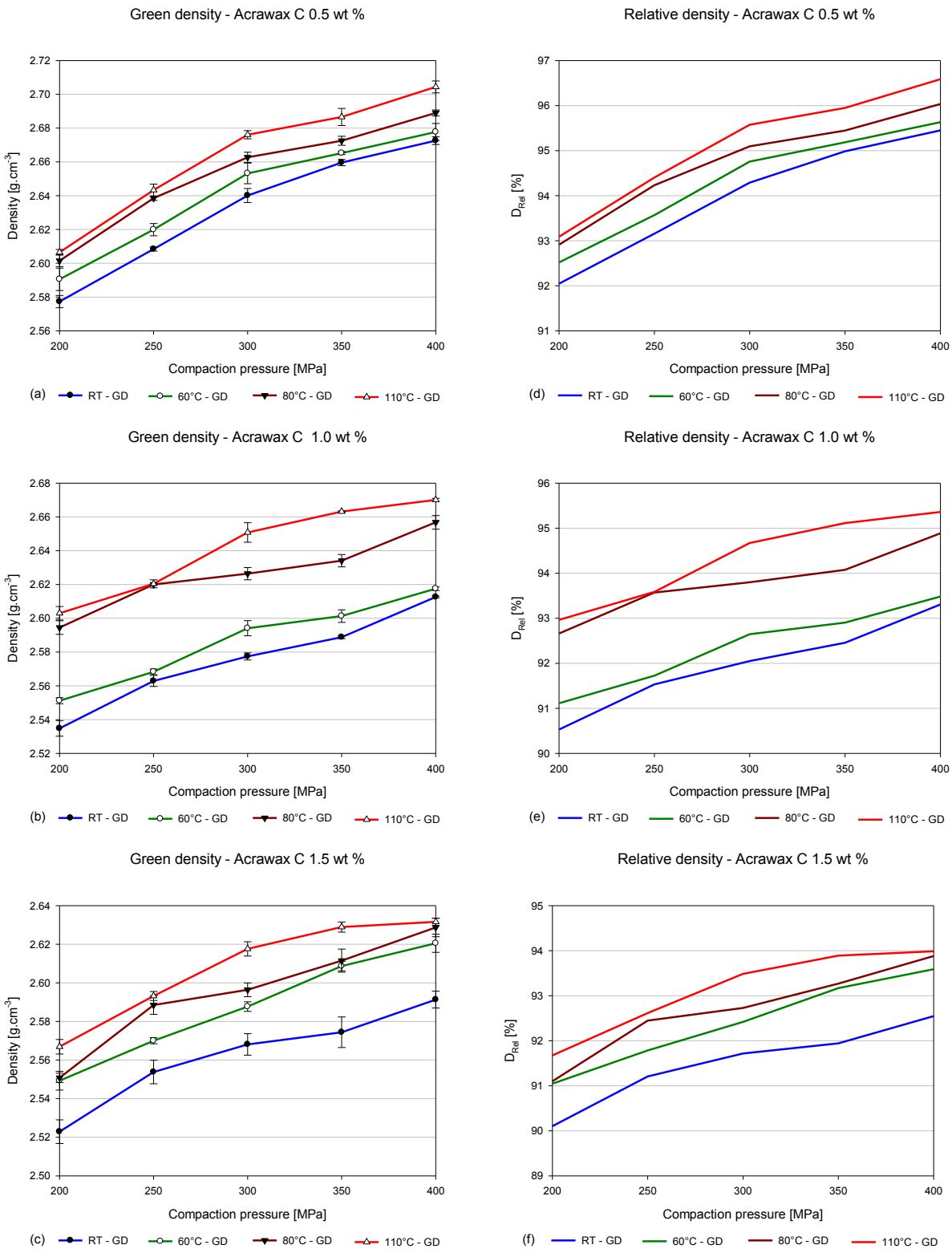

Figure 4.10: Green density (a-c) and D_{Rel} - relative green density (d-f) of Alumix 123 compacts as a function of pressure and temperature with Acrawax C contents of 0.5 wt %, 1.0 wt % and 1.5 wt %. (GD – green density of the specimens)

The specimens with Acrawax C content of 0.5 wt % compacted at 110°C and 400 MPa reached a green density of over 96.58 % (2.704 g/cm^3) of the theoretical density (TD), while specimens compacted at RT and 400 MPa reached a green density just over 95.45 % (2.672 g/cm^3) of TD. A similar trend of increased green density was also found in specimens with a higher amount of admixed lubricant. For the specimens with Acrawax C content of 1.0 wt % compacted at 110ºC and 400 MPa the green density was measured to be 95.36 % (2.670 g/cm^3) of TD and for the specimens compacted at RT and 400 MPa the green density was 92.73 % (2.612 g/cm^3) of TD. The green density of the specimens with 1.5 wt % of Acrawax C compacted at 110ºC was over 93.98 % (2.631 g/cm^3) of TD and at RT it was 92.54 % (2.591 g/cm^3) of TD. This shows that the specimens with Acrawax C content of 0.5 wt % compacted at RT reached higher green density than the specimens with Acrawax C content of 1.5 wt % compacted at 110ºC. The list of measured green densities and calculated relative green densities can be found in table A3 in the appendix.

4.3.2 Kenolube P11

Figure 4.11 shows the green density (a-c) and relative green density (d-f) as a function of compaction pressure, temperature and amount of admixed Kenolube P11. The specimens with Kenolube P11 followed the same tendency in the green densities as the specimens with Acrawax C; i.e. higher compaction temperature, higher pressing pressure and lower amount of admixed lubricant led to improved densities. It was observed that specimens compacted at 110ºC reached highest green density in all Kenolube P11 contents.

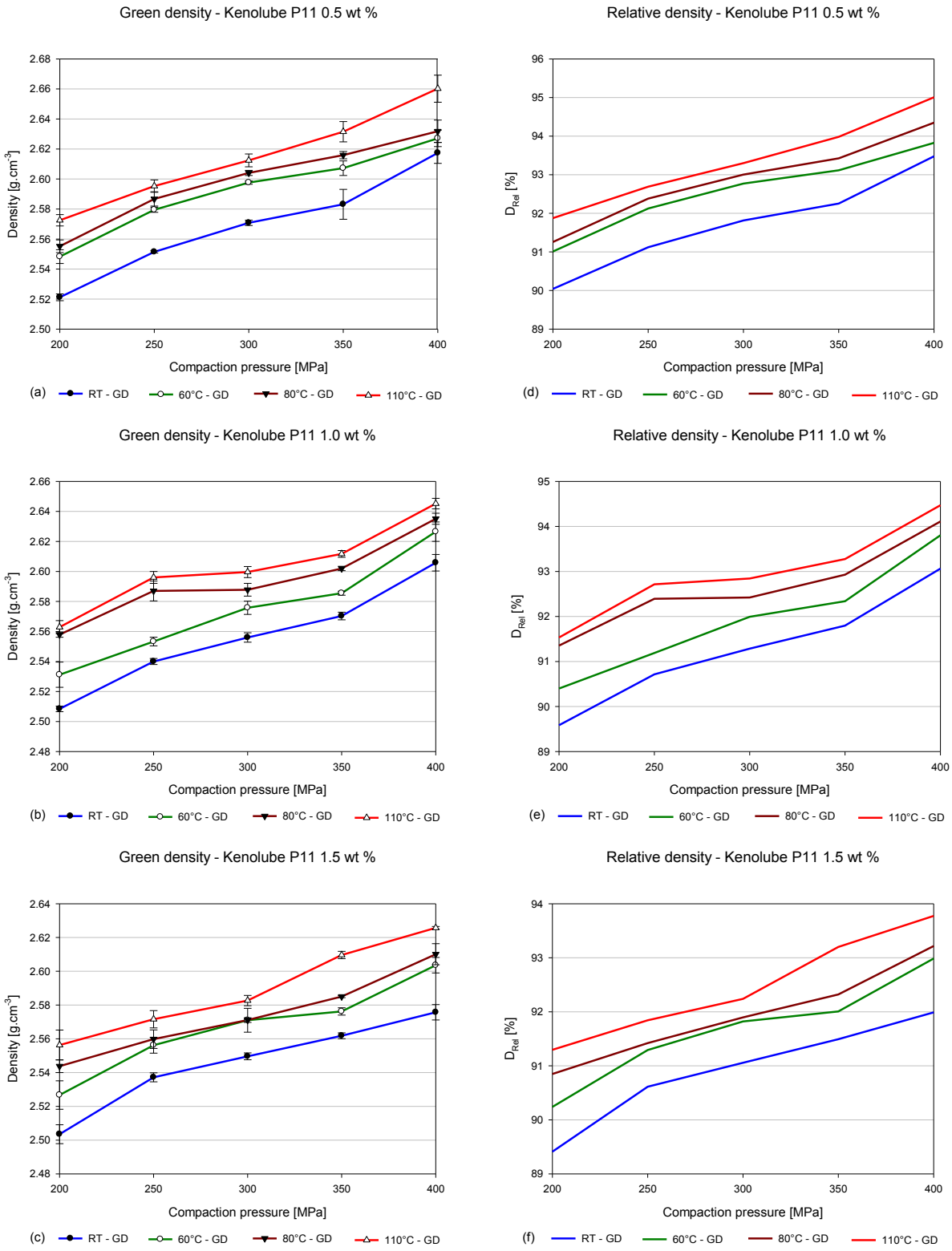

Figure 4.11: Green density (a-c) and D_{Rel} - relative green density (d-f) of Alumix 123 compacts as a function of pressure and temperature with Kenolube P11 content of 0.5 wt %, 1.0 wt % and 1.5 wt %. (GD – green density of the specimens)

The green density of the specimens with 0.5 wt % of Kenolube P11 reached 95 % (2.660 g/cm^3) of TD and 93.47 % (2.617 g/cm^3) of TD (Figure 4.17 (a-c)) when compacted at 110 ºC for 400 MPa and at RT for 400 MPa, respectively. The specimens with 1.0 wt % of Kenolube P11 achieved a green density of 94.47 % (2.645 g/cm^3) and 93.06 % (2.605 g/cm^3) of TD when compacted at 110ºC for 400 MPa and at RT for 400 MPa, respectively. The specimens with 1.5 wt % of Kenolube P11 obtained the green density of 93.77 % (2.625 g/cm^3) of TD and 91.98 % (2.617 g/cm^3) of TD when compacted at 110ºC for 400 MPa and at RT for 400 MPa, respectively. The list of measured green and relative green densities for compacts with Kenolube P11 is shown in table A4 in the appendix.

The effect of warm compaction on the green density of aluminium powder was reported by Simchi *et al.* [89]. They reported that compaction at RT and 350 MPa leads to green density as high as 95.5 % of TD and warm compacted specimens compacted at 110ºC reached up to 98 % of TD.

Martín *et al.* [134] in their study of Alumix 123 with Microwax C as admixed lubricant achieved green density of 2.58 g/cm^3 at compaction pressure of 400 MPa and RT with lubricant content of 1.5 wt %. This is comparable with present study where Alumix 123 with 1.5 wt % of Acrawax C and Kenolube P11 reached green density of 2.571 and 2.576 g/cm^3, respectively.

4.4 Relationship between Compaction Pressure and Green Density of Alumix 123 Compacts

The green density results show that compaction at elevated temperatures, even at same compaction pressure, gives higher deformability, through better compressibility of powder constituents. This can be explained by the temperature dependence of yield strength in Al powder. (Figure 2.18, Section 2.3.2).

Heckel describes the relationship between compaction pressure and relative density by equation 2.5 (Section 2.3).

As mentioned in section 2.3, the Heckel relationship is very sensitive to variations in experimental conditions, such as compaction under exceptionally high pressure with high loading, weight of the compact and temperature, the maximum compression pressure and temperature. Owing this sensitivity the figures 4.12 and 4.13 show deviations from the linear relationship. Apparent density, for each lubricant contents, was used as starting point of the plots to include pressureless region to the Heckle equation.

4.4.1 Acrawax C

Figure 4.12 shows the Heckel relationship of compaction pressure versus $\ln\left(\frac{1}{1-D}\right)$ for different compaction temperatures and Acrawax C contents. It was found that with increasing compaction temperature and reduction in admixed lubricant the slope k_H increases, thus the yield strength of powder is decreasing. Tables 4.3 and 4.4 shows the Heckel slope k_H and yield strength for Acrawax C using various amounts of lubricant and compaction temperatures, respectively.

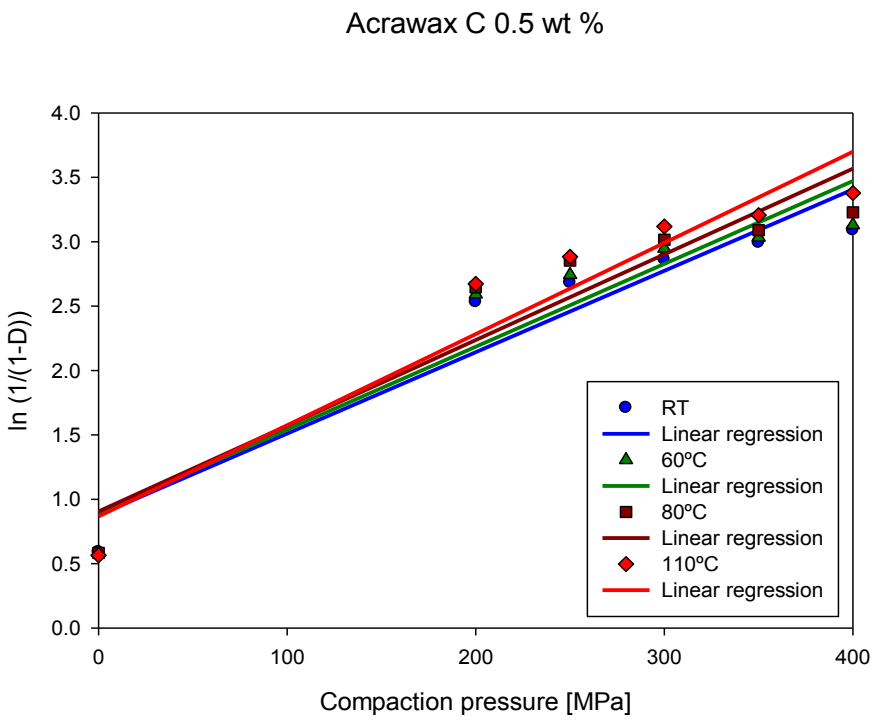

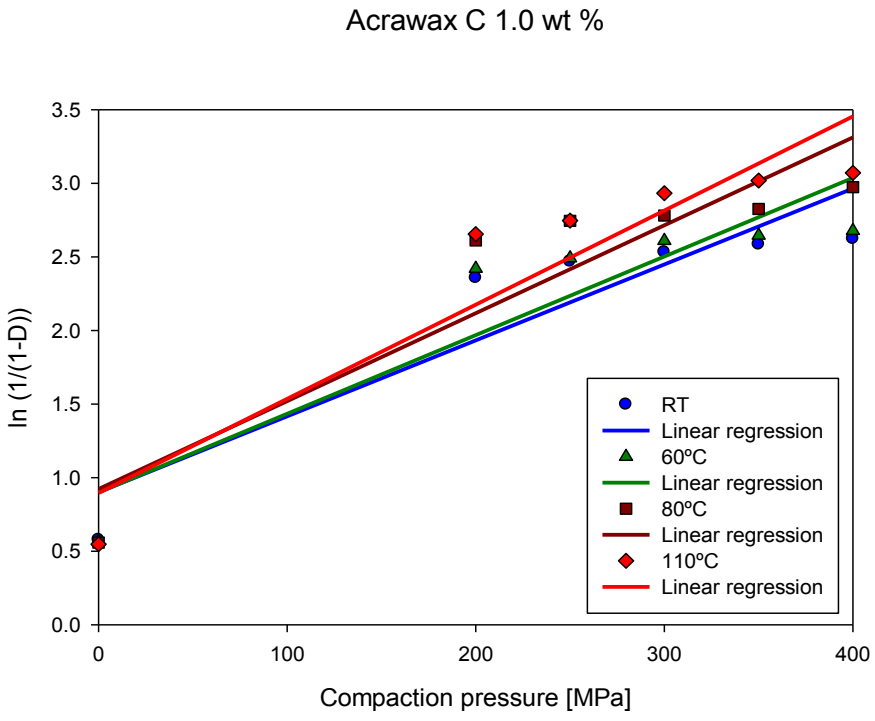

Figure 4.12 (a-b): Heckle relationship between compaction pressure and ln (1/ (1-D)) with different compaction temperatures and Acrawax C contents of (a) 0.5 wt % and (b) 1.0 wt %. (D is the relative density)

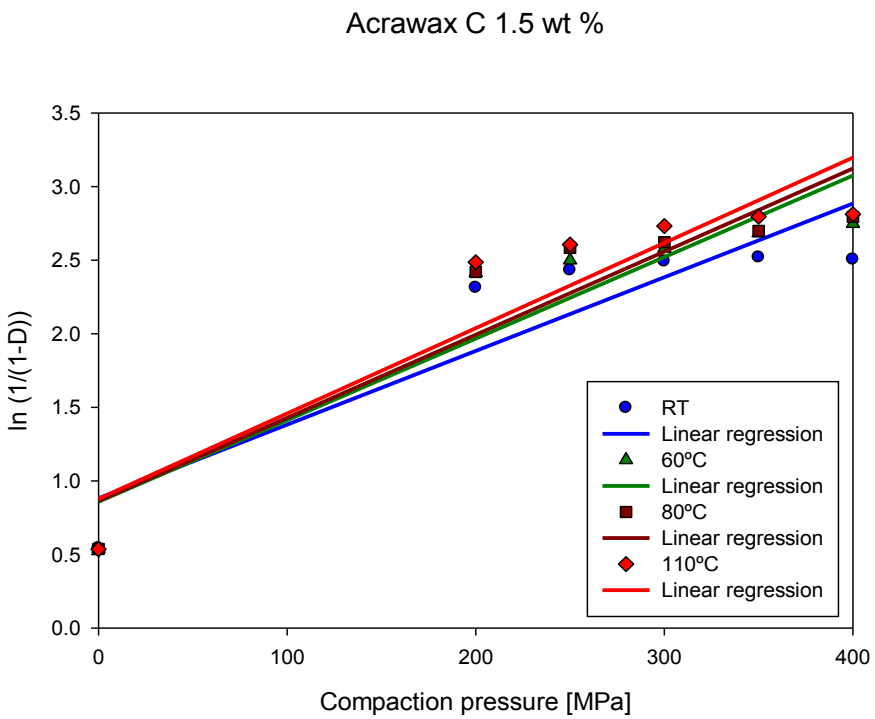

Figure 4.12 (c): Heckle relationship between compaction pressure and the ln (1/ (1-D)) with different compaction temperatures and with Acrawax C content of 1.5 wt %.(D is the relative density).

Table 4.3: Heckel slope k_H for different compaction temperatures and Acrawax C contents

Lubricant	**Heckel slope k_H [MPa^{-1}]**			
	Compaction temperature [ºC]			
	RT	**60**	**80**	**110**
Acrawax C 0.5 wt %	0.005488	0.00557	0.006055	0.006526
Acrawax C 1.0 wt %	0.00516	0.00534	0.005764	0.006052
Acrawax C 1.5 wt %	0.00501	0.00554	0.00565	0.0058

Table 4.4: Yield strength for different compaction temperatures and Acrawax C contents

Lubricant	Yield strength [MPa]			
	Compaction temperature [°C]			
	RT	60	80	110
Acrawax C 0.5 wt %	60.74	59.84	55.05	51.08
Acrawax C 1.0 wt %	64.6	62.42	57.83	55.08
Acrawax C 1.5 wt %	66.53	60.17	59	57.47

4.4.2 Kenolube P11

A similar observation of an increase of the slope k_H with increasing compaction temperature and decreasing amount of admixed lubricant was found for Kenolube P11 compared with Acrawax C. Figure 4.13 shows the Heckel relationship of compaction pressure versus $\ln\left(\frac{1}{1-D}\right)$ for various compaction temperatures and Kenolube P11 contents.

The calculated slope k_H and yield strength for various lubricant contents and temperatures are listed in tables 4.5 and 4.6, respectively.

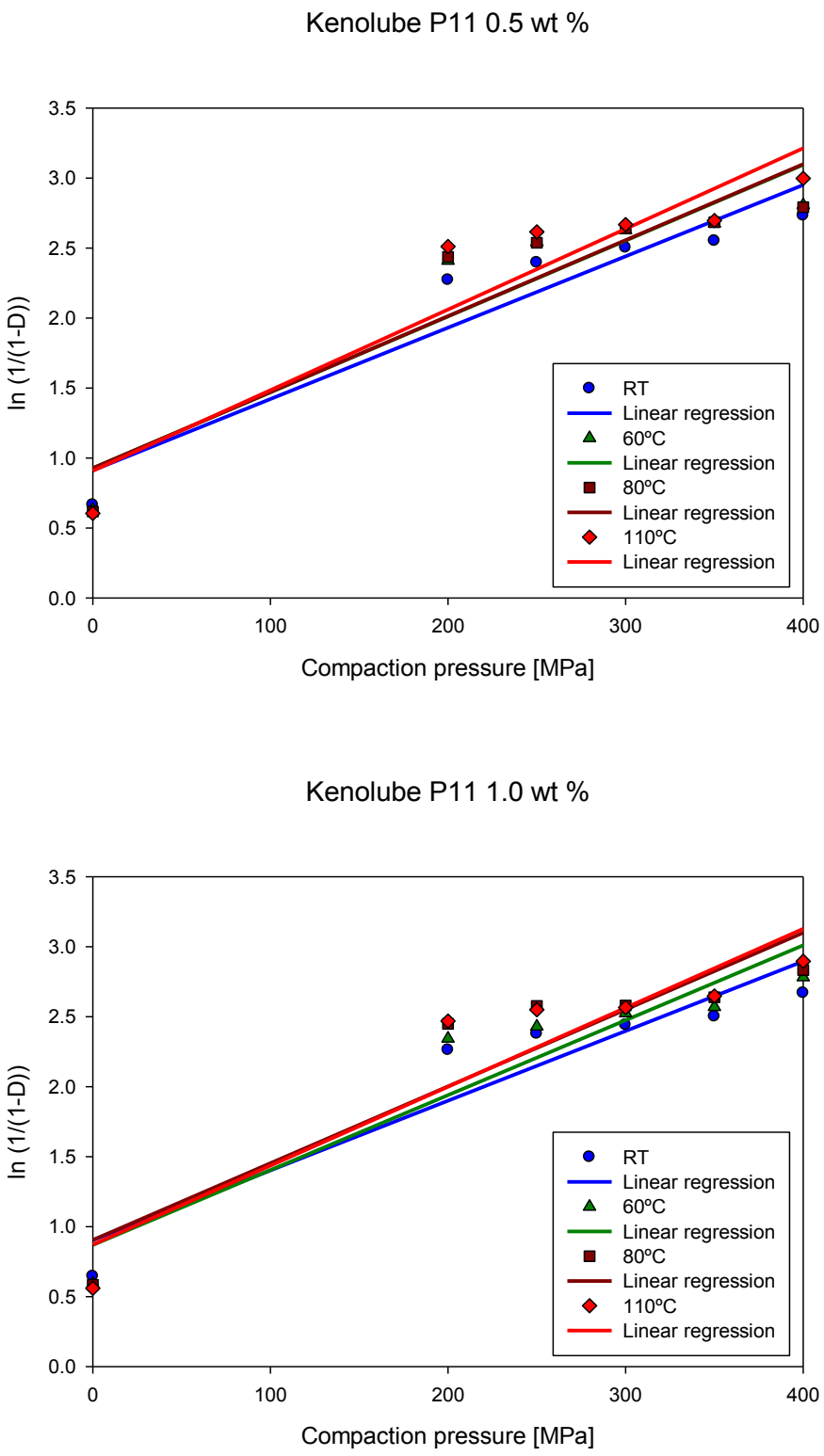

Figure 4.13 (a-b): Heckle relationship between compaction pressure and ln (1/ (1-D)) with different compaction temperatures and Kenolube P11 contents of (a) 0.5 wt % and (b) 1.0 wt %. (D is the relative density)

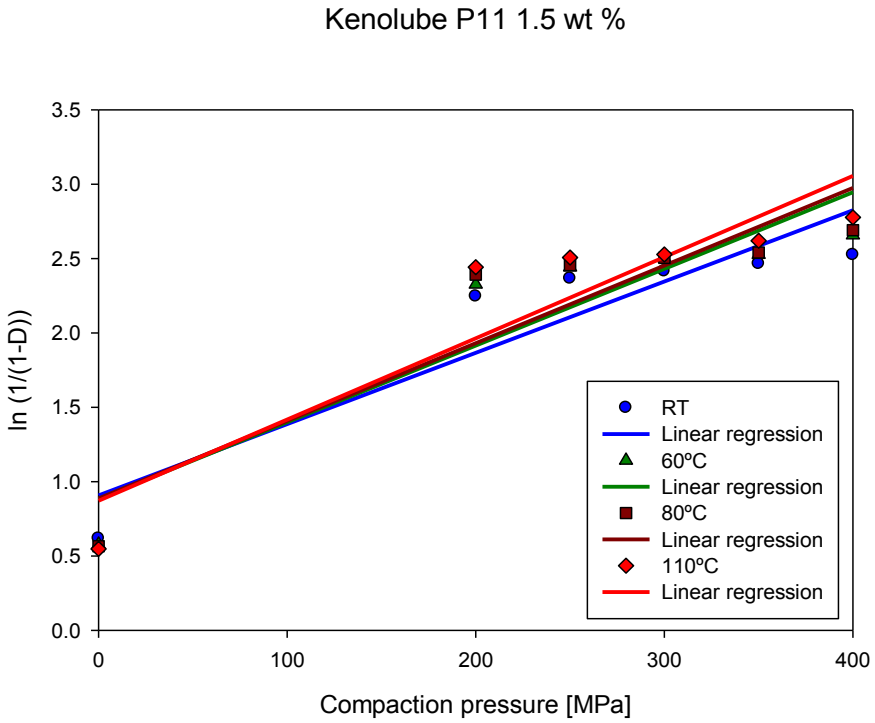

Figure 4.13 (c): Heckle relationship between compaction pressure and ln (1/ (1-D)) with different compaction temperature and with Kenolube P11 content of 1.5 wt %. (D is the relative density)

Table 4.5: Heckel slope k_H for different compaction temperatures and Kenolube P11 contents

Lubricant	**Heckel slope k_H [MPa^{-1}]**			
	Compaction temperature [ºC]			
	RT	**60**	**80**	**110**
Kenolube P11 0.5 wt %	0.00501	0.00538	0.00560	0.00589
Kenolube P11 1.0 wt %	0.00498	0.00535	0.00550	0.00572
Kenolube P11 1.5 wt %	0.00479	0.00515	0.00525	0.00554

Table 4.6: Yield strength for different compaction temperatures and Kenolube P11 contents

Lubricant	**Yield strength [MPa]**			
	Compaction temperature [ºC]			
	RT	**60**	**80**	**110**
Kenolube P11 0.5 wt %	66.53	61.95	59.52	56.59
Kenolube P11 1.0 wt %	66.93	62.31	60.61	58.27
Kenolube P11 1.5 wt %	69.59	64.72	63.49	60.17

4.5 Microstructure of Alumix 123 Green Compacts

Figure 4.14 shows the typical microstructure of the green compacts. The microstructure corresponds to Alumix 123 with 1.5 wt % of Acrawax C as admixed lubricant compacted at 80ºC and 300 MPa. The grey region represents elemental Al or Al-12Si particles. The black regions represent pores and bright regions are Cu particles. There were regions characterised as Al-50Mg by EDX. Figure 4.15 shows the EDX spectrum of Al-50Mg region with percentage of the elements, as is illustrated in table 4.7.

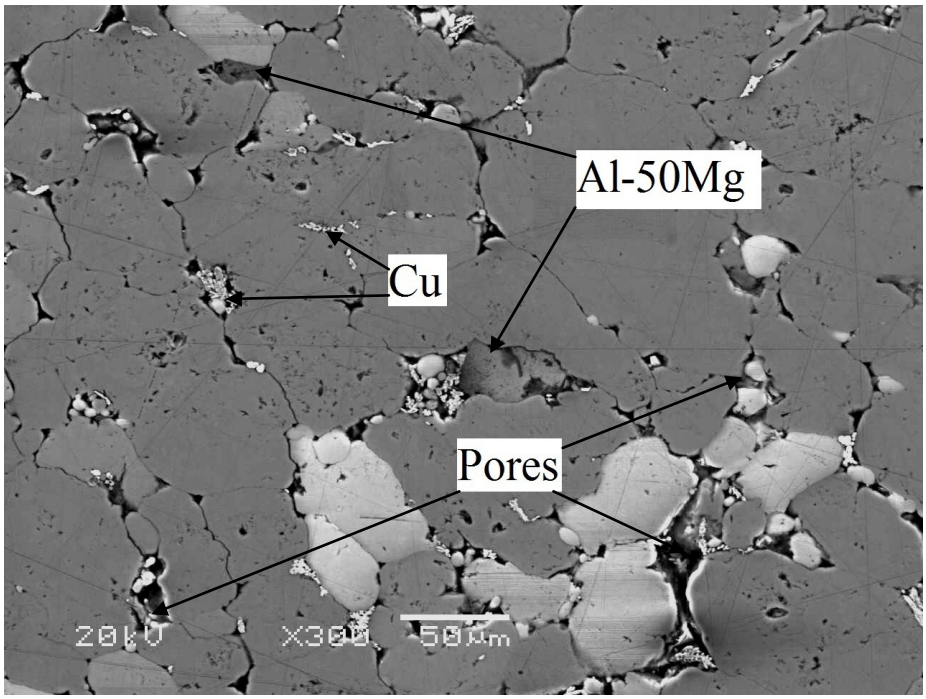

Figure 4.14: Typical microstructure of Alumix 123 green compact (BSI).

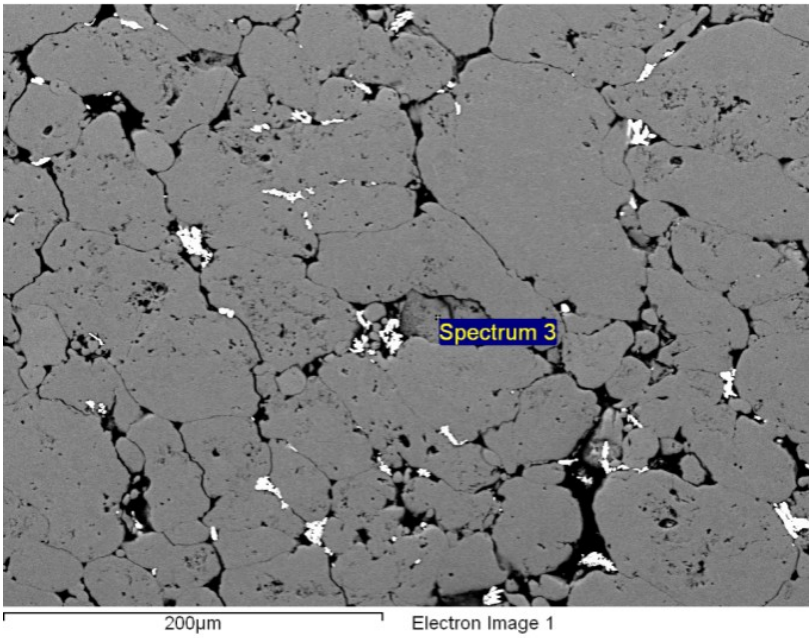

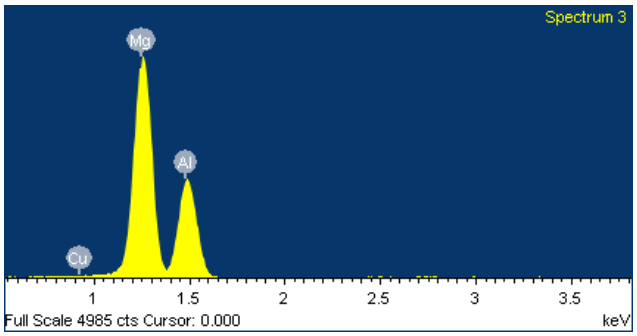

Figure 4.15: EDX spectrum of the Al-50Mg region.

Table 4.7: Percentage representation of Al-50Mg region

Element	**Weight %**	**Atomic %**
Mg	51.14	53.79
Al	48.52	45.99
Si	0.15	0.14
Cu	0.19	0.08
Totals	100.00	100.00

4.5.1 Effect of Lubricant Content on Microstructure of Alumix 123 Green Compacts

Figure 4.16 shows the microstructures of green compacts prepared at room temperature and pressures 400 MPa, using Acrawax C and Kenolube P11 with contents of 0.5, 1.0, and 1.5 wt %, respectively. Room temperature was chosen to visibly present the improvement in green compact microstructure with decreasing amount of lubricant in terms of porosity level.

From measured data of green density the overall porosity of the single lubricant contents increased with increasing lubricant content as can be seen at table 4.8. Data in table 4.8 are average values for specimens compacted at RT and 400 MPa for a given lubricants contents.

Table 4.8: The overall porosity of the green specimens compacted at RT and 400 MPa.

	Overall porosity [%]	
Lubricant content	**Acrawax C**	**Kenolube P11**
0.5 wt %	4.5	6.5
1.0 wt %	6.6	6.9
1.5 wt %	7.4	8.1

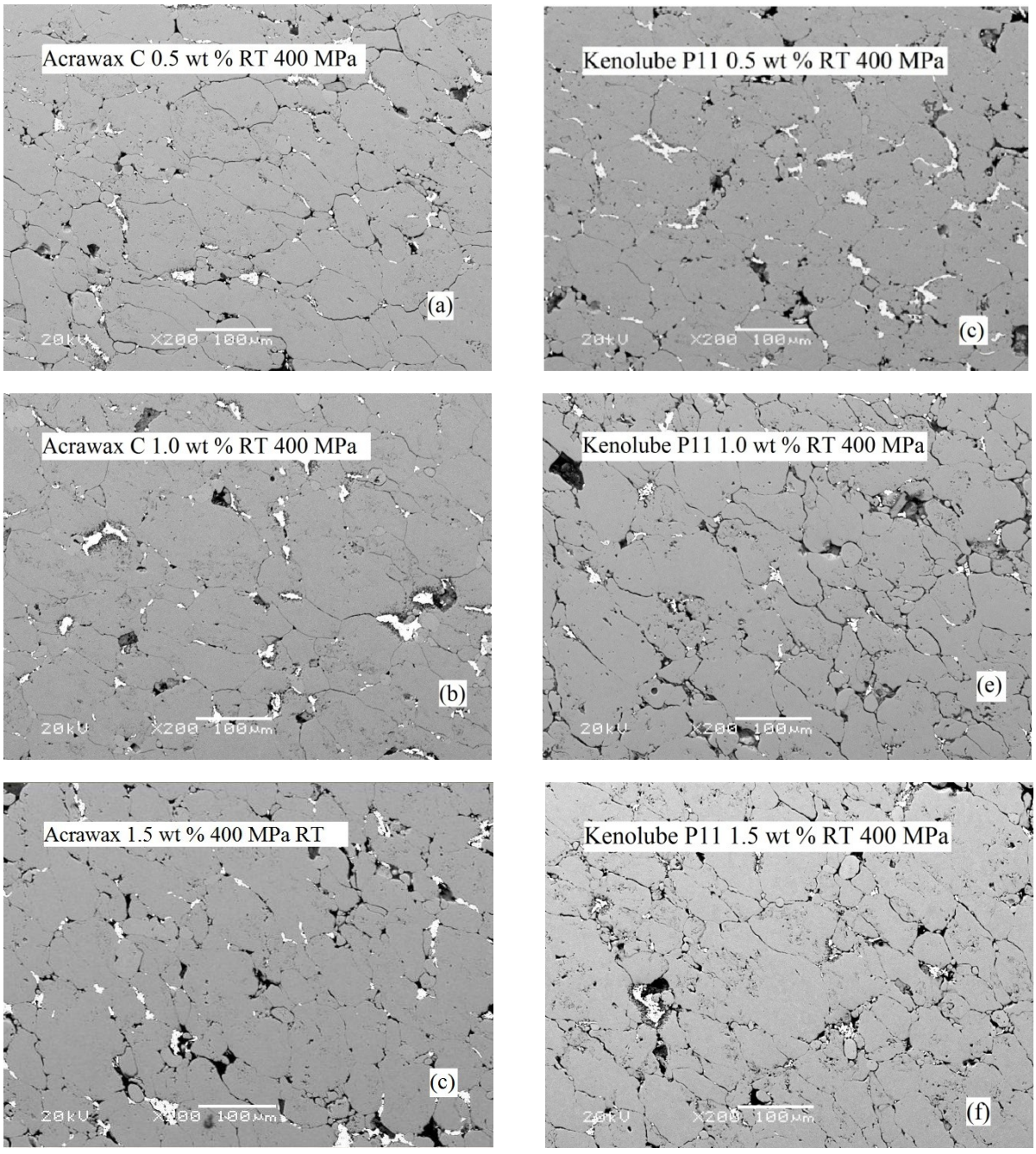

Figure 4.16: Microstructures of green compacts; (a-c) Acrawax C, (d-f) Kenolube P11 with different lubricant contents, compacted at RT by pressure of 400 MPa.

4.5.2 Distribution of Porosity in Alumix 123 Green Compacts

Figure 4.17 shows the distribution of porosity in a specimen with 0.5 wt % of Acrawax C compacted at 110ºC and 400 MPa and a specimen with 1.5 wt % of Acrawax C compacted at RT and 200 MPa.

As mentioned above, higher compaction pressure, compaction temperature and lower lubricant content result in decreasing amount of porosity in the compact. However, compaction at low pressure (200 MPa) and temperature (RT) with lubricant content of 1.5 wt % shows that overall porosity at the edge of specimen was significantly higher (10.2 %) than at the centre of specimen (4.3 %). For specimens compacted at 400 MPa at 110ºC with lubricant content 0.5 wt % the distribution of porosity is more uniform. Porosity at the edge and at the centre of specimen was represented by 1.7 % and 0.8 %, respectively. To evaluate the porosity level, Zeiss KS 300 4.0 image analysis software was used.

A similar observation on distribution of porosity using Kenolube P11 compared with Acrawax C has occurred. For specimens compacted at RT and 200 MPa with Kenolube P11 content of 1.5 wt %, porosity at the edge and at the centre was 11.7 % and 6.1 %, respectively. For specimens with 0.5 wt % of Kenolube P11 compacted at 110ºC and 400 MPa, porosity at the edge and at the centre was represented by 2.7 % and 1.5 %, respectively.

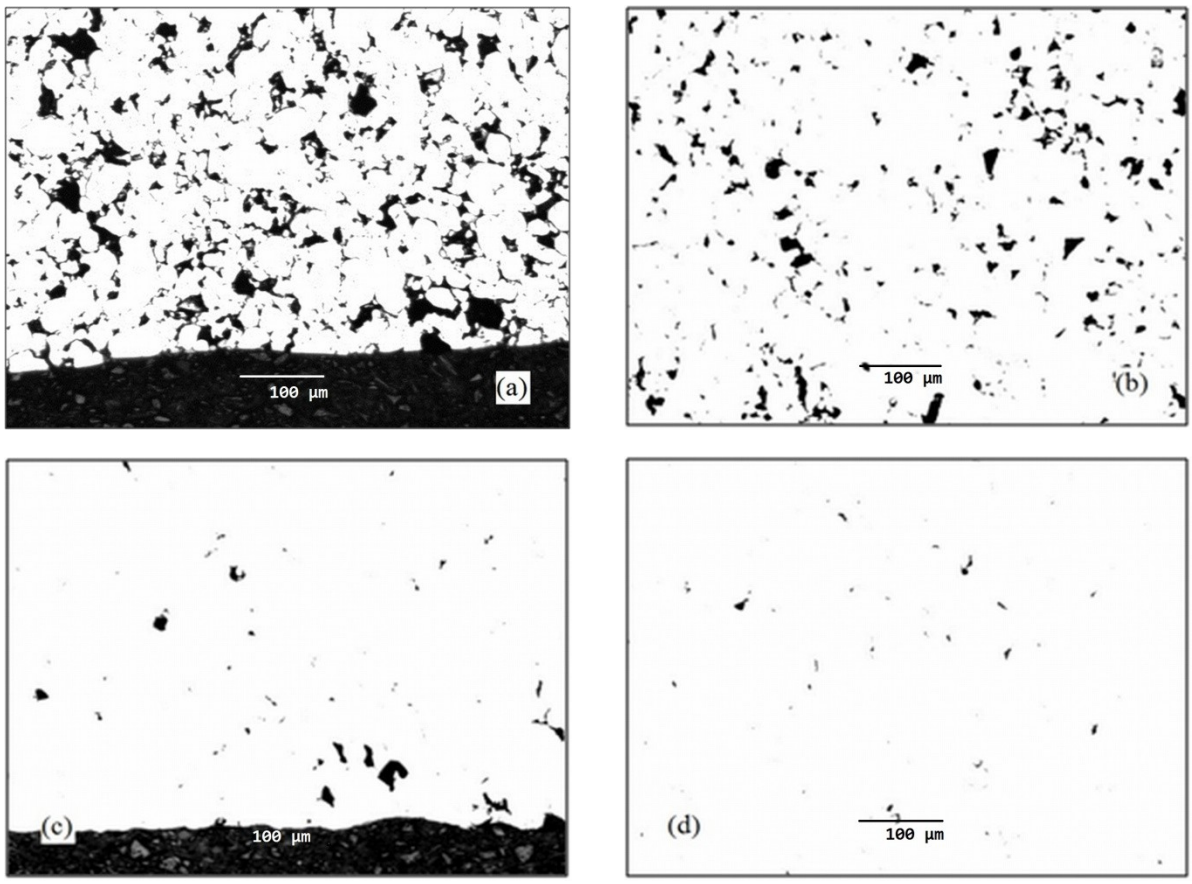

Figure 4.17: Distribution of porosity (a-b) specimen with 1.5 wt % of Acrawax C, (c-d) specimen with 0.5 wt % of Acrawax C; (a) and (c) the edge of the specimen and (b) and (d) the centre of specimen.

4.6 Effect of Compaction Pressure and Temperature on Sintered/Aged Density of Alumix 123 Compacts

Higher compaction pressure, compaction temperature and reduction in lubricant content led to higher green density, subsequently resulted in higher sintered density of specimens.

4.6.1 Acrawax C

Figure 4.18 shows the sintered/aged density (a-c) and relative sintered/aged density (d-f) as a function of various compaction pressures, temperatures and Acrawax C contents. It can be said that sintered density followed the tendency of green compacts with Acrawax C contents. As mentioned above, higher green density gives higher sintered density.

The maximum sintered density for specimens with Acrawax C content of 0.5 wt % was measured to be 98.26 % (2.751 g/cm^3) of TD. The specimens were compacted by a pressure of 400 MPa at a temperature of 110ºC. For Acrawax C content of 1.0 wt % the maximum sintered density reached for specimens compacted at a pressure of 400 MPa and temperature of 110ºC was of 97.28 % (2.724 g/cm^3) of TD. The highest sintered density for specimens with Acrawax C content of 1.5 wt % was measured to be 95.68 % (2.679 g/cm^3) of TD at pressing conditions of 400 MPa and 110ºC. The list of sintered/aged and relative sintered/aged densities for specimens with Acrawax C can be found in table A5 in the appendix.

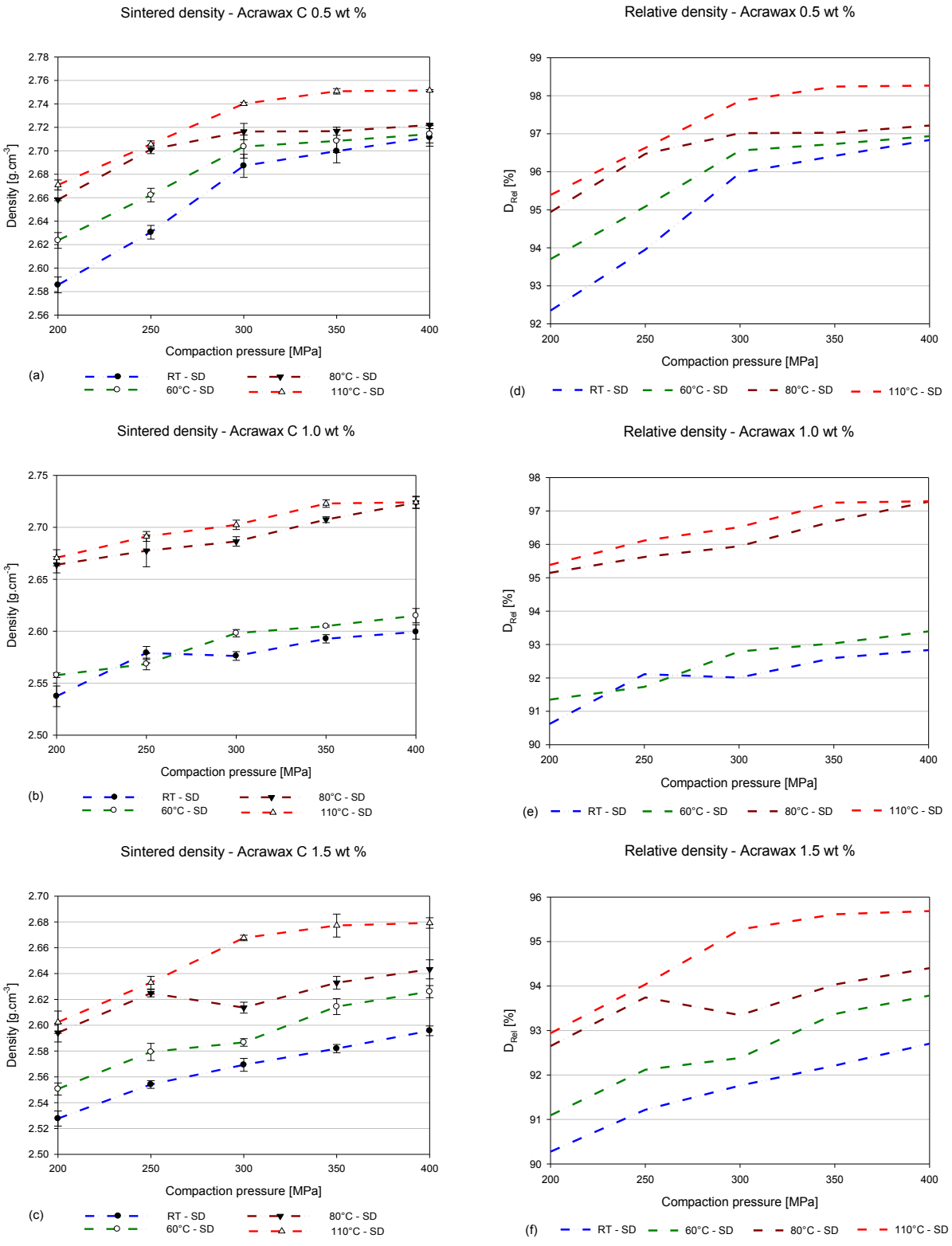

Figure 4.18: Sintered/aged density (a-c) and D_{Rel} - relative sintered/aged density (d-f) of Alumix 123 specimens as a function of pressure and temperature with Acrawax C contents of 0.5 wt %, 1.0 wt % and 1.5 wt %. (SD – green density of the specimens)

4.6.2 Kenolube P11

Figure 4.19 shows the sintered/aged density of specimens (a-c) and relative sintered/aged density (d-f) versus different compaction pressures, temperatures and various Kenolube P11 contents. As with Acrawax C, the higher green density resulted in higher sintered density. However, the sintered densities of specimens with Kenolube P11 are slightly lower than those with Acrawax C. For all lubricant contents, the specimens compacted at 110ºC and pressure 400 MPa reached the highest sintered density as compared to other compaction pressures and temperatures.

The highest sintered density for 0.5 wt % Kenolube P11 was measured to be 95.83 % (2.683 g/cm^3) of TD. For Kenolube P11 content of 1.0 wt % the maximum sintered density reached 94.77 % (2.654 g/cm^3) of TD and for 1.5 wt % of Kenolube P11 the greatest sintered density was 94.69 % (2.651 g/cm^3) of TD. The list of sintered/aged and relative sintered/aged densities for specimens with Kenolube P11 can be found in table A6 in the appendix.

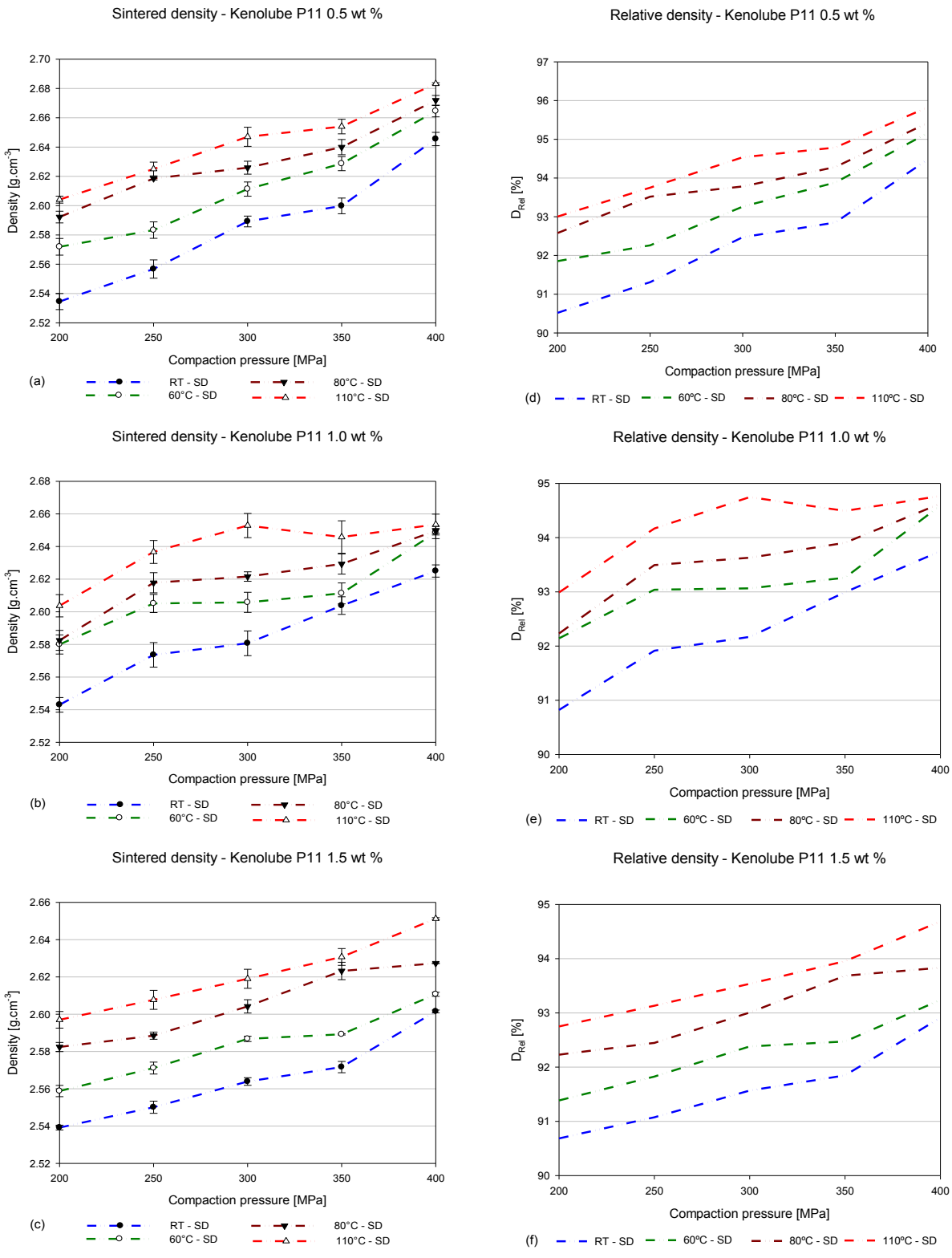

Figure 4.19: Sintered/aged density (a-c) and D_{Rel} - relative sintered/aged density (d-f) of Alumix 123 specimens as a function of pressure and temperature with Kenolube P11 contents of 0.5 wt %, 1.0 wt % and 1.5 wt %. (SD – green density of the specimens)

The sintered densities of Alumix 123 specimens with Acrawax C and Kenolube P11 content of 1.5 wt % were found to be similar to the sintered density of Alumix 123 specimens with Microwax C represented in table 1.1. When comparing the sintered densities of specimens compacted at RT and 250 MPa, sintered in nitrogen atmosphere at 590°C to 600ºC (low value of the sintered density in Table 1.1.), specimens with Acrawax C gave a slight increase in sintered density (2.554 g/cm^3) compared to specimens with Kenolube P11 and Microwax C (both 2.55 g/cm^3).

For green density, as well for sintered density Martín *et al.* [134] showed similar observation of the sintered density for Alumix 123. The sintered densities of specimens achieved value of 2.584 g/cm^3 for compaction pressure of 400 MPa at RT with 1.5 wt % of Microwax C. The increase between green and sintered density is 0.15 %. This is similar to Alumix 123 with 1.5 wt % of Kenolube P11 whereby densities increased by 0.19 % after sintering. In the case of specimens with Acrawax C the improvement was 0.92 %. However, in their study, specimens were sintered at 590ºC for 20 minutes, which is lower than to traditional sintering temperature of 600ºC for 30 minutes, respectively.

4.7 Mechanical Properties of Sintered/Aged Alumix 123 Compacts

4.7.1 Effect of Compaction Pressure and Temperature on Tensile Strength of Sintered/Aged Alumix 123 Compacts

4.7.1.1 Acrawax C

Figure 4.20 shows the tensile strength of sintered/aged specimens compacted at different temperatures and pressing pressures with Acrawax C contents of 0.5, 1.0 and 1.5 wt %. It was noted, that the green/sintered density and subsequent tensile strength increased with increasing compaction pressure, temperature and using lower lubricant content.

At a pressure of 400 MPa and temperature of 110ºC the specimens reached the maximum tensile strength values of 365.65, 343.51 and 324.90 MPa using Acrawax C contents of 0.5, 1.0 and 1.5 wt %, respectively.

For 0.5 wt % of Acrawax C (Figure 4.20 (a)) the tensile strength increased by 9.01 % when the compaction pressure changed from 200 to 400 MPa at RT. For a compaction temperature of 60ºC, the tensile strength increased by 6.68 % (when the compaction pressure increased from 200 to 400 MPa). The tensile strength increased by 14.4 and 11.48 % for compaction temperatures of 80 and 110ºC, respectively when the compaction pressure changed from 200 to 400 MPa.

For Acrawax C content of 1.0 wt % (Figure 4.20 (b)) the tensile strength increased by 5.3 % when the compaction pressure changed from 200 to 400 MPa at RT. At compaction temperatures of 60, 80 and 110ºC, the tensile strength increased by 8.3, 10.4 and 7.2 %, respectively when the compaction pressure changed from 200 to 400 MPa.

For Acrawax C content of 1.5 wt % (Figure 4.20 (c)) the tensile strength increased by 8.1 % when the compaction pressure changed from 200 to 400 MPa at RT. At a compaction temperature of 60ºC, the tensile strength increased by 7.5 %, for a given change of compaction pressures. The tensile strength increased by 6.5 and 10.8 % for compaction temperatures of 80 and 110ºC, respectively when the compaction pressure changed from 200 to 400 MPa.

The list of measured tensile strength values of sintered/aged specimens with Acrawax C is illustrated in table A7 in the appendix.

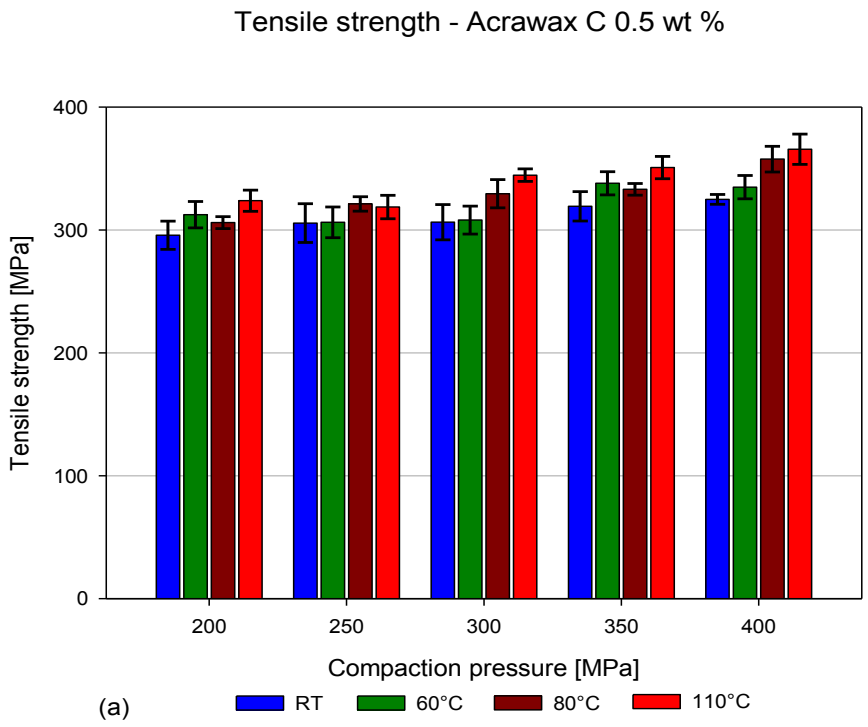

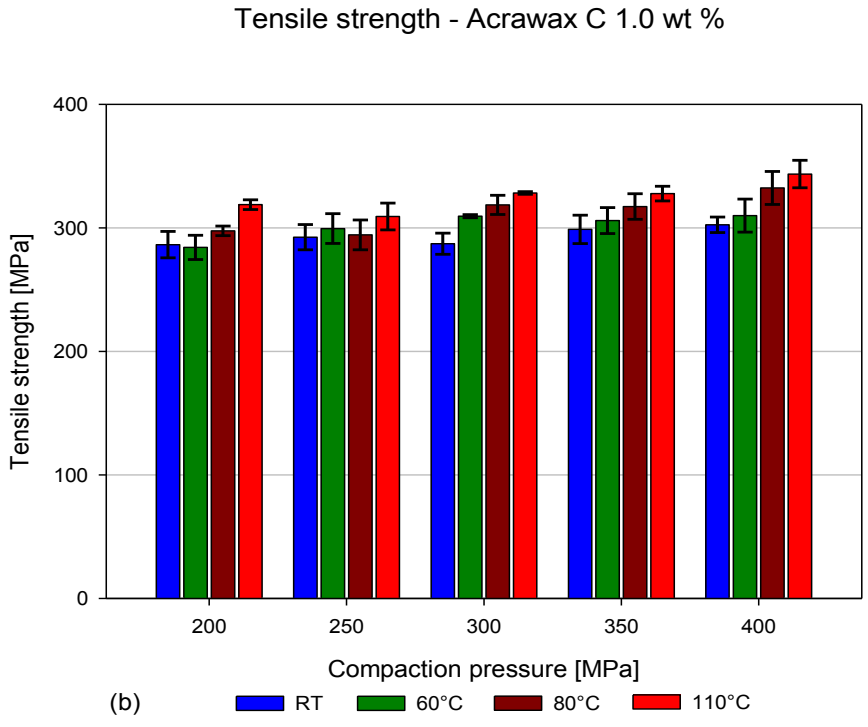

Figure 4.20 (a-b): Tensile strength of sintered/aged specimens compacted at different compaction pressures and temperatures with Acrawax C contents of (a) 0.5 wt % and (b) 1.0 wt %.

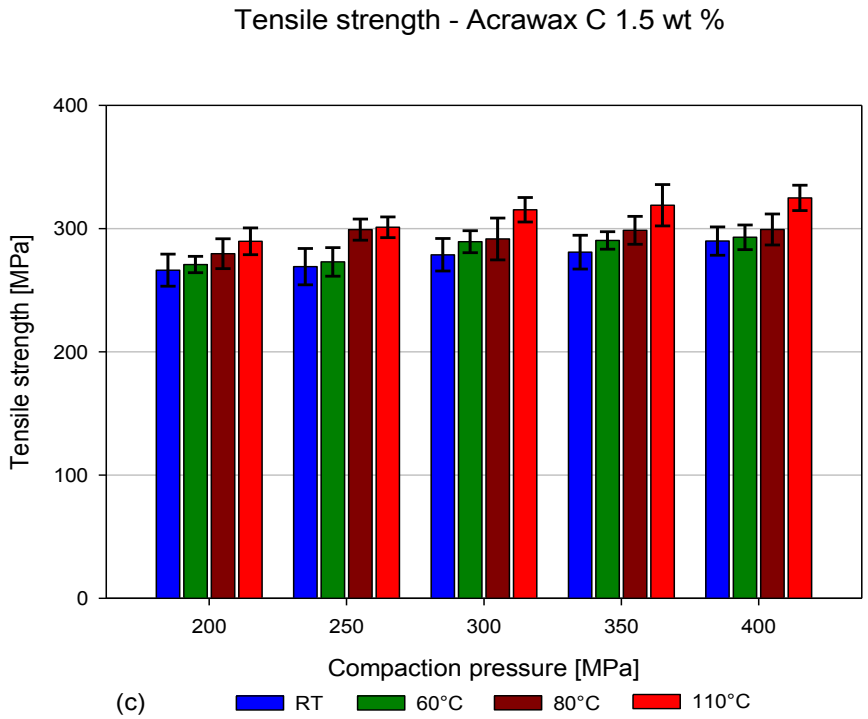

Figure 4.20 (c): Tensile strength of sintered/aged specimens compacted at different compaction pressures and temperatures with Acrawax C content of 1.5 wt %.

4.7.1.2 Kenolube P11

Figure 4.21 shows the tensile strength of sintered/aged specimens compacted with various compaction temperatures, pressures and Kenolube P11 contents. A similar trend on the effect of compaction pressure, temperature and lubricant amount on the tensile strength of specimens was found in Kenolube P11 as compared with Acrawax C.

At compaction pressure of 400 MPa and temperature of 110ºC the specimens reached the maximum values for tensile strength of 351.74, 320.87 and 309.98 MPa when using Kenolube P11 contents of 0.5, 1.0 and 1.5 wt %, respectively.

For 0.5 wt % of Kenolube P11 (Figure 4.21 (a)) the tensile strength increased by 10.6 % when compaction pressure changed from 200 to 400 MPa at RT. The tensile strength

increased by 11.9, 11.6 and 12.6 %, for compaction temperatures of 60, 80 and 110ºC, respectively for a given change of compaction pressures.

For 1.0 wt % of Kenolube P11 (Figure 4.21 (b)) the tensile strength increased by 5.7 % when compaction pressure changed from 200 to 400 MPa at RT. At a compaction temperature of 60ºC, the tensile strength increased by 10.6 % for a given change of compaction pressures. The tensile strength increased by 8.7 and 8.8 %, for compaction temperature of 80 and 110ºC, respectively for a given change of compaction pressures.

For Kenolube P11 content of 1.5 wt % (Figure 4.21 (c)) the tensile strength increased by 6.8 % when compaction pressure changed from 200 to 400 MPa at RT. At a compaction temperature of 60ºC, the tensile strength increased by 8.6 %, when compaction pressure increased from 200 to 400 MPa. The tensile strength increased by 13 and 10.6 % for compaction temperatures of 80 and 110ºC, respectively, when compaction pressure changed from 200 to 400 MPa.

The list of measured value of the tensile strength of sintered/aged specimens with Kenolube P11 can be found in table A8 in the appendix.

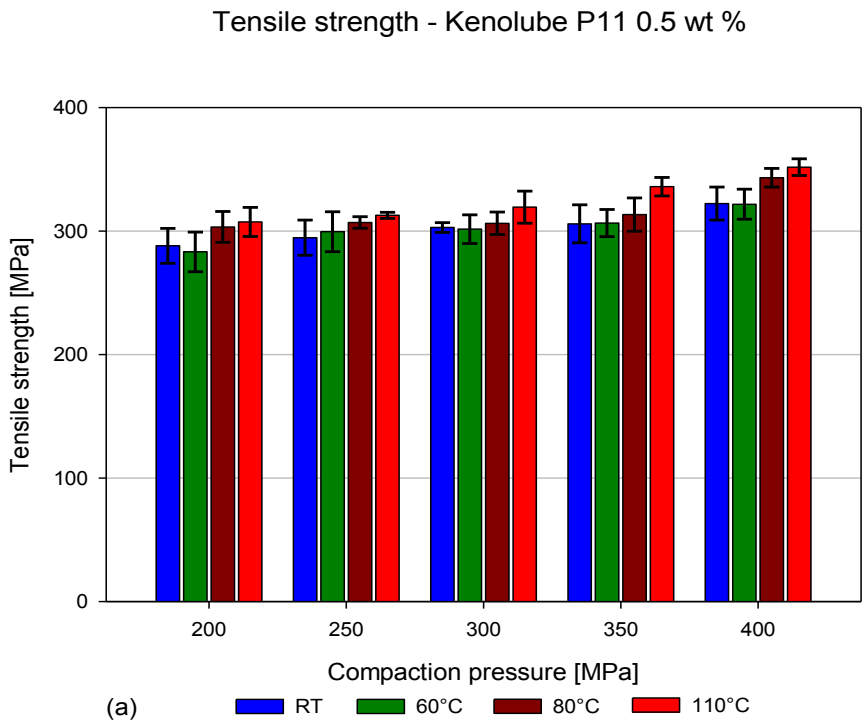

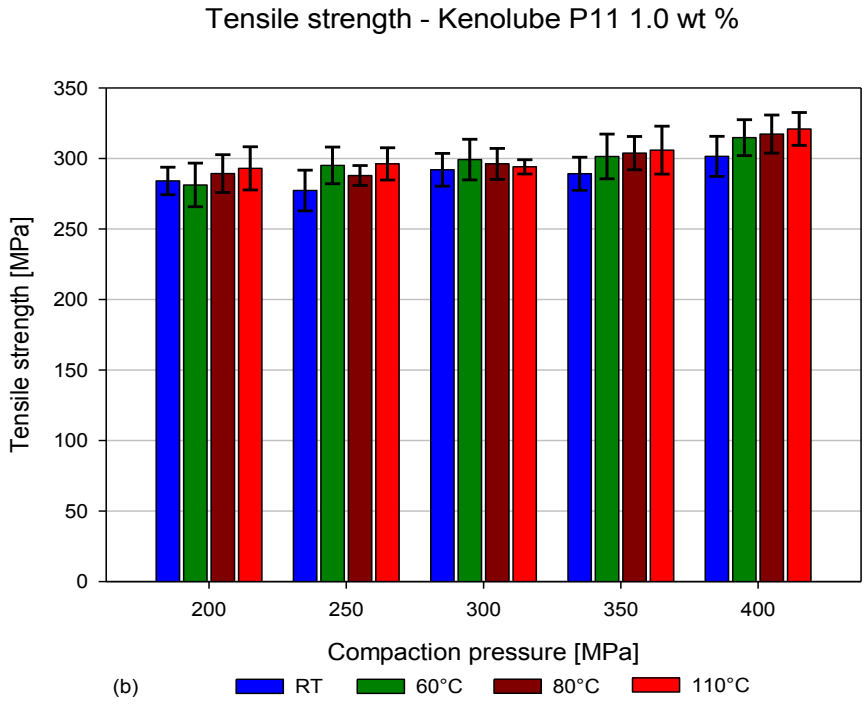

Figure 4.21 (a-b): Tensile strength of sintered/aged specimens compacted at different compaction pressures and temperatures with Kenolube P11 contents of (a) 0.5 wt % and (b) 1.0 wt %.

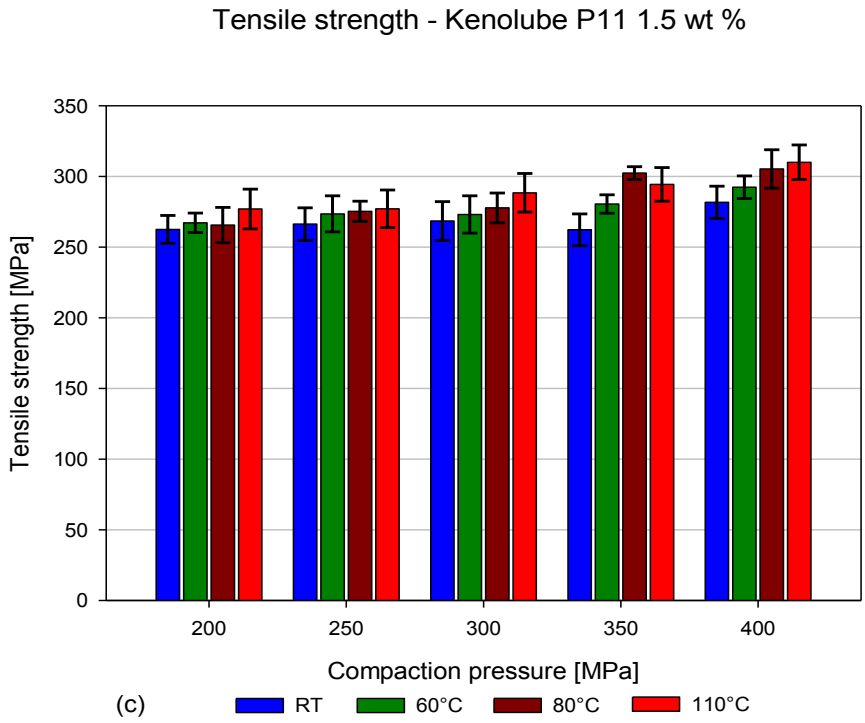

Figure 4.21 (c): Tensile strength of sintered/aged specimens compacted at different compaction pressures and temperatures with Kenolube P11 content of 1.5 wt %.

Martín *et al.* [159] found the tensile strength of sintered/aged Alumix 123 specimens with Microwax C to be 388 ± 26 MPa. This value is comparable to tensile strengths of Alumix 123 with Acrawax C and Kenolube P11 (365.65 ± 12.36 and 351.74 ± 6.74 MPa, respectively) in this present study. It was noted that specimens in the Martín *et al.* work were prepared at RT and 400 MPa with green/sintered density of 2.61 ± 0.02 and 2.745 ± 0.006 g/cm^3, respectively. However, in the present study the similar values of densities were obtained by compaction at 110ºC and 400 MPa. This is due to using single punch pressing.

4.7.2 Effect of Compaction Pressure and Temperature on Hardness of Sintered/Aged Alumix 123 Compacts

4.7.2.1 Acrawax C

Figure 4.22 shows the hardness of sintered/aged specimens obtained from compacts prepared using various compaction pressures and temperatures with Acrawax C contents of 0.5, 1.0 and 1.5 wt %. By decreasing the amount of Acrawax C and increasing compaction temperature and pressure, the hardness of specimens increased.

At compaction pressure of 400 MPa and temperature 110ºC the maximum hardness of sintered/aged specimens was 128.6, 119.51 and 117.31 HV for Acrawax C contents of 0.5, 1.0 and 1.5 wt %, respectively.

For Acrawax C content 0.5 wt % (Figure 4.22 (a)) when compaction temperatures changed from RT to 110ºC the hardness increased by 6.2, 10, 13.7, 14 and 15 %, for compaction pressures 200, 250, 300, 350 and 400 MPa, respectively.

For Acrawax C content 1.0 wt % (Figure 4.22 (b)) when compaction temperatures changed from RT to 110ºC the hardness increased by 6.6, 9.7, 3.9, 6.4 and 13.5 %, for compaction pressures 200, 250, 300, 350 and 400 MPa, respectively.

For Acrawax C content 1.5 wt % (Figure 4.22 (c)) when compaction temperatures changed from RT to 110ºC the hardness increased by 4.9, 4, 9.2, 6.4 and 11 %, for compaction pressures 200, 250, 300, 350 and 400 MPa, respectively.

The list of the hardness values of sintered/aged specimens with Acrawax C is illustrated in table A9 in the appendix.

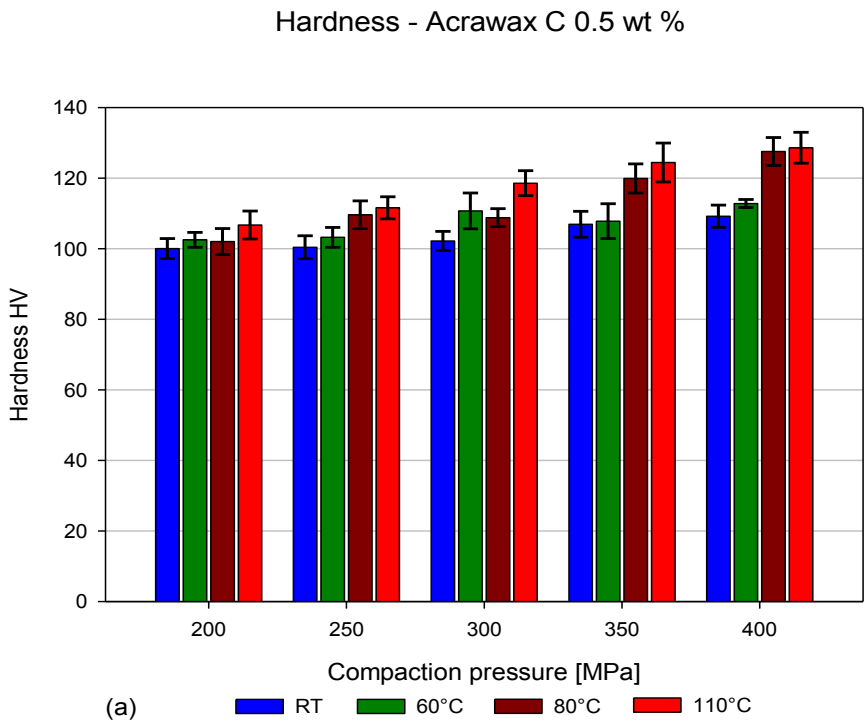

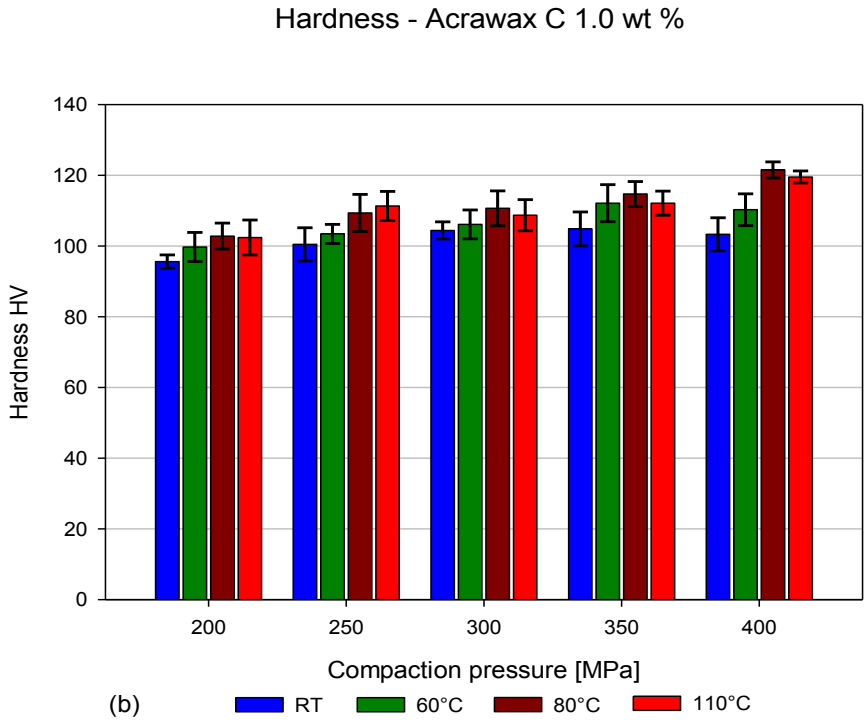

Figure 4.22 (a-b): Hardness of sintered/aged specimens obtained from compacts prepared at various compression pressures and temperatures with Acrawax C contents of (a) 0.5 wt % and (b) 1.0 wt %.

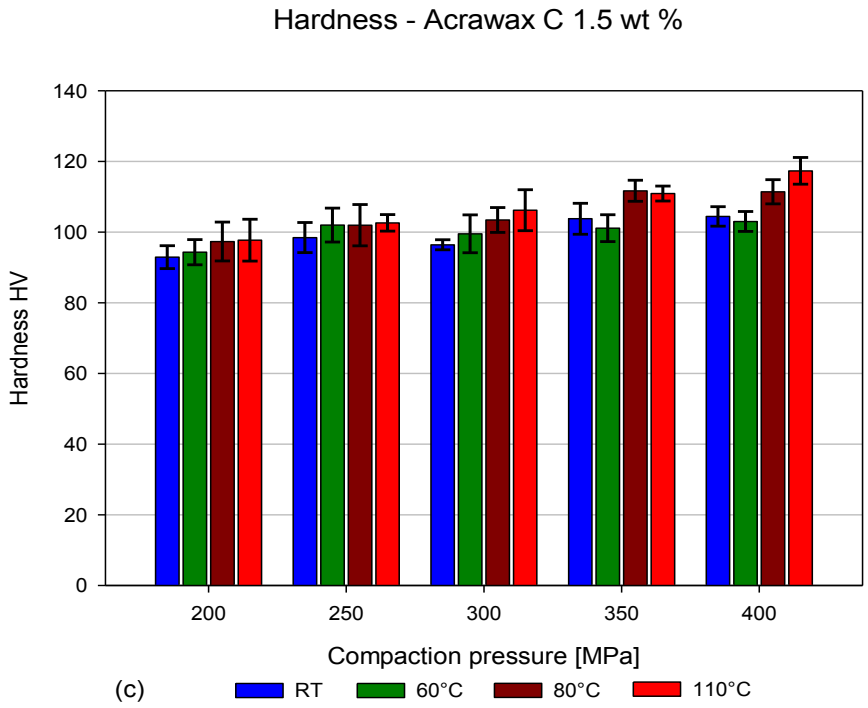

Figure 4.22 (c): Hardness of sintered/aged specimens obtained from compacts prepared at various compression pressures and temperatures with Acrawax C content of 1.5 wt %.

4.7.2.2 Kenolube P11

Figure 4.23 shows the hardness of sintered/aged specimens with Kenolube P11 contents of 0.5, 1.0 and 1.5 wt % compacted at different pressures and temperatures.

At a compaction pressure of 400 MPa and temperature of 110ºC the maximum hardness of sintered/aged specimens was found to be 117.93, 115.45 and 113.25 HV for Kenolube P11 contents of 0.5, 1.0, 1.5 wt %, respectively.

For Kenolube P11 content 0.5 wt % (Figure 4.23 (a)) when compaction temperatures changed from RT to 110ºC the hardness increased by 5, 9, 8.7, 9.6 and 7.6 %, for compaction pressures 200, 250, 300, 350 and 400 MPa, respectively.

For Kenolube P11 content of 1.0 wt % (Figure 4.23 (b)) when compaction temperatures changed from RT to 110ºC the hardness improved by 7.3, 8, 8.6, 9 and 11.3 %, for compaction pressures 200, 250, 300, 350 and 400 MPa, respectively.

For Kenolube P11 content of 1.0 wt % (Figure 4.23 (c)) when compaction temperatures changed from RT to 110ºC the hardness increased by 4.3, 8.2, 10.2, 9.9 and 10.3 %, for compaction pressures 200, 250, 300, 350 and 400 MPa, respectively.

The list of the hardness values of sintered/aged specimens with Kenolube P11 can be found in table A10 in the appendix.

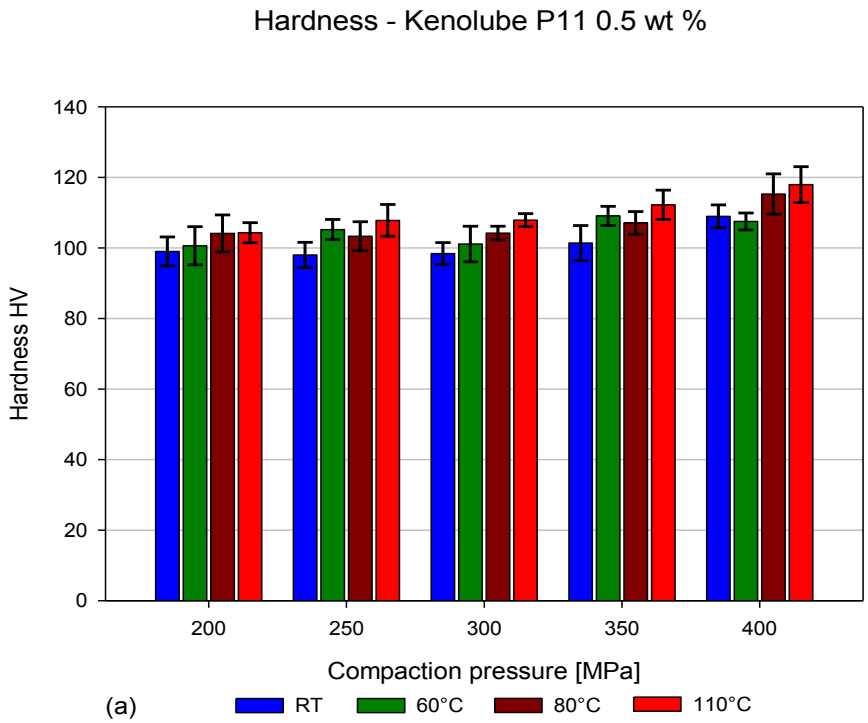

Figure 4.23 (a): Hardness of sintered/aged specimens obtained from compacts prepared at various compression pressures and temperatures with Kenolube P11 content of 0.5 wt %.

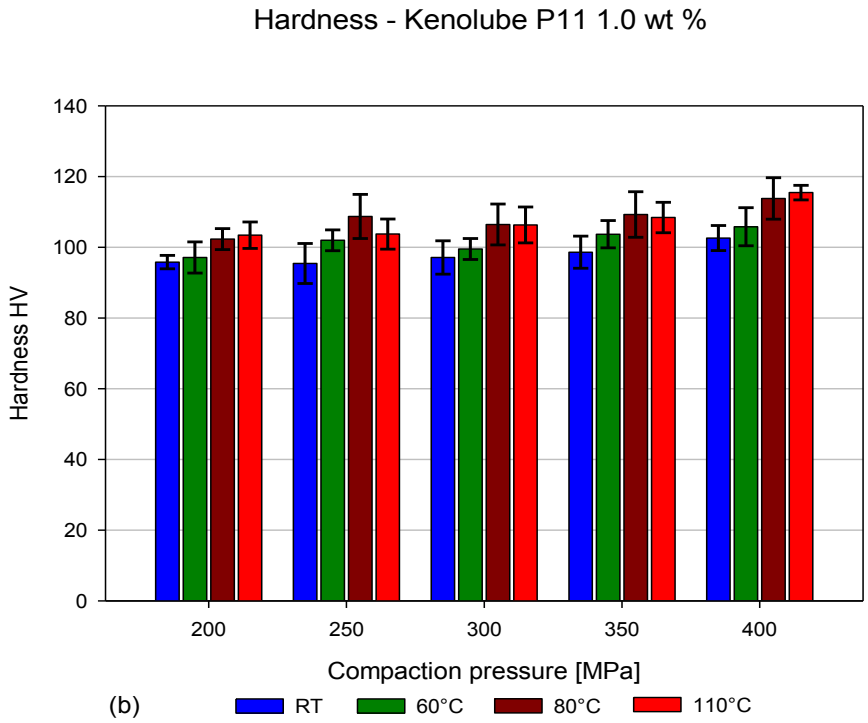

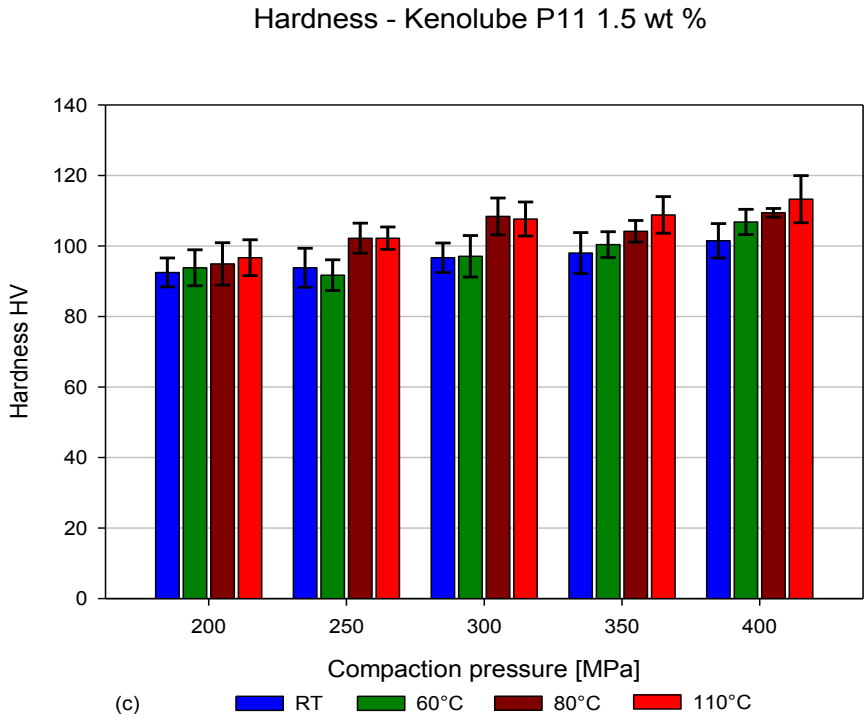

Figure 4.23 (b-c): Hardness of sintered/aged specimens obtained from compacts prepared at various compression pressures and temperatures with Kenolube P11 contents of (b) 1.0 wt % and (c) 1.5 wt %.

Martín *et al.* [159] found the hardness of Alumix 123 specimens with sintered density 2.73 g/cm^3 to be 76 HV (HRF = 73) in as-sintered state with sintering at 590ºC for 20 minutes. After heat treatment T6 at 160ºC for 16 hour the hardness increased to 131 HV (HRF = 97). These results are comparable with the hardness obtained in this study, where hardness of sintered/aged specimens with density of 2.75 g/cm^3 was measured to be 128 HV.

4.7.3 Effect of Compaction Pressure and Temperature on Elongation of Sintered/Aged Alumix 123 Compacts

As observed before (Section 4.7.1) with increasing green/sintered density the tensile strength of the specimens increases. Comparable behaviour is visible at the elongation of sintered/aged specimens, where specimens compacted with higher pressure and elevated compaction temperature and lower amounts of admixed lubricant reached better elongation. Figure 4.24 shows typical plots of force versus elongation development for the specimens with Acrawax C content of 0.5 and 1.5 wt %. Acrawax C content of 1.0 wt % has similar progress of elongation as specimens with lubricant content of 1.5 wt %. Specimens were compacted at 400 MPa and temperatures of RT and 110ºC. The plots validate that higher green/sintered density results in higher tensile strength and subsequently larger elongation.

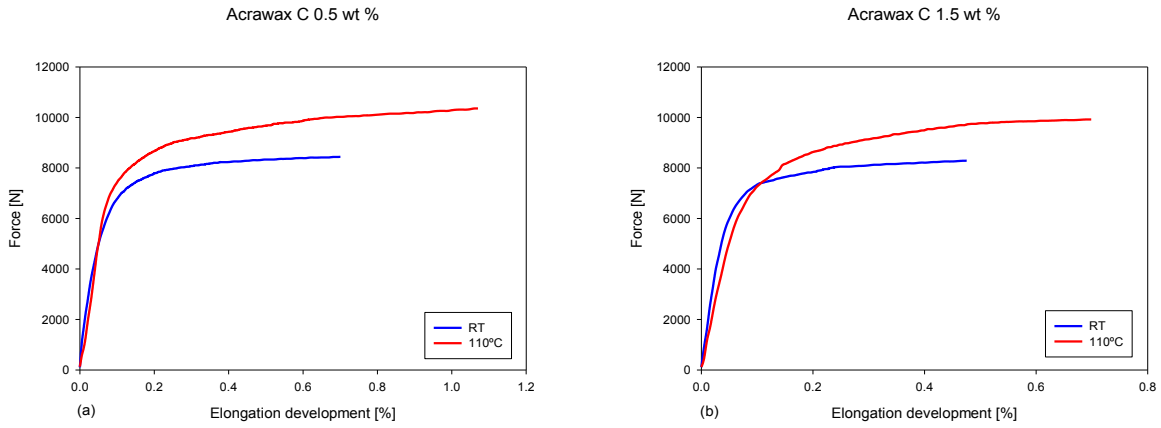

Figure 4.24: Process dependence between force versus elongation development for the sintered/aged specimens compacted at 400 MPa and compaction temperature RT and 110ºC with Acrawax C contents of (a) 0.5 wt % and (b) 1.5wt %.

4.7.3.1 Acrawax C

Figure 4.25 shows the elongation of the sintered/aged specimens with different compaction pressures and temperatures and Acrawax C contents of 0.5, 1.0 and 1.5 wt %. It can be seen, that higher compaction pressure, temperature and lower lubricant content led to an increase in the elongation.

For compaction pressure of 400 MPa and temperature of 110ºC the maximum values of the elongation were measured to be 1.11, 0.82 and 0.7 % for specimens prepared using 0.5, 1.0 and 1.5 wt % of Acrawax C, respectively.

For Acrawax C content of 0.5 wt % (Figure 4.25 (a)) the increase of the elongation between compaction temperatures RT and 110ºC was found to be 37.6, 40, 26.5, 28.2 and 26.9 %, for compaction pressures of 200, 250, 300, 350 and 400 MPa, respectively.

For 1.0 wt % of Acrawax C (Figure 4.25 (b)) the increase of the elongation between compaction temperatures of RT and 110ºC was found to be 29.8, 23.8, 26.8, 33.6 and 31.8 % for compaction pressures of 200, 250, 300, 350 and 400 MPa, respectively.

For Acrawax C content of 1.5 wt % (Figure 4.25 (c)) the increase of the elongation between compaction temperatures of RT and 110ºC was found to be 10.34, 19.7, 20.1, 21.9, and 23.8 % for compaction pressures 200, 250, 300, 350 and 400 MPa, respectively.

The list of measured elongation values of sintered/aged specimens with Acrawax C is illustrated in table A11 in the appendix.

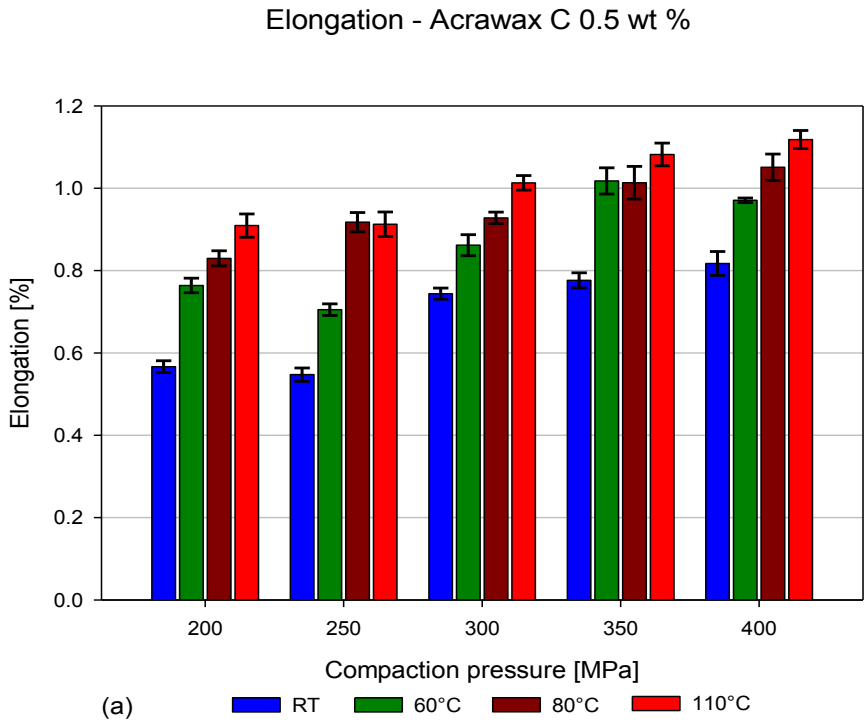

Figure 4.25 (a): Elongation of sintered/aged specimens using various compaction pressures and temperatures with Acrawax C content of 0.5 wt %.

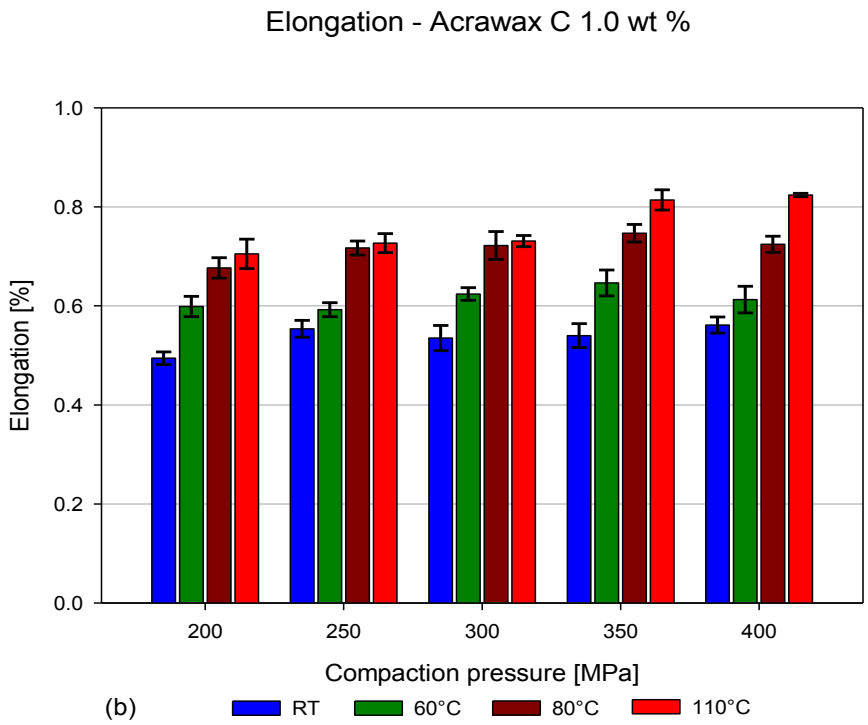

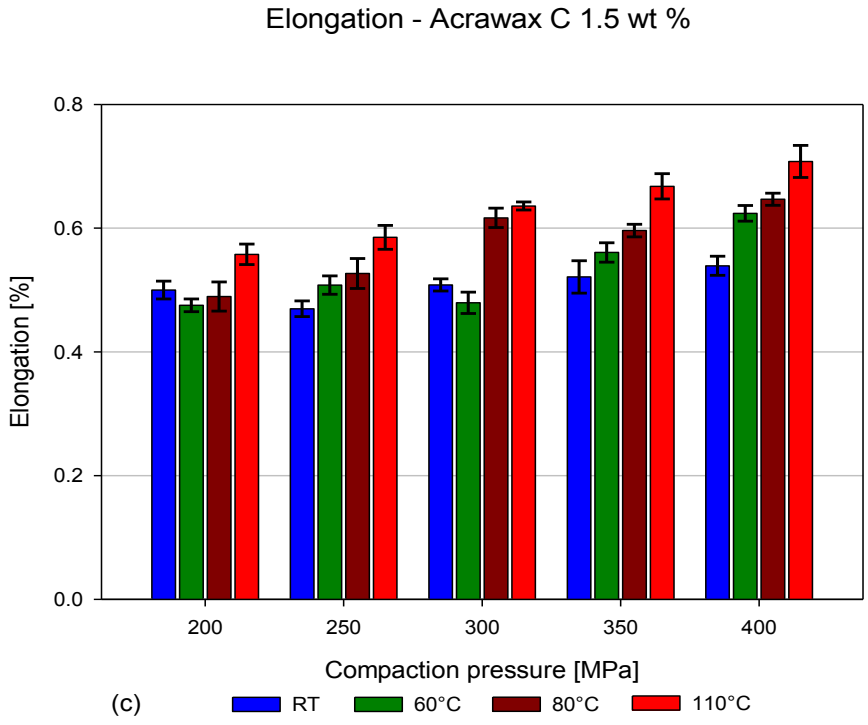

Figure 4.25 (b-c): Elongation of sintered/aged specimens using various compaction pressures and temperatures with Acrawax C contents of (b) 1.0 wt % and (c) 1.5 wt %.

4.7.3.2 Kenolube P11

The elongation of sintered/aged specimens with different compaction pressures, temperatures and various Kenolube P11 contents is plotted in figure 4.26.

For compaction pressure of 400 MPa and temperature of 110ºC the maximum values of the elongation were measured to be 0.93, 0.72 and 0.7 % for specimens prepared using 0.5, 1.0 and 1.5 wt % of Kenolube P11, respectively.

For Kenolube P11 content of 0.5 wt % (Figure 4.26 (a)) the improvement of the elongation between compaction temperatures of RT and 110ºC was found to be 28.5, 16.1, 21.1, 18.5 and 27.1 % for compaction pressures of 200, 250, 300, 350 and 400 MPa, respectively.

For Kenolube P11 content of 1.0 wt % (Figure 4.26 (b)) the improvement of the elongation between compaction temperatures of RT and 110ºC was found to be 9.6, 11.6, 7.6, 8.9 and 16.4 % for compaction pressures of 200, 250, 300, 350 and 400 MPa, respectively.

For Kenolube P11 content of 1.5 wt % (Figure 4.26 (c)) the improvement of the elongation measured between compaction temperatures of RT and 110ºC was found to be 13.5, 17.9, 28.4, 21.3 and 25.5 % for compaction pressures 200, 250, 300, 350 and 400 MPa, respectively.

The list of measured elongation values of sintered/aged specimens with Kenolube P11 is located in table A12 in the appendix.

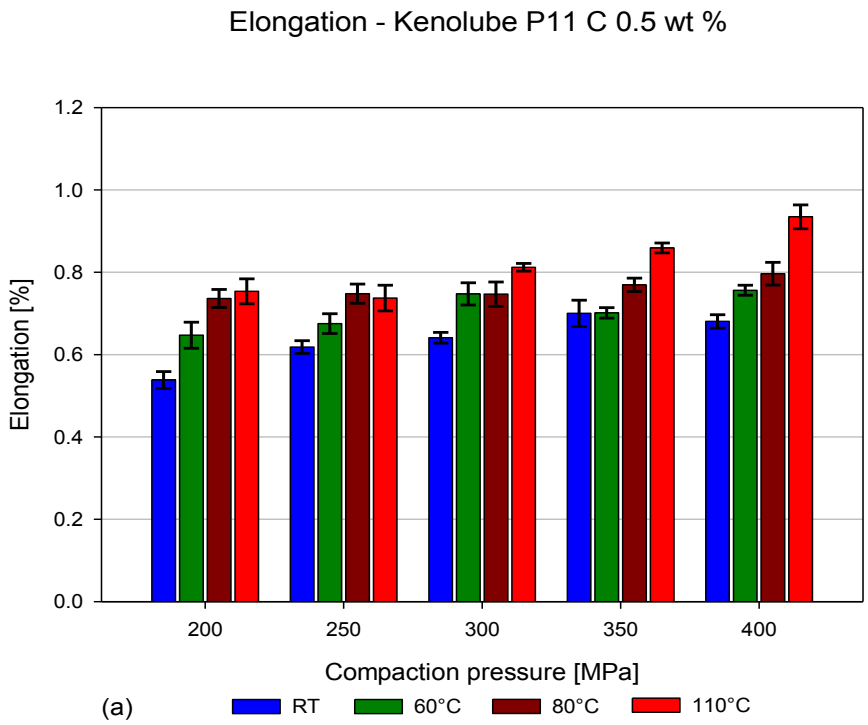

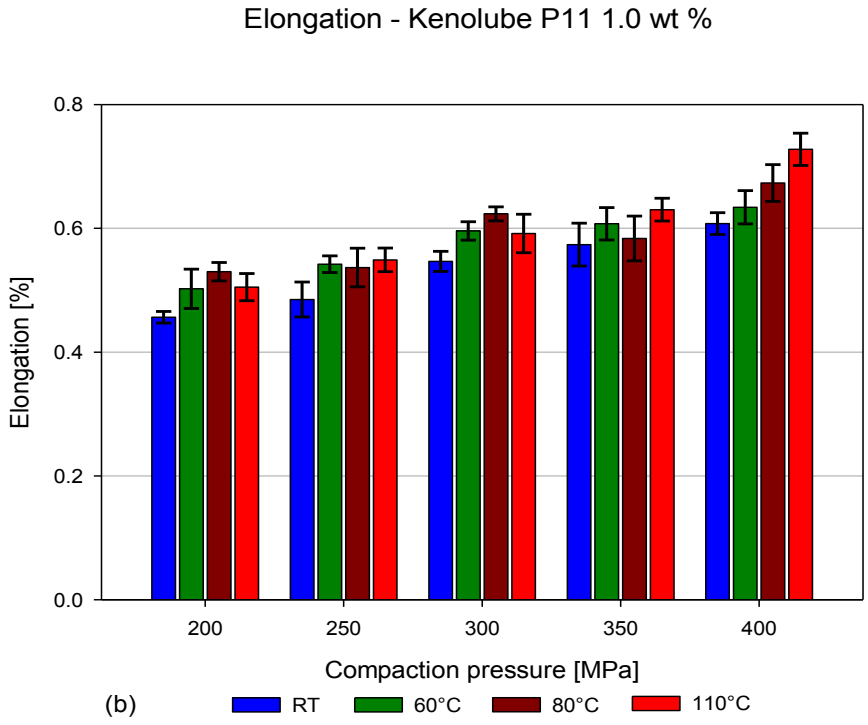

Figure 4.26 (a-b): Elongation of sintered/aged specimens using various compaction pressures and temperatures with Kenolube P11contents of (a) 0.5 wt % and (b) 1.0 wt %.

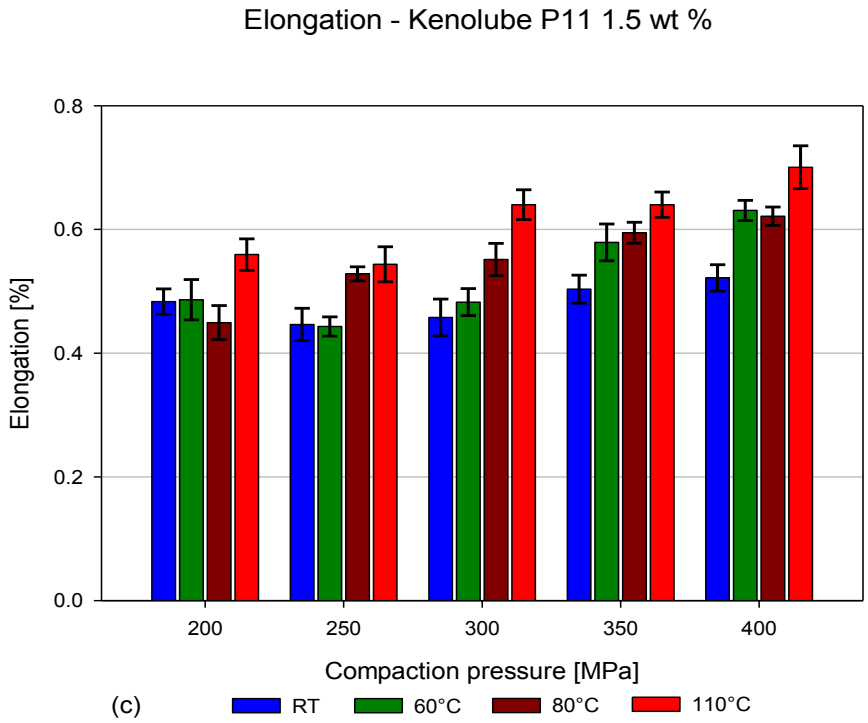

Figure 4.26 (c): Elongation of sintered/aged specimens using various compaction pressures and temperatures with Kenolube P11 content of 1.5 wt %.

The elongation of Alumix 123 specimens with Acrawax C and Kenolube P11 content of 1.5 wt % is close to the elongation of Alumix 123 specimens with Microwax C which is given in table 1.1. The lower values of elongation are affected by porosity level and heat treatment. When precipitation hardening is applied, the hardness and strength of specimens increased and there was also a moderate loss of elongation. [160] This trend was also observed in a study by Martín *et al.* [159]. They found that elongation after T6 (aging at 160ºC for 16 hours) decreased to 0.26 ~ 0.73 % compared to as-sintered where the elongation reached 2.9 ± 1.2 %. A recent study by Hearda *et al.* [161] on another aluminium system (Alumix 231) showed similar trends in sintered/aged elongation, thus age hardening decreased the elongation of the specimens.

4.7.4 Effect of Compaction Pressure and Temperature on Young's Modulus of Sintered/Aged Alumix 123 Compacts

4.7.4.1 Acrawax C

Figure 4.27 shows Young's modulus of sintered/aged specimens compacted at various compaction pressures, temperatures and Acrawax C contents.

For a compaction pressure of 400 MPa and temperature of 110ºC the maximum values of Young's modulus of sintered/aged specimens were measured to be 69.73, 67.88 and 65.88 GPa, for Acrawax C contents of 0.5, 1.0 and 1.5 wt %, respectively.

When the pressure for Acrawax C content 0.5 wt % (Figure 4.27 (a)) increased from 200 to 400 MPa, the Young's modulus increased by 8.5, 6.7, 8.7 and 10.6 % at RT, 60 , 80 and 110ºC, respectively,

When the pressure for Acrawax C content of 1.0 wt % (Figure 4.27 (b)) increased from 200 to 400 MPa, the Young's modulus increased by 5.8, 6.3, 9.5 and 9.6 % for RT, 60 , 80 and 110ºC, respectively.

When the pressure for Acrawax C content of 1.5 wt % (Figure 4.27 (c)) increased from 200 to 400 MPa, the Young's modulus increased by 10.5, 6.3, 6.4 and 7.1 % for RT, 60, 80 and 110ºC, respectively.

The list of calculated Young's modulus values for sintered/aged specimens with Acrawax C is shown in table A13 in the appendix.

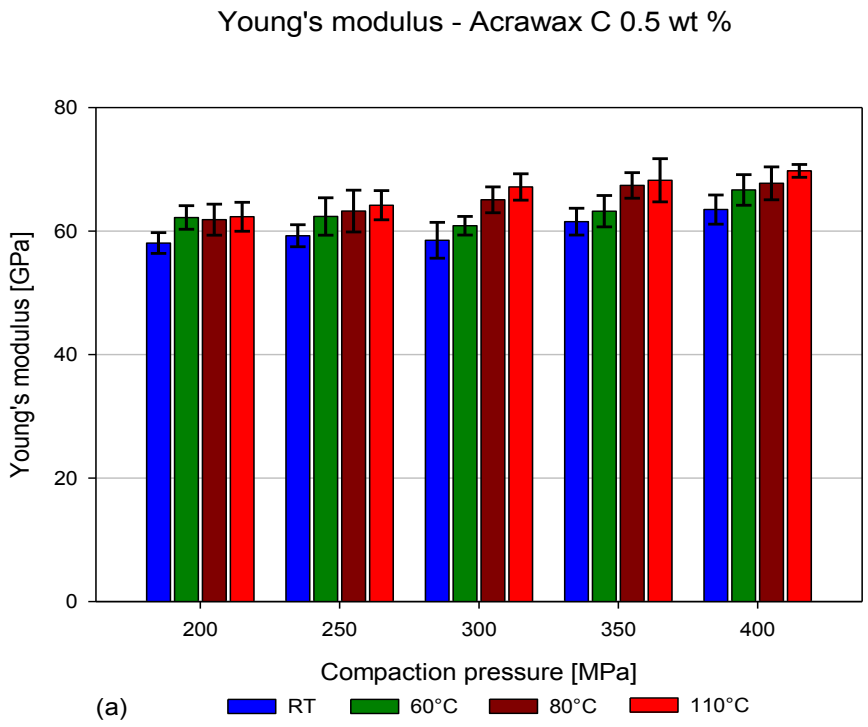

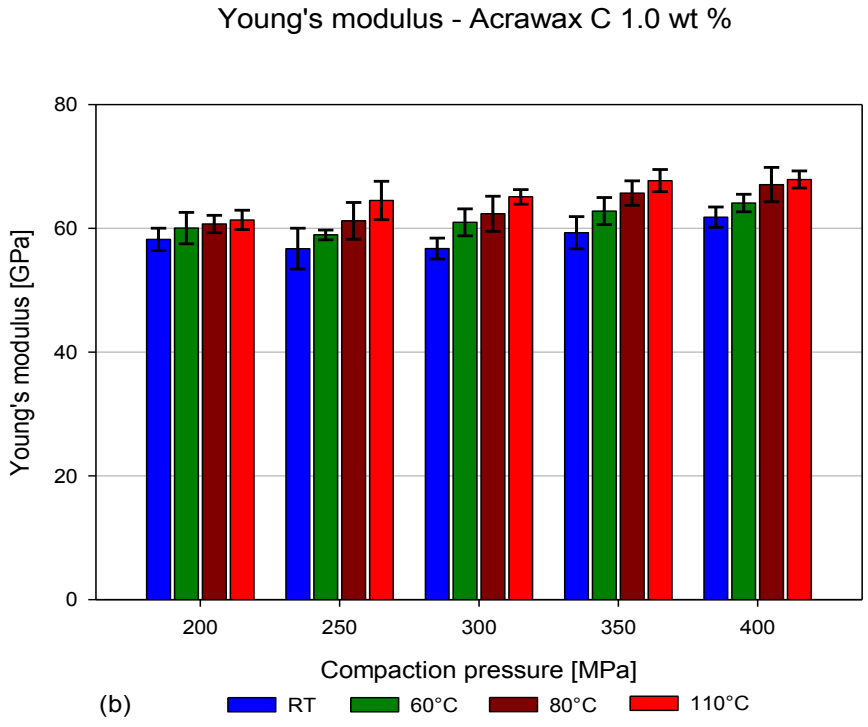

Figure 4.27 (a-b): Young's modulus of sintered/aged specimens using various compaction pressures and temperatures with Acrawax C contents of (a) 0.5 wt % and (b) 1.0 wt%.

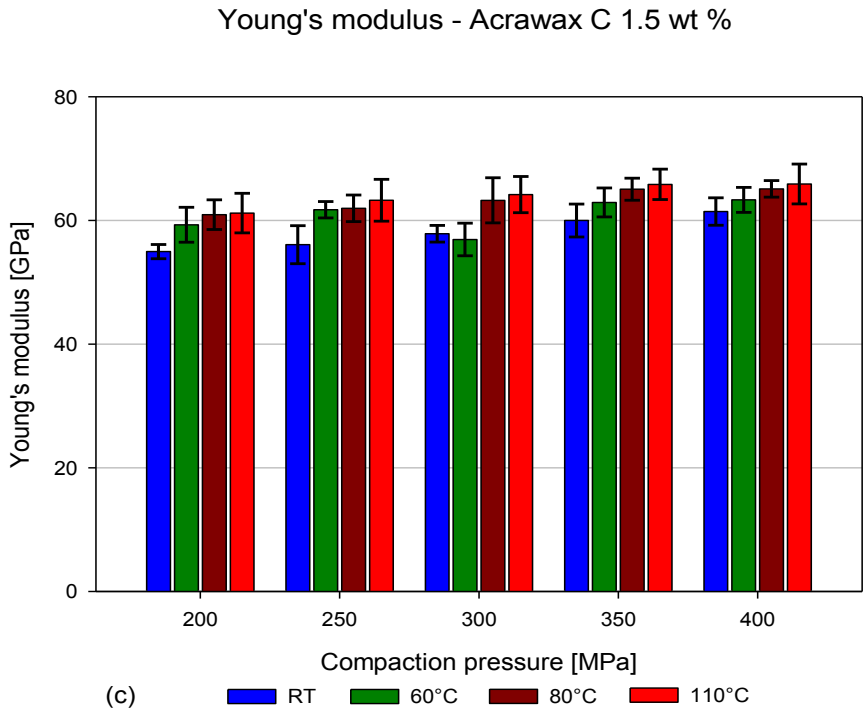

Figure 4.27 (c): Young's modulus of sintered/aged specimens using various compaction pressures and temperatures with Acrawax C content of 1.5 wt %.

4.7.4.2 Kenolube P11

Figure 4.28 shows Young's modulus of sintered/aged specimens compacted at various pressures, temperatures and Kenolube P11 contents. A similar trend as for Acrawax C was noted. The higher compaction pressures and temperatures, and lower amount of lubricant led to higher values of Young's modulus.

For compaction pressure of 400 MPa and temperature of 110ºC, the maximum values of Young's modulus for sintered/aged specimens were found to be 68.44, 66.78 and 65.34 GPa for lubricant contents of 0.5, 1.0 and 1.5 wt %, respectively.

When the compaction pressure for Kenolube P11 content of 0.5 wt % (Figure 4.28 (a)) increased from 200 to 400 MPa the Young's modulus increased by 8.7, 9.1, 8.2 and 6.5 % for RT, 60, 80 and 110ºC, respectively.

When the compaction pressure for Kenolube P11 content of 1.0 wt % (Figure 4.28 (b)) increased from 200 to 400 MPa the Young's modulus increased by 11.1, 7.2, 7.6 and 8.5 % for RT 60, 80 and 110ºC, respectively.

When the compaction pressure for Kenolube P11 content of 1.5 wt % (Figure 4.28 (c)) increased from 200 to 400 MPa the Young's modulus increased by 8.8, 11.9, 7.8 and 7.8 % for RT, 60, 80 and 110ºC, respectively.

The list of calculated Young's modulus values for sintered/aged specimens with Kenolube P11 is illustrated in table A14 in the appendix.

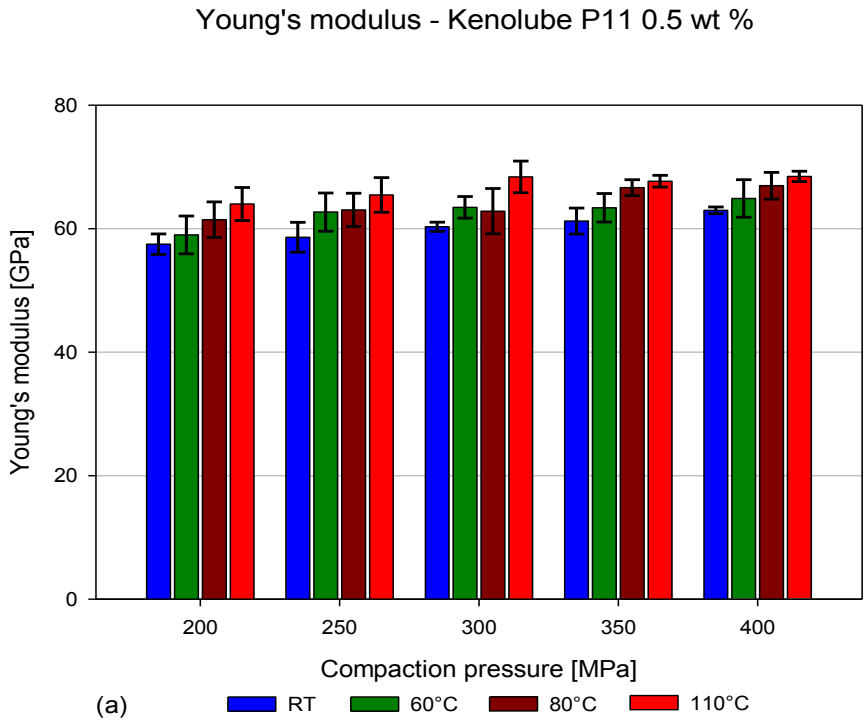

Figure 4.28 (a): Young modulus of sintered/aged specimens using various compaction pressures and temperatures with Kenolube P11 content of 0.5 wt %.

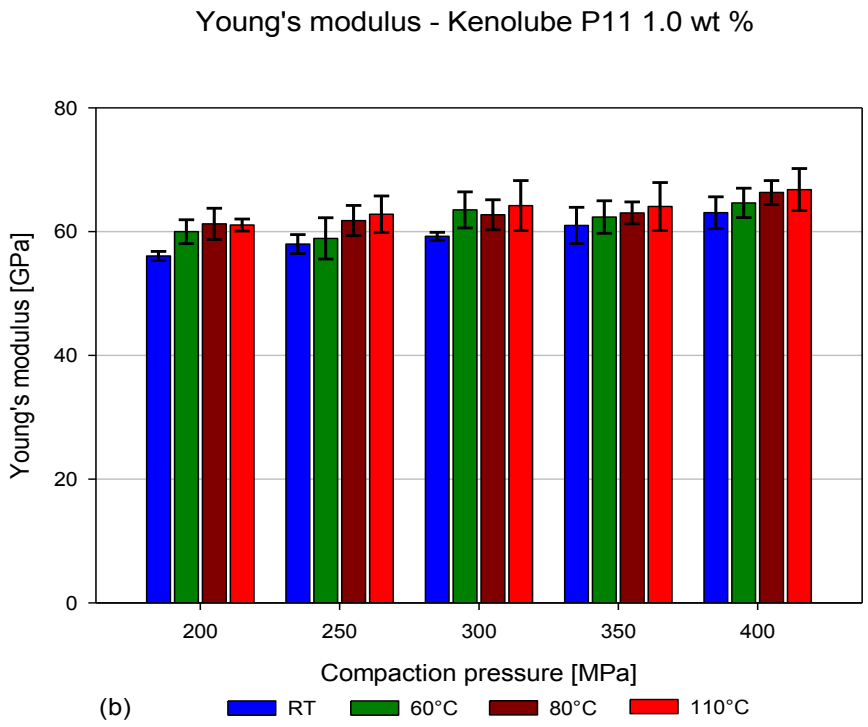

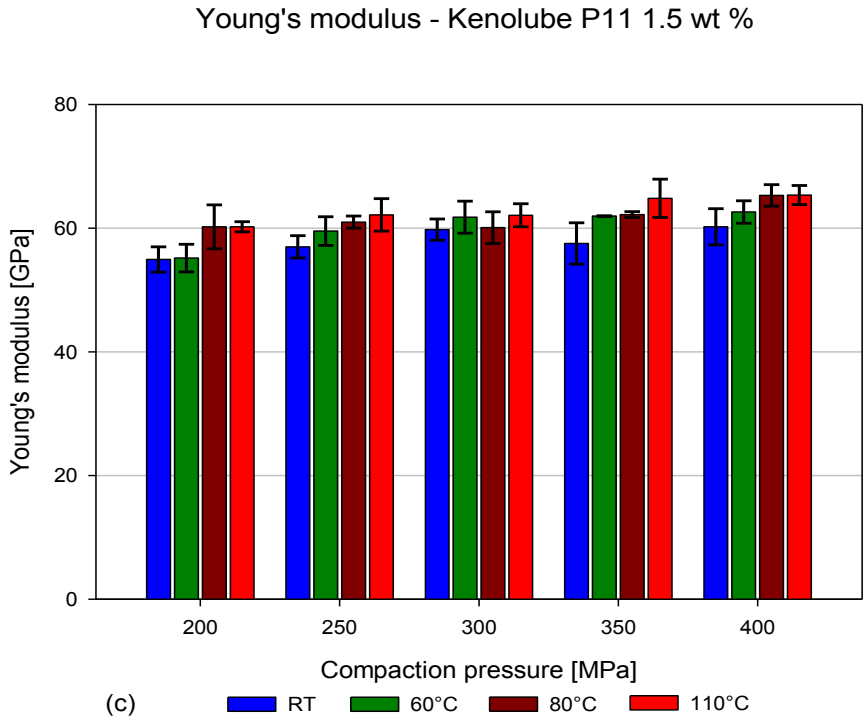

Figure 4.28 (b-c): Young modulus of sintered/aged specimens using various compaction pressures and temperatures with Kenolube P11 contents of (b) 1.0 wt % and (c) 1.5 wt %.

The highest value of Young's modulus was found to be 69.73 GPa for Acrawax C content of 0.5 wt %, which is 94.52 % of Young's modulus for wrought Al 2014A alloy (73 GPa). A study by Martín *et al.* [159] on Alumix 123 with Microwax C showed similar values of Young's Modulus (70 ± 10 GPa).

4.7.5 Correlation between Tensile Strength, Young's Modulus and Porosity

Generally, increased porosity detrimentally affects the mechanical property of powder compacts. It reduces the effective cross sectional area such that the mechanical property is dependent on the minimum solid-contact area. In addition, porosity leads to stress concentration near the pores so that under mechanical loading, the true stress in the material is higher near the pores than farther away from them. [162]

4.7.5.1 Correlation between Tensile Strength and Porosity

Several empirical or theoretical expressions for the relationship between tensile strength and porosity of powder metallurgy compacts have been proposed. Assuming that tensile strength is function of sintered density Salak *et.al* [163] found that the tensile strength of a powder compact relative to the fully dense material can be represented by:

$$\sigma_{rel} = \frac{\sigma}{\sigma_0} = exp(-4.3\eta) \qquad \text{(eq. 4.2)}$$

where σ_{rel} is the relative tensile strength of the sintered powder compact, σ is the tensile strength of the powder compact, σ_0 is the tensile strength of the fully dense material, and η is the fractional porosity.

Fleck and Smith [164] reported a simple model where the relative tensile strength of a sintered compact is related to the fractional porosity. In this model the pores and particles in the compact are represented as a layered, randomly organized array of cubes. Using the probability that a pore exists at a specific location, they formulate the equation:

$$\sigma_{rel} = \frac{\sigma}{\sigma_0} = (1 - \eta^{\frac{2}{3}})^2 \qquad \text{(eq. 4.3)}$$

with the same notation as in equation 4.2.

Tronshenko [165] found the relative strength of sintered ferrous compacts follows the relationship:

$$\sigma_{rel} = \frac{\sigma}{\sigma_0} = \frac{(1-\alpha\eta)}{(1+\alpha\beta\eta)} \qquad \text{(eq. 4.4)}$$

where α is a factor relating to the surface area of the transverse cross section occupied by the pores, and β is a parameter determining the non-uniformity of the stress distribution over the cross section. For spherical pores, α is estimated to be 1.5. For ferrous compacts, β is known to be 2.

Exner and Pohl [166] have determined that the relationship between the relative tensile strength and fractional porosity of sintered compacts can be shown by the following equation:

$$\sigma_{rel} = \frac{\sigma}{\sigma_0} = exp(-k\eta) \quad \text{(eq. 4.5)}$$

which is a generalization of equation 4.2. The slope k of the plots is related to the morphology of the pores. In the ideal model, if the k value is close to 1, pores are spherical or cylindrical. However, by empirical investigation it was found that the k value can be close up to 10. Hong *et al.* [167] reported the k value for SiC_w 2124 Al to be 15.5 due to high sensitivity of the pores to the tensile strength of the composite. The high value of k is due to irregularly shaped pores which lead to a stress concentration effect around the pores. So the higher value of k the greater the stress concentration effect becomes.

4.7.5.1.1 Acrawax C

Figure 4.29 displays the relative tensile strength values (σ_{rel}) plotted as a function of fractional porosity (η) for 0.5, 1.0 and 1.5 wt % of Acrawax C.

Equation 4.4 is presented four times, with different values of α and β. Equation 4.5 is presented twice with different values of k. By adjusting these parameters the equations can take into account the pore morphology. The adjusted parameters for 0.5, 1.0 and 1.5 wt % of Acrawax C are in table 4.9.

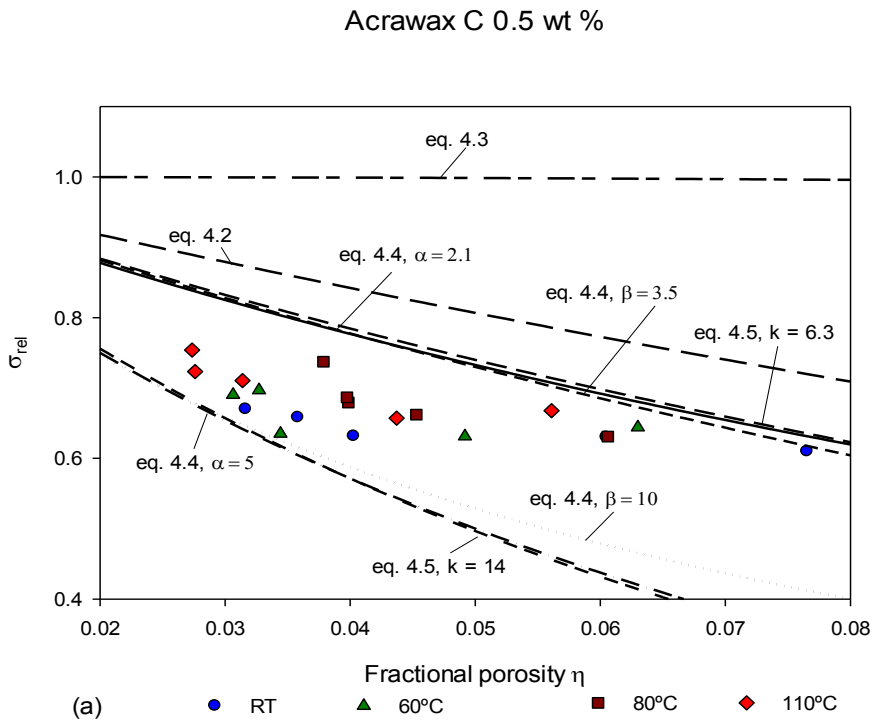

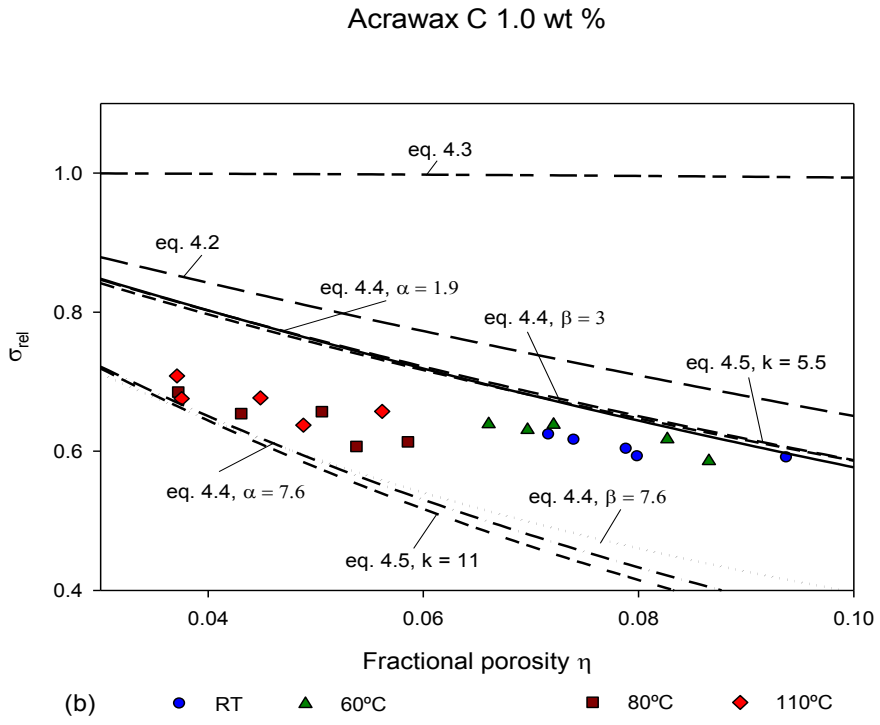

Figure 4.29 (a-b): Relative tensile strength values (σ_{rel}) plotted as a function of fractional porosity (η) for Acrawax C contents of (a) 0.5 wt % and (b) 1.0 wt %.

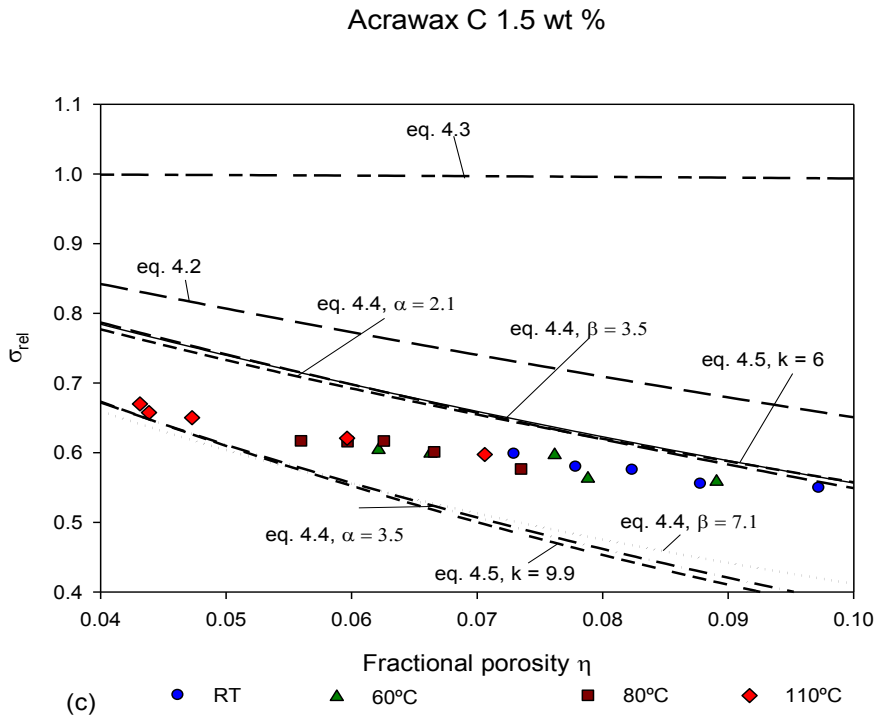

Figure 4.29 (c): Relative tensile strength values (σ_{rel}) plotted as a function of fractional porosity (η) for Acrawax C content of 1.5 wt %.

Table 4.9: The adjusted parameters to incorporate the pore morphology

Acrawax C	**Limit**	**α [β = 2]**	**β [α = 1.5]**	**k**
0.5 wt %	Upper	2.1	3.5	6.3
	Lower	5	10	14
1.0 wt %	Upper	1.9	3	5.5
	Lower	3.8	7.6	11
1.5 wt %	Upper	2.1	3.5	6
	Lower	3.5	7.1	9.9

4.7.5.1.2 Kenolube P11

Figure 4.30 shows the relative tensile strength values (σ_{rel}) plotted as a function of fractional porosity (η) for 0.5, 1.0 and 1.5 wt % of Kenolube P11.

Equation 4.4 is presented four times, with different values of α and β, and equation 4.5 is presented twice with different values of k. The adjusted parameters for 0.5, 1.0 and 1.5 wt % of Kenolube P11 are in table 4.10.

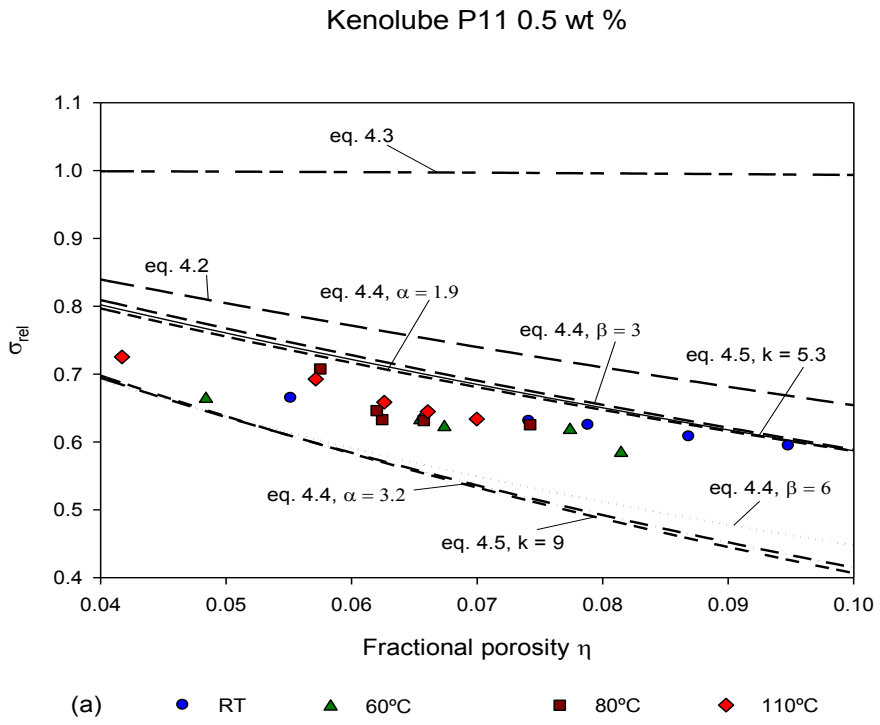

Figure 4.30 (a): Relative tensile strength values (σ_{rel}) plotted as a function of fractional porosity (η) for Kenolube P11 content of 0.5 wt %.

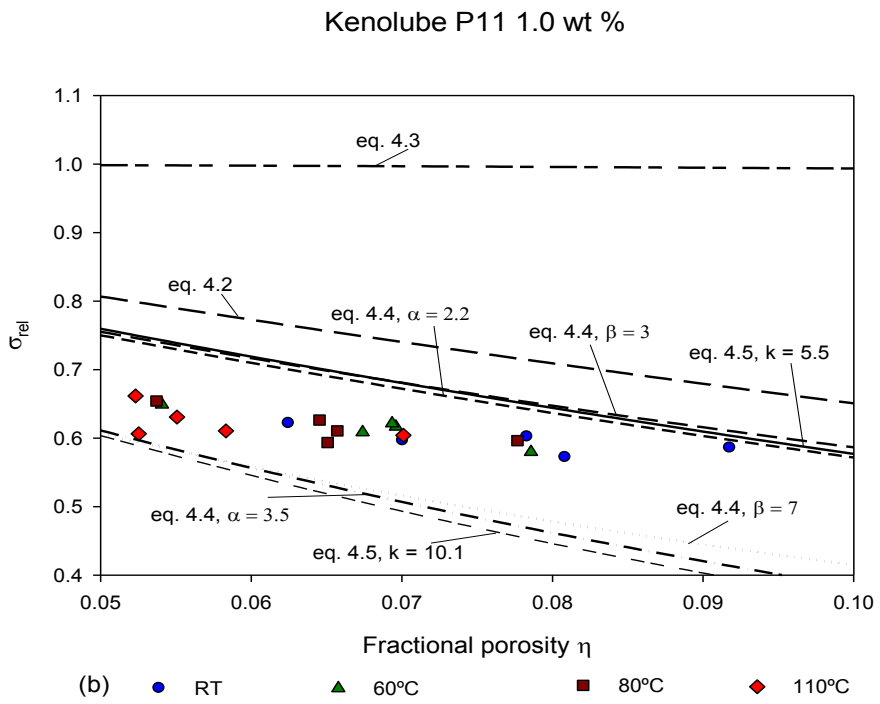

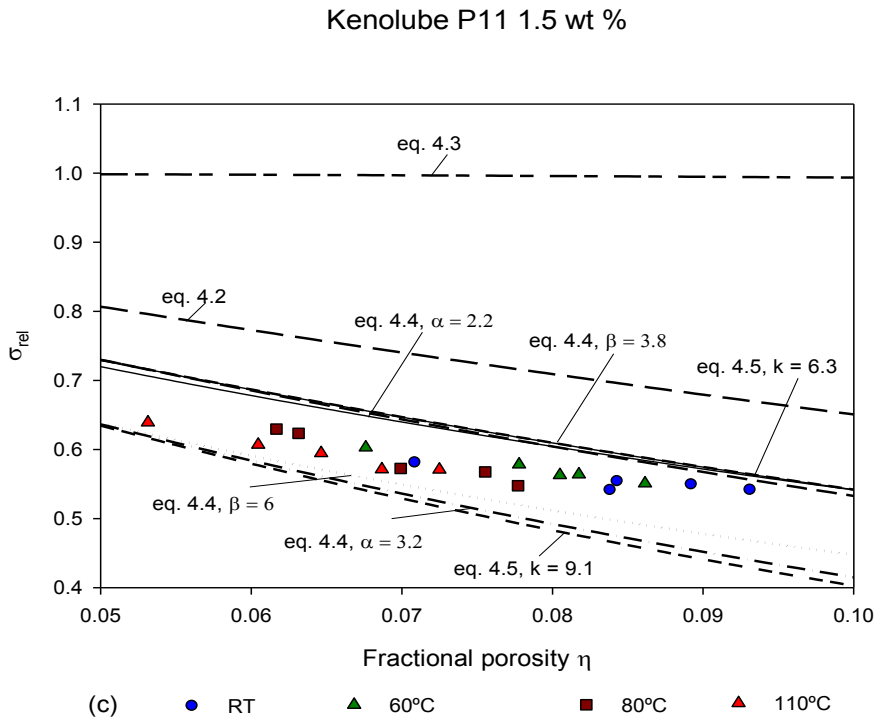

Figure 4.30 (b-c): Relative tensile strength values (σ_{rel}) plotted as a function of fractional porosity (η) for Kenolube P11 contents of (b) 1.0 wt % and (c) 1.5 wt %.

Table 4.10: The adjusted parameters to incorporate the pore morphology

Kenolube P11	**Limit**	**α [β = 2]**	**β [α = 1.5]**	**k**
0.5 wt %	Upper	1.9	3	5.3
	Lower	3.2	6	9
1.0 wt %	Upper	2.2	3	5.5
	Lower	3.5	7	10.1
1.5 wt %	Upper	2.2	3.8	6.3
	Lower	3.2	6	9.1

4.7.5.2 Correlation between Young's Modulus and Porosity

Various models have been developed for prediction of Young's modulus for a porous material at given porosity. These models include linear dependence, exponential dependence or semi-empirical equations.

Fryxell and Chandler [168] reported a linear relationship between Young's modulus and fractional porosity which is represented by the following equation:

$$E = E_0(1 - a\eta) \qquad \text{(eq. 4.6)}$$

where E is the Young's modulus of the compact, E_0 is the Young's modulus of the fully dense material, a is a material constants and η is the fractional porosity.

Spriggs [169] found that the Young's modulus of porous material relative to the fully dense material can be evaluated by equation:

$$E = E_0 \exp(-b\eta) \quad \text{(eq. 4.7)}$$

with the same notation as in equation 4.6; b is a material constant.

Wagh *et al.* [170] developed a model in which they take into consideration randomness of the microstructure, i.e. shapes, sizes and distributions of pores. The model is formulated by equation:

$$E = E_0(1-\eta)^n \quad \text{(eq. 4.8)}$$

with the same notation as in equation 4.6.

In addition, they also observed that the value of the exponent n depends on grain size and pore size of the porous ceramic material under investigation and that the value could vary from 2 to 5. Wong *et al.* [171] using this model, showed that there is very little difference between open and total porosity, implying a negligibly small fraction of closed pores. This justifies the use of the open porosity model in this case, even at low porosity.

Ramakrishnan and Arunachalam [172] developed a model in which a single spherical pore is surrounded by a spherical matrix. In addition, this model also considers the intensification of pressure on the pore surface due to interaction of pores in the material. Considering this, the Young's modulus of a material with a given fractional porosity, is governed by the following equation:

$$E = E_0 \left[\frac{(1-\eta)^2}{1+\kappa_E \eta}\right] \quad \text{(eq. 4.9)}$$

with the same notation as in equation 4.6. κ_E is a constant which is related to the Poisson's ratio v_0 of the fully dense material:

$$\kappa_E = 2 - 3v_0 \quad \text{(eq. 4.10)}$$

For a fully dense wrought Al 2014 T6, Poisson's ratio is approximately 0.33.

4.7.5.2.1 Acrawax C

Figure 4.31 plots the relationship of E/E_0 as a function of fractional porosity η for 0.5, 1.0 and 1.5 wt % of Acrawax C. As in correlation of tensile strength and porosity, adjustment of parameters in equations 4.6, 4.7 and 4.8 can incorporate the pore morphology. The adjusted parameters for equation 4.6, 4.7 and 4.8 for 0.5, 1.0 and 1.5 wt % of Acrawax C are listed in table 4.11.

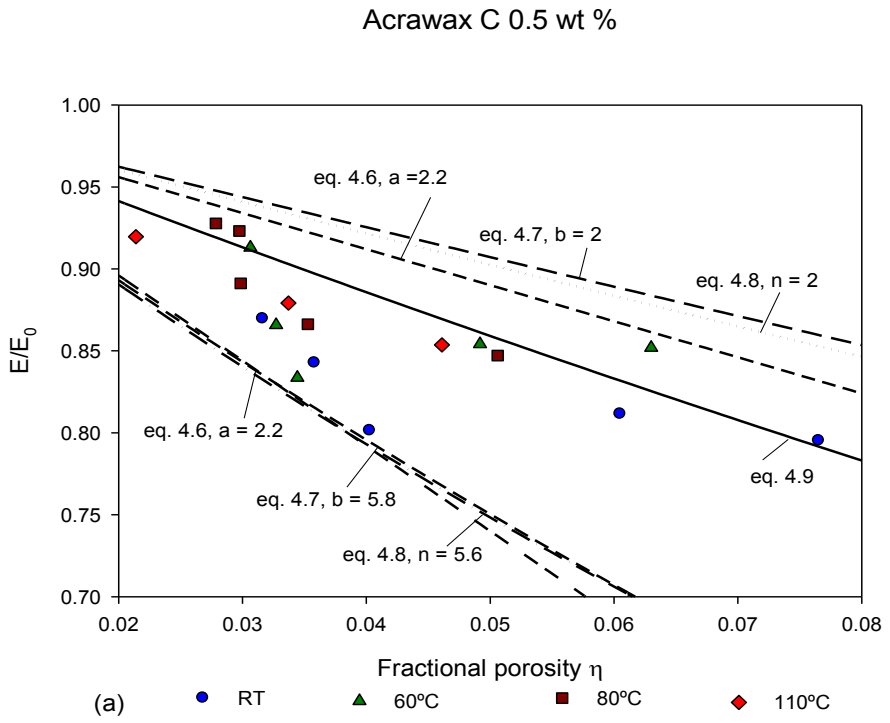

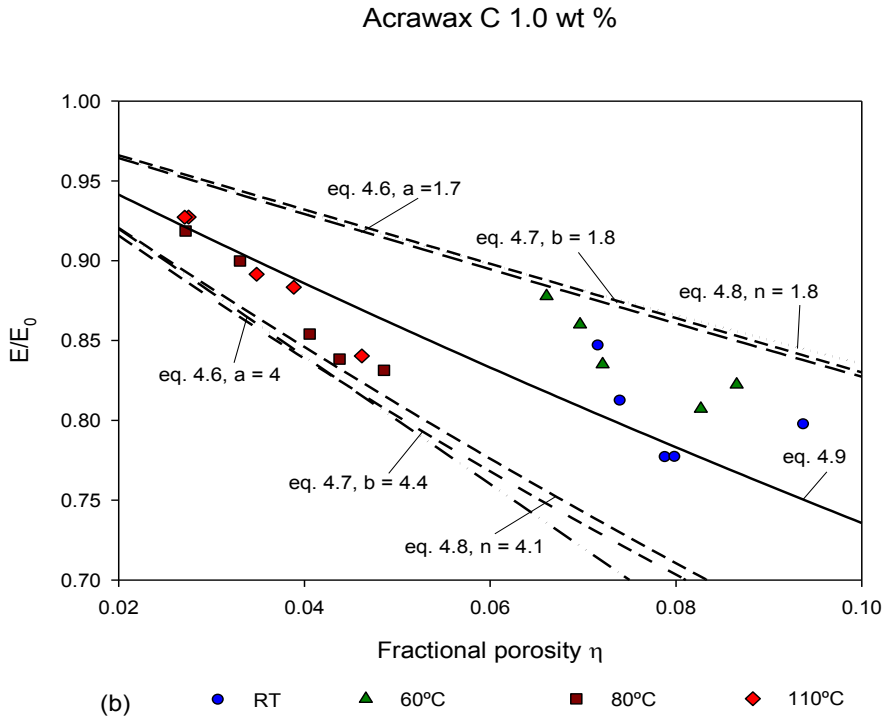

Figure 4.31 (a-b): The relationship of E/E_0 as a function of fractional porosity η for Acrawax C contents of (a) 0.5 wt % and (b) 1.0 wt %.

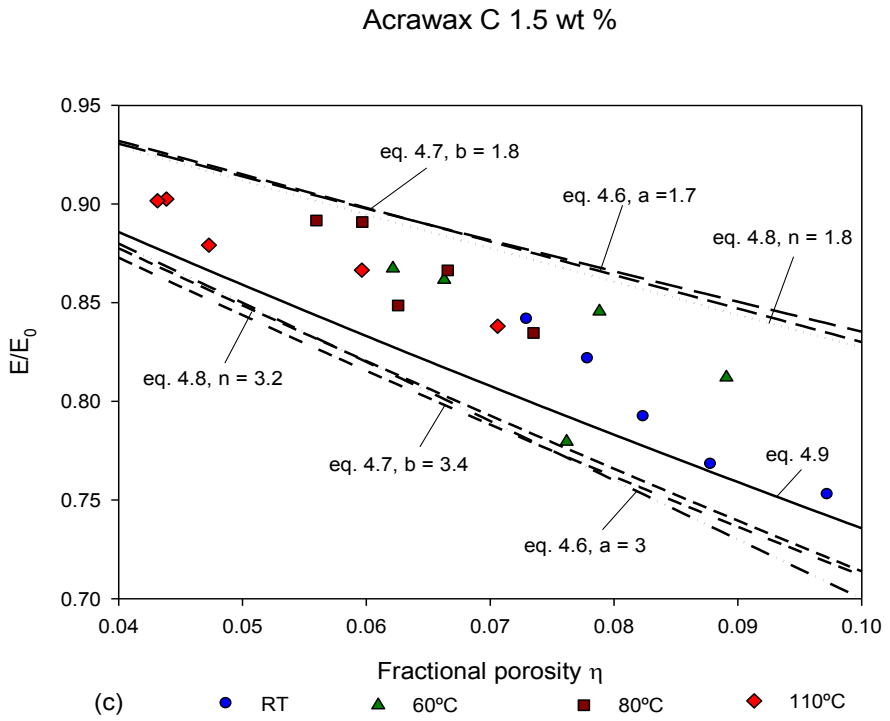

Figure 4.31 (c): The relationship of E/E_0 as a function of fractional porosity η for Acrawax C content of 1.5 wt %.

Table 4.11.: The adjusted parameters to incorporate the pore morphology

Acrawax C	**Limit**	**a**	**b**	**n**
0.5 wt %	Upper	2.2	2	2
	Lower	5.2	5.8	5.6
1.0 wt %	Upper	1.7	1.8	1.8
	Lower	4	4.5	4.1
1.5 wt %	Upper	1.7	1.8	1.8
	Lower	3	3.4	3.2

4.7.5.2.2 Kenolube P11

Figure 4.32 shows the relationship of E/E_0 as a function of fractional porosity η for 0.5, 1.0 and 1.5 wt % of Kenolube P11. The values of the adjusted parameters for equation 4.6, 4.7 and 4.8 for 0.5, 1.0 and 1.5 wt % of Kenolube P11 are in table 4.12.

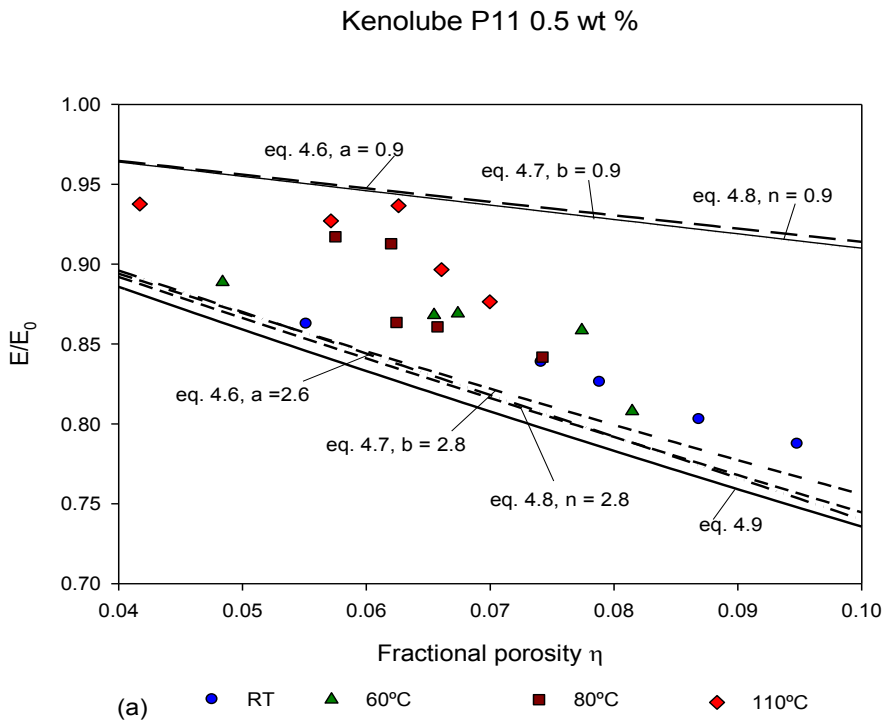

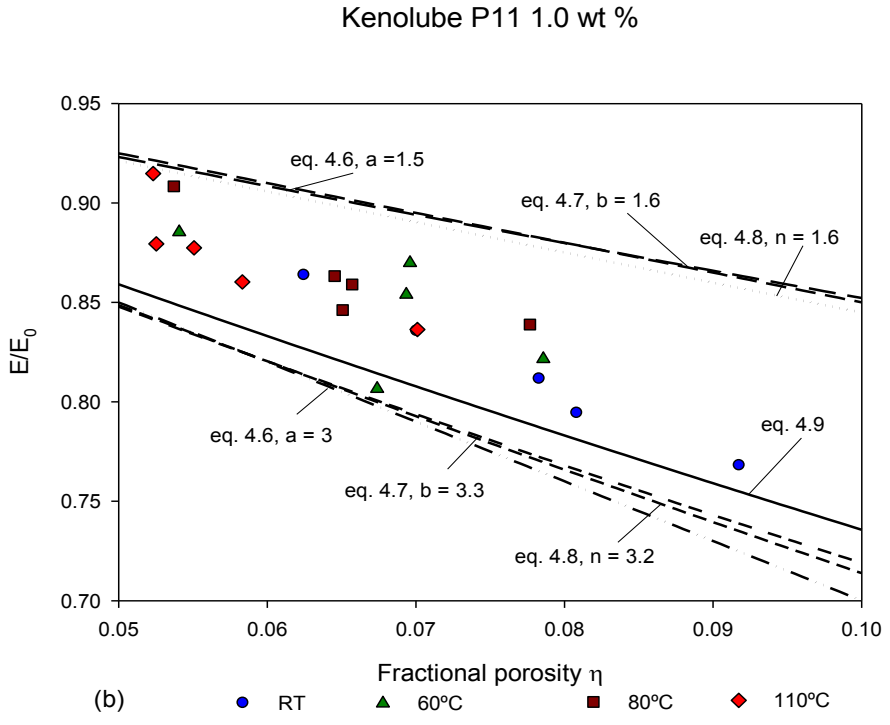

Figure 4.32 (a-b): The relationship of E/E_0 as a function of fractional porosity η for Kenolube P11 contents of (a) 0.5 wt % and (b) 1.0 wt %.

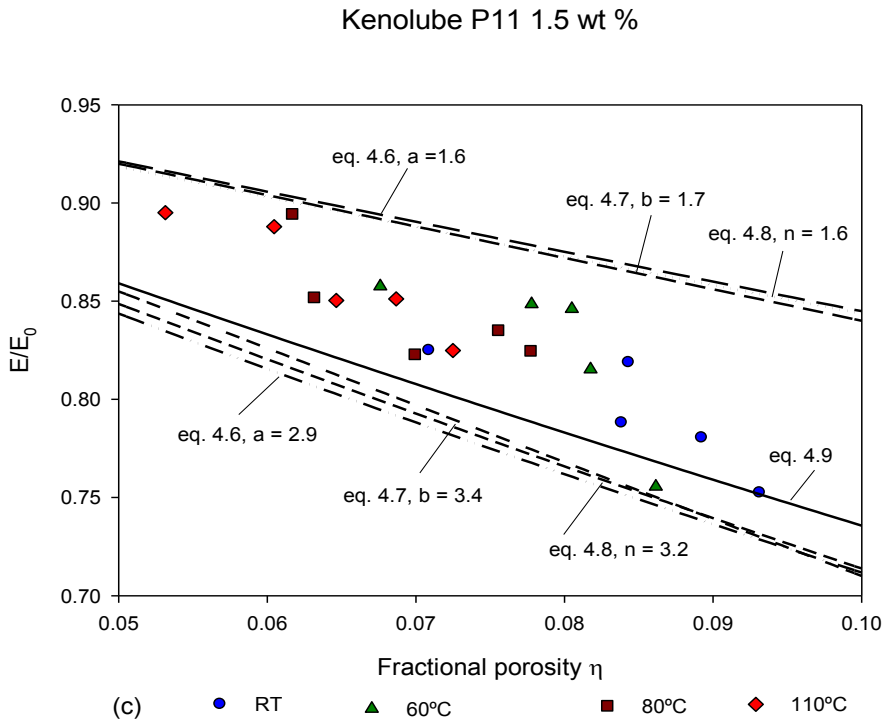

Figure 4.32 (c): The relationship of E/E_0 as a function of fractional porosity η for Kenolube P11content of 1.5 wt %.

Table 4.12.: The adjusted parameters to incorporate the pore morphology

Kenolube P11	**Limit**	**a**	**b**	**n**
0.5 wt %	Upper	0.9	0.9	0.9
	Lower	2.6	2.8	2.8
1.0 wt %	Upper	1.5	1.6	1.6
	Lower	3	3.3	3.2
1.5 wt %	Upper	1.6	1.7	1.6
	Lower	2.9	3.4	3.2

4.8 Microstructure of Sintered/Aged Alumix 123 Compacts

Figure 4.33 shows the typical microstructure of sintered/aged specimens compacted at 400 MPa and 110ºC with Acrawax C content of 1.0 wt %.

In figure 4.34 the pores are represented by dark regions; bright regions correspond to eutectic Al-Cu-Si-Mg, or Cu rich phase, or Al_2Cu. Al_2Cu phase is more visible in figure 4.35, especially where Acrawax C content is 0.5 wt %.

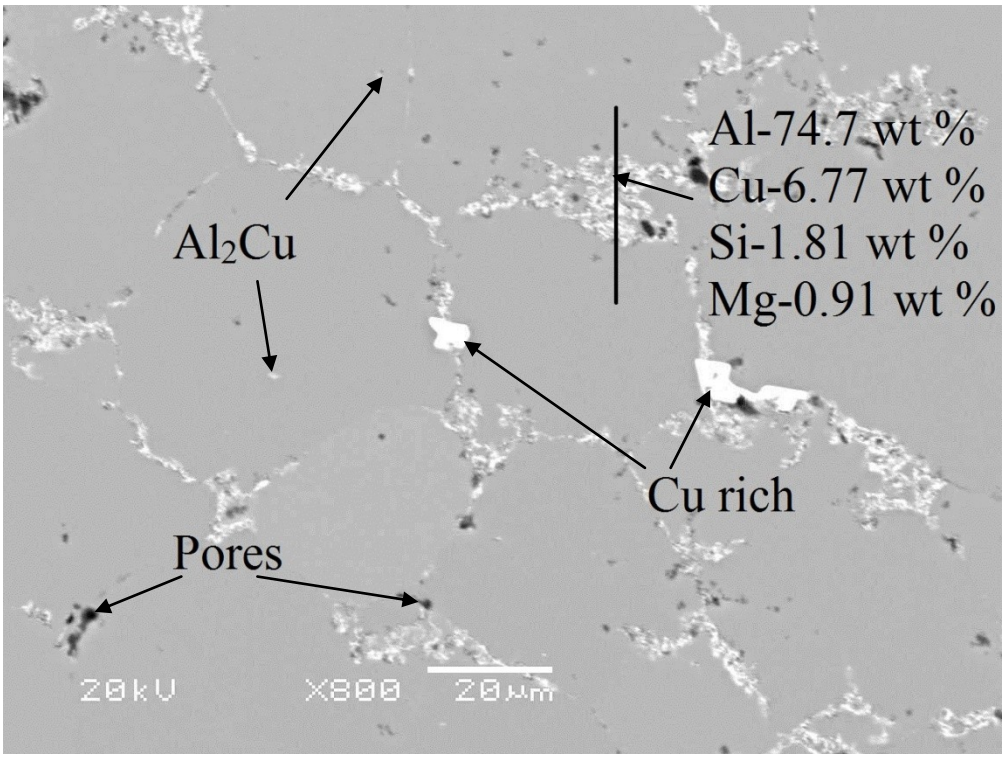

Figure 4.34: Sintered/aged microstructure of specimen compacted by 400 MPa at 110ºC, with Acrawax C content of 1.0 wt %.

Figure 4.35 shows the microstructure of sintered/aged specimens prepared by compaction at 110ºC and 400 MPa with various Acrawax C and Kenolube P11 contents. It was noted that sintered density/microstructure strongly depends on green density/microstructure. Lower porosity in green compacts therefore indicates lower porosity in sintered specimens. In addition, specimens with Acrawax C generally have smaller amounts of pores compared to those with Kenolube P11, caused higher density of specimens with Acrawax C.

From measured data of sintered/aged density the overall porosity of the single lubricant contents increased with increasing lubricant content as can be seen at table 4.13. Data in table 4.13 are average values for specimens compacted at 110°C and 400 MPa for a given lubricants contents.

Table 4.13: The overall porosity of the sintered/aged specimens compacted at 110°C and 400 MPa.

	Overall porosity [%]	
Lubricant content	**Acrawax C**	**Kenolube P11**
0.5 wt %	1.7	4.1
1.0 wt %	2.7	5.2
1.5 wt %	4.3	5.3

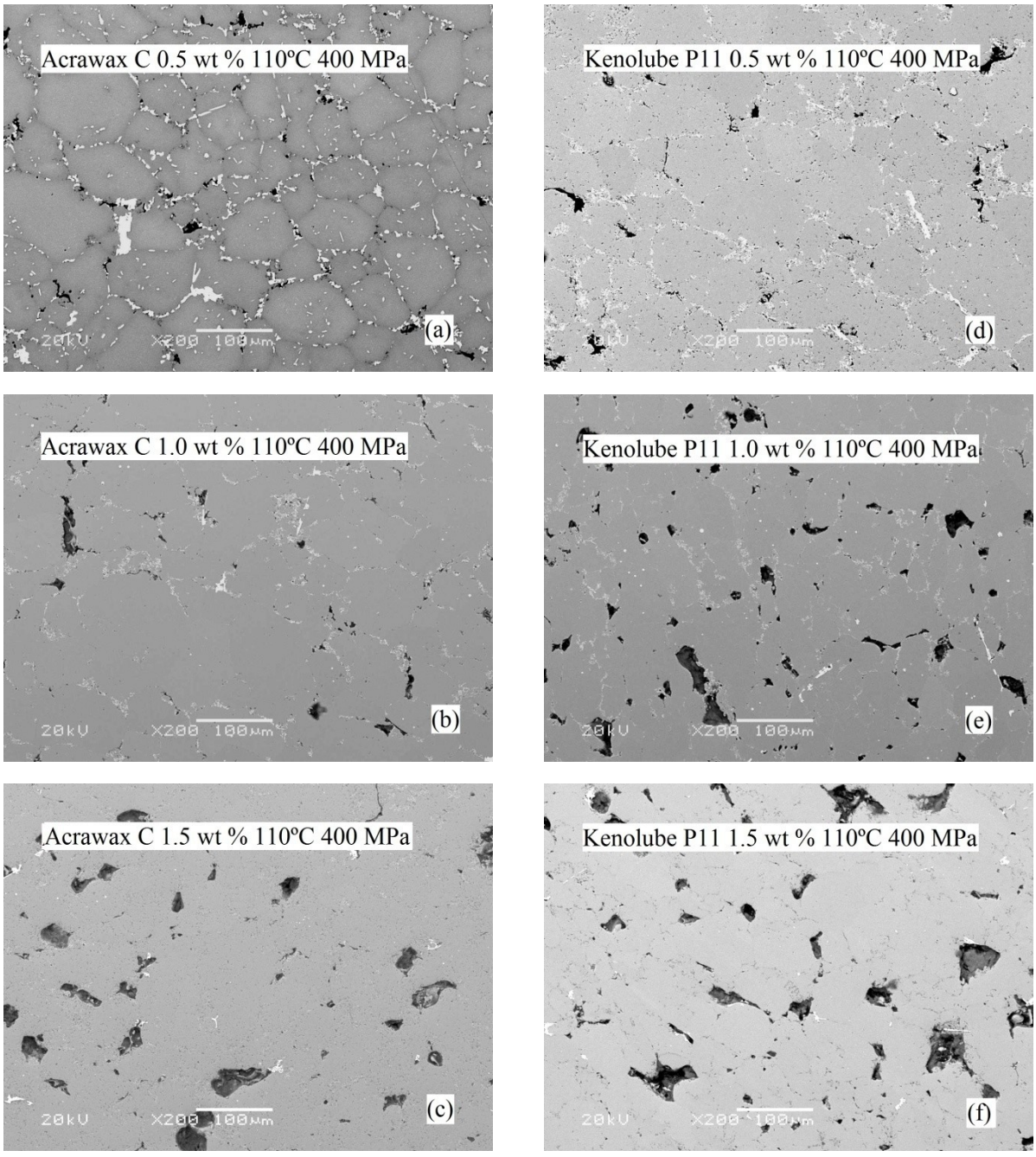

Figure 4.35: Sintered/aged microstructure of specimens with (a-c) Acrawax C and (e-f) Kenolube P11contents of 0.5 wt %, 1.0 wt % and 1.5 wt %.

4.9 Fracture Surface of Sintered/Aged Alumix 123 Compacts

Figure 4.36 shows SEM micrographs of the fracture surface of broken sintered/aged specimens with Acrawax C content of 1.5 wt %. Specimens were compacted by a pressure of 400 MPa at RT or 110ºC. Figure 4.36 (a) shows that fracture was developed through grain boundaries and along the pores as the lack of any dimpled feature and cup cone feature, indicating an intergranular fracture. The bright areas at figure 4.36 (a) represent Al-Cu-Si-Mg liquid phase formed during the sintering. [141, 173, 174]

Figure 4.36 (b) shows that tear ridges were found on a large amount of particles, fracture leaving the grain remnant with faceted cleavages, indicating a transgranular fracture. [174]

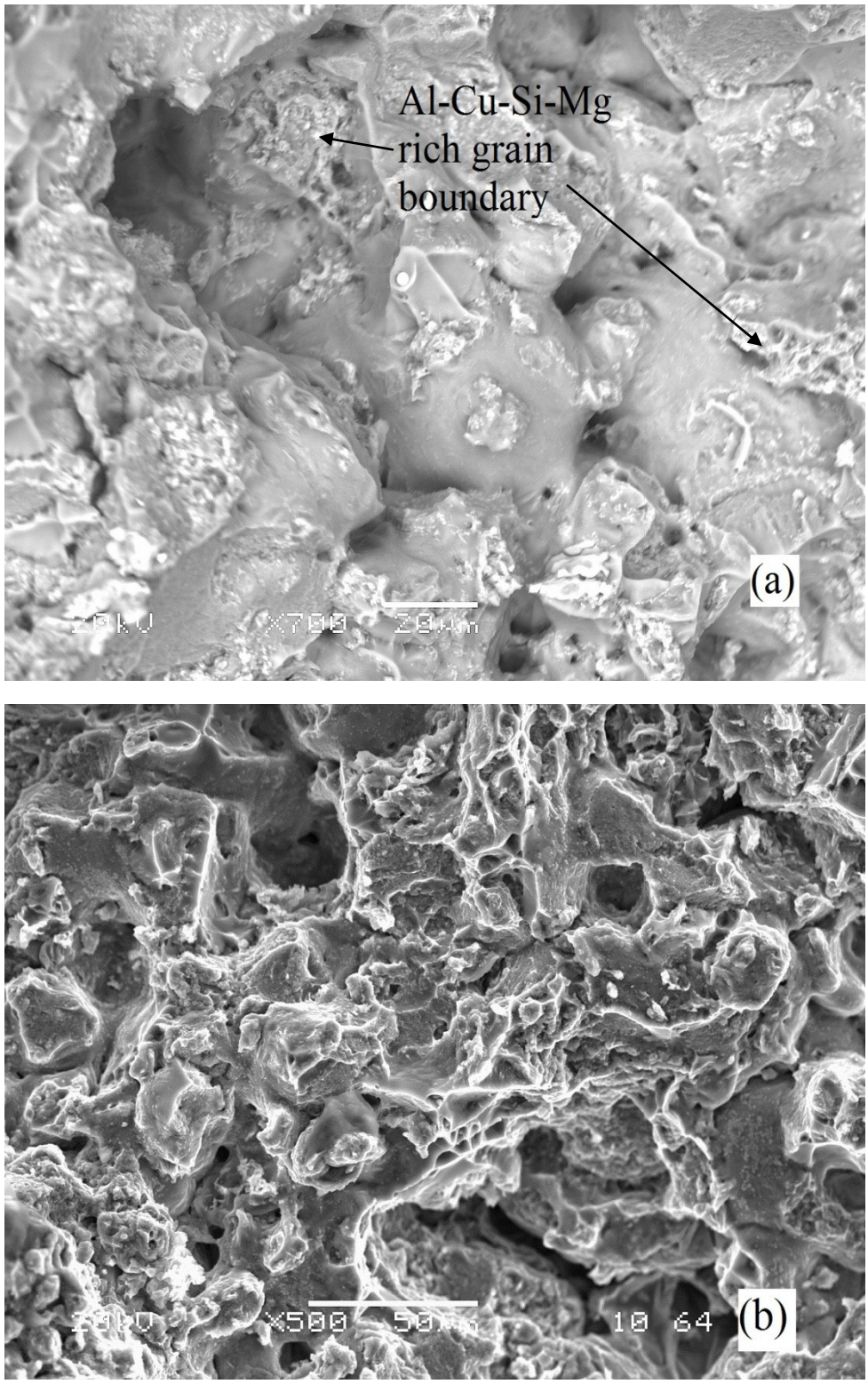

Figure 4.36: Fracture surface of Alumix 123 sintered/aged specimens compacted at (a) RT and (b) 110ºC.

4.10 Taguchi design

By application of Taguchi design it is possible to optimize which parameter influences the final properties the most. [175] The compaction pressure, compaction temperature and amount of admixed lubricant were chosen as parameters for this study. For compaction pressures 200, 300 and 400 MPa were selected. For compaction temperature RT, 80 and 110ºC were selected, and three lubricant contents of 0.5, 1.0 and 1.5 wt % were selected, and are shown in table 4.14. Because each parameter has three factors an L9 array was applied. A typical L9 orthogonal array used in this study is illustrated in 4.15.

Table 4.14: Parameters and factors for Taguchi design

Parameter	**Factor 1**	**Factor 2**	**Factor 3**
Compaction pressure	200	300	400
Compaction temperature	RT	80	110
Lubricant content	0.5	1.0	1.5

Table 4.15: L9 Array for Taguchi design

Experiment	**P1**	**P2**	**P3**	**Experiment**	**P1**	**P2**	**P3**
1	1	1	1	1	200	RT	0.5
2	1	2	2	2	200	80	1.0
3	1	3	3	3	200	110	1.5
4	2	1	2	4	300	RT	1.0
5	2	2	3	5	300	80	1.5
6	2	3	1	6	300	110	0.5
7	3	1	3	7	400	RT	1.5
8	3	2	1	8	400	80	0.5
9	3	3	2	9	400	110	1.0

This setup allows the testing of all three variables without having to run 27 [=3^3= (3 Pressures), (3 Temperatures), (3 Lubricant contents)] separate trials. For each experiment, three trial runs were conducted for a given variable. For calculation of the signal-to-noise (S/N) ratio, equation 2.10 (larger is better, to maximize the response) for each experiment was used. For the target properties (i.e. green/sintered density, tensile strength, elongation, Young's modulus and hardness), the parameters that gave the highest and lowest effect on the properties were determined.

For example, the calculation of the S/N ratio for Acrawax C with target property of green density is shown in the following steps.

Calculation steps [175]:

1. Calculation of S/N ratio.

a) Signal-to-noise ratio of the trials for experiment no. 1, S/N_1

$$\frac{S}{N_1} = -10\,log\left[\frac{1}{n}\sum_{i=1}^{n}\frac{1}{y_i^2}\right] = -10log\left[\frac{1}{3(2.577^2+2.574^2+2.581^2)}\right] = 17.76582 \qquad \text{(eq. 4.11)}$$

Similar steps for calculation of the S/N ratio for remaining experiments were used. The S/N ratio for each experiment for Acrawax C with target property of green density is shown in table 4.16.

Table 4.16: Response table of the S/N ratio for each experiment for Acrawax C with target property of green density

Experiment	P1	P2	P3	Trial 1	Trial 2	Trial 3	S/N
1	1	1	1	2.577	2.574	2.581	17.76582
2	1	2	2	2.595	2.594	2.589	17.81814
3	1	3	3	2.562	2.570	2.562	17.72226
4	2	1	2	2.575	2.578	2.576	17.76329
5	2	2	3	2.592	2.568	2.598	17.79523
6	2	3	1	2.674	2.684	2.671	18.09245
7	3	1	3	2.573	2.573	2.571	17.74872
8	3	2	1	2.687	2.689	2.691	18.13408
9	3	3	2	2.674	2.667	2.668	18.07179

2. The effect of the parameter

a) Sum of the S/N ratio at parameter 1 and level 1, $S_{P1(1)}$

$$S_{P1(1)} = \frac{(17.76582 + 17.81814 + 17.72226)}{3} = 17.76874 \quad \text{(eq. 4.12)}$$

b) Sum of the S/N ratio at parameter 1 and level 2, $S_{P1(2)}$

$$S_{P1(2)} = \frac{(17.76329 + 17.79523 + 18.09245)}{3} = 17.88365 \quad \text{(eq. 4.13)}$$

c) Sum of the S/N ratio at parameter 1 and level 3,$S_{P1(3)}$

$$S_{P1(3)} = \frac{(17.74872 + 18.13408 + 18.07179)}{3} = 17.98487 \quad \text{(eq. 4.14)}$$

d) The effect of the parameter 1 Δ, is then calculated by difference of the relative magnitude of effects,

$$\Delta = Max - Mix = 17.98487 - 17.76874 = 0.21613 \quad \text{(eq. 4.15)}$$

Table 4.17: Effect of the parameters on green density of the specimens with Acrawax C

Level	P1 (Pressure)	P2 (Temperature)	P3 (Lubricant)
1	17.76874	17.75928	17.99745
2	17.88365	17.91582	17.88441
3	17.98487	17.96217	17.7554
Δ	0.21613	0.20289	0.24205
Rank	2	3	1

From the results above it can be seen that largest effect on green density of Acrawax C is the lubricant content.

The same calculation steps were applied on the other output values: sintered density, tensile strength, elongation, Young's modulus and hardness for both lubricants Acrawax C and Kenolube P11. The results are listed in tables 4.18 and 4.19.

Table 4.18 shows the effect of the single parameters with their percentage contribution on the densities and mechanical properties of the specimens with Acrawax C. As can be seen, the lubricant content parameter exhibits the greatest influence on green density, tensile strength and elongation. Followed by compaction temperature, this has the most influence on sintered density and Young's modulus. For hardness, compaction pressure has the highest influence.

Table 4.18: Effect of the parameters on the output values for specimens with Acrawax C

Acrawax C (rank)	**Pressure**	**Temperature**	**Lubricant content**	**Residual error [%]**
	Contribution of single parameters [%]			
Green density	2 (31.06)	3 (29.94)	1 (38.89)	0.11
Sintered density	3 (16.69)	1 (53.2)	2 (26.29)	3.82
Tensile strength	2 (30.67)	3 (29.72)	1 (39.48)	0.13
Elongation	2 (30.99)	3 (25.85)	1 (41.4)	1.76
Young's modulus	2 (24.13)	1 (57.65)	3 (11.81)	6.41
Hardness	1 (50.62)	3 (16.42)	2 (31.33)	1.63

Table 4.19 shows the effect of the single parameters with their percentage contribution on the densities and mechanical properties of the specimens with Kenolube P11. Similar observation as for Acrawax C has occurred; the lubricant content influenced the most green density, tensile strength and elongation. The second parameter with the highest influence on sintered density and hardness is compaction pressure. The third parameter with the highest influence is compaction temperature and this parameter influence the most Young's modulus.

Table 4.19: Effect of the parameters on the output values for specimens with Kenolube P11

Kenolube P11 (rank)	**Pressure**	**Temperature**	**Lubricant content**	**Residual error [%]**
	Contribution of single parameters [%]			
Green density	2 (30.81)	3 (24.75)	1 (44.19)	0.25
Sintered density	1 (52.17)	2 (41.23)	3 (3.7)	2.9
Tensile strength	2 (41.62)	3 (8.6)	1 (47.55)	2.23
Elongation	2 (33.58)	3 (25.67)	1 (37)	3.75
Young's modulus	2 (32.69)	1 (53.27)	3 (11.8)	2.24
Hardness	1 (45.88)	2 (34.38)	3 (8.85)	10.89

CHAPTER 5

DISCUSSIONS

5.1 The Influence of Compaction Pressure, Temperature and Lubricant Content on Ejection Force of Alumix 123 Compacts

Figures 4.8 and 4.9 show that the higher compaction pressure, reduction of lubricant content and lower compaction temperature requires a relatively higher ejection force. This is due to increased friction between powder particles and die walls during compaction. [176] When the force is overcome the particles slide relative over the die wall. This interaction can be described by the sliding coefficient, η. [177] The relation between the slide coefficient η and the friction coefficient μ is formulated as: [89]

$$\eta = e^{-4\,\mu \tan \varphi} \qquad \text{(eq. 5.1)}$$

where φ is the angle of the pressure transmission from the top to the die's wall. Yet, no reliable method has been presented for the determination of φ so an accurate friction coefficient μ cannot be obtained. [178] However, for practical purposes, a similar approach

has been used to establish an empirical relationship between the slide coefficient and compacting parameters. For a cylindrical specimen, compacted by single action press, the sliding coefficient at completion of compaction is given by Ballhausen–Gasiorek model: [179]

$$\eta = \left(\frac{P_t}{P_a}\right)^{\left(\frac{4F}{SH}\right)} \qquad \text{(eq. 5.2)}$$

where P_t is the pressure transmitted to the stationary punch, P_a is the pressure applied to the punch, F is the cross-section area, S is the cross-section perimeter and H is the height of the cylinder. These parameters can be easily measured. Consequently, the sliding coefficient can be determined. Numerical values of η vary from 0 to 1. [177] According *Simchi et al.* [89] the value 0.7 is considered moderate. They noticed that the sliding coefficient of cold compacted aluminium powder and its elemental blends is below 0.6 and for prealloyed powder is around 0.7. For warm compaction at 140°C the sliding coefficient of elemental powder blends increase to 0.8 and for Al-12Si prealloyed powder to 0.9. Thus, for the elemental blends and the prealloyed powder, good compaction properties can be expected. It can be said, that the higher the sliding coefficient, the lower the friction between powder particles and die walls. Therefore a lower ejection force is required resulting in more uniform the density through the compact.

Referring again to figures 4.8 and 4.9 compaction at elevated temperature reduced the ejection force in all conditions, i.e. different compaction pressures and different amounts of admixed lubricant. Li *et al.* [180] found that with increasing compaction temperature, the

friction coefficient on the die wall decreased through viscosity of the lubricant, and the higher compaction temperature the lower viscosity of the lubricant. This resulted in the reduction of the friction and subsequently in the increase of green density of the compact. The viscosity of lubricant must be sufficiently high to provide adequate lubrication at the die walls. Compaction above the melting temperature of lubricant led to the formation of a partially molten film between the die wall and green compact. However, if the compaction temperature increased further, to the temperature range in which lubricant and its additives become unstable by their degradation, the viscosity would decrease and the friction coefficient increase. [181] Rabinowicz [182] showed that some lubricants remained solid over one temperature range and liquid over another and then become desorbed and lose their function at higher temperatures. This was demonstrated with octadecyl alcohol lubricant between copper sliders. Below 40°C, at solid lubricant state, the friction coefficient was about 0.11. When, the temperature has increased to 60°C, the lubricant became liquefied and the friction coefficient increased to 0.33. Friction remained constant until about 120°C, then another transition occurred and the friction coefficient increased to 1.0 as the liquid was desorbed, which increased the friction. Gegel *et al.* [183] pointed out that pressing at temperatures above the melting point of the lubricant may reduce the friction but can leave a residue on the compaction die, which requires additional cleaning operation.

5.2 The Influence of Compaction Pressure, Temperature and Lubricant Content on Green Density of Alumix 123 Compacts

The effect of compaction pressure on the green density with Acrawax C (Figure 4.10) contents shows that an increase in compaction pressure from 200 to 400 MPa using the same compaction temperature is similar to increase in green density between different compaction temperatures and the same compaction pressure. For example, the green density of specimens compacted at 110ºC and 200 MPa for Acrawax C content of 1.5 wt % was measured to be 2.566 g/cm^3 and the green density of specimens compacted at 400 MPa reached 2.631 g/cm^3. For a given compaction pressure of 400 MPa, the green density of specimens compacted at RT was measured to be 2.591 g/cm^3 and specimens compacted at 110ºC reached the green density of 2.631 g/cm^3. This represents an increase of 2.47 % by varying compaction pressure from 200 to 400 MPa at a given temperature of 110ºC, and an increase of 1.44 % by varying temperature from RT to 110ºC for a given compaction pressure of 400 MPa.

A similar effect of compaction pressure on the green density with Kenolube P11 (Figure 4.11) contents compared to Acrawax C was observed. The increase between compaction pressure of 200 MPa and 400 MPa at the same compaction temperature is similar to increase in density between different compaction temperatures at the same compaction pressure. For example, the green density of specimens with 1.5 wt % of Kenolube P11 was 2.556 g/cm^3 and 2.626 g/cm^3 when compacted at 110ºC for 200 MPa and at 110ºC for 400 MPa, respectively. At constant compaction pressure of 400 MPa but with changing compaction temperatures, the green density of specimens compacted at RT was measured to be 2.576 g/cm^3 and specimens compacted at 110ºC reached the green density of

2.626 g/cm^3. This represents an increase of 2.48 % by varying compaction pressure from 200 to 400 MPa while there is an increase of 1.79 % by varying compaction temperature for RT to 110ºC.

The effect of admixed lubricants on the green density of Alumix 123 specimens pressed at different compaction pressure and temperature is also shown in figures 4.10 and 4.11. A constant decrease in green density with increasing lubricants (Acrawax C and Kenolube P11) contents can be observed. For example, for specimens with Acrawax C compacted at 400 MPa and 110°C the green density decrease as the amount of lubricant increase. At lubricant content of 0.5, 1.0 and 1.5 wt % the green density decreased as follow 2.704, 2.670 and 2.632 g/cm^3.For specimens with Kenolube P11 at lubricant content 0.5, 1.0 and 1.5 wt % the green density decreased from 2.660, 2.645 and 2.626 g/cm^3 for a given compaction pressure and temperature.

The increase in green density with pressure is due to the increasing forces causing porosity to close up. The increase in green density with temperature is due to a combination of higher degree of plastic deformation of Al powder occurring at elevated temperature, and softening/melting of lubricant and its subsequent expulsion from the powder compact through pores towards the die walls. The mechanism of expulsion of the lubricant from the green compact is complex. In compaction at elevated temperature if the lubricant is in a semi-liquid or a liquid state, the lubricant flows into the porous compact by pressure-assisted capillary flow. [177] Washburn [184] describe the model of penetration of a liquid into porous medium by relation:

$$L^2 = \left(\frac{\sigma D \cos(\theta)}{4\mu} t\right) \quad \text{(eq. 5.3)}$$

where L is the depth of penetration of the liquid, σ is the surface tension of the liquid, D is the average pore diameter, θ is the contact angle between the solid and the liquid, t is the time, and μ is the dynamic viscosity of the liquid.

As compaction temperature and pressure increase, the viscosity of the lubricant decreases and this facilitates movement of lubricant from interparticle space towards the die wall. The expulsion of lubricant towards the die walls continues as long as the applied pressure is higher than the capillary pressure due to the surface tension of the liquid lubricant. [177] This improves compressibility, reduces the amount of trapped lubricant between particles, and enhances metal-to-metal contacts, subsequently increasing green density. [185] At higher amounts of admixed lubricant more lubricant is trapped inside the pores and the green density decreases.

The figures 4.10 and 4.11 also display the compressibility curve for each lubricant content and compaction temperature. At lower pressure the initial increase in density is due to rearrangement of powder particles. The further increases of pressure caused deformation and work hardening, generating more resistance to compaction until densification was halted. This mechanism was explained by Thummler and Oberacker. [186] Kim *et al.* [187] confirmed that at certain point of pressurizing, bulk deformation causes the formation of closed pores which proved to be detrimental to sinterability.

Simchi [188] and Rahman *et al.* [189] reported similar observations of the effect of lubricant content on green density for iron powder (ASC 100.29 from Hoeganaes). Simchi found that higher amount of admix lubricant (0.8 wt % of ethylene bisstearoylamide) increase densification in the lower pressure region, while limiting the denisty at high

pressures. In addition, he showed that warm compaction results in the formation of more metal-to-metal contacts during compacting. Rahman showed that specimens with 0.5 wt % of zinc stearate, for similar iron-based composition, led to higher green density compared to specimens with 0.75, 1, 1.15 and 2 wt % of lubricant.

5.3 Heckel Relationships

Figures 4.12 and 4.13 show the Heckel relationship between ln (1/ (1-D)) and the applied pressure during compaction. In both lubricants, the increase of slope k_H with increasing compaction temperature is mainly due to a decrease in the yield strength of aluminium powder (Figure 2.18) and also with increasing pressure due to closing up of pores. In addition, as mentioned in section 5.2 with higher compaction temperature and pressure the amount of the admixed lubricant is reduced through partial movement of lubricant towards the die wall which results in higher green density of the compacts.

Specimens with Kenolube P11 gave slightly higher value of k_H which assume higher value of yield strength than specimens with Acrawax C for given amount of lubricant and compaction temperature.

Table 5.1 suggests the main contribution to yield strength of compacts is from aluminium rather than copper. It should be noted that the overall yield strength is represented by powder constituent(s) which yield first.

It can be said that calculated yield strength (based on Heckel study) of the powder Alumix 123 in given conditions is comparable to Al in at its cast state.

Table 5.1: Yield strength of powder constituents at their cast state under room temperature [136]

Constituent	**Yield strength** [MPa]
Al 99.99 %	20-105
Cu 99.9 %	70
Al 2014 T_0	~ 100
Al 3xxx series	80-300
Al 4xxx series	80-320

5.4 The Influence of Compaction Pressure, Temperature and Lubricant Content on Sintered/Aged Density of Alumix 123 Compacts

In this study, sintering temperature, sintering time, protective atmosphere and subsequent thermal treatment where chosen based on the previous work as mentioned in section 2.4.4. The results show that the specimens with Acrawax C reached higher sintered densities against those specimens where Kenolube P11 was used. If comparing the highest value of sintered densities achieved at 110ºC and 400 MPa for specimens with Acrawax C and Kenolube P11 (2.751 and 2.683 g/cm^3, respectively) the sintered densities of specimens with Acrawax C improve by 2.47 %. This follows the trend of green densities where specimens with Acrawax C obtained higher green densities. It can be assume that the specimens with high green density would have higher sinter density for given lubricants.

This study also pointed out that green density of specimens compacted at 110°C, for both lubricants, increased after sintering over two times (~2 %) than specimens compacted at room temperature (~1 %). It is believed, that warm compaction on relative high temperature

has resulted in large plastic deformation of the powders (Section 2.3.2), breaking of the oxide layers and formation of more contacts between copper and aluminium particles. [188]

In a work by Babakhani *et al.* [190] a similar trend of increase between green and sintered density with increasing compaction temperature and reduction of lubricant for prealloyed powder (Fe–3Cr–0.5Mo) with/without 0.6 wt % lithium stearate was found. For specimens with/without 0.6 wt % of lubricant compacted at 500 MPa, when compaction temperature increased from RT to 150ºC, the green density increased by 0.2 and 0.24 g/cm^3, respectively. After sintering of these specimens density increased by 0.2 and 0.22 g/cm^3, respectively. This was due to evaporation of admixed lubricant (if any) and elimination of the pores by sintering.

5.5 The Influence of Compaction Pressure, Temperature and Lubricant Content on Tensile Strength and Hardness of Sintered/Aged Alumix 123 Compacts

The sintered density and the heat treatment have a major effect on the mechanical properties. Increased density will increase strength, hardness and elongation. The highest densities are achieved by using higher compaction pressures.

The heat treatment, or the age hardening, of Al-Cu-Si-Mg alloy is caused by the precipitation of intermetallic phases during the decomposition of a metastable supersaturated solid solution obtained by solution treatment and quenching. [191] In Al-Cu alloys, during artificial ageing, a second phase, such as coherent intermetallic precipitate of Al_2Cu (θ') is formed. The fine θ' phase effectively impedes the movement of dislocations and since

dislocations are often the dominant carriers of plasticity, this imparts strength and hardness to the alloy. [191,192] Dislocations can be generated as a result of: a) quenching stresses, which occurs from retention of an excess concentration of vacancies, b) cold work or c) misfit of stresses created during the nucleation of a phase. [193]

The precipitates restrict dislocation motion via dislocation bowing (Figure 5.1), or cutting mechanisms (Figure 5.2)

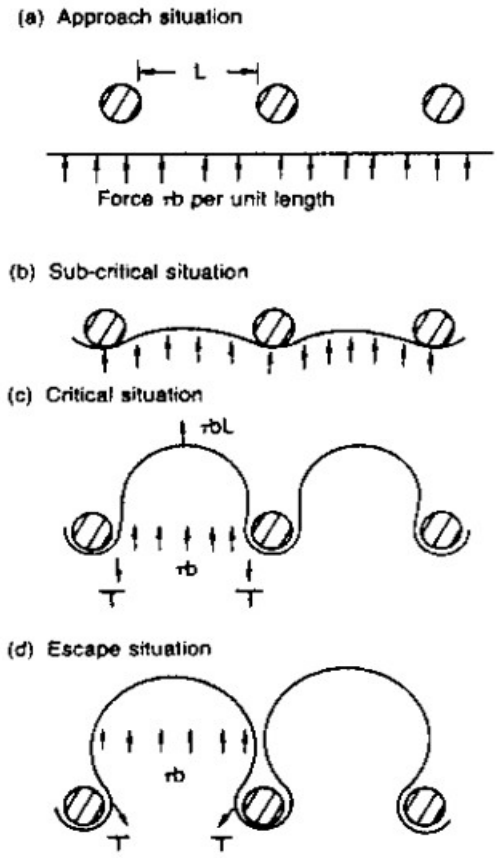

Figure 5.1: Schematic of Orowan strengthening due to bowing of dislocations between precipitates: (a) dislocation approaching particles; (b) dislocation extruding through particles; (c) critical situation when extruded dislocation reaches semicircular configuration; (d) escape situation. [192]

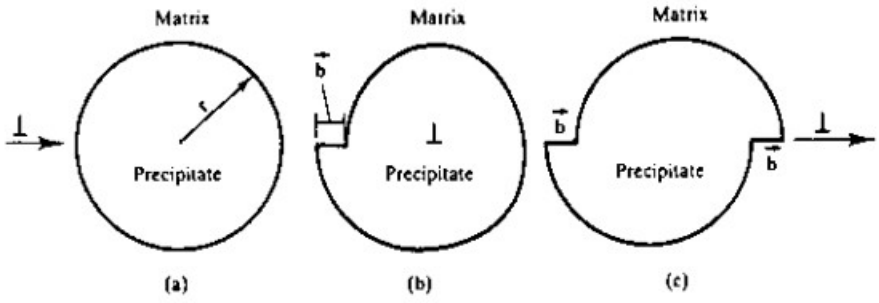

Figure 5.2: Schematic illustration of ledge formation and precipitation strengthening due to dislocation cutting of precipitates: (a) before cutting; (b) during cutting; (c) after cutting. [192]

Dislocation bowing (Figure 5.1) occurs when sub-micrometer precipitates pin two segments of a dislocation. The residual of the dislocation line is then extruded between the two pinning points due to the additional applied shear stress $\Delta\tau$. This mechanism was first described by Orowan, and is given by relation: [192, 194]

$$\Delta\tau = \frac{Gb}{L-2r} \qquad \text{(eq. 5.4)}$$

where $\Delta\tau$ is the material strength, G is the shear modulus, b is the magnitude of the Burgers vector, L is the distance between pinning points, and r is the second phase particle radius. This equation shows that when dislocation bowing around particle the strength is inversely proportional to the second phase particle radius r. This mechanism is more likely to occur when there are large particles present in the material. [192]

A dislocations cutting mechanism through particles may result in the formation of ledges at the interfaces between the particle and the matrix, in the regions where dislocation entry or exit occur. The mechanism is given by relation:

$$\Delta\tau = \frac{r\gamma\pi}{bL} \qquad \text{(eq. 5.5)}$$

where $\Delta\tau$ is material strength, r is the second phase particle radius, γ is the surface energy, b is the magnitude of the Burgers vector, and L is the spacing between pinning points. The equation shows that when dislocation cutting through particles occurs, the strength is proportional to r, the radius of the precipitate particles. This means that it is easier for dislocations to cut through a material with smaller second phase particles (small r). With increasing size of the second phase particles, dislocation movement is impeded and it becomes more difficult for the particles to cut through the material. Therefore, the strength of a material increases with increasing r. In addition, if the particles have a small radius and there are many close together, this can also increase the strength of a material due to small interparticle spacing, L. [192, 194]

In this study, tensile strength and hardness of specimens compacted at elevated temperature is higher than those produced by compaction at room temperature. This is due to the decrease in the yield strength of Al powder during compaction at elevated temperature (Section 2.3.2). Thus at the same compaction pressure but at higher compaction temperature specimens are more dense. This reduces the amount of the pores in specimens which act as crack initiators. A similar effect of compaction temperature on tensile strength was observed by Li *et al.* [195] in iron based system. They found that tensile strength increased from 546 to 751 MPa, when the compaction temperature changed from RT to 175ºC.

The same trend of higher tensile strength and hardness was observed with increasing compaction pressure. The higher compaction pressure caused better rearrangement and closed up porosity, this led to higher tensile strength and hardness values.

Comparison the relationship between the cold compacted and warm compacted tensile specimens with different lubricants are shown in figures 4.20 and 4.21. When compared with each other for a single lubricant, there is a similar behavior among the tensile test results. This suggests that the tensile strength of specimens is closely related to their green/sintered density. Eski *et al* [196] found that if cold/warm compacted specimens after sintering reached similar sintered densities, due to same green densities, they also reached similar tensile properties.

The maximum sintered/aged tensile strength of warm compacted specimens was measured to be 365.65 MPa. The maximum sintered/aged strength of cold compacted specimens was measured to be 324.86 MPa. This represents a difference of 11 % between warm and cold compacted specimens. However, the summary of the tensile strength study hinted that not just increasing compaction temperature and compaction pressure, and lowering the amount of admixed lubricant, but the type of lubricant also has a nominal influence on the final strength. The comparison of maximum measured values of admixed lubricant, Acrawax C (365.65 MPa) and Kenolube P11 (351.74 MPa), represents a difference of around 4 % in higher tensile strength for Acrawax C. This could be caused by composition of lubricants and their de-binding behaviour.

Figures 4.22 and 4.23 show the effect of compaction condition on the hardness of specimens with different lubricants. Similar effect as for tensile strength has occurred. The hardness of sintered/aged specimens increased with increasing compaction pressures and temperatures and decreasing amounts of lubricant. The highest hardness of specimens with 0.5 wt % of Acrawax C compacted at 400 MPa and RT or 110ºC was found to be 109.2 and 128.6 HV, respectively. This represents an increase in hardness of 15 % due to temperature

change. The highest hardness of specimens with 0.5 wt % of Kenolube P11 compacted at 400 MPa and RT or 110ºC was found to be 108.9 and 117.9 HV, respectively. This represents improvement of the hardness of 7.6 % due to temperature change.

As mentioned above, hardness is mostly affected by precipitation hardening. The impact of precipitation hardening on hardness is clearly seen when comparing the hardness values of this study and the hardness value from table 1.1, where as-sintered specimens of wrought alloy Al 2014 A and Alumix 123 reached the hardness of 57 and 68 HV (HB = 55 and 64), respectively. After heat treatment T6 the hardness of wrought alloy increased to 150 HV (HB = 140).

5.6 The Influence of Compaction Pressure, Temperature and Lubricant Content on Elongation of Sintered/Aged Alumix 123 Compacts

As mentioned in the previous section, a normal consequence of precipitation hardening mechanisms is an accompanying reduction in elongation. Consequently, most age hardenable alloys have high strength but low elongation, due to reduction of grain size in the hardened state and also because additions and small impurities bind the main alloying element into insoluble particles and decrease their content in the supersaturate solid solution. [197]

The elongation depends on the green/sintered density of specimens where the higher compaction pressures and temperature, and lower amount of admixed lubricant decrease the

porosity level in the specimens. Generally, specimens with higher green/sintered density achieved higher elongation.

From the data and from the figures 4.25 and 4.26, it was noted that increasing lubricant content decreased the elongation values. This is due to higher porosity levels in specimens with high lubricant content. [188] Like sintered materials, castings are also not usually fully dense but contain pores from a variety of sources. It has been shown for cast aluminium alloys that higher porosity leads to reduction of the elongation. Sintered aluminium may be expected to be similar. [198, 199]

The maximum elongation of specimens with 0.5 wt % of Acrawax C compacted at 400 MPa at RT or 110ºC, was found to be 0.81 and 1.11 %, respectively. This represents an improvement of the elongation of 27.02 % through temperature change. The maximum elongation of specimens with 0.5 wt % of Kenolube P11 compacted at 400 MPa at RT or 110ºC was measured to be 0.68 and 0.93 %, respectively. This represents an increase of the elongation of 26.8 % by temperature change.

The results reveal that specimens with Acrawax C attain higher values of elongation. By comparing the elongation for specimens compacted at 110ºC and 400 MPa with lubricant content of 0.5 wt %, the elongation for Acrawax C was 1.11 % and for Kenolube P11 was 0.93 %, which is a difference of 16.2 %.

5.7 The Influence of Compaction Pressure, Temperature and Lubricant Content on Young's modulus of Sintered/Aged Alumix 123 Compacts

From figures 4.27 and 4.28, it can be seen that Young's modulus is increasing with increasing compaction pressures and temperatures, and decreasing lubricant content, which resulted from higher green/sintered density. It can be said, the Young's modulus of materials is largely dependent on the densities of material. Young's modulus of material increases as the density of the material increases. This relation was described by many authors (Section 4.7.5.2). [200]

The maximum Young's modulus of specimens with 0.5 wt % of Acrawax C compacted at 400 MPa and RT or 110ºC was found to be 63.47 and 69.73 GPa, respectively. This represents an increase of the Young's modulus of 8.9 % by temperature change. The maximum Young's modulus of specimens with 0.5 wt % of Kenolube P11 compacted 400 MPa and RT or 110ºC was found to be 62.95 and 68.44 GPa respectively. This represents improvement of the Young's modulus of 8.1 % by temperature change. It can be seen that there is similar improvement for both of the lubricants used.

5.8 Correlation between Tensile Strength, Young's Modulus and Porosity

The equations described in section 4.7.5.1 have been applied to the results obtained in this study. As seen in figures 4.29 and 4.30, any equation proposed so far can not explain the relation between tensile strength and porosity. This is believed to be due to the fact that the range of porosity used in development of model equations was very narrow and restricted to a high porosity level. In addition, the pore morphology may significantly affect the mechanical properties. Without incorporating the pore geometry effect, the equations fail as the porosity level increases. [201]

However, equations 4.4 and 4.5 contain parameters - α, β and k, respectively, - which can be adjusted to incorporate the pore morphology. By adjusting the numerical value of these variables (i.e. changing their constant characteristic) the limits of the region in which the equations can be used to estimate relative strength of the high porosity compacts can be established. [202] It can be seen that Tronshenko equation with constant α and changing β parameter can include most of the porosity range of the specimens with Acrawax C and Kenolube P11.

All the specimens with Acrawax C and Kenolube P11 additions showed significantly higher value of α, β and k. This clearly shows that the pores of the sintered compacts with either Acrawax C or Kenolube P11 are irregular shape.

The theoretical equations describing the effect of porosity on Young's modulus (Section 4.7.5.2) have been applied to the results acquired in this study. From figures 4.31 and 4.32, can be seen that none of these equations can explain the relation between Young's modulus and porosity/density of the specimens in this study. As with the correlation between tensile strength and porosity, the inability of the equations to fit the experimental data is caused by the fact that most numerical modelling studies of the elastic behaviour of P/M materials assume the pores to be perfectly spherical and distributed homogeneously in the matrix. However, the results of this study indicate that the elastic properties appear to be significantly influenced by the shape and morphology of the porosity microstructure. As seen from tables 4.11 and 4.12, the n exponent gave lower numerical values than those obtained by other authors. [170, 171] This is believed to be due to a wider range of porosity in the specimens in this study.

When the a, b and n values in equations 4.6, 4.7 and 4.8, respectively, are not treated as constant, it is possible to find the limits of the regions in which the equations correlating the Young's modulus and porosity can be used. The figures 4.31 and 4.32 show that Spriggs equation with changing b parameter can include the most porosity of range of the specimens with Acrawax C and Kenolube P11.

5.9 Microstructure of Sintered/Aged Alumix 123 Compacts

Figure 4.34 shows the microstructure of sintered/aged Alumix 123 (Al-4.5Cu-0.6Si-0.5Mg) specimens with 1.0 wt % of Acrawax C compacted at 110°C and 400 MPa.

Falticeanu *et al.* [203] and Martin *et al.* [159] in their studies of sintering behaviour of Al-4.4Cu-0.8Si-0.5Mg and Al-4.4Cu-0.7Si-0.5Mg, respectively, showed that sintering of these alloys occurred in several endothermic events. The first two events occurred at temperatures below 460ºC. The first event started at ~ 449ºC, with the possibility of fusion of the β-phase (Mg_2Al_3 or Mg_5Al_8) or, alternatively, formation of Al-Mg eutectic liquid at the Al-Mg interface. The second events started at 457ºC and related to melting of the γ-phase ($Al_{12}Mg_{17}$). Further events occurred as heating continued towards the sintering temperature at ~505ºC and then up to ~ 550ºC, which relates to the formation of a liquid phase, following the reaction:

$$Al + Al_2Cu + Al_2CuMg \rightarrow \text{Liquid phase} \qquad \text{(eq. 5.6)}$$

In the presence of Si, the reaction is:

$$Al + Al_2Cu + Al_2CuMg + Mg_2Si \rightarrow \text{Liquid phase} \qquad \text{(eq. 5.7)}$$

$$Al + Al_2Cu + Si + Al_5Cu_2Mg_8Si_6 \rightarrow \text{Liquid phase} \qquad \text{(eq. 5.8)}$$

According to the literature the reactions in equations 5.6, 5.7 and 5.8 occurred at 507, 500 and 507ºC, respectively. [204] At 549ºC another endothermic reaction occurred;

$Al + Al_2Cu \rightarrow$ Liquid phase (eq. 5.9)

This reaction took place in locations where copper particles are far removed from the Mg particles so did not interfere with reactions (eq. 5.6) to (eq. 5.8) due to insufficient concentration of Mg. If the temperature is greater than 646ºC the composition is completely molten.

It was noted, that increasing lubricant content increased the amount of the porosity in all specimens. It is believed that during the sintering, the admixed lubricant trapped at particle interfaces evaporates and escapes through the open pores or permeates to the surface through inter-particle voids. However, when the amount of lubricant is high, gases from the evaporated lubricant can become trapped inside the specimen. [190, 205]

In addition, It was noted than sinter/aged specimens microstructures with Acrawax C contained lower amounts of large pores (> 75 μm) than sinter/aged specimens with Kenolube P11 for a given pressure and lubricant content. However, higher content of admixed lubricant increased the amount of pores in both waxes.

5.10 Fracture Surface of Sintered/Aged Alumix 123 Compacts

Figure 4.36 shows SEM micrographs of the fracture surface of broken sintered/aged specimens with 1.5 wt % of Acrawax C compacted at 400 MPa and RT or 110ºC, respectively. Figure 4.36 (a) shows that fracture was developed through grain boundaries and along the pores as the lack of any dimpled feature and cup cone feature, indicating an intergranular fracture. The bright areas at figure 4.36 (a) represent Al-Cu-Si-Mg liquid phase formed at grain boundaries during the sintering. [173, 174] Falticeanu [141] suggested that this eutectic phase might be detrimental to the mechanical properties as its presence on the grain boundaries together with the remnant porosities that concentrate the load at the triple point between the neighbouring grains have a cumulative effect.

With the higher compaction temperature of 110ºC tear ridges were found on a large amount of particles, (Figure 4.36 (b)). This points towards the occurrence of transgranular fracture. The transgranular fracture indicates the increase of the strengthening effect of the grain boundaries. [174] Additional external stress and energy is required to fracture the specimens which have larger proportions of transgranular fracture features present. It is assumed that warm compacted specimens (with better sinterability) would have higher values of tensile strength and elongation than cold compacted ones.

Božić *et al.* [206] and Saage *et al.* [207] found that there is a correlation between the fracture morphology and the elongation, i.e. higher elongation corresponds to transgranular fracture, while the minimum elongation is a consequence of intergranular fracture.

5.11 Taguchi analysis

Tables 4.18 and 4.19 show the effect of the single parameters with their percentage contribution on the densities and mechanical properties of the specimens with Acrawax C and Kenolube P11.

Taguchi analysis shows that lubricant content has the most significant influence on green density, tensile strength and elongation of Alumix 123 specimens for both lubricants. In specimens with Acrawax C the second parameter with highest influence was compaction temperature, followed by compaction pressure. In specimens with Kenolube P11 the compaction pressure was followed by compaction temperature.

However, the percentage contribution of single parameters pointed that difference between their influences are balanced.

The present study is based on single parameter influences which do not take into account of any interaction between process parameters (i.e. compaction pressure, temperature and lubricant content). This may affect the order of influence if the interaction of parameters is included in the analysis.

The effect of the lubricant content has been observed by many authors mentioned in this study [e.g. 185, 186 and 205]. Where the presence of lubricant causes an increase in porosity levels, the required properties of the specimens are therefore limited.

CHAPTER 6

CONCLUSIONS AND FUTURE WORK

6.1 Conclusions

In this project the effect of admixed lubricant and compaction processes (cold and warm compaction) on mechanical properties and microstructure of aluminium alloy Alumix 123 was investigated. It was found that, by compaction at elevated temperature:

- The green density of Alumix123 P/M parts with an Acrawax C content of 1.5 wt % can be increased from 2.57 to 2.63 g/cm^3 by increasing compaction temperature from RT to 110°C, respectively. Further increase in green density to 2.71 g/cm^3 of Alumix 123 can be achieved by reducing the amount of lubricant to 0.5 wt % of the warm compaction at temperature of 110ºC. This is due to a reduction in temperature dependent yield strength of the powder mixture. This resulted in better rearrangement of powder particles during warm compaction. The compaction at elevated temperature softens the lubricant and helps to reduce particle-to-particle friction and die wall friction.

- Reducing the amount of admixed lubricant increases the green and sintered densities for cold and warm compaction, respectively. However, compaction using lower amount of lubricant requires frequent tool and die wall cleaning.

- The highest green density was achieved at a compaction pressure of 400 MPa, temperature of 110ºC and lubricant content of 0.5 wt %.

- Increasing compaction temperature also reduced the ejection force required to remove the compacts from the die by 40 % due to reduction of friction between particles and die wall, as lubricant softens during warm compaction.

- The warm compacted specimens can reach similar mechanical properties using less compaction pressure as compared to those compacted at higher pressure and room temperature.

- Acrawax C significantly improves the density and mechanical properties of specimens as compared to those prepared using Kenolube P11.

- The Taguchi analysis shows that Alumix 123 specimens are most affected by lubricant content.

6.2 Suggestions for further work

1. The present study of warm compaction of Alumix 123 showed enhanced static mechanical properties. This study can be extended to determine if warm compaction can improve the dynamic mechanical behaviour (e.g. fatigue).

2. In this study the aging of the specimens was carried out under the same conditions. However, further investigation of the effect of warm compaction on the aging characteristic of Alumix 123 is needed.

3. The current study indicates lower lubricant content can give greater enhancement in the density and mechanical properties. Therefore, it would be interesting to study warm compaction without admix lubricant but with only die wall lubrication.

4. In this study, the specimens were compacted by single punch pressing. It would be interesting to extend warm compaction to a double punch die set to determine if density can be more uniform within the compact.

5. It has been determined, that warm compaction process can increase mechanical properties of aluminium Alumix 123. With reference to this, warm compaction process could be applied to other Al based P/M alloys (e.g. Alumix 231, Alumix 431).

6. In this study, lubricant content is the process parameter which most influences the most green/sintered densities and mechanical properties according to Taguchi analysis. However, this can be extended to study interaction of all the processing parameters.

APPENDIX

Table A1: Ejection force of Alumix 123 compacts with Acrawax C

Acrawax C 0.5 wt %				
Compaction pressure [MPa]	**Compaction temperature [°C]**			
	RT	**60**	**80**	**110**
	Ejection force [kN] (Standard error) [kN]			
200	9.40 (±0.21)	8.00 (±0.14)	5.90 (±0.12)	6.27 (±0.13)
250	11.53 (±0.21)	9.13 (±0.21)	6.90 (±0.21)	6.73 (±0.24)
300	12.10 (±0.28)	9.03 (±0.14)	8.03 (±0.07)	6.53 (±0.16)
350	13.37 (±0.14)	8.23 (±0.21)	8.77 (±0.21)	7.17 (±0.16)
400	12.97 (±0.07)	9.87 (±0.14)	9.80 (±0.23)	6.80 (±0.26)
Acrawax C 1.0 wt %				
200	5.33 (±0.17)	4.30 (±0.17)	4.95 (±0.17)	3.63 (±0.17)
250	5.85 (±0.17)	4.08 (±0.35)	5.78 (±0.15)	3.55 (±0.12)
300	6.47 (±0.13)	4.63 (±0.30)	5.55 (±0.17)	3.03 (±0.24)
350	6.53 (±0.29)	4.83 (±0.17)	5.03 (±0.17)	3.55 (±0.15)
400	7.20 (±0.05)	4.53 (±0.15)	5.18 (±0.35)	3.25 (±0.15)
Acrawax C 1.5 wt %				
200	7.58 (±0.14)	6.39 (±0.17)	4.85 (±0.10)	4.27 (±0.14)
250	7.90 (±0.15)	6.94 (±0.18)	5.20 (±0.20)	5.40 (±0.12)
300	8.10 (±0.06)	6.77 (±0.12)	6.12 (±0.14)	5.50 (±0.11)
350	8.20 (±0.27)	7.47 (±0.11)	6.80 (±0.10)	5.93 (±0.15)
400	10.10 (±0.18)	8.70 (±0.15)	6.31 (±0.14)	6.05 (±0.16)

Table A2: Ejection force of Alumix 123 compacts with Kenolube P11

Kenolube P11 0.5 wt %				
Compaction pressure [MPa]	**Compaction temperature [ºC]**			
	RT	**60**	**80**	**110**
	Ejection force [kN] (Standard error) [kN]			
200	7.35 (±0.13)	5.33 (±0.16)	4.65 (±0.11)	4.73 (±0.16)
250	7.80 (±0.22)	5.55 (±0.11)	4.80 (±0.16)	4.50 (±0.16)
300	8.03 (±0.26)	5.18 (±0.11)	4.58 (±0.22)	4.35 (±0.16)
350	8.65 (±0.18)	5.48 (±0.13)	4.88 (±0.13)	4.95 (±0.18)
400	10.58 (±0.13)	8.25 (±0.16)	6.03 (±0.16)	7.58 (±0.22)
Kenolube P11 1.0 wt %				
200	7.20 (±0.21)	5.63 (±0.21)	4.28 (±0.21)	3.90 (±0.16)
250	6.98 (±0.11)	5.78 (±0.21)	4.13 (±0.21)	3.45 (±0.22)
300	6.83 (±0.13)	5.63 (±0.21)	3.90 (±0.13)	4.05 (±0.13)
350	7.68 (±0.22)	5.55 (±0.13)	4.13 (±0.11)	3.60 (±0.18)
400	10.75 (±0.09)	7.13 (±0.15)	7.35 (±0.13)	5.18 (±0.13)
Kenolube P11 1.5 wt %				
200	6.95 (±0.23)	5.40 (±0.15)	4.50 (±0.22)	4.90 (±0.17)
250	7.05 (±0.20)	4.85 (±0.17)	4.38 (±0.22)	4.65 (±0.15)
300	6.93 (±0.25)	4.83 (±0.11)	4.40 (±0.15)	4.38 (±0.18)
350	7.75 (±0.20)	5.03 (±0.18)	4.15 (±0.07)	5.03 (±0.12)
400	10.13 (±0.25)	5.85 (±0.17)	6.83 (±0.20)	5.05 (±0.22)

Table A3: Green density of Alumix 123 compacts with Acrawax C

Acrawax C 0.5 wt %				
Compaction pressure [MPa]	**Compaction temperature [ºC]**			
	RT	**60**	**80**	**110**
	Green density (Standard error) [g/cm^3]			
	Relative density [%]			
200	2.577 (±0.018) 92.05	2.591 (±0.033) 92.52	2.602 (±0.018) 92.91	2.607 (±0.008) 93.09
250	2.608 (±0.006) 93.16	2.620 (±0.018) 93.57	2.639 (±0.007) 94.23	2.643 (±0.018) 94.40
300	2.640 (±0.021) 94.29	2.653 (±0.031) 94.76	2.663 (±0.015) 95.10	2.676 (±0.012) 95.58
350	2.660 (±0.009) 94.99	2.665 (±0.004) 95.19	2.673 (±0.013) 95.45	2.687 (±0.025) 95.95
400	2.673 (±0.012) 95.45	2.678 (±0.025) 95.63	2.689 (±0.009) 96.04	2.704 (±0.018) 96.59
Acrawax C 1.0 wt %				
200	2.535 (±0.024) 90.52	2.551 (±0.009) 91.11	2.595 (±0.021) 92.66	2.603 (±0.020) 92.96
250	2.563 (±0.017) 91.53	2.568 (±0.009) 91.73	2.620 (±0.002) 93.57	2.620 (±0.012) 93.59
300	2.577 (±0.011) 92.05	2.594 (±0.023) 92.65	2.626 (±0.019) 93.80	2.651 (±0.029) 94.67
350	2.589 (±0.004) 92.45	2.601 (±0.019) 92.90	2.634 (±0.019) 94.08	2.663 (±0.002) 95.11
400	2.613 (±0.005) 93.31	2.617 (±0.001) 93.48	2.657 (±0.021) 94.89	2.670 (±0.005) 95.36
Acrawax C 1.5 wt %				
200	2.523 (±0.032) 90.10	2.549 (±0.025) 91.05	2.551 (±0.013) 91.10	2.567 (±0.020) 91.68
250	2.554 (±0.032) 91.21	2.570 (±0.008) 91.79	2.589 (±0.025) 92.45	2.593(±0.012) 92.61
300	2.568 (±0.029) 91.72	2.588 (±0.013) 92.42	2.596 (±0.018) 92.73	2.618 (±0.019) 93.49
350	2.574 (±0.021) 91.94	2.609 (±0.013) 93.17	2.612 (±0.031) 93.27	2.629 (±0.014) 93.89
400	2.591 (±0.043) 92.54	2.621 (±0.024) 93.59	2.629 (±0.025) 93.88	2.632 (±0.010) 93.99

Table A.4: Green density of Alumix 123 compacts with Kenolube P11

Kenolube P11 0.5 wt %				
Compaction pressure [MPa]	**Compaction temperature [ºC]**			
	RT	**60**	**80**	**110**
	Green density (Standard error) [g/cm^3]			
	Relative density [%]			
200	2.511 (±0.012) 89.69	2.548 (±0.024) 91.01	2.555 (±0.022) 91.26	2.573 (±0.020) 91.88
250	2.545 (±0.004) 90.89	2.580 (±0.009) 92.13	2.579 (±0.025) 92.10	2.595 (±0.022) 92.69
300	2.571 (±0.009) 91.81	2.598 (±0.006) 92.77	2.601 (±0.009) 93.01	2.612 (±0.023) 93.30
350	2.581 (±0.032) 92.25	2.607 (±0.026) 93.11	2.616 (±0.013) 93.42	2.631 (±0.026) 93.98
400	2.617 (±0.027) 93.48	2.627 (±0.029) 93.82	2.631 (±0.020) 94.35	2.660 (±0.018) 95.01
Kenolube P11 1.0 wt %				
200	2.508 (±0.009) 89.59	2.531 (±0.021) 90.40	2.558 (±0.009) 91.35	2.563 (±0.022) 91.53
250	2.540 (±0.010) 90.71	2.553 (±0.014) 91.19	2.587 (±0.013) 92.39	2.596 (±0.020) 92.71
300	2.556 (±0.0160 91.29	2.576 (±0.022) 91.99	2.588 (±0.021) 92.42	2.599 (±0.018) 92.84
350	2.570 (±0.013) 91.80	2.586 (±0.007) 92.34	2.600 (±0.007) 92.85	2.612 (±0.011) 93.27
400	2.606 (±0.028) 93.06	2.627 (±0.032) 93.80	2.635 (±0.018) 94.11	2.645 (±0.018) 94.47
Kenolube P11 1.5 wt %				
200	2.504 (±0.030) 89.41	2.527 (±0.025) 90.24	2.544 (±0.020) 90.85	2.556 (±0.027) 91.30
250	2.537 (±0.014) 90.61	2.556 (±0.025) 91.29	2.560 (±0.029) 91.42	2.572 (±0.027) 91.84
300	2.550 (±0.011) 91.06	2.571 (±0.018) 91.82	2.571 (±0.007) 91.83	2.582 (±0.016) 92.23
350	2.562 (±0.009) 91.49	2.576 (±0.012) 92.01	2.579 (±0.003) 92.12	2.609 (±0.012) 93.20
400	2.576 (±0.024) 91.99	2.604 (±0.024) 92.99	2.610 (±0.033) 93.22	2.626 (±0.004) 93.78

Table A5: Sintered/aged density of Alumix 123 compacts with Acrawax C

Acrawax C 0.5 wt %				
Compaction pressure [MPa]	**Compaction temperature [ºC]**			
	RT	**60**	**80**	**110**
	Sintered/aged density (Standard error) [g/cm^3]			
	Relative density [%]			
200	2.586 (±0.015) 92.35	2.624 (±0.025) 93.70	2.658 (±0.004) 94.94	2.671 (±0.022) 95.39
250	2.631 (±0.020) 93.95	2.662 (±0.010) 95.08	2.701 (±0.019) 96.47	2.706 (±0.015) 96.63
300	2.687 (±0.022) 95.97	2.704 (±0.012) 96.56	2.716 (±0.016) 97.01	2.740 (±0.006) 97.86
350	2.700 (±0.022) 96.42	2.708 (±0.022) 96.73	2.717 (±0.018) 97.03	2.751 (±0.010) 98.24
400	2.711 (±0.019) 96.84	2.714 (±0.019) 96.94	2.722 (±0.003) 97.21	2.751 (±0.011) 98.26
Acrawax C 1.0 wt %				
200	2.537 (±0.026) 90.62	2.558 (±0.016) 91.35	2.664 (±0.021) 95.14	2.671 (±0.021) 95.38
250	2.579 (±0.017) 92.11	2.569 (±0.015) 91.73	2.677 (±0.021) 95.62	2.691 (±0.013) 96.11
300	2.576 (±0.011) 92.01	2.598 (±0.019) 92.79	2.686 (±0.012) 95.94	2.702 (±0.012) 96.51
350	2.593 (±0.011) 92.60	2.605 (±0.012) 93.03	2.707 (±0.017) 96.69	2.723 (±0.020) 97.25
400	2.625 (±0.069) 93.78	2.634 (±0.068) 94.08	2.724 (±0.015) 97.28	2.724 (±0.015) 97.29
Acrawax C 1.5 wt %				
200	2.528 (±0.019) 90.28	2.551 (±0.015) 91.09	2.594 (±0.024) 92.65	2.602 (±0.028) 92.94
250	2.554 (±0.010) 91.22	2.579 (±0.022) 92.12	2.625 (±0.024) 93.74	2.633 (±0.016) 94.04
300	2.569 (±0.016) 91.76	2.587 (±0.020) 92.38	2.614 (±0.014) 93.34	2.668 (±0.007) 95.27
350	2.582 (±0.011) 92.21	2.614 (±0.020) 93.37	2.633 (±0.016) 94.03	2.677 (±0.029) 95.61
400	2.611 (±0.037) 93.23	2.626 (±0.015) 93.79	2.643 (±0.024) 94.40	2.679 (±0.013) 95.69

Table A6: Sintered/aged density of Alumix 123 compacts with Kenolube P11

Kenolube P11 0.5 wt %				
Compaction pressure [MPa]	**Compaction temperature [ºC]**			
	RT	**60**	**80**	**110**
	Sintered/aged density (Standard error) [g/cm^3]			
	Relative density [%]			
200	2.535 (±0.026) 90.52	2.572 (±0.027) 91.85	2.592 (±0.019) 92.58	2.604 (±0.011) 93.00
250	2.557 (±0.030) 91.31	2.583 (±0.027) 92.26	2.618 (±0.009) 93.51	2.625 (±0.049) 93.75
300	2.579 (±0.018) 92.11	2.611 (±0.023) 93.26	2.625 (±0.044) 93.78	2.647 (±0.056) 94.53
350	2.592 (±0.026) 92.59	2.628 (±0.039) 93.88	2.639 (±0.052) 94.28	2.654 (±0.049) 94.78
400	2.646 (±0.022) 94.48	2.665 (±0.019) 95.16	2.671 (±0.016) 95.42	2.683 (±0.004) 95.83
Kenolube P11 1.0 wt %				
200	2.543 (±0.022) 90.82	2.580 (±0.019) 92.14	2.583 (±0.021) 92.23	2.604 (±0.014) 92.99
250	2.574 (±0.017) 91.91	2.605 (±0.055) 93.03	2.618 (±0.021) 93.49	2.637 (±0.015) 94.17
300	2.581 (±0.018) 92.17	2.606 (±0.061) 93.06	2.621 (±0.029) 93.62	2.653 (±0.017) 94.75
350	2.604 (±0.027) 92.99	2.611 (±0.064) 93.26	2.629 (±0.061) 93.90	2.646 (±0.020) 94.49
400	2.625 (±0.019) 93.75	2.649 (±0.019) 94.59	2.650 (±0.007) 94.63	2.654 (±0.022) 94.77
Kenolube P11 1.5 wt %				
200	2.539 (±0.007) 90.69	2.559 (±0.015) 91.39	2.582 (±0.013) 92.23	2.597 (±0.023) 92.75
250	2.550 (±0.017) 91.08	2.571 (±0.016) 91.83	2.589 (±0.010) 92.45	2.608 (±0.026) 93.13
300	2.564 (±0.010) 91.57	2.586 (±0.007) 92.38	2.604 (±0.018) 93.01	2.619 (±0.026) 93.54
350	2.565 (±0.015) 91.61	2.589 (±0.012) 92.47	2.623 (±0.024) 93.69	2.631 (±0.023) 93.95
400	2.602 (±0.004) 92.91	2.611 (±0.016) 93.24	2.627 (±0.011) 93.83	2.651 (±0.013) 94.69

Table A7: Tensile strength of sintered/aged Alumix 123 compacts with Acrawax C

Acrawax C 0.5 wt %				
Compaction pressure [MPa]	**Compaction temperature [ºC]**			
	RT	**60**	**80**	**110**
	Tensile strength [MPa] (Standard error) [MPa]			
200	295.66 (±11.47)	312.42 (±10.75)	305.96 (±4.87)	323.79 (±8.63)
250	305.56 (±15.79)	306.18 (±12.48)	321.16 (±5.88)	318.65 (±9.53)
300	306.31 (±14.36)	308.02 (±11.36)	329.48 (±11.49)	344.57 (±5.10)
350	319.20 (±11.92)	337.98 (±9.44)	333.07 (±4.76)	350.76 (±9.05)
400	324.86 (±3.99)	334.84 (±9.48)	357.61 (±10.50)	365.65 (±12.36)
Acrawax C 1.0 wt %				
200	286.39 (±10.73)	284.13 (±9.84)	297.55 (±3.85)	318.76 (±3.95)
250	292.43 (±10.22)	299.40 (±12.08)	294.30 (±12.09)	309.20 (±10.81)
300	287.12 (±8.58)	309.45 (±1.26)	318.62 (±7.77)	328.21 (±1.13)
350	298.75 (±11.46)	305.88 (±10.52)	317.21 (±10.33)	327.72 (±5.98)
400	302.43 (±6.28)	309.89 (±13.35)	332.29 (±13.38)	343.51 (±11.15)
Acrawax C 1.5 wt %				
200	266.22 (±12.98)	270.80 (±6.65)	279.59 (±12.15)	289.67 (±10.82)
250	269.07 (±14.76)	272.92 (±11.58)	299.15 (±8.57)	301.03 (±8.39)
300	278.71 (±13.19)	289.29 (±8.89)	291.55 (±16.93)	315.25 (±9.93)
350	280.86 (±13.71)	290.34 (±7.13)	298.60 (±11.30)	318.87 (±16.78)
400	289.84 (±11.50)	292.92 (±10.03)	299.21 (±12.57)	324.90 (±10.29)

Table A8: Tensile strength of sintered/aged Alumix 123 compacts with Kenolube P11

Kenolube P11 0.5 wt %				
Compaction pressure [MPa]	**Compaction temperature [ºC]**			
	RT	**60**	**80**	**110**
	Tensile strength [MPa] (Standard error) [MPa]			
200	288.01 (±14.15)	283.12 (±16.05)	303.31 (±12.55)	307.37 (±11.80)
250	294.62 (±14.21)	299.48 (±16.17)	306.92 (±4.68)	312.72 (±2.48)
300	302.88 (±3.92)	301.53 (±11.59)	306.26 (±9.11)	319.33 (±12.96)
350	305.80 (±15.34)	306.44 (±10.99)	313.31 (±13.46)	335.90 (±7.47)
400	322.22 (±13.35)	321.71 (±12.16)	343.17 (±7.58)	351.74 (±6.74)
Kenolube P11 1.0 wt %				
200	284.00 (±9.70)	281.19 (±15.49)	289.24 (±13.43)	292.95 (±15.31)
250	277.25 (±14.44)	295.08 (±13.02)	287.88 (±7.05)	296.12 (±11.42)
300	291.94 (±11.60)	299.14 (±14.39)	296.12 (±10.95)	294.03 (±5.04)
350	289.12 (±11.75)	301.38 (±15.87)	303.74 (±11.78)	305.85 (±16.99)
400	301.45 (±14.19)	314.73 (±12.74)	317.27 (±13.47)	320.87 (±11.63)
Kenolube P11 1.5 wt %				
200	262.46 (±9.86)	267.17 (±6.88)	265.55 (±12.53)	276.91 (±14.03)
250	266.25 (±11.49)	273.48 (±12.77)	275.27 (±7.17)	277.05 (±13.26)
300	268.44 (±13.68)	273.05 (±13.18)	277.71 (±10.56)	288.39 (±13.64)
350	262.23 (±11.24)	280.45 (±6.53)	302.34 (±4.51)	294.35 (±11.85)
400	281.65 (±11.43)	292.38 (±7.99)	305.26 (±13.60)	309.98 (±12.26)

Table A9: Hardness of sintered/aged Alumix 123 compacts with Acrawax C

Acrawax C 0.5 wt %				
Compaction pressure [MPa]	**Compaction temperature [ºC]**			
	RT	**60**	**80**	**110**
	Vickers hardness [HV] (Standard error) [HV]			
200	100.02 (±2.86)	102.50 (±2.12)	102.01 (±3.68)	106.70 (±3.96)
250	100.40 (±3.25)	103.20 (±2.83)	109.60 (±3.96)	111.58 (±3.11)
300	102.20 (±2.69)	110.70 (±5.09)	108.80 (±2.55)	118.55 (±3.54)
350	106.90 (±3.68)	107.80 (±4.95)	119.90 (±4.10)	124.43 (±5.52)
400	109.20 (±3.12)	112.80 (±1.13)	127.53 (±3.96)	128.60 (±4.38)
Acrawax C 1.0 wt %				
200	95.60 (±1.84)	99.70 (±4.10)	102.80 (±3.68)	102.40 (±4.95)
250	100.45 (±4.67)	103.40 (±2.71)	109.33 (±5.23)	111.30 (±4.10)
300	104.40 (±2.43)	106.10 (±4.08)	110.65 (±4.95)	108.70 (±4.38)
350	104.83 (±4.81)	112.10 (±5.23)	114.70 (±3.54)	112.10 (±3.39)
400	103.30 (±4.67)	110.25 (±4.50)	121.50 (±2.26)	119.51 (±1.70)
Acrawax C 1.5 wt %				
200	92.90 (±3.25)	94.30 (±3.54)	97.31 (±5.49)	97.70 (±5.94)
250	98.43 (±4.25)	101.98 (±4.80)	101.94 (±5.82)	102.60 (±2.33)
300	96.39 (±1.41)	99.50 (±5.37)	103.42 (±3.54)	106.17 (±5.80)
350	103.76 (±4.38)	101.10 (±3.82)	111.68 (±2.97)	110.90 (±2.13)
400	104.41 (±2.76)	103.00 (±2.84)	111.39 (±3.42)	117.31 (±3.79)

Table A10: Hardness of sintered/aged Alumix 123 compacts with Kenolube P11

Kenolube P11 0.5 wt %				
Compaction pressure [MPa]	**Compaction temperature [ºC]**			
	RT	**60**	**80**	**110**
	Vickers hardness [HV] (Standard error) [HV]			
200	99.00 (±4.10)	100.60 (±5.41)	104.10 (±5.26)	104.30 (±2.83)
250	98.00 (±3.59)	105.20 (±2.86)	103.30 (±4.13)	107.80 (±4.50)
300	98.40 (±3.11)	101.10 (±5.02)	104.20 (±1.94)	107.85 (±1.84)
350	101.37 (±4.96)	109.05 (±2.71)	107.06 (±3.25)	112.20 (±4.18)
400	108.93 (±3.25)	107.50 (±2.40)	115.26 (±5.71)	117.93 (±5.09)
Kenolube P11 1.0 wt %				
200	95.80 (±1.89)	97.10 (±4.42)	102.30 (±2.97)	103.40 (±3.75)
250	95.40 (±5.66)	101.97 (±2.93)	108.70 (±6.22)	103.73 (±4.27)
300	97.10 (±4.71)	99.50 (±2.97)	106.44 (±5.78)	106.30 (±5.08)
350	98.60 (±4.53)	103.67 (±3.86)	109.26 (±6.45)	108.40 (±4.31)
400	102.60 (±3.54)	105.80 (±5.37)	113.80 (±5.88)	115.45 (±2.05)
Kenolube P11 1.5 wt %				
200	92.48 (±4.10)	93.80 (±5.09)	94.90 (±5.99)	96.67 (±5.09)
250	93.80 (±5.55)	91.70 (±4.37)	102.20 (±4.27)	102.20 (±3.20)
300	96.65 (±4.19)	97.05 (±5.89)	108.37 (±5.23)	107.63 (±4.81)
350	97.97 (±5.81)	100.37 (±3.65)	104.14 (±3.08)	108.80 (±5.19)
400	101.48 (±4.88)	106.80 (±3.59)	109.40 (±1.20)	113.25 (±6.68)

Table A11: Elongation of sintered/aged Alumix 123 compacts with Acrawax C

Acrawax C 0.5 wt %				
Compaction pressure [MPa]	**Compaction temperature [ºC]**			
	RT	**60**	**80**	**110**
	Elongation [%] (Standard error) [%]			
200	0.57 (±0.01)	0.76 (±0.02)	0.83 (±0.02)	0.91 (±0.03)
250	0.55 (±0.02)	0.71 (±0.01)	0.93 (±0.02)	0.91 (±0.03)
300	0.74 (±0.01)	0.86 (±0.03)	0.93 (±0.01)	1.01 (±0.02)
350	0.78 (±0.02)	1.02 (±0.03)	1.01 (±0.04)	1.08 (±0.03)
400	0.82 (±0.03)	0.97 (±0.01)	1.05 (±0.03)	1.12 (±0.02)
Acrawax C 1.0 wt %				
200	0.49 (±0.01)	0.60 (±0.02)	0.68 (±0.02)	0.71 (±0.03)
250	0.55 (±0.02)	0.59 (±0.01)	0.72 (±0.01)	0.73 (±0.02)
300	0.54 (±0.03)	0.62 (±0.01)	0.72 (±0.03)	0.73 (±0.01)
350	0.54 (±0.02)	0.65 (±0.03)	0.75 (±0.02)	0.81 (±0.02)
400	0.56 (±0.02)	0.61 (±0.03)	0.72 (±0.02)	0.82 (±0.01)
Acrawax C 1.5 wt %				
200	0.50 (±0.01)	0.48 (±0.01)	0.49 (±0.02)	0.56 (±0.02)
250	0.47 (±0.01)	0.51 (±0.01)	0.53 (±0.02)	0.59 (±0.02)
300	0.51 (±0.01)	0.48 (±0.02)	0.62 (±0.02)	0.64 (±0.01)
350	0.52 (±0.03)	0.56 (±0.02)	0.60 (±0.01)	0.67 (±0.02)
400	0.54 (±0.02)	0.62 (±0.01)	0.65 (±0.01)	0.71 (±0.03)

Table A12: Elongation of sintered/aged Alumix 123 compacts with Kenolube P11

Kenolube P11 0.5 wt %				
Compaction pressure [MPa]	**Compaction temperature [ºC]**			
	RT	**60**	**80**	**110**
	Elongation [%] (Standard error) [%]			
200	0.54 (±0.02)	0.65 (±0.03)	0.74 (±0.02)	0.75 (±0.03)
250	0.62 (±0.02)	0.68 (±0.02)	0.75 (±0.02)	0.74 (±0.03)
300	0.64 (±0.01)	0.75 (±0.03)	0.75 (±0.03)	0.81 (±0.01)
350	0.70 (±0.03)	0.70 (±0.01)	0.77 (±0.02)	0.86 (±0.01)
400	0.68 (±0.02)	0.76 (±0.01)	0.80 (±0.03)	0.93 (±0.03)
Kenolube P11 1.0 wt %				
200	0.46 (±0.01)	0.50 (±0.03)	0.53 (±0.01)	0.51 (±0.02)
250	0.49 (±0.03)	0.54 (±0.01)	0.54 (±0.03)	0.55 (±0.02)
300	0.55 (±0.02)	0.60 (±0.01)	0.62 (±0.01)	0.59 (±0.03)
350	0.57 (±0.03)	0.61 (±0.03)	0.58 (±0.04)	0.63 (±0.02)
400	0.61 (±0.02)	0.63 (±0.03)	0.67 (±0.03)	0.73 (±0.03)
Kenolube P11 1.5 wt %				
200	0.48 (±0.02)	0.49 (±0.03)	0.45 (±0.03)	0.56 (±0.03)
250	0.45 (±0.03)	0.44 (±0.02)	0.53 (±0.01)	0.54 (±0.03)
300	0.46 (±0.03)	0.48 (±0.02)	0.55 (±0.03)	0.64 (±0.02)
350	0.50 (±0.02)	0.58 (±0.03)	0.59 (±0.02)	0.64 (±0.02)
400	0.52 (±0.02)	0.63 (±0.02)	0.62 (±0.01)	0.70 (±0.03)

Table A13: Young's modulus of sintered/aged Alumix 123 compacts with Acrawax C

Acrawax C 0.5 wt %				
Compaction pressure [MPa]	**Compaction temperature [ºC]**			
	RT	**60**	**80**	**110**
	Young's modulus [GPa] (Standard error) [GPa]			
200	58.05 (±1.68)	62.19 (±1.91)	61.84 (±2.51)	62.31 (±2.34)
250	59.24 (±1.78)	62.35 (±3.04)	63.24 (±3.38)	64.18 (±2.36)
300	58.50 (±2.90)	60.86 (±1.51)	65.06 (±2.09)	67.14 (±2.13)
350	61.52 (±2.17)	63.21 (±2.54)	67.39 (±2.07)	68.22 (±3.50)
400	63.48 (±2.37)	66.66 (±2.47)	67.73 (±2.65)	69.74 (±1.04)
Acrawax C 1.0 wt %				
200	58.20 (±1.82)	60.04 (±2.54)	60.69 (±1.40)	61.35 (±1.56)
250	56.70 (±3.30)	58.93 (±0.79)	61.20 (±2.98)	64.49 (±3.12)
300	56.71 (±1.69)	60.96 (±2.19)	62.35 (±2.83)	65.08 (±1.18)
350	59.28 (±2.61)	62.78 (±2.19)	65.69 (±1.97)	67.70 (±1.80)
400	61.80 (±1.65)	64.08 (±1.42)	67.06 (±2.77)	67.69 (±1.39)
Acrawax C 1.5 wt %				
200	54.95 (±1.15)	59.29 (±2.83)	60.93 (±2.40)	61.18 (±3.19)
250	56.07 (±3.07)	61.73 (±1.32)	61.95 (±2.15)	63.26 (±3.37)
300	57.84 (±1.35)	56.91 (±2.64)	63.24 (±3.65)	64.18 (±2.93)
350	59.98 (±2.67)	62.90 (±2.35)	65.03 (±1.78)	65.89 (±2.46)
400	61.44 (±2.22)	63.32 (±2.02)	65.09 (±1.34)	65.82 (±3.23)

Table A14: Young's modulus of sintered/aged Alumix 123 compacts with Kenolube P11

Kenolube P11 0.5 wt %				
Compaction pressure [MPa]	**Compaction temperature [ºC]**			
	RT	**60**	**80**	**110**
	Young's modulus [GPa] (Standard error) [GPa]			
200	57.47 (±1.68)	58.98 (±3.06)	61.45 (±2.88)	63.98 (±2.68)
250	58.60 (±2.41)	62.68 (±3.10)	63.04 (±2.68)	65.45 (±2.80)
300	60.30 (±0.74)	63.45 (±1.75)	62.83 (±3.67)	68.37 (±2.57)
350	61.21 (±2.10)	63.37 (±2.31)	66.63 (±1.28)	67.68 (±0.95)
400	62.96 (±0.55)	64.88 (±3.03)	66.95 (±2.16)	68.45 (±0.83)
Kenolube P11 1.0 wt %				
200	56.06 (±0.73)	59.98 (±1.93)	61.24 (±2.53)	61.05 (±0.97)
250	57.98 (±1.53)	58.88 (±3.33)	61.77 (±2.45)	62.80 (±2.94)
300	59.24 (±0.64)	63.50 (±2.92)	62.71 (±2.43)	64.20 (±4.04)
350	60.99 (±2.92)	62.34 (±2.62)	63.02 (±1.77)	64.05 (±3.86)
400	63.04 (±2.57)	64.63 (±2.38)	66.31 (±1.94)	66.78 (±3.39)
Kenolube P11 1.5 wt %				
200	54.93 (±2.06)	55.16 (±2.22)	60.21 (±3.56)	60.22 (±0.81)
250	56.97 (±1.81)	59.52 (±2.33)	60.97 (±0.98)	62.14 (±2.63)
300	59.77 (±1.72)	61.77 (±2.58)	60.08 (±2.55)	62.08 (±1.86)
350	57.53 (±3.34)	61.94 (±0.06)	62.19 (±0.46)	64.82 (±3.10)
400	60.22 (±2.93)	62.61 (±1.82)	65.30 (±1.74)	65.34 (±1.55)

REFERENCES

1. M. Capus, *Metal Powders A Global Survey of Production, Applications and Markets to 2010*, Fourth Edition, Elsevier Advanced Technology, Oxford, 2005, p. 98;
2. http://www.metalpowderproducts.com/index.asp?action=manufacturing_basics, accessed: 27th February 2009;
3. http://www.smcpowdermetallurgy.com/advantages.htm, accessed: 27th February 2009;
4. http://www.keytometals.com/Article62.htm, accessed: 27th February 2009;
5. M. L. Bauccio, *ASM Metals Reference Book*, American Society for Metals, Third Edition, ASM International, 1993, p. 531;
6. http://aluminium.matter.org.uk/aluselect/09_mech_browse.asp, accessed: 27th February 2009;
7. http://www.ecka-granules.com/index.php?id=153&typ=15&anwendung=3&L=2, accessed: 27th February 2009;
8. H.Rutz, J. Khanuja, S. Kassam, *Single Compaction to Achieve High Density in Ferrous P/M Materials in Automotive Applications*, Presented at PM^{2}TEC '96 World Congress;
9. ASM handbook Vol.7, *Powder Metal Technologies and Applications / Prepared Under the Direction of the ASM International Handbook Committee*, Materials Park, ASM, 1998, p. 834;
10. P. Enghag, *Encyclopedia of the Elements*, *Technical Data History Processing Applications,* WILEY-VCH Verlag GmbH & Co. KGaA, 2004 p. 819-843;
11. Lambda research, *Efficiently optimizing manufacturing processes using interactive Taguchi analysis*, Diffraction Notes, No. 25, Cincinnati, 2000, p. 1-4;
12. J. M. Capus, *Metal Powders A Global Survey of Production, Applications and Markets to 2010*, Fourth Edition, Elsevier Advanced Technology, Oxford, 2005, p. 153;
13. G. Dowson, *Powder Metallurgy: The Process and its Products*, Hilger, Bristol, 1990, p. 19;
14. D. Yarnton, M. Argyle, *A Practical Course in Powder Metallurgy*, Cassell, London, 1962, p. 4;

15. F. Thummler, R. Oberacker, *Introduction to Powder Metallurgy*, Institute of Materials, London, 1993, p. 7;

16. A. Havalda, *Prášková Metalurgia*, STU Bratislava, 2000, p. 16-18;

17. ASM handbook Vol.7, *Powder Metal Technologies and Applications / Prepared Under the Direction of the ASM International Handbook Committee*, Materials Park, ASM, 1998, p. 89;

18. F. Thummler, R. Oberacker, *Introduction to Powder Metallurgy*, Institute of Materials, London, 1993, p. 23;

19. ASM handbook Vol.7, *Powder Metal Technologies and Applications / Prepared Under the Direction of the ASM International Handbook Committee*, Materials Park, ASM, 1998, p. 111-114;

20. J. M. Capus, *Metal Powders A Global Survey of Production, Applications and Markets to 2010*, Fourth Edition, Elsevier Advanced Technology, Oxford, 2005, p. 157;

21. N. Dombrowski, W.R. Johns, *The Aerodynamic Instability and Disintegration of Viscous Liquid Sheets*, Chemical Engineering Science., Vol. 18, 1963, p. 203-214;

22. W. Schatt, K. P. Wieters, *Powder Metallurgy : Processing and Materials*, EPMA Publications, 1997, p. 13;

23. G. Dowson, *Powder Metallurgy: The Process and its Products*, Hilger, Bristol, 1990, p. 26;

24. R. M. German, *Powder Metallurgy Science*, Metal Powder Industries Federation, NJ, 1984, p. 78;

25. F. Thummler, R. Oberacker, *Introduction to Powder Metallurgy*, Institute of Materials, London, 1993, p. 21;

26. http://www.substech.com/dokuwiki/lib/exe/fetch.php?w=&h=&cache=cache&media=atomization.png; accessed: 13th March 2009;

27. A. R. Kaufman, *Method and Aperture for Making of Powder*, United States Patent 3099041, 1963;

28. A. Lawley, Atomization: *The Production of Metal Powders*, Metal Powder Industries Federation, Princeton, NJ, 1992;

29. A. Havalda, *Prášková Metalurgia*, STU Bratislava, 2000, p. 26;

30. G. Dowson, *Powder Metallurgy: The Process and its Products*, Hilger, Bristol, 1990, p. 28;

31. R. M. German, *Powder Metallurgy Science*, Metal Powder Industries Federation, NJ, 1984, p. 81;

32. A. R. Kaufman, *Production of Pure, Spherical Powders*, United States Patent 3802816, 1974;

33. S. P. Bhat, T. R. Ramachandran, A. K. Jena, *Splat Cooling of Aluminium -Manganese Alloys*, Journal of Materials Science, Vol. 9, 1974, p. 1759-1763;

34. Ch. C. Thompson, *Splat Cooling of Liquid Metal Droplets*, United States Patent 4375440, 1983;

35. W. Schatt, K. P. Wieters, *Powder Metallurgy: Processing and Materials*, EPMA Publications, 1997, p. 18 - 21;

36. http://www.magnets.bham.ac.uk/images/melt_spin.gif, accessed 13th March 2009;

37. http://electrochem.cwru.edu/ed/encycl/art-m03-machining.htm, accessed 13th March 2009;

38. F. Thummler, R. Oberacker, *Introduction to Powder Metallurgy*, Institute of Materials, London, 1993, p. 44;

39. W. Schatt, K. P. Wieters, *Powder Metallurgy: Processing and Materials*, EPMA Publications, 1997, p. 30;

40. http://electrochem.cwru.edu/ed/encycl/art-p04-metalpowder.htm; accessed 13th March 2009;

41. V. Kraus, *Tepelné Zpracování a Slinování Přednášky*, ZČU, Plzeň, 2000, p. 170-173;

42. A. Salak, M. Selecka, H. Danninger, *Machinability of Powder Metallurgy Steels*, Cambridge, International Science Publishing, 2005, p. 6-11;

43. A. Chatterjee, *Beyond the Blast Furnace,* CRC Press, 1993, p. 92-114;

44. L. F. Pease, III, *Advances in Powder Metallurgy - 1991: P/M Materials*, Metal Powder Industries Federation, 1991, p. 32;

45. J. M. Capus, *A Global Survey of Production, Applications and Markets*, Elsevier, 2000 p. 112;

46. Elsevier Scientific Publishing Company, *Applied Catalysis*, 1984, p. 22-25;

47. A. Parmaliana, *Natural Gas Conversion*, Elsevier, 1998, p. 116-126;

48. R. L. Sands, C.R. Shakespeare, *Powder Metallurgy*, William Clowes and Sons, London, 1966, p. 24-25;

49. V. Kraus, *Tepelné Zpracování a Slinování Přednášky*, ZČU, Plzeň, 2000, p. 166-167;

50. http://www.emeraldinsight.com/fig/1820210204012.png; accessed 30th March 2009;

51. A. Havalda, *Prášková Metalurgia*, STU Bratislava, 2000, p. 41-43;

52. W. Schatt, K. P. Wieters, *Powder Metallurgy: Processing and Materials*, EPMA Publications, 1997, p. 47;

53. V. Kraus, *Tepelné Zpracování a Slinování Přednášky*, ZČU, Plzeň, 2000, p. 166-167;

54. W.V. Knopp, *Effect of Type of Lubricant on Green Strength*, Advances in Powder Metallurgy and Particulate Materials, Metal Powder Industries Federation, Vol. 2, 1993, p. 27-33;

55. V. G. Melnikov, N. I. Zamyatina, T. G. Komarova, *Combined Effect of Solid Lubricants and Inclusions in P/M Composite Materials*, Powder Metallurgical Materials, No. 5, 1985, p. 30-32;

56. E. R. Booser, *Handbook of Lubrication: Monitoring, Materials, Synthetic Lubricants, and Applications,* CRC Press, 1994, p. 150-160;

57. W. Schatt, K. P. Wieters, *Powder Metallurgy: Processing and Materials*, EPMA Publications, 1997, p. 50, 163;

58. E. Geijer, R.B. Jamison, *Lubricants for Powder Metallurgy Parts Manufacturing*, Hoeganaes report, No. 142, 1965;

59. K.H. Moyer, *The Burn Off Characteristics of Common Lubricants in 316L Powder Compacts*, International Journal of Powder Metallurgy, Vol. 7, 1971, p. 33-43;

60. P.E. Matthews, *Brass and Nickel Silver Powders*, Copper Base Powder Metallurgy, Metal Powder Industries Federation, Vol. 7, 1980;

61. J. McGraw and M.J. Koczak, *A Laboratory/Production Comparison of Powder Compacting and Ejection Response*, International Journal of Powder Metallurgy, Vol. 16 (No. 1), 1980;

62. W. Schatt, K. P. Wieters, *Powder Metallurgy: Processing and Materials*, EPMA Publications, 1997, p. 51;

63. B. H. Kaye, *Powder Mixing*, Springer, 1997, p. 11-13, 19-26;

64. R. M. German, *Powder Metallurgy Science*, Metal Powder Industries Federation, NJ, 1984, p. 102;

65. N. M Shima, H. Jones, J. B Shamsul, M. N Mazlee, K. R Ahmad, M. W. M Fitri, *Mechanical Properties of Al-4.4Cu-0.8Si-0.5Mg Produced by Powder Metallurgy*, ICRAMME 2005, Paper No. 230;

66. N. A. Belov, D. G. Eskin, A. A. Aksenov, *Multicomponent Phase Diagrams: Applications for Commercial Aluminum Alloys*, Elsevier, 2005, p: 83-88, 193-202;

67. R.W. Heckel, *Density pressure relationship in powder compaction*, Transactions of the Metallurgical Society of AIME, Vol.221, 1961, p. 671-675;

68. http://aluminium.matter.org.uk/content/html/eng/default.asp?catid=214&pageid=2144417086, accessed 27th February 2009;

69. G. S. Upadhyaya, *Powder Metallurgy Technology*, Cambridge, International Science Publishing, 1997, p. 42-57;

70. G. Dowson, *Powder Metallurgy: The Process and its Products*, Hilger, Bristol, 1990, p. 43;

71. R. M. German, *Powder Metallurgy Science*, Metal Powder Industries Federation, NJ, 1984, p. 114;

72. F. Thummler, R. Oberacker, *Introduction to Powder Metallurgy*, Institute of Materials, London, 1993, p. 122;

73. W. D. Jones, *Fundamental Principles of Powder Metallurgy*, London, Edward Arnold, 1960;

74. W. Schatt, K. P. Wieters, *Powder Metallurgy: Processing and Materials*, EPMA Publications, 1997, p. 103;

75. A. Havalda, *Prášková Metalurgia*, STU Bratislava, 2000, p. 56-67;

76. R. L. Sands, C.R. Shakespeare, *Powder Metallurgy*, William Clowes and Sons, London, 1966, p. 41-47;

77. V. Kraus, *Tepelné Zpracování a Slinování Přednášky*, ZČU, Plzeň, 2000, p. 178-184;

78. G. Kaletunc, G. Kaletunç, K. Breslauer, *Characterization of Cereals and Flours: Properties, Analysis, and Applications*, CRC Press, 2003;

79. L. L. Augsburger, F. X. Muller, *The Role of The Displacement-Time Waveform in the Determintion of Heckel Behaviour Under Dynamic Conditions in a Compaction Simulator and a Fully Instrumented Rotary Tablet Machine*, Journal of Pharmacy and Pharmacology, Vol. 46, 1994, p. 468-475;

80. J. M. Sonnergaard, *A Critical Evaluation of the Heckel Equation*, International Journal of Pharmaceutics, Vol. 193, 1999, p. 63–71;

81. G.F. Bocchini, *The Warm Compaction Process: Basics, Advantages, and Limitations*, Society of Automotive Engineers, 1998;

82. U. Engstrom, B. Johansson, H. Rutz, F. Hanejko, S. Luk, *High Density Materials for Future Applications*, Advances in Powder Metallurgy and Particulate Materials 1995, Metal Powders Industries Federation, Vol. 3, 1995, p. 106-126;

83. K. Ueda, T. Machida, M. Iwakiri, H. Fukagawa, *Effect of Powder Lubricants and Compacting Temperature on the Higher Density of Iron-based Green Compacts*, Hitachi Powder Metals Technical Report Vol. 1,2002;

84. Y. Ozaki, S. Unami, S. Uenosono, *Pre-mixed Partially Alloyed Iron Powder for Warm Compaction: KIP Clean Mix HW Series*, Kawasaki Steel Technical Report, No. 47, 2002;

85. C. C. Degnan, P. H. Shipway, A. R. Kennedy, *Comparison of The Green Strength of Warm Compacted Astaloy CrM and Distaloy AE Densimix Powder Compacts*, Materials Science and Technology, Vol. 20, 2004, p. 731;

86. H. Yu, S. Liu, Q. J. Wang and Y. W. Chung, *Influence of Temperature-dependent Yield Strength on Thermomechanical Asperity Contacts*, Tribology Letters, Vol. 17, No. 2, 2004;

87. H. G. Rutz, F. G. Hanejko, *High Density Processing of High Performance Ferrous Materials*, Advances in Powder Metallurgy and Particulate Materials 1994, Metal Powder Industries Federation, Vol. 5, 1994, p. 117-133;

88. O. Grinder, *The Puzzle of Warm Compaction's Cool Reception*, PM Technology AB, Stockholm, Sweden, 1995;

89. A. Simchi, G. Veltl*, Investigation of Warm Compaction and Sintering Behaviour of Aluminium Alloys*, Powder Metallurgy, Vol. 46, No. 2, 2003;

90. A. Eksi, G. Veltl, F. Petzoldt, K. Lipp, C. M. Sonsino, *Tensile and Fatigue Properties of Cold and Warm Compacted Alumix 431 alloy*, Powder Metallurgy, Vol. 47, No. 1, 2004;

91. Z. Jiang, C. L. Falticeanu, I. T. H. Chang, *Warm Compression of Al Alloy PM Blends*, Materials Science Forum, Vol. 534-36, 2007, p. 333-336;

92. W. Schatt, K. P. Wieters, *Powder Metallurgy: Processing and Materials*, EPMA Publications, 1997, p. 117-118;

93. W. B. James, *An Optimized Double Press-double Sinter Powder Metallurgy Method*, European Patent Application 0457418A1, 1991;

94. V. Kraus, *Tepelné Zpracování a Slinování Přednášky*, ZČU, Plzeň, 2000, p. 185-186;

95. R. L. Sands, C.R. Shakespeare, *Powder Metallurgy*, William Clowes and Sons, London, 1966, p. 67-70;

96. W. Schatt, K. P. Wieters, *Powder Metallurgy: Processing and Materials*, EPMA Publications, 1997, p. 121-124, 132-134;

97. G. S. Upadhyaya, *Powder Metallurgy Technology*, Cambridge, International Science Publishing, 1997, p. 57-62;

98. G. Friedman, *Fabrication, Characterization and Thermal Conductivity of Porous Copper and Stainless Steel Materials*, NASA CR-72755, 1970;

99. H. F. Fischmeister, *Modern Techniques for Powder Metallurgical Fabrication of Low-alloy and Tool Steels*, Sweden, 1975, p. 157-166;

100. W. Schatt, K. P. Wieters, *Powder Metallurgy: Processing and Materials*, EPMA Publications, 1997, p. 134-138;

101. G. S. Upadhyaya, *Powder Metallurgy Technology*, Cambridge, International Science Publishing, 1997, p. 105-109;

102. ASM handbook Vol.7, *Powder Metal Technologies and Applications / Prepared Under the Direction of the ASM International Handbook Committee*, Materials Park, ASM, 1998, p. 1493, 1498-1501, 2008-2012;

103. R. L. Sands, C.R. Shakespeare, *Powder Metallurgy*, William Clowes and Sons, London, 1966, p. 72-73;

104. W. Schatt, K. P. Wieters, *Powder Metallurgy: Processing and Materials*, EPMA Publications, 1997, p. 131-132;

105. M. Bauser, G. Sauer, K. Siegert, *Extrusion*, ASM International, 2006, p 289-298;

106. V. Kraus, *Tepelné Zpracování a Slinování Přednášky*, ZČU, Plzeň, 2000, p. 187-188;

107. http://www.efunda.com/processes/metal_processing/extrusion.cfm, accessed 30th March 2009;

108. W. Schatt, K. P. Wieters, *Powder Metallurgy: Processing and Materials*, EPMA Publications, 1997, p. 147-149;

109. Suk-Joong L. Kang, *Sintering, Densification, Grain Growth and Microstructure*, Elsevier Butterworth-Heinemann, Oxford, 2005, p. 3-8, 37-75;

110. M. N. Rahaman, *Ceramic processing*, CRC / Taylor & Francis, 2006, p. 376;

111. R. L. Sands, C.R. Shakespeare, *Powder Metallurgy*, William Clowes and Sons, London, 1966, p. 78-81;

112. Suk-Joong L. Kang, *Sintering, Densification, Grain Growth and Microstructure*, Elsevier Butterworth-Heinemann, Oxford, 2005, p. 197-247;

113. R.M. German, *Liquid Phase Sintering,* Springer, 1985, p. 2-10;

114. A. Salak, *Ferrous Powder Metallurgy*, Cambridge International Science Publishing, 1995;

115. http://sweb.cz/JHamernik/Metalurgie.htm; accessed 7th May 2009;

116. A. Havalda, *Prášková Metalurgia*, STU Bratislava, 2000, p. 97-100;

117. P. Gummeson, A. Stosuy, *Iron-Carbon Behaviour During Sintering*, Technical Bulletin D 164, Hoeganaes Corp., 1972;

118. R. L. Sands, C.R. Shakespeare, *Powder Metallurgy*, William Clowes and Sons, London, 1966, p. 149;

119. ASM handbook Vol.7, *Powder Metal Technologies and Applications / Prepared Under the Direction of the ASM International Handbook Committee*, Materials Park, ASM, 1998, p. 372, 1078-1086;

120. http://www.weatheronline.co.uk/reports/wxfacts/Dew-Point.htm; accessed 7th May 2009;

121. A. Salak, M. Selecka, H. Danninger, *Machinability of Powder Metallurgy Steels*, Cambridge, International Science Publishing, 2005, p: 181-185;

122. D. Gard, K. R. Berger, D. J. Bowe, J. G. Marsden, *Sintering of Carbon Steel Components in Endothermic and Nitrogen-hydrogen Atmospheres,* Industrial Heating, 1999,

123. F. Thummler, R. Oberacker, *Introduction to Powder Metallurgy*, Institute of Materials, London, 1993, p. 244;

124. R. Fabian, *Vacuum Technology: Practical Heat Treating and Brazing*, ASM International, 1993, p. 179;

125. K. H. Moyer, W. R. Jones, *Vacuum Sinter Hardening*, Heat Treating Progress, 2002;

126. D. J. Bowe, K. R. Berger, J. G. Marsden, D. Gard, *Optimization of Nitrogen/hydrogen Sintering Atmosphere Composition for Carbon Steel,* Journal of Powder Metallurgy, Vol. 31, 1995, p. 29-37;

127. http://www.praxair.com/praxair.nsf/AllContent/704FEF424DF1C3108525654F004FF267?OpenDocument&URLMenuBranch=996847C0023A54D58525706F004F1665, accessed 7th May 2009;

128. M. N. Rahaman, *Sintering of Ceramics*, CRC Press, 2007, p. 320-330;

129. R. M German, G. L. Messing, R. G. Cornwall, *Sintering Technology*, CRC Press, 1996;

130. G. E. Totten, M. A. H. Howes, T. Inoue, *Handbook of Residual Stress and Deformation of Steel*, ASM International, 2002, p. 402-403;

131. P. King, B. Lindsley, *Chromium Steels for High Performance PM Applications*, Presented at Powder Metallurgy 2007, USA, 2007;

132. R. Davis & Associates, *Aluminium and Aluminium Alloys*, ASM International Handbook Committee, Edition: 4, 1993, p. 282-283;

133. J. Liu, H. A. Kuhn, *Innovative Approach to Sintering Aluminium and Aluminium Alloy Powders for Rapid Manufacturing Applications*, KPMI, PM 2006, p. 246;

134. J. M. Martin, F. Castro, *Liquid Phase Sintering of P/M Aluminium Alloys: Effect of Processing Conditions*, Journal of Materials Processing Technology, 143–144, 2003, p. 814–821;

135. K. H. Min, S. P. Kang, B.-H. Lee, J.-K. Lee, Y. D. Kim, *Liquid Phase Sintering of the Commercial 2xxx Series Al Blended Powder,* Journal of Alloys and Compounds, 2005, p. 58;

136. P. Enghag, *Encyclopedia of the Elements, Technical Data History Processing Applications,* WILEY-VCH Verlag GmbH & Co. KGaA, Weinheim, 2004, p. 834;

137. J. M. Silcock, T. J. Heal, H. K. Hardy, *Structural Ageing Characteristics of Binary Aluminium–copper Alloys*, Journal of the Institute of Metals, Vol. 82, 1953, p. 239-248;

138. K. Raviprasad, C. R. Hutchinson, T. Sakuraic and S. P. Ringer, *Precipitation Processes in An Al-2.5Cu-1.5Mg (wt. %) Alloy Microalloyed with Si*, Acta Materialia Vol. 51, Issue 17, 2003, p. 5037-5050;

139. W. Q Song, P Krauklis, A. P Mouritz and S Bandyopadhyay, *The Effect of Thermal Ageing on the Abrasive Wear Behaviour of Age-hardening 2014 Al/SiC and 6061 Al/SiC Composites,* Wear, Vol. 185, Issues 1-2, 1995, p. 125-130;

140. T. B. Sercombe, *On the Sintering of Uncompacted, Pre-alloyed Al Powder Alloys*, Materials Science and Engineering A341, 2003, 163/168;

141. C. L. Falticeanu, *Powder Metallurgy of Al-Cu-Si-Mg blends*, Thesis, The University of Birmingham, 2007;

142. http://controls.engin.umich.edu/wiki/index.php/Design_of_experiments_via_taguchi_methods:_orthogonal_arrays, accessed 14th May 2009;

143. http://www.scribd.com/doc/7024941/Orthogonal-Array-Testing, accessed 4th April 2009;

144. P. Erto, *Statistics for Innovation*, Springer, 2009, p. 81-83;

145. T. P. Ryan, *Modern Engineering Statistics*, Wiley, 2007, p. 419-420;

146. R. K. Roy, *A Primer on the Taguchi Method*, SME, 1990, p. 145;

147. G. A. Lewis, D. M. Roger T. L. Phan, M. Dekker, *Pharmaceutical Experimental Design*, 1999;

148. M. Tjantele, *Parameter Design Using the Taguchi Methodology*, Microelectronic Engineering 10, 1991, p. 277-286;

149. E. Ozbay, A. Oztas, A. Baykasoglu, H. Ozbebek, *Investigating Mix Proportions of High Strength Self Compacting Concrete by Using Taguchi Method*, Construction and Building Materials, Vol. 23, 2009, p. 694-702;

150. http://www.public.iastate.edu/~vardeman/IE361/s00mini/maurer.htm, accessed 4th April 2009;

151. S. H. Hong, K. H. Chung, *The Effects of Processing Parameters on Mechanical Properties of SiC/$_w$ 2124Al Composites*, Journal of Materials Processing Technology , Vol. 48, 1995, p. 349-355;

152. C. Selcuk , J. V. Wood, *Reactive Sintering of Porous Tungsten: A Cost Effective Sustainable Technique for the Manufacturing of High Current Density Cathodes to be Used in Fashlamps*, Journal of Materials Processing Technology, Vol. 170, 2005, p. 471-476;

153. K. R. Jamaludin , N. Muhamad , M. N. A. Rahman , S. Y. M. Amin , S. Ahmad , M.H.I. Ibrahim, *Sintering Parameter Optimisation of the SS316L Metal Injection Molding (MIM) Compacts For Final Density Using Taguchi Method,* Accepted for Advances in Materials and Processing Technologies Conference, 2009;

154. Material Safety Data Sheet for Acrawax C, V50, V150, IMS Company, OH;

155. Material Safety Data Sheet for Kenolube P11, Hoganas AB, Sweden, MSDS code: 027575;

156. Standard Test Methods for Metal Powders and Powder Metallurgy Products, 2nd second edition, Metal Powders Industries Federation 2002;

157. W. Schatt, K. P. Wieters, *Powder Metallurgy: Processing and Materials,* EPMA Publications, 1997, p. 183;

158. G. Poszmik, S. H. Luk, *Binder Treated Products for Higher Densities and Better Precision*, Hoeganaes Corporation, Presented at PM2TEC2003, 2003, USA;

159. J. M. Martín, F. Castro, *Sintering Response &Microstructural Evolution of an Al-Cu-Mg-Si Premix,* International Journal of Powder Metallurgy, Vol. 43, 2007, p. 59-68;

160. J. Zhou, J. Duszczyk, *Aging Response of an AA2014-based Composite Prepared from an Elemental Powder Mixture*, Journal of Materials Science Letters, Vol. 18, 1999, p.1111-1113; 219;

161. D. W. Hearda, I. W. Donaldsonb, D. P. Bishop, *Metallurgical Assessment of a Hypereutectic Aluminum–silicon P/M Alloy*, Journal of Materials Processing Technology, 2009;

162. F. W Nyongesa, B. O. Aduda, *Fracture Strength of Porous Ceramics: Stress Concentration vs. Minimum Solid Area Models*, African Journal of Science and Technology, Vol. 5, 2004, p. 19-27;

163. A. Salak, V. Miskovic, E. Dudrova, E. Rudnayova, *The Dependence of Mechanical Properties of Sintered Iron Compacts upon Porosity*, Powder Metallurgy International 6, Vol. 128, 1974, p. 128-132;

164. N. A. Fleck, R. A. Smith, *Use of Simple Models to Estimate Effect of Density on Fracture Behaviuor of Sintered Steel,* Powder Metallurgy, No. 3, 1981, p: 126-130;

165. V. T. Troshchenko, *The Strength of Porous Sintered Materials,* Powder Metallurgy and Metal Ceramics, Vol. 2, 1963;

166. H. E. Exner, D. Pohl, *Fracture behavior of sintered iron*, Powder Metallurgy International, Vol. 10, 1978, p. 193-196;

167. S. H. Hong, K. H. Chung, *Effects of Vacuum Hot Pressing Parameters on the Tensile Properties and Microstructure of SiC – 2124 Al Composites*, Materials Science and Engineering, 1995, p. 165-170;

168. R. E. Fryxell, B. A. Chandler, *Creep, Strength, Expansion, and Elastic Moduli of Sintered BeO As a Function of Grain Size, Porosity, and Grain Orientation,* Journal of the American Ceramic Society, Vol. 47, 1964, p. 283-291;

169. R. Spriggs, *Expression for Effect of Porosity on Elastic Modulus of Polycrystalline Refractory Materials, Particularly Aluminum Oxide,* Journal of the American Ceramic Society, Vol. 44, 1961, p. 628-629;

170. A. S. Wagh, J. P. Singh, R. B. Poeppel, *Dependence of Ceramic Fracture Properties on Porosity,* Journal of Material Science, Vol. 28, 1993, p. 3589-3593;

171. P. Wong, J. Koplik , J. P. Tomanic, *Conductivity and Permeability of Rocks*, Physical Review B, Vol. 30, 1984, p. 6606-6614;

172. N. Ramakrishnan, V. S. Arunachalam, *Effective Elastic Moduli of Porous Solids*, Journal of Materials Science, Vol. 25, 1990, p. 3930-3937;

173. http://www.tech.plym.ac.uk/sme/interactive_resources/tutorials/FailureAnalysis/Fractography/Fractography_Resource5.htm; accessed 14th May 2009;

174. T. Pardoena; D. Dumont, A. Deschampsd, Y. Brechet; *Grain Boundary Versus Transgranular Ductile Failure*, Journal of the Mechanics and Physics of Solids, Vol. 51, 2003, p. 637-665;

175. http://controls.engin.umich.edu/wiki/index.php/Design_of_experiments_via_taguchi_methods:_orthogonal_arrays, accessed 14th May 2009;

176. S. S. M. Nora, M. M. Rahmana, F. Tarlochana, B. Shahidaa, A. K. Ariffinb, *The Effect of Lubrication in Reducing Net Friction in Warm Powder Compaction Process*, Journal of Materials Processing Technology, 207, 2008, p. 118-124;

177. L. Azzi, Y. Thomas, S. St-Laurent, *Lubricants for High-density Compaction at Moderate Temperatures*, International Journal of Powder Metallurgy, Vol. 43, 2007, p. 39-45;

178. B. Azhdar, B. Stenberg, L. Kari, *Determination of Dynamic and Sliding Friction, and Observation of Stick-slip Phenomenon on Compacted Polymer Powders During High-velocity Compaction,* Polymer Testing, Vol. 25, 2006, p: 1069-1080;

179. P. Izak, *Generalized Model for Densification of Granulated Ceramic Powders*, Zeramische Zeitschrift, Vol.53, 2001, p: 912-915;

180. Y. Y. Li, T. L. Ngai, S. L. Wang, M. Zhu, W. P. Chen, *Effects of Lubricant's Friction Coefficient on Warm Compaction Powder Metallurgy*, Transactions of Nonferrous Metals Society of China, Vol. 15, No. 1., 2005;

181. P. J. Blau, *Friction Science and Technology: From Concepts to Applications*, Taylor & Francis Group, 2009, p.242;

182. E. Rabinowicz, *Friction and Wear of Materials*, Wiley, 1965, p.211;

183. G. A. Gegel, S. Luk, *Test Device and Method for Evaluation of Lubricants for P/M Compaction*, Caterpillar Inc., Hoeganaes Corporation;

184. E. W. Washburn, *The Dynamic of Capillary Flow*, Physical Review, 1921, Vol. 17, p. 273-283;

185. A. Babakhani, A. Haerian, *Effect of Carbon Content and Sintering Temperature on Mechanical Properties of Iron - based PM Parts Produces by Warm Compaction,* Powder Metallurgy Progress, Vol.8, No 2, 2008. p. 156-163;

186. F. Thummler, R. Oberacker, *Introduction to Powder Metallurgy*, 1st ed, London, The Institute of Materials, 1993. p. 121-124;

187. D. G. Kim, K. H. Min, S. Y. Chang, Y. D. Kim, *Effect of Compacting Pressure on Sintering Characteristics of Commercial 2xxx Series Al Alloy Powders*, Journal of Korean Powder Metallurgy Institute, Vol.9, 2002, p. 116-123;

188. A. Simchi, *Effects of Lubrication Procedure on the Consolidation, Sintering and Microstructural Features of Powder Compacts,* Materials & Design, Vol. 24, Issue 8, 2003, p. 585-594;

189. M. M. Rahman, S. S. M. Nor, *An Experimental Investigation of Metal Powder Compaction at Elevated Temperature*, Mechanics of Materials, Vol. 41, 2009, p. 553-560;

190. A. Babakhani, A. Haerian, M. Ghambari, *On the Combined Effect of Lubrication and Compaction Temperature on Properties of Iron-based P/M Parts*, Materials Science and Engineering, 2006, p. 360–365;

191. Z. Huda, *Precipitation Strengthening and Age-Hardening in 2017 Aluminum Alloy for Aerospace Application*, European Journal of Scientific Research, Vol.26, 2009, p.558-564;

192. W. Soboyejo, *Mechanical Properties of Engineered Materials*, Marcel Dekker, Inc., NY, 2003, p. 234-244;

193. G. E. Totten, D. S. MacKenzie, *Handbook of Aluminium*, Physical Metallurgy and Processes, Vol. 1, Marcel Dekker, Switzerland, p. 86-91;

194. R. E. Smallman, R. J. Bishop, *Modern Physical Metallurgy and Materials Engineering ,Science, Process, Applications*, Sixth Edition, Reed Educational and Professional Publishing Ltd 1995, 1999, p. 259-263;

195. Y. Y. Li, T. L. Ngai, Z. Y. Xiao; *Study on Mechanical Properties of Warm Compacted Iron-base Materials,* Journal of Central South University of Technology, Vol. 9, 2002, p.154-158;

196. A. K. Eksi, K. Lipp, C.M. Sonsino, G. Veltl, F. Petzoldt, *Static and Fatigue Properties of the Cold and Warm Compacted Sintered Aluminium Alloy Alumix 431 (Al-5.5 Zn-2.5 Mg-1.5 Cu),* Materialwissenschaft und Werkstofftechnik, Vol. 37, 2006, p. 374-382;

197. Z. Horita, K. Ohashi, T. Fujita, K. Kaneko, T. G. Langdon, *Achieving High Strength and High Ductility in Precipitation-hardened Alloys*, Advanced Materials, Vol. 17, 2005, p. 1599-1602;

198. G. E. Totten, K. Funatani, L. Xie, *Handbook of Metallurgical Process Design,* Vol. 24, 2004, p. 380-383;

199. B. J. Hall, G. B. Schaffer, *Statistical Experimental Design of Al–Cu–Mg–Si P/M Alloys,* Journal of Light Metals, Vol. 2, 2002, p. 229-238;

200. H. S. Choi, T. Lee, H. Lee, J. Kim, K. H. Hong, K. H. Kim, J. Shin, H. J. Shin, H. D. Jung, S. H. Choi, *Prediction of Young's Moduli of Low Dielectric Constant Materials by Atomistic Molecul Dynamics Simulation,* Materials Research Society, 2006, p. 0891-EE07-08.1-6;

201. H. J. Sung, T. K. Ha, S. Ahn, Y. W. Chang, *Powder Injection Molding of a 17-4 PH Stainless Steel and the Effect of Sintering Temperatures on its Microstructure and Mechanical Properties,* Journal of Materials Processing Technology, 2002, p. 321-327;

202. R. P. Baron, F. E. Wawner, J. A. Wert, *Relationship Between Fractional Porosity and Tensile Strength for High-porosity Sintered Ferrous Powder Compacts*, Scripta Materialia, Vol. 39, No. 3, 1998, p. 269-275;

203. C. L. Falticeanu, I. T. H. Chang; J. S. Kim, R. Cook; *Sintering Behaviour of Al-Cu-Mg-Si Blends,* Materials Science Forum, 2007, p. 597-600;

204. L.F. Mondolfo, *Aluminum Alloys: Structure and Properties*, Butterworth & Co. Ltd., UK, 1976;

205. A. Gökçe, F. Fındik, *Mechanical and Physical Properties of Sintered Aluminum Powders*, Journal of Achievements in Materials and Manufacturing Engineering, Vol. 30, 2008, p. 157-164;

206. D. Božić, N. Ilić, M. Mitkov, M.T. Jovanović, *A Comparative Study of Microstructure, Mechanical and Fracture Properties of Ni_3Al-based Intermetallics Produced by Powder Metallurgy and Standard Melting and Casting Processes*, Journal of Materials Science, Vol. 31, 1996, p. 3213-3221;

207. H. Saage, M. Krüger, D. Sturm, M. Heilmaier, J. H. Schneibel, E. George, L. Heatherly, Ch. Somsen, G. Eggeler, Y. Yang, *Ductilization of Mo–Si Solid Solutions Manufactured by Powder Metallurgy,* Acta Materialia Vol. 57, 2009, p. 3895-3901;